Replication Stress Links Structural and Numerical Chromosomal Instability in Colorectal Cancer

Rebecca Alison Burrell

University College London

and

Cancer Research UK London Research Institute

PhD Supervisor: Professor Charles Swanton

A thesis submitted for the degree of

Doctor of Philosophy

University College London

September 2012

Declaration

I, Rebecca Burrell, confirm that the work presented in this thesis is my own. Where information has been derived from other sources, I confirm that this has been indicated in the thesis.

Abstract

Chromosomal instability (CIN), describing an increased rate of numerical and structural chromosome aberrations, is a principal driver of inter-cellular genetic heterogeneity in tumours. CIN is widely observed in solid malignancies, and is associated with poor patient outcome and drug resistance. Despite the prevalence and clinical impact of CIN in cancer, the underlying mechanisms still remain poorly characterised.

Systematic characterisation of CIN+ colorectal cancer cells revealed that structurally abnormal chromosomes, generated through pre-mitotic defects, cause the majority of anaphase segregation errors. This contradicts a widely held hypothesis that CIN is caused by mitotic dysfunction. An investigation of the origins of these structural chromosome aberrations found that CIN+ cells display elevated DNA replication stress. Further experiments to investigate the link between replication stress and CIN demonstrated that induction of replication stress in diploid cells initiated both numerical and structural chromosomal instability.

Through an integrative genomics approach, three novel putative CIN-suppressor genes (PIGN, RKHD2 and ZNF516) were identified, encoded on chromosome 18q, a genomic region subject to copy number loss in 80 per cent of CIN+ colorectal cancers. Silencing each of these three genes resulted in anaphase segregation errors and structural chromosome abnormalities. Cells depleted of the CIN-suppressors displayed evidence of DNA replication stress, phenocopying observations in CIN+ cells. Supplementing cells with exogenous nucleosides, which may alleviate replication stress, reduced both segregation errors induced by CIN-suppressor gene silencing, and endogenous segregation errors in cells with 18q loss.

In summary, CIN in colorectal cancer appears to be driven through pre-mitotic generation of structurally abnormal chromosomes that are subsequently missegregated at anaphase, rather than through mitotic defects. These structurally abnormal chromosomes may result from elevated levels of DNA replication stress in CIN+ cells, which may be linked to the loss of three syntenic CIN-suppressor genes encoded on chromosome 18q.

Acknowledgement

First and foremost, I would like to thank my supervisor Charlie for his endless supply of enthusiasm and ideas, and for all the encouragement and opportunities he has given me throughout my PhD.

I would also like to thank the entire Translational Cancer Therapeutics Laboratory, past and present, for being such a great group of people to work alongside. In particular, I would like to thank Sarah McClelland, Andrew Rowan and Alvin Lee for all that they taught me at the bench in the early days. Special thanks must also go to Andrew for all the cheesecakes, and to Eva, Sally, Chloe and Sarah for their help in proofreading this thesis.

This work would not have been possible without collaboration. Within the lab I would like to thank Sarah McClelland and David Endesfelder, with whom I have worked on this project from the outset. I am also very grateful to our external collaborators, Professors Jiri Bartek, Thomas Helleday and Ian Tomlinson, for all their advice and input to this project, in particular to Prof. Bartek for his encouragement over the last two years.

Within the LRI, I would like to acknowledge my thesis committee (Professors Julian Downward and Gordon Peters), the core service labs, our lab aides Ian and Chris, and my fellow students. I would also like to thank Kay Penicud and Nnennaya Kanu for their technical assistance and advice in the journey from mitotic cell biology into the world of DNA damage and replication stress. At UCL, I would like to thank Prof. Gordon Stewart and the UCL MB PhD programme for the opportunity to undertake this research during my medical studies.

To my friends and family – thank you for all your patience and support. It has been invaluable.

I would like to dedicate this thesis to the memory of my brother Edd Burrell

Table of Contents

Abstract **3**
Acknowledgement **4**
Table of Contents **5**
Table of figures **9**
List of tables **11**
Abbreviations **12**
Chapter 1. Introduction **14**
1.1 Chromosomal instability and aneuploidy in cancer **15**
1.1.1 Measuring CIN in tumour specimens 15
1.1.2 CIN and poor prognosis in cancer 16
1.2 Mechanisms of CIN **19**
1.2.1 Classifying anaphase chromosome segregation errors 20
1.3 Mitotic causes of chromosome missegregation **22**
1.4 The mitotic checkpoint **23**
1.4.1 Mitotic checkpoint defects and CIN 24
1.5 Correcting improper kinetochore-microtubule attachments **26**
1.5.1 Abnormal spindle geometry promotes improper kinetochore-microtubule attachments 27
1.5.2 Hyper-stable microtubules and defective error correction 30
1.6 Mitotic causes of chromosome missegregation - summary **30**
1.7 Pre-mitotic mechanisms of CIN **31**
1.8 DNA damage and structural chromosome abnormalities **32**
1.8.1 Types of DNA damage 33
1.8.2 Mechanisms of DNA repair 34
1.8.3 Recognition of DNA damage 36
1.8.4 Replication fork stalling – restart and repair 41
1.8.5 The cell cycle checkpoint response to DNA damage 44
1.9 DNA damage and CIN **46**
1.9.1 Defective DNA damage response and chromosomal abnormalities 47
1.9.2 Increased generation of endogenous DNA damage 49
1.9.3 Telomere Uncapping 49
1.9.4 DNA replication stress 51
1.10 Defects in chromosome assembly **56**
1.11 Pre-mitotic mechanisms of CIN – summary **58**
1.12 Can one mechanism explain structural and numerical CIN? **58**
1.13 Mechanisms of CIN – summary **60**
1.14 Genetic instability in colorectal cancer **60**
1.15 Microsatellite instability **61**
1.16 CIN in colorectal cancer **62**
1.16.1 Is there a mutational basis for CIN in colorectal cancer? 62
1.16.2 Recurrent copy number changes in CIN colorectal cancer 65
1.17 Conclusion **68**
Chapter 2. Materials & Methods **69**
2.1 Cell lines **69**
2.1.1 Cell line classification 69
2.2 Transfections **70**

2.2.1 Plasmid preparation 70
2.2.2 Plasmid transfections 70
2.2.3 SiRNA transfections 70
2.3 Immunostaining 71
2.3.1 Immunofluorescence on coverslips 71
Abcam ab6046 **..... 72**
2.3.2 Immunofluorescence on chromosome spreads 72
2.3.3 DNA fibre assays 73
2.4 Fluorescence *in-situ* hybridization (FISH) 74
2.4.1 Sample preparation 74
2.4.2 Probe hybridisation and analysis: 75
2.5 Microscopy 76
2.5.1 Image Acquisition 76
2.5.2 Image analysis 76
2.5.3 Time-lapse microscopy 80
2.6 Flow cytometry 81
2.6.1 Mitotic index: 81
2.6.2 Mitotic checkpoint 81
2.6.3 G2-M Checkpoint 81
2.6.4 Intra-S phase checkpoint 82
2.7 Miscellaneous cell treatments 82
2.7.1 Monastrol washout 82
2.7.2 Irradiation 82
2.7.3 Aphidicolin 82
2.7.4 Blebbistatin 83
2.8 Characterisation of genes encoded on chromosome 18q 83
2.8.1 siRNA transfections 83
2.8.2 RNA extraction and RT-qPCR 83
2.8.3 Western blotting 85
2.8.4 shRNA cell lines 86
2.9 Nucleoside supplementation 87
2.9.1 Segregation error and mitotic DNA damage quantification 87
2.9.2 Proliferation assays 87
2.9.3 Cellular ATP measurement 87
2.10 Tumour specimen analysis 88
2.10.1 Ploidy analysis - flow cytometry 88
2.10.2 Carcinoma-in-adenoma Patient samples 89
2.11 Bioinformatics Analysis 90
2.11.1 Aneuploid tumour analysis 90
2.11.2 Defining Consistent Regions of Somatic Copy Number Loss – cell lines 90
2.11.3 TCGA (The Cancer Genome Atlas) data 92
2.11.4 Structural/Numerical Complexity 92
Chapter 3. Results 1 – CIN+ colorectal cancer cell lines display elevated replication stress 93
3.1 Introduction 93
3.2 Classification of segregation errors in CIN+ CRC 93
3.3 Structural and numerical instability in CIN+ CRC 97
3.3.1 Structural and Numerical karyotypic complexity in CIN+ CRC cell line 97

3.3.2 Structural chromosome defects in CIN+ CRC 99
3.3.3 Numerical instability in CIN+ CRC 101
3.4 Mitotic defects in CIN+ CRC 102
3.4.1 Mitotic progression 103
3.4.2 Mitotic Checkpoint Function and sister chromatid cohesion 105
3.4.3 Spindle defects and merotelic attachments 106
3.5 Pre-mitotic defects in CIN+ CRC 111
3.5.1 CIN+ cells display evidence of elevated DNA replication stress 112
3.5.2 G2-M DNA damage checkpoint function 113
3.5.3 Telomere dysfunction does not account for CIN+ cell prometaphase damage 114
3.6 Slow replication fork rates in CIN+ cell lines 116
3.7 Inducing replication stress in CIN- cells initiates chromosomal instability 117
3.8 Conclusions and discussion 126
Chapter 4. Results 2 – Identifying CIN-suppressors encoded on chromosome 18q 128
4.1 A recurrent CIN-specific genome architecture 129
4.1.1 Recurrent loss of chromosome 18q in CIN+ Colorectal Cancer 130
4.1.2 A temporal association of 18q copy number loss with aneuploidy onset 133
4.2 Screening for novel suppressors of chromosomal instability 136
4.2.1 Identification of candidate CIN-suppressor genes 136
4.2.2 SiRNA screen for chromosome segregation error induction 137
4.3 SiRNA screen validation 140
4.3.1 siRNA pool deconvolution, silencing efficiency 140
4.3.2 Excluding common off-target effects 141
4.3.3 Validation in additional cell lines 142
4.4 Candidate CIN-suppressors are lost together in tumours, and copy number loss correlates with decreased expression 143
4.5 CIN-suppressors: background 144
4.5.1 PIGN 145
4.5.2 RKHD2 146
4.5.3 ZNF516 146
4.6 Silencing candidate CIN suppressors results in structural instability 147
4.7 CIN-suppressor silencing results in numerical instability 150
4.8 Conclusions and discussion 152
Chapter 5. Results 3 – Depletion of CIN-suppressors is associated with pre-mitotic rather than mitotic defects 153
5.1 Assessment of DNA replication stress following CIN-suppressor silencing 153
5.1.1 DNA damage induction 154
5.1.2 Ultra-fine bridges 156
5.1.3 53BP1 bodies in G1 cells 158
5.1.4 53BP1 bodies induced by CIN-suppressor silencing are not a consequence of chromosome damage during cytokinesis 158
5.1.5 DNA fibre analysis reveals slow replication rates after CIN-suppressor silencing 160
5.1.6 Pre-mitotic dysfunction following CIN-suppressor silencing 161
5.2 Examining mitotic dysfunction following CIN-suppressor silencing 163

5.2.1 Time-lapse microscopy following CIN-suppressor silencing reveals no alterations in mitotic progression following CIN silencing 163
5.2.2 Segregation errors induced by CIN-suppressor silencing do not arise specifically from micronuclei 165
5.2.3 The mitotic checkpoint is not compromised after CIN-suppressor silencing 167
5.2.4 Defective spindle geometry 169
5.2.5 Merotelic kinetochore-microtubule attachments 170
5.3 Summary – pre-mitotic versus mitotic defects after CIN-suppressor silencing 171
5.4 Further characterisation of pre-mitotic defects induced by CIN-suppressor silencing 173
5.4.1 G2-M DNA damage checkpoint function 173
5.4.2 Intra-S checkpoint function 176
5.5 Conclusions and discussion 177
5.5.1 CIN-suppressor gene function 180
Chapter 6. Results 4 – Nucleoside supplementation reduces segregation error frequency in CIN+ cell lines with 18q loss 184
6.1 Exogenous nucleosides reduce endogenous segregation error frequency in CIN+ cell lines 185
6.2 Cell cycle distribution and mitotic entry after nucleoside supplementation 185
6.3 Nucleoside supplementation does not affect proliferation 189
6.4 Nucleoside supplementation does not increase ATP levels 191
6.5 Nucleoside supplementation does not reduce segregation error frequency in CIN- or 18q normal CIN+ cells. 192
6.6 Conclusions and discussion 194
Chapter 7. Discussion 196
7.1 Mechanisms of CIN in colorectal cancer 196
7.1.1 Structural chromosome aberrations are the main cause of segregation errors in CIN+ CRC 196
7.1.2 CIN+ cells are characterised by elevated replication stress 197
7.1.3 CIN and oncogene-induced replication stress 199
7.2 18q and CIN in colon cancer 201
7.2.1 Using RNA interference to identify CIN-suppressor genes on 18q 201
7.2.2 Copy number alterations as a cause of CIN 202
7.2.3 Clinical implications 203
7.3 Strategies to target CIN in tumours 204
7.4 Conclusion 206
Chapter 8. Appendix 207
8.1 Appendix 1: List of genes screened by RNA interference 207
8.2 Appendix 2 - List of papers and reviews published during the production of this thesis 212
Reference List 213

Table of figures

Chapter 1

Figure 1.1 Classification of anaphase segregation errors 20
Figure 1.2 The stages of mitosis 23
Figure 1.3 Monitoring kinetochore-microtubule attachments before anaphase 25
Figure 1.4 Abnormal spindle geometry results in improper attachments 29
Figure 1.5 Mechanisms generating dicentric and acentric chromosomes 33
Figure 1.6 Non-homologous end-joining (NHEJ) 37
Figure 1.7 Homologous recombination mediated repair (HR) 38
Figure 1.8 Recognition of double strand breaks 40
Figure 1.9 Restart and repair of stalled replication forks 43
Figure 1.10 DNA damage checkpoint signalling 45
Figure 1.11 Replication-stress associated phenotypes 56

Chapter 2

Figure 2.1 Segregation error classification 78
Figure 2.2 Structural abnormalities in metaphase chromosomes 79

Chapter 3

Figure 3.1 Anaphase segregation errors in CIN+ CRC cell lines 96
Figure 3.2 Monastrol washout specifically induces lagging chromosomes 97
Figure 3.3 Karyotypic complexity in CRC cell lines 98
Figure 3.4 Structural chromosome aberrations in CIN+ CRC cells 100
Figure 3.5 Numerical heterogeneity in CIN+ CRC cell lines 102
Figure 3.6 Mitotic progression in CIN+ vs CIN- CRC cell lines 104
Figure 3.7 Mitotic checkpoint activity in CIN+ CRC cells 107
Figure 3.8 Sister chromatid cohesion in CIN+ CRC cells 108
Figure 3.9 Spindle geometry and merotelic attachments in CIN+ CRC cell lines 109
Figure 3.10 CIN+ cells display elevated DNA replication stress 113
Figure 3.11 G2-M DNA damage checkpoint function in CIN+ CRC cell lines 114
Figure 3.12 DNA damage are not confined to chromsome termini 115
Figure 3.13 Slow replication fork rates in CIN+ CRC cell lines 118
Figure 3.14 Pharmacological induction of replication stress in HCT-116 122
Figure 3.15 Comparison of PICH and RPA as markers of ultra-fine bridges 123
Figure 3.16 Pharmacological induction of replication stress induces chromosome segregation errors 124
Figure 3.17 Pharmacological induction of replication stress results in structural and numerical instability 125

Chapter 4

Figure 4.1 Somatic copy number losses in aneuploid/CIN+ colorectal cancer 131
Figure 4.2 18q loss in CIN+ CRC cell lines 132
Figure 4.3 Temporal association of 18q loss and aneuploidy 134
Figure 4.4 18q loss usually precedes polyploidy in CRC development 136

Figure 4.5 siRNA screen of 18q genes to identify suppressors of chromosome segregation errors 138
Figure 4.6 Screen deconvolution and validation 139
Figure 4.7 Validation in addition CRC cell lines 143
Figure 4.8 Gene expression correlates with copy number loss in tumours and cell lines 145
Figure 4.9 Structural aberrations after CIN-suppressor silencing 148
Figure 4.10 Chromosome non-disjunction initiated by CIN-suppressor silencing 149
Figure 4.11 Cytokinesis block chromosome non-disjunction assay 151

Chapter 5

Figure 5.1. CIN-suppressor silencing results in DNA damage 155
Figure 5.2 Induction of ultra-fine bridges after CIN-suppressor silencing 157
Figure 5.3 Induction of 53BP1 bodies in G1 cells 159
Figure 5.4 Reduced replication fork rates after CIN-suppressor silencing 162
Figure 5.5 Time-lapse microscopy of HCT-116 H2B-mRFP cells after CIN-suppressor silencing 164
Figure 5.6 Segregation errors do not arise specifically in cells with micronuclei 166
Figure 5.7 The mitotic checkpoint is functional after CIN-suppressor silencing 168
Figure 5.8 Examining spindle geometry after CIN-suppressor silencing 172
Figure 5.9 Evaluation of kinetochore-microtubule attachments after CIN-suppressor silencing 173
Figure 5.10 RKHD2 depletion leads to a defective G2/M DNA damage checkpoint .. 175
Figure 5.11 Intra-S phase checkpoint function after CIN-suppressor silencing 178
Figure 5.12 Intra-S phase checkpoint dysfunction after RKHD2 silencing 179
Figure 5.13 Replication block induces double-strand breaks in siRKHD2 cells 180
Figure 5.14 Preliminary localisation of GFP tagged RKHD2 and ZNF516 181

Chapter 6

Figure 6.1 Nucleoside supplementation reduces segregation error frequency in CIN+ colorectal cancer cell lines 187
Figure 6.2 Nucleoside supplementation does not affect cell cycle distribution 188
Figure 6.3 Nucleoside supplementation does not affect proliferation rate 190
Figure 6.4 Nucleoside supplementation does not increase cellular ATP levels 191
Figure 6.5 Nucleosides do not reduce segregation errors in CIN- or 18q normal CIN+ cell lines 194

List of tables

Table 1.1 CIN is associated with poor prognosis in multiple cancer types 17
Table 1.2 Hereditary syndromes caused by mutations in components of the DNA damage response 48
Table 1.3 Mismatch repair genes commonly mutated in Lynch Syndrome 61
Table 1.4 Mutations in CRC 67
Table 2.1 Antibodies used for immunofluorescence 72
Table 2.2 siRNA and shRNA sequences used in this study 84
Table 2.3 Taqman Probe catalogue numbers used for qRT-PCR 85
Table 3.1 Details of cell lines used in this study 95
Table 3.2 Replication fork rates of a range of cell lines 119
Table 4.1 Frequency of 18q loss in CIN+ CRC cell lines and aneuploid colorectal tumours (BAC array and TCGA cohort) 133
Table 4.2 Frequency of CIN-suppressor loss 144
Table 5.1 Predicted ATM phosphorylation sites in CIN-suppressor proteins 183
Table 6.1 Summary of effects of nucleoside supplementation 192

Abbreviations

APC/C – anaphase promoting complex/cyclosome

BER – base excision repair

CDK- cyclin dependent kinase

CIN – Chromosomal instability

CRC – Colorectal Cancer

DDR – DNA damage response

DFS – disease free survival

dNTP – deoxyribonucleotide tri-phosphates

DSB – DNA double strand break

FISH – Fluorescence *in-situ* hybridisation

γH2AX – phosphorylated (gamma) histone variant 2.AX

HR – homologous recombination

H2B – histone 2B

GFP – green fluorescent protein

LOH – loss of heterozygosity

LCC – last chromosome congressed

MIN – microsatellite instability

MMR – mismatch repair

MSI – microsatellite instability

MFS – metastasis-free survival

NCS – numerical complexity score

NEBD – nuclear envelope breakdown

NER – nucleotide excision repair

NHEJ – non homologous end joining

NSCLC – non small-cell lung cancer

OS – overall survival

RFP – red fluorescent protein

RFS – relapse free survival

RPA – replication protein A

SCNL – somatic copy number loss

siRNA - small interfering ribonucleic acid

shRNA – small hairpin RNA

SNP – single nucleotide polymorphism

ssDNA – single stranded DNA

UFB – ultra-fine bridge

UV – ultra-violet

Chapter 1. Introduction

Intra-tumour heterogeneity is observed in both solid tumours and haematopoietic malignancies, contributing to the development of drug resistance and metastases (Gerlinger and Swanton, 2010, Ding et al., 2012, Wu et al., 2012, Su et al., 2012, Anderson et al., 2011, Gerlinger et al., 2012, Snuderl et al., 2011). Intra-tumour heterogeneity provides a substrate to overcome selection pressures encountered during tumour growth, and may furthermore decrease the efficacy of personalised cancer medicine approaches that use single biopsies to inform treatment choice (Gerlinger and Swanton, 2010, Yap et al., 2012).

One mechanism through which intra-tumour heterogeneity may be generated is through chromosomal instability (CIN). CIN describes an elevated rate of change in chromosome number and structure, generating profound genetic variation between cells that may foster continual evolution and adaptation in the face of new selection pressures. CIN is observed in the majority of solid tumours (Lengauer et al., 1997, Thompson et al., 2010) and is associated with both poor prognosis and with intrinsic and acquired drug resistance (McGranahan et al., 2012, Lee et al., 2011, Swanton et al., 2009, McClelland et al., 2009, Duesberg et al., 2000).

CIN+ cancer cells exhibit segregation defects during anaphase (Thompson and Compton, 2008). CIN may be caused by various defects, including improper attachments of chromosomes during mitosis, faulty DNA repair and DNA replication stress (Thompson and Compton, 2011b). Structural and numerical chromosome aberrations are usually observed together in tumours (Demirhan et al., 2010, Lengauer et al., 1998, Beroukhim et al., 2010) and mechanisms that may explain the initiation of both numerical and structural CIN have begun to be elucidated (Janssen et al., 2011, Crasta et al., 2012, Pampalona et al., 2010b, Ichijima et al., 2010). However, which of the possible mechanisms that generate instability are most prevalent in CIN+ cancer cells has not been determined. Furthermore, it is unclear whether there are any consistent genomic changes that may determine the patterns of CIN observed. Refining our understanding of mechanisms contributing to numerical and structural CIN in tumours may facilitate development of rational therapeutic approaches for this high-risk patient subgroup.

1.1 Chromosomal instability and aneuploidy in cancer

CIN results in aneuploidy, a state of abnormal chromosomal number widely observed in cancers. Aneuploidy, however, is not always associated with CIN. For example, some leukaemias and neuroblastomas exhibit a stable aneuploid karyotype and patients have a favourable prognosis relative to those with CIN+ tumours (Paulsson and Johansson, 2009, Kaneko and Knudson, 2000). The distinction between the dynamic process of CIN and the state of aneuploidy is therefore important in considering the impact of CIN upon prognosis (Roylance et al., 2011, Birkbak et al., 2011, McGranahan et al., 2012). Nevertheless, in tumour specimens, measuring aneuploidy remains the most widespread and robust method for identifying tumours that are likely to be chromosomally unstable.

1.1.1 Measuring CIN in tumour specimens

Tumour CIN status is not currently assessed in the clinical setting, although existing clinical parameters, like tumour grade, correlate with CIN (Endesfelder et al., 2011, Smid et al., 2011, Dunn et al., 2011). Measuring CIN requires assessment of cell-to-cell variability in chromosome complement, as well as an assessment of the rate at which these chromosomal changes occur.

Due to its dynamic nature, direct methods for determining CIN from fixed tumour tissue are currently limited to the assessment of the frequency of anaphase segregation errors. This method has been used to assess CIN status in diffuse large B-cell lymphoma specimens but is not amenable to less proliferative or more morphologically disordered tumours (Bakhoum et al., 2011). An alternative method for assessing CIN in tumour specimens measures cell-to-cell variability in chromosome number by fluorescence *in-situ* hybridization (FISH), using centromere-specific probes (Roylance et al., 2011, Farabegoli et al., 2001, Lingle et al., 2002). This allows the assessment of the chromosomal state of hundreds of cells and distinguishes between stable and unstable aneuploidy (CIN).

However, the most widely used tools for assessing CIN status are DNA image and flow cytometry, which measure cellular DNA content (McGranahan et al., 2012, Darzynkiewicz et al., 2010). CIN status can be inferred from aneuploidy together with heterogeneity in tumour cell DNA content (Kronenwett et al., 2004, Habermann et al.,

2009). The ability of cytometry techniques to identify CIN+ tumours is supported by the observation that anaphase segregation errors were only observed in sections from those tumours defined as CIN by cytometry, in a small cohort of sarcomas, colorectal and pancreatic carcinomas (Montgomery et al., 2003).

Alternative methods to measure CIN sample an aggregated population of cells. These techniques provide a measure of chromosome complexity or of a CIN-associated gene-expression signature across the population, rather than sampling cell-to-cell heterogeneity. A range of methods including whole genome sequencing, spectral karyotyping and single-nucleotide polymorphism arrays (SNP arrays) can be used to assess cancer karyotypes and genomic rearrangements. An advantage of these measures, relative to centromeric FISH on tissue sections, is the ability to capture both structural and numerical chromosome complexity. Gene expression signatures and copy-number-based scores correlate well with direct measures of CIN (Birkbak et al., 2011) and quantifying the proportion of the genome that shows copy number aberrations has allowed the definition of genome integrity indices and CIN scores that have prognostic value (Chin et al., 2007, Smid et al., 2011, Birkbak et al., 2011, Carter et al., 2006, Mettu et al., 2010).

1.1.2 CIN and poor prognosis in cancer

CIN is associated with poor patient outcome in multiple cancer types, including lung, breast and colon cancer, summarised in Table 1.1. This association may be driven by intra-tumour heterogeneity, as CIN results in genetic and phenotypic variation across the cell population, facilitating selection in the face of environmental and stromal pressures (Gerlinger and Swanton, 2010, Cahill et al., 1999, McClelland et al., 2009, McGranahan et al., 2012). Evolutionary and murine models suggest that CIN might be selected for by increasing the rate at which tumour suppressor genes are lost from the genome (Baker et al., 2009, Komarova, 2004).

Given the heterogeneity that arises as a consequence of CIN, and the propensity for selection and adaptation, it is likely that the relationship of CIN with poor prognosis could ultimately be explained by the emergence of drug resistance and an increased

Cancer Type	Method of measuring CIN	IN associated with	Additional details	Reference
Lung cancer (NSCLC)	FISH (n=63)	Poor prognosis (OS & DFS)		(Choi et al., 2009)
	FISH (n=50)	Poor prognosis (OS)		(Nakamura et al., 2003)
	12-gene signature(n=647)	Poor prognosis (OS)	Multiple datasets	(Mettu et al., 2010)
	CIN70 signature (n=62)	Poor clinical outcome		(Carter et al., 2006)
Breast cancer	SSI (Image cytometry) (n=890)	Poor prognosis (OS)	CIN measured within diploid, tetraploid and aneuploid classified tumours	(Kronenwett et al., 2004)
	SNP array (n=313)	Poor prognosis (MFS)	Significant in ER positive, luminal B and her2/neu subtypes, (not in ER negative patients)	(Smid et al., 2011)
	12-gene signature (n=469)	Poor prognosis (DFS & RFS)	Multiple datasets	(Habermann et al., 2009)
	CIN70 signature (n=1866)	Poor clinical outcome	Multiple datasets	(Carter et al., 2006)
	FISH (n=31)	Lymph-node metastasis and ER negativity.		(Takami et al., 2001)
Endocrine pancreatic tumors	CGH (n=62)	Metastasis		(Jonkers et al., 2005)
Colon cancer	12 gene genomic instability signature (n=92)	Recurrence of colon cancer	Multiple datasets	(Mettu et al., 2010)
	Flow / image cytometry (n = 10 126)	Poor prognosis.	Meta-analysis	(Walther et al., 2008)
Ovarian cancer	12-gene genomic instability signature(n=124)	Poor prognosis (RFS)		(Mettu et al., 2010)
Endometrial cancer	SNP array (n=31)	Poor prognosis (OS)		(Murayama-Hosokawa et al., 2010)
Diffuse Large B-cell Lymphoma	Anaphase segregation errors (n=54)	Poor prognosis (RFS)		(Bakhoum et al., 2011)

Table 1.1 CIN is associated with poor prognosis in multiple cancer types
Adapted from (McGranahan et al., 2012). Abbreviations: NSCLC, non-small cell lung cancer; SCC, squamous cell carcinoma; FISH, fluorescence *in situ* hybridisation; SSI, stem line scatter index; CGH, comparative genome hybridisation; SNP, single-nucleotide polymorphism, OS, overall survival; DFS, disease-free survival; MFS, metastasis-free survival; RFS, relapse free survival.

capacity to metastasize to distant sites (Lee et al., 2011, Swanton et al., 2009, Duesberg et al., 2000, Li et al., 2005, Takami et al., 2001, Jonkers et al., 2005). Consistent with this hypothesis, mouse models suggest that CIN promotes early tumour relapse (Sotillo et al., 2010), and CIN+ cancer cell lines acquire multi-drug resistance at an elevated rate compared to chromosomally stable, diploid cells (Duesberg et al., 2000). CIN was also associated with intrinsic taxane resistance in both cancer cell lines and in a small clinical trial cohort of taxane-treated patients with ovarian cancer (Swanton et al., 2009). Our laboratory has previously shown that CIN+ colorectal cancer cells are intrinsically multi-drug resistant relative to CIN- colorectal cancer cell lines and a meta-analysis of tumour drug response in colorectal cancer supported a relationship between tumour CIN status and drug resistance (Lee et al., 2011).

An alternative, although not mutually exclusive, hypothesis explaining the relationship between CIN and drug resistance, is the existence of a CIN survival state (McClelland et al., 2009, Lee et al., 2011). Adaptations required to avoid cell death in response to continual genome remodelling might render cells inherently resistant to therapy, particularly if in the therapy in someway mimics the mechanisms of genome instability of the cancer cell. This intrinsic resistance would also facilitate the eventual outgrowth of an optimally resistant clone during the course of drug treatment. Intrinsic drug resistance could therefore be a feature of cells with elevated levels of CIN, as opposed to being purely a consequence of the intra-tumour heterogeneity promoted by CIN (Lee et al., 2011).

Another implication of a CIN survival state is that there is a limit beyond which CIN cannot be tolerated. In a mouse model of CIN, tumours were actually suppressed in tissues with a higher underlying level of aneuploidy (Weaver et al., 2007) and furthermore, massive chromosome missegregation (for example during multipolar anaphases or after mitotic checkpoint ablation) results in cell lethality (Kops et al., 2004, Ganem et al., 2009). Consistent with these observations our laboratory has found that patients whose tumours displayed high levels of CIN had an improved long-term survival relative to those with intermediate levels of CIN (Birkbak et al., 2011, Roylance et al., 2011). This may reflect a deleterious effect of high levels of CIN on cell viability, rendering tumour cells more susceptible to chemotherapy.

Taken together, these studies suggest a central role for CIN in determining patient outcome: increased levels of CIN might facilitate Darwinian adaptation and selection, thus having a negative impact on prognosis. Paradoxically, extreme CIN may be associated with improved outcome. This association highlights the clinical relevance of CIN in cancer and suggests that CIN status could potentially be exploited in the clinical setting, both therapeutically and as a prognostic marker.

1.2 Mechanisms of CIN

CIN is often subdivided into two categories: numerical and structural. Numerical CIN refers to gains and losses of whole chromosomes. Structural CIN refers to a wide range of changes in chromosome structure, including translocations, deletions, amplifications and inversions (Thompson and Compton, 2011b, Gisselsson, 2008). While often considered separately from a mechanistic point of view, numerical and structural CIN are almost always observed together in tumours (Venkitaraman, 2007, Abdel-Rahman et al., 2001, Gaasenbeek et al., 2006, Demirhan et al., 2010). These observations have led to suggestions that the two forms of CIN may be governed by unified mechanisms (Venkitaraman, 2007), and recent evidence, discussed below, has lent further support to this hypothesis (Pampalona et al., 2010b, Crasta et al., 2012, Janssen et al., 2011, Stewenius et al., 2005).

Cytogenetic analysis of a variety of CIN+ cell lines has revealed an increased rate of chromosome non-disjunction at anaphase relative to CIN- cell lines (Lengauer et al., 1997, Roschke et al., 2003, Roschke et al., 2002, Thompson and Compton, 2008, Klein et al., 2006). CIN+ cells also display elevated frequencies of anaphase segregation errors relative to CIN- cells (Ganem et al., 2009, Silkworth et al., 2009, Thompson and Compton, 2008). More recently, anaphase segregation errors have been quantified directly in tumour specimens (Bakhoum et al., 2011). These anaphase errors are a likely explanation for inaccurate partitioning of chromosomes into daughter cells in CIN+ cell lines and tumours.

1.2.1 Classifying anaphase chromosome segregation errors

Anaphase segregation errors can be grouped according to whether they are more likely to have arisen directly as a consequence of mitotic dysfunction, or indirectly due to defects in interphase (Gisselsson, 2008, Thompson and Compton, 2011b, Acilan et al., 2007). As illustrated in Figure 1.1, the majority of segregation errors can be classified as being lagging chromosomes, acentric chromosomes or anaphase bridges. The morphological criteria for defining these different classes of segregation errors are described below, followed by a more detailed examination of possible mechanisms causing chromosome missegregation.

Mitotic defects converge upon the formation of improper attachments of chromosomes to the mitotic spindle, which results in the generation of lagging chromosomes (Thompson et al., 2010, Bakhoum et al., 2009b, Bakhoum et al., 2009a, Cahill et al., 1998, Ganem et al., 2009, Silkworth et al., 2009). These chromosomes are

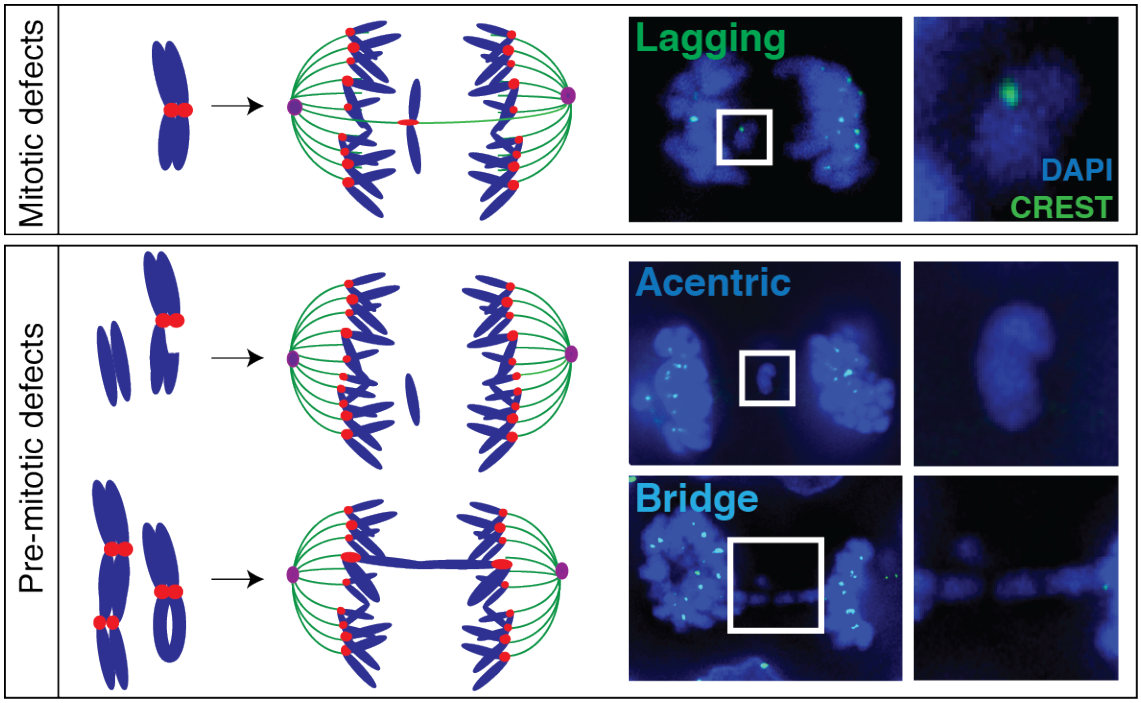

Figure 1.1 Classification of anaphase segregation errors
Schematic illustrating different types of anaphase segregation error. Mitotic defects cause lagging chromosomes, while pre-mitotic defects result in acentric chromosomes and anaphase bridges (Gisselsson, 2008). Right hand side: Images of SW1116 cells stained with DAPI (blue – to mark DNA) and CREST patient serum, which marks centromeres (green)

spatially separated from the segregating chromosomes, and stain positively for centromeric DNA, and centromere/kinetochore components (Gisselsson, 2008, Thompson and Compton, 2011a)(see Figure 1.1). Mitotic dysfunction may also result in chromosome segregation errors that do not lag at anaphase, which can only be identified using cytogenetics approaches. However, these are thought to occur at very low frequencies (Thompson and Compton, 2011a, Gisselsson et al., 2008, Jin et al., 2007). More extreme chromosome segregation defects can arise as a consequence of multipolar division, which usually occurs as a consequence of the presence of extra-centrioles (Gisselsson et al., 2008, Ganem et al., 2009, Silkworth et al., 2009). However, in the cell lines studied so far, multipolar divisions appear to generate pre-dominantly non-viable cells (Ganem et al., 2009, Stewenius et al., 2005), suggesting that they are unlikely to be a major cause of CIN. It should also be noted that lagging chromosomes can be generated as a consequence of pre-mitotic defects in chromosome assembly, for example defective sister chromatid decatenation or failure to establish adequate sister chromatid cohesion (Baxter and Diffley, 2008, Wang et al., 2008, Chan et al., 2007, Solomon et al., 2011, Barber et al., 2008, Cimini et al., 1997).

In contrast to mitotic dysfunction, pre-mitotic defects in genome duplication, such as defects in DNA replication or repair, may result in the generation of structurally abnormal chromosomes, visible in anaphase cells as i) anaphase bridges and ii) acentric chromosome fragments (see Figure 1.1)(Gisselsson, 2008, Thompson and Compton, 2011b). Anaphase bridges, which extend fully between the segregating chromosome masses, are generated through fusion of either sister chromatids, or of two chromosomes, to form dicentric or multivalent chromosomes. Chromatid and chromosome fusion may occur following DNA damage, inappropriate recombination or telomere uncapping (Pampalona et al., 2010a, Pampalona et al., 2010b, Gisselsson, 2008, Acilan et al., 2007, Hsiao and Smith, 2009, Xia et al., 2001).

Acentric chromosome fragments do not stain for centromere proteins. These fragments segregate at random, or are lost during anaphase, due to an inability to attach to the mitotic spindle, and are generated as a consequence of DNA damage (Thompson and Compton, 2011b, Gisselsson, 2008, Pauletti et al., 1990, Kawabata et al., 2011). Studies have indicated that acentric chromosomes may segregate by being tethered to the ends of mitotic chromosomes (Kanda and Wahl, 2000, Kanda et al., 2001, Royou et

al., 2010). However, the direction of the segregation of these acentrics is random, and furthermore, due to the lack of a centromere, there is no mechanism to separate replicated sister DNA molecules, which will result in segmental copy number gains and losses.

Various mechanisms have been identified as possible causes of chromosome missegregation. These either affect the accuracy of chromosome attachment during mitosis (mitotic causes of chromosome segregation errors) or destabilise the chromosomes themselves through compromised structural integrity or chromosome assembly (pre-mitotic causes of chromosome segregation errors). Mitotic causes of chromosome missegregation result primarily in lagging chromosomes, while the majority of segregation errors caused by pre-mitotic defects will be acentric or dicentric chromosomes, as illustrated in Figure 1.1. Both mitotic and pre-mitotic defects that can cause CIN will now be considered in more detail.

1.3 Mitotic causes of chromosome missegregation

During a normal mitosis, chromosome attachment to the mitotic spindle is tightly regulated to ensure equal partitioning of chromosomes into daughter cells. The stages of mitosis are illustrated in Figure 1.2. Two main pathways monitor kinetochore-microtubule attachments: 1) the mitotic checkpoint, which signals constitutively until all kinetochores are attached, preventing anaphase onset; and 2) the error correction machinery, which depolymerises microtubules at improperly attached kinetochores. Once all chromosomes are correctly attached in a bi-oriented fashion (amphitelic attachment – see Figure 1.3), the mitotic checkpoint is satisfied, sister chromatid cohesion is cleaved and anaphase onset ensues. Chromosome segregation errors stem from failure to correct or detect improper kinetochore-microtubule attachments, which can arise through defects in the pathways monitoring kinetochore-microtubule attachments. Alternatively, saturation of the capacity to correct improper attachments prior to anaphase onset may precipitate chromosome missegregation.

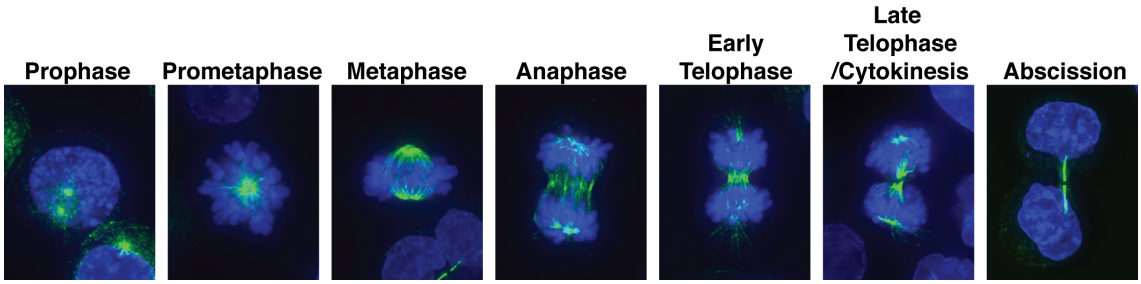

Figure 1.2 The stages of mitosis
Images of HCT-116 cells in the different stages of mitosis (DNA is stained with DAPI in blue and the mitotic spindle with anti-tubulin antibodies in green). Following nuclear envelope breakdown at the end of prophase, spindle microtubules are nucleated from the centrosomes and attach to chromosomes via their microtubule-binding components, the kinetochores. By the end of prometaphase, a bipolar spindle is formed and all chromosomes are aligned at the middle of the cell, at which point the cell is in metaphase. Chromosomes segregate towards the spindle poles at anaphase and the cytokinesis furrow begins to ingress during telophase, during which the nuclear envelope reforms, before cytokinesis completes and abscission occurs, dividing the cell into two genetically identical daughter cells. An 'abscission checkpoint', analogous to the yeast 'no-cut' pathway, may operate at this stage in cell division.

1.4 The mitotic checkpoint

The mitotic checkpoint is fundamental in ensuring the fidelity of chromosome segregation, halting cell division until every kinetochore is attached to the spindle (Rieder et al., 1995). This arrest is achieved through preventing the degradation of two proteins (securin and cyclin B) by the anaphase-promoting complex (APC/C) ubiquitin ligase (Musacchio and Salmon, 2007) (see Figure 1.3). Securin inhibits the enzyme separase, which is responsible for breaking down the cohesin complexes that hold sister chromatids together, while cyclin B is the activating subunit of the mitotic cyclin-dependent kinase CDK1, the inactivation of which leads to anaphase onset and mitotic exit. APC/C inhibition occurs through the negative regulation of CDC20, a co-activator and substrate recruitment subunit of the APC/C (Chao et al., 2012). When the mitotic checkpoint is satisfied, CDC20 inhibition is relieved and the APC/C ubiquitylates securin and cyclin B, promoting their degradation and permitting progress through mitosis.

Inactivation of CDC20 is achieved by its sequestration in a 'mitotic checkpoint complex' with the mitotic checkpoint proteins MAD2 and BUBR1, which binds and inhibits the APC/C (Sudakin et al., 2001, Herzog et al., 2009). MAD2 localises to

kinetochores that are not bound by microtubules, and induces a conformational switch in cytosolic MAD2 that facilitates its binding to CDC20 (Musacchio and Salmon, 2007, De Antoni et al., 2005, Kulukian et al., 2009, Santaguida et al., 2010). CDC20-MAD2 is then able to bind BUBR1 to form a complex competent to inhibit the APC/C (Chao et al., 2012, Burton and Solomon, 2007). One a kinetochore is attached, MAD2 is shuttled away from the kinetochore along microtubules (Howell et al., 2001), and once all kinetochores are attached, the kinetochore bound MAD2 template required for checkpoint activity is no longer available, and the checkpoint is silenced.

The signal from a single unattached kinetochore is sufficient to prevent anaphase onset (Rieder et al., 1995) and a number of proteins not described here are involved in the amplification of the checkpoint signal from single or small numbers of unattached kinetochores (Musacchio and Salmon, 2007). In addition there are multiple regulators of the mitotic checkpoint involved in facilitating kinetochore recruitment of checkpoint components, for example MPS1, BUB1, CENP-E, Aurora kinase B, the ROD/ZWILCH/ZWINT complex and NDC80/HEC1 (Musacchio and Salmon, 2007). The mitotic checkpoint complex is also antagonised by $p31^{comet}$, which competes with BUBR1 to prevent formation of the mitotic checkpoint complex (Chao et al., 2012), and the APC/C specific ubiquitin-conjugating enzyme UBCH10, which ubiquitylates CDC20 to promote dissociation of MAD2 and BUBR1. UBCH10 activity is counteracted by USP44, a de-ubiquitinating enzyme (Reddy et al., 2007).

1.4.1 Mitotic checkpoint defects and CIN

Defects in mitotic checkpoint function have been linked to CIN in a number of studies (Cahill et al., 1998, Jelluma et al., 2008, Jacquemont et al., 2002, Hanks et al., 2004).

Heterozygous mutations in the checkpoint gene *BUB1* were associated with weakened checkpoint function in CIN+ colorectal cancer (CRC) cell lines, and expressing the mutant BUB1 in CIN- CRC lines revealed that the mutation acted in a dominant negative fashion. The same study also described rare mutations in *BUB1B* (which encodes BUBR1)(Cahill et al., 1998). This study initiated further investigations into mitotic checkpoint function in CIN+ cancers. Later work from the same laboratory found mutations in genes encoding the ZW10, ROD and ZWILCH proteins, which

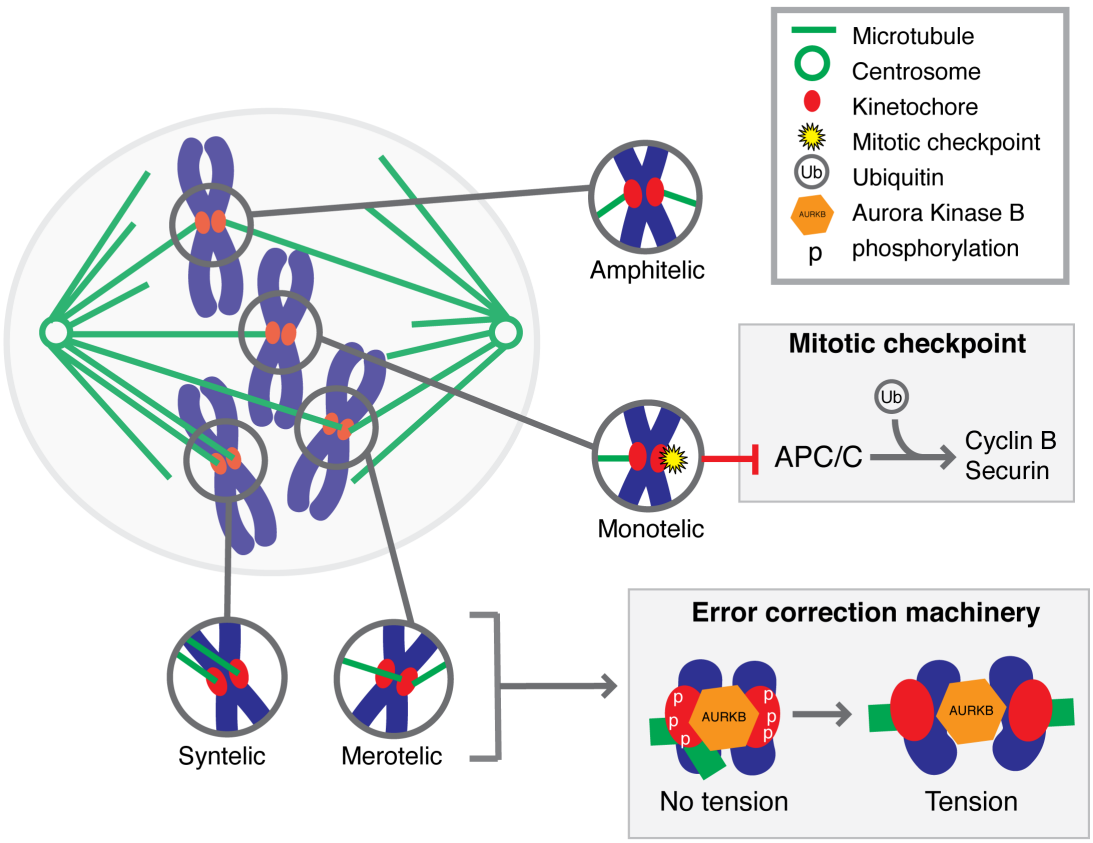

Figure 1.3 Monitoring kinetochore-microtubule attachments before anaphase
Spindle microtubules are nucleated from the centrosome and attach stochastically to kinetochores. Four different types of attachment are shown: **amphitelic attachment** (both kinetochores attached to microtubules originating from opposite spindle poles), **monotelic attachment** (only one sister kinetochore attached to spindle, resulting in sustained activation of the mitotic checkpoint, shown to the right), **syntelic attachment** (both kinetochores attached to the same pole) and **merotelic attachment** (one kinetochore attached to both poles). Syntelic and merotelic attachments are corrected by the error correction machinery, a schematic of which is shown: when sister kinetochores are not under tension, AURKB phosphorylates substrates on the outer kinetochore, which in turn depolymerise microtubules to remove the incorrect attachment.

localise to the kinetochore and function in the mitotic checkpoint by anchoring the MAD2 receptor MAD1 to the kinetochore (Wang et al., 2004b, Kops et al., 2005). The checkpoint was further implicated in aneuploidy and CIN when biallelic germline mutations in *BUB1B* were found in patients with Mosiac Variegated Aneuploidy, who have a high risk of malignancy (Hanks et al., 2004).

Nevertheless, the role of the mitotic checkpoint in driving CIN remains controversial. All CIN+ cell lines tested so far, excluding those with *BUB1* mutations,

have been demonstrated to mount a robust checkpoint response to Nocodazole treatment (which depolymerises microtubules and chronically activates the checkpoint) and other anti-mitotic agents (Tighe et al., 2001, Gascoigne and Taylor, 2008). In addition, ablation of the mitotic checkpoint has been shown on a number of occasions to cause lethality (Kops et al., 2004, Baker et al., 2004, Wang et al., 2004a), suggesting that, similar to multipolar divisions, this is unlikely to be a common route to CIN (Ganem et al., 2009, Stewenius et al., 2005).

The profound compromise to viability observed following mitotic checkpoint ablation has given rise to the idea that the checkpoint may be weakened rather than completely abrogated in CIN+ cancer cells. Overexpression of the checkpoint antagonistic ubiquitin ligase *UBCH10* results in chromosome segregation errors, aneuploidy and an increased rate of tumour formation in transgenic mouse models, with only a mild checkpoint defect (van Ree et al., 2010). *UBCH10* is expressed at high levels in some cancers and could represent a mechanism by which the SAC may be aberrantly regulated, allowing chromosome missegregation and the development of CIN (Berlingieri et al., 2007, Wagner et al., 2004, van Ree et al., 2010). However, by live-cell imaging, three CIN+ cell lines never exhibited premature anaphase (anaphase onset before chromosome congression)(Gascoigne and Taylor, 2008). This indicates that checkpoint function in these cell lines is likely to be sufficient to detect even a single unattached kinetochore, and does not support the hypothesis of weakened checkpoint function in CIN+ cells.

Hence defects in the mitotic checkpoint can cause CIN, but it appears that this may be a relatively infrequent mechanism of CIN in cancer cells. A more exhaustive analysis of checkpoint function in CIN+ cell lines is required.

1.5 Correcting improper kinetochore-microtubule attachments

Incorrect attachments may occur that satisfy the mitotic checkpoint (because all kinetochores are bound by microtubules) but which require correction prior to anaphase onset. In syntelic attachments both sister kinetochores are attached to the same spindle pole, while in merotelic attachments one kinetochore is attached simultaneously to both poles (Cimini et al., 2001)(see Figure 1.3). Both syntelic and merotelic attachments

occur frequently during the early stages of a normal mitosis, but are corrected by the error correction machinery prior to anaphase onset (Cimini et al., 2003, Thompson and Compton, 2011a). The central regulator of the error correction machinery is Aurora kinase B, which localises to the centromere (Cimini, 2007, Hauf et al., 2003). In the absence of sister kinetochore bi-orientation, the lack of tension across the centromere allows Aurora kinase B to access and phosphorylate its outer kinetochore substrates (see Figure 1.3) (Liu et al., 2009). These are principally microtubule depolymerases such as MCAK, which depolymerise the microtubules attached to the kinetochore, generating an unattached kinetochore that signals to the mitotic checkpoint and thus delays anaphase onset. Once amphitelic attachment is achieved, centromere stretch prevents Aurora B from accessing its substrates, and the activity of its counteracting phosphatase (PP1) dominates at the outer kinetochore, stabilising the kinetochore-microtubule attachment (Figure 1.3) (Liu et al., 2010). Depletion of components of the error correction machinery, or inhibition of Aurora kinase B, increases the frequency of both merotely and syntely, indicating that this pathway usually corrects these attachments (Hauf et al., 2003, Lens et al., 2003, Bakhoum et al., 2009b, Knowlton et al., 2006).

In situations where merotelic and syntelic attachments are generated at high frequencies, these attachments go uncorrected. In addition, merotelic attachments may persist into anaphase uncorrected if attachment of the sister kinetochore generates sufficient tension across the centromere to inactivate Aurora B activity. Merotelic attachments have been described in CIN+ cell lines, although the proportion of segregation errors arising due to merotely has not been quantified (Thompson and Compton, 2008, Ganem et al., 2009, Silkworth et al., 2009, Cimini et al., 2001). Proposed causes of merotelic attachments in CIN+ cells include abnormal spindle geometry, and hyperstable microtubules, discussed below.

1.5.1 Abnormal spindle geometry promotes improper kinetochore-microtubule attachments

Both transient mono- and multipolar spindle morphology have been demonstrated to elevate improper kinetochore-microtubule attachments, resulting in elevated frequencies of lagging chromosomes at anaphase (Silkworth et al., 2012, Silkworth et al., 2009, Ganem et al., 2009).

In normal cells, centrosome separation to opposite poles to form a bipolar spindle can occur either before or after nuclear envelope breakdown (Toso et al., 2009)(see Figure 1.4). If centrosome separation occurs after nuclear envelope breakdown, then spindle formation goes through a transient monopolar stage, which may elevate the frequency of improper attachments and chromosome segregation errors (McClelland et al., 2009). Evidence supporting this hypothesis has recently been reported in rat kangaroo cells (PtK1 cells) (Silkworth et al., 2012) and in HeLa cells (Andrew McAinsh, personal communication), although the increase in segregation errors in cells passing through a monopolar spindle is small. In addition, drug washout strategies that transiently arrest cells with monopolar spindles result in increased frequencies of lagging chromosomes (Mailhes et al., 2004, Thompson and Compton, 2008). It is as yet unknown whether transient monopolar spindle morphology is a cause of chromosome segregation errors in CIN+ cells.

In the presence of extra centrioles, cells may pass through a transient multipolar spindle during prometaphase, with extra spindle poles eventually coalescing to form a pseudo-bipolar spindle prior to anaphase onset, as illustrated in Figure 1.4 (Kwon et al., 2008, Ganem et al., 2009). It is proposed that spindle pole coalescence generates improper attachments and, subsequently, chromosome segregation errors (Ganem et al., 2009, Silkworth et al., 2009). In a panel of seven CIN+ cell lines of mixed tissue types, higher frequencies of segregation errors were observed in bipolar anaphase cells that had extra centrioles, than in anaphases with a normal centriole number. These anaphase cells may have passed through a multipolar spindle intermediate during prometaphase, or alternatively may have clustered the extra centrioles prior to mitosis (Ganem et al., 2009). This mechanism could explain the observation that centriole amplification has frequently been associated with aneuploidy and CIN in tumours, (Lingle et al., 2002, Zhou et al., 1998) and cell lines (Ghadimi et al., 2000, Ganem et al., 2009, Silkworth et al., 2009).

However, the observation of elevated segregation errors in anaphases with extra-centrioles could be coincidental, as defects in DNA replication or repair may simultaneously deregulate centriole duplication and generate structurally abnormal chromosomes that missegregate during anaphase (Nigg and Stearns, 2011, Prosser et al., 2009, McDermott et al., 2006, Inanc et al., 2010). Direct live-cell analysis linking

multipolar spindle intermediates with chromosome segregation errors in mitosis is still lacking; it is not known how frequently multipolar spindles cluster to form bipolar anaphases, and the fate of cells arising from these aberrant mitoses is also yet to be examined. Finally, the overall contribution of transient multipolar spindles to the segregation errors observed in CIN+ cell lines remains to be evaluated.

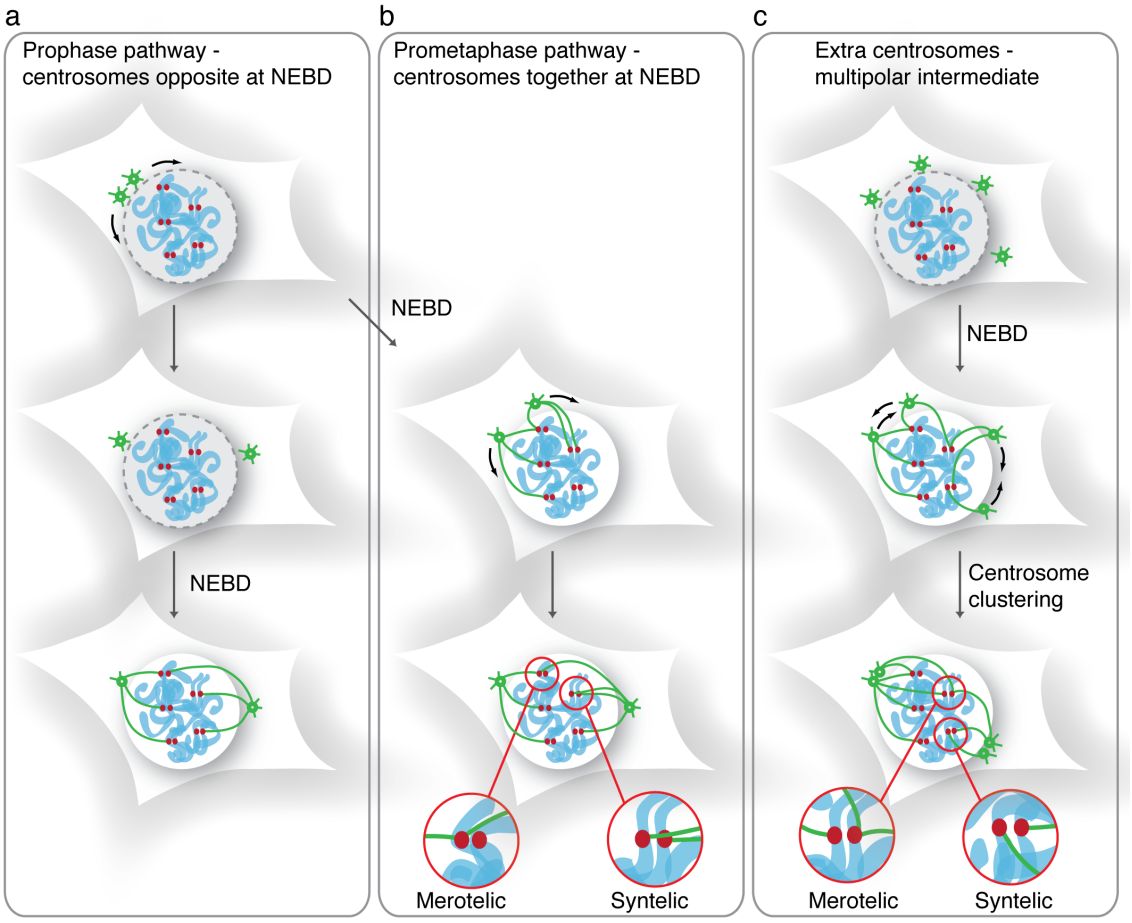

Figure 1.4 Abnormal spindle geometry results in improper kinetochore microtubule attachments
Reproduced from (McClelland et al., 2009) a) centrioles are separated prior to spindle formation – no monopolar intermediate b) centrioles are together at spindle formation, resulting in a transient monopolar spindle stage and a small elevation in the frequency of improper attachments that persist to anaphase c) extra centrioles result in the formation of a multipolar spindle. Extra spindle poles are then clustered to form a pseudo-bipolar spindle, with concurrent formation of syntelic and merotelic attachments.

1.5.2 Hyper-stable microtubules and defective error correction

Hyper-stability of spindle microtubules has also been linked to the generation of improper attachments and segregation errors in CIN+ cancer cells (Bakhoum et al., 2009a, Bakhoum et al., 2009b). Silencing the microtubule depolymerases MCAK and KIF2B results in the persistence of improper kinetochore-microtubule attachments through an inability to depolymerise the erroneously attached microtubules, leading to lagging chromosomes at anaphase (Bakhoum et al., 2009b). Overexpression of KIF2B or MCAK in CIN+ U2OS osteosarcoma and MCF7 breast cancer cells reduced both the frequency of lagging chromosomes and modal deviation in chromosome number across the cell population, indicating that microtubules might be hyper-stable in CIN+ cells (Bakhoum et al., 2009b). A further study by the same group examined microtubule dynamics directly in CIN+ cells (Bakhoum et al., 2009a). By expressing tubulin tagged with photo-activatable green fluorescent protein (GFP), and examining fluorescence dissipation after photo-activation, the authors demonstrated increased microtubule stability in either prometaphase or metaphase (measured as a longer half-life of kinetochore microtubules) in five CIN+ cell lines relative to the immortalised non-transformed epithelial cell line RPE-1-hTERT. However, the magnitude of this effect was highly variable between cell lines, and it remains possible that these results could be explained by differences in the cell type of origin of these cell lines; the control cell line (RPE-1) was the only epithelial cell line examined, while the other cell lines were of neuronal or mesenchymal origins. The mechanism through which microtubules may be hyper-stabilised in these CIN+ cell lines is also not known.

1.6 Mitotic causes of chromosome missegregation - summary

In summary, the failure to establish correct kinetochore-microtubule attachments during mitosis results in lagging chromosomes at anaphase. Mitotic defects generating improperly attached chromosomes that are suggested to contribute to CIN include defects in the mitotic checkpoint, abnormal spindle geometry and hyper-stable microtubules. Studies depleting or inhibiting components of the error correction machinery suggest that mutations or altered expression of components of the error

correction machinery might also lead to mitotic dysfunction, although this has not been reported in CIN+ cell lines or tumours. In general, studies examining CIN+ cell lines have been conducted in small numbers of cell lines of heterogeneous tissue types and genetic backgrounds, and hence the findings of these studies should not be extrapolated to all CIN+ cancer cells.

1.7 Pre-mitotic mechanisms of CIN

As described in section 1.2.1, structurally abnormal chromosomes generated prior to mitosis may cause anaphase segregation errors. During a normal cell cycle, DNA is replicated, and sister chromatid cohesion established, during S-phase. DNA is then condensed into chromosomes, and any persistent DNA catenation resolved both at the G2-M transition, and at metaphase, prior to chromosome segregation at anaphase. Cohesin is removed from chromosome arms during prometaphase, and is cleaved at the centromere following satisfaction of the mitotic checkpoint.

Defects that directly affect DNA structural integrity may generate acentric chromosomes and anaphase bridges (Gisselsson, 2008, Richardson and Jasin, 2000). In addition, disruption of chromosome assembly prior to mitosis may also cause segregation errors. For example, defects in chromosome condensation, sister chromatid cohesion or the resolution of sister chromatid catenation may result in the generation of anaphase bridges and lagging chromosomes (independently of improper kinetochore-microtubule attachment) (Solomon et al., 2011, Samoshkin et al., 2009, Cimini et al., 1997).

Alterations in chromosome structure that affect the accuracy of chromosome segregation most often result from the generation of double-strand breaks (DSBs), followed by either aberrant DNA repair, generating chromosome fusions, or failure to repair the damage, generating acentric chromosome fragments (Thompson and Compton, 2011b, Gisselsson, 2008), illustrated in Figure 1.5 a-c. In addition, it appears that loci under replication stress may rupture to form chromosome breaks during chromosome condensation at the onset of mitosis (Lukas et al., 2011a, Kawabata et al., 2011, Chan et al., 2009). DSBs are particularly toxic (Kastan and Bartek, 2004) and can result in both gene conversion and gross genome rearrangements (Richardson and Jasin,

2000). In addition, chromosome translocations and acentric chromosomes may be generated through recombination, both between chromosomes and intra-chromosomally, illustrated in Figure 1.5 d and e (Colnaghi et al., 2011, Hastings et al., 2009, Liu et al., 2011, Branzei, 2011). Recombination between chromosomes may be a feature of DSB repair (see section 1.8.2) or the restart of stalled replication forks (see section 1.8.4). These structurally abnormal chromosomes are not accurately segregated; acentric chromosomes cannot attach to the mitotic spindle, while dicentric chromosomes are likely to form improper attachments that result in anaphase bridges (see Figure 1.5f). Chromatid fusions cannot be fully separated and therefore also result in anaphase bridging (Figure 1.5b) (Gisselsson, 2008, Pampalona et al., 2010b, Pampalona et al., 2010a, Acilan et al., 2007).

The following section is an overview of the mechanisms that may generate structurally abnormal chromosomes, or which may disrupt chromosome assembly. Defects that may generate chromosomal abnormalities, through a faulty DNA damage response, or through elevated generation of DNA damage, will be considered, with a focus on the role of DNA replication stress. The contribution to chromosome missegregation of abnormal chromosome assembly as a consequence of cohesin defects will also be discussed.

1.8 DNA damage and structural chromosome abnormalities

The genome is susceptible to an array of different forms of DNA damage. In order to deal with the plethora of sources and types of DNA damage, all living organisms employ a complex network of pathways to maintain genome stability, which function to repair different types of DNA damage and arrest the cell cycle to permit repair to take place. Defects in cellular responses to DNA damage have long been associated with cancer, due to the existence of cancer predisposition syndromes caused by mutations in key components of the DNA damage response (German, 1980). Many of these syndromes are associated with gross chromosomal aberrations. In addition, activation of the DNA damage response and somatic mutations in DNA damage response components are observed in a high proportion of tumours, alongside complex structural karyotypic rearrangements.

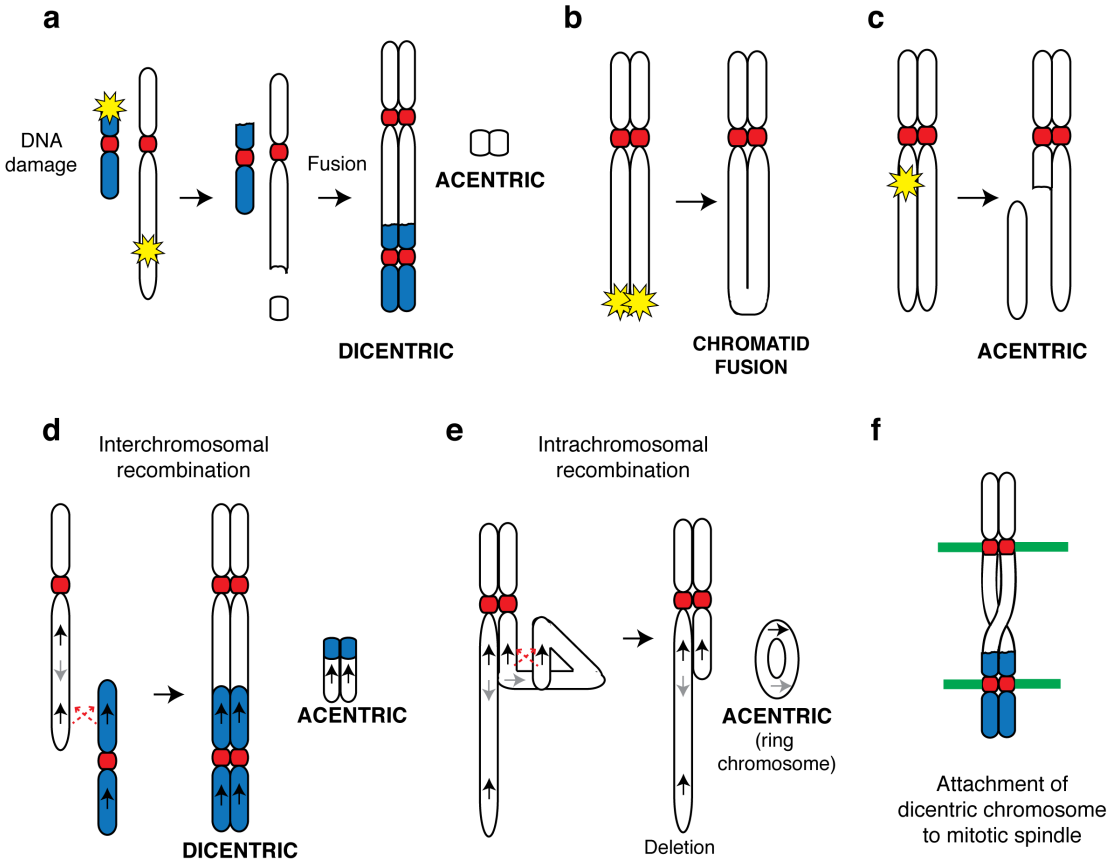

Figure 1.5 Mechanisms generating dicentric and acentric chromosomes
DNA damage results in a) fusion of damaged chromosomes to form dicentric and acentric chromosomes, prior to DNA replication b) fusion of sister chromatids c) generation of acentric chromatids (after DNA replication). Recombination between non-allelic homologous sequences may result in d) inter-chromosomal recombination, generating dicentric and acentric chromosomes e) intra-chromosomal recombination, generating deletions and acentric ring chromosomes. f) Acentric chromosomes cannot attach to the mitotic spindle, while dicentric chromosomes are likely to attach improperly, illustrated here (microtubules are shown in green).

1.8.1 Types of DNA damage

DNA is susceptible to multiple forms of damage, both exogenous and endogenous. Exogenous sources of DNA damage include ionising radiation, ultra-violet (UV) light and a number of chemical agents, including those found in tobacco smoke, and those used as cancer chemotherapeutics. Ionising radiation generates reactive oxygen species, which can lead to the generation of both double and single-stranded DNA breaks. UV light results in the formation of cross-links between adjacent thymine bases (pyrimidine dimers), which represent an obstacle to DNA replication fork progression in S phase.

Chemical agents can generate cross-links both within and between DNA strands or may generate bulky DNA adducts that again block replication fork progression (Jackson and Bartek, 2009).

There are also multiple endogenous sources of DNA damage. Spontaneous depurination generates abasic sites through fission of the base-sugar link, while spontaneous deamination generates uracil from cytosine, which obstructs DNA replication (Kouzminova and Kuzminov, 2006). Reactive oxygen species, generated as a natural by-product of cellular metabolism, can generate both single and double stranded DNA lesions, in addition to modified guanine residues (8-oxo-guanine), which can pair erroneously with adenine during replication, leading to base substitutions (Cheng et al., 1992, Kasai et al., 1986). Finally, DNA damage may occur through errors of the DNA replication and repair machinery.

1.8.2 Mechanisms of DNA repair

Multiple pathways exist to repair damaged DNA, specialised for particular types of DNA damage and cell cycle stage. This section will briefly summarise mechanisms for repairing 1) single strand DNA breaks, base modifications and replication errors and 2) double strand breaks.

1.8.2.1 Repair of ssDNA gaps, base modifications and replication errors

The broken DNA ends at a ssDNA gap are first processed to restore 3'-hydroxyl and 5'-phosphate moieties, which are required for DNA polymerases to resynthesise DNA in the ssDNA gap. After gap-filling, DNA ligases reseal the nicked DNA backbone (Caldecott, 2008). Alternatively, recombination may be used to fill in daughter strand gaps behind the DNA replication fork (Branzei, 2011). Repair of chemically modified DNA bases or bulky DNA-protein adducts, for example those generated by topoisomerase inhibitors, requires either base- or nucleotide-excision repair. In base excision repair, the abnormal base is excised by DNA glycosylases, after which the sugar backbone is cleaved at the abasic site to generate the single-strand break, which is then repaired as described above. In nucleotide-excision repair, for example of UV-induced thymine dimers, endonucleases cut the sugar backbone slightly up- and downstream of the lesion, resulting in removal of a longer stretch of DNA

encompassing the lesion. The ssDNA gap is then processed, filled and ligated. Excision repair is required downstream from translesion synthesis, which allows replication forks to bypass DNA lesions, using error-prone DNA polymerases (Sale et al., 2012).

Mismatch repair (MMR) functions primarily during DNA replication, when it functions to excise incorrectly incorporated bases (mismatches) or looped DNA that results from polymerase slippage at repetitive sequences. A MSH2/MSH6 heterodimer recognises small mismatches and looped DNA, while MSH2/MSH3 recognises larger mismatches. Binding of an MSH2-containing heterodimer recruits MLH1, in complex with PMS2. MLH1-PMS2 then coordinate the recruitment of other factors, including PCNA, exonuclease 1 and DNA polymerases, to excise the mismatch or looped DNA and resynthesise DNA.

Repair of ssDNA gaps and modified bases is important to the maintenance of chromosomal stability, as when a progressing replication fork encounters a ssDNA gap, the replication fork will collapse and a double-strand break will be generated (Jackson and Bartek, 2009, Petermann and Helleday, 2010). Forks that stall irreversibly at modified DNA bases may also be cleaved to generate double strand breaks (Constantinou et al., 2002), or require recombination mediated restart.

1.8.2.2 Double strand break repair

There are two main mechanisms of double strand break (DSB) repair – non-homologous end joining (NHEJ) and homologous recombination (HR). Which repair pathway is employed varies with cell cycle stage (Branzei and Foiani, 2008, Hartlerode and Scully, 2009) and is most likely regulated by CDK mediated phosphorylation (Hartlerode and Scully, 2009, Falck et al., 2012). HR occurs in S and G2 when a homologous sister DNA molecule is available, while NHEJ is the dominant form of repair in G1 (but can occur at any point throughout the cell cycle).

In NHEJ, broken DNA ends are directly re-ligated and repair is error-prone. Broken DNA ends are bound by the Ku70/Ku80 heterodimer and DNA-dependent protein kinase, which facilitates processing of the DNA ends. After end processing the XRCC4 homodimer binds to Ku and acts as a scaffold, stimulating ligase IV activity to seal the DSB (Hartlerode and Scully, 2009). A schematic of NHEJ is shown in Figure

1.6. Inappropriate NHEJ mediated repair between two chromosomes may result in chromosome fusions (see Figure 1.5a) (Smogorzewska et al., 2002, Wang et al., 2001).

In HR, DNA ends are resected by MRE11 and CtIP, generating ssDNA tracts either side of the DSB (Sartori et al., 2007, Buis et al., 2008, Garcia et al., 2011). The resected ends are then bound by the ssDNA binding protein RPA (Replication Protein A), which melts any secondary structures. Then BRCA2, among other proteins (including BRCA1), is required to exchange RPA for RAD51, creating nucleoprotein filaments that can mediate strand invasion to find a homologous sequence for repair. If the second end of the DSB is captured during strand invasion then a double Holliday junction will form (illustrated in Figure 1.7). Alternatively, after extension of the initial invading strand, the newly synthesised DNA may be displaced and engage the second resected DSB end, in a process called synthesis-dependent strand annealing (Paques and Haber, 1999).

Resolution of recombination intermediates can occur with or without crossing over, and can require Holliday junction migration (Constantinou et al., 2001, Karow et al., 2000, Constantinou et al., 2000). The Bloom helicase (BLM), mutated in patients with Bloom's syndrome, is important for resolution of recombination intermediates without crossing over (Wu and Hickson, 2003). The MUS81-EME1 complex, on the other hand, can cleave Holliday junctions to produce crossovers (Constantinou et al., 2002). However, crossing over is rare during somatic homologous recombination (Richardson et al., 1998), preventing erroneous chromosome translocations (Richardson and Jasin, 2000). BLM is also likely to be important for the resolution of recombination intermediates generated during recombination-mediated bypass (template switching) of DNA lesions during DNA replication (Branzei, 2011). Defective HR may result in the dominance of repair by NHEJ and the generation of chromosome fusions, as is observed in tumour cells harbouring BRCA1/2 mutations (Xia et al., 2001, Wang et al., 2001). Alternatively, non-allelic homologous recombination may result in the generation of dicentric or acentric chromosomes, illustrated in Figure 1.5 (Colnaghi et al., 2011).

1.8.3 Recognition of DNA damage

DNA double strand breaks (DSBs) result in the formation of nuclear foci consisting of a plethora of proteins, some with roles in in activating cell cycle checkpoint responses,

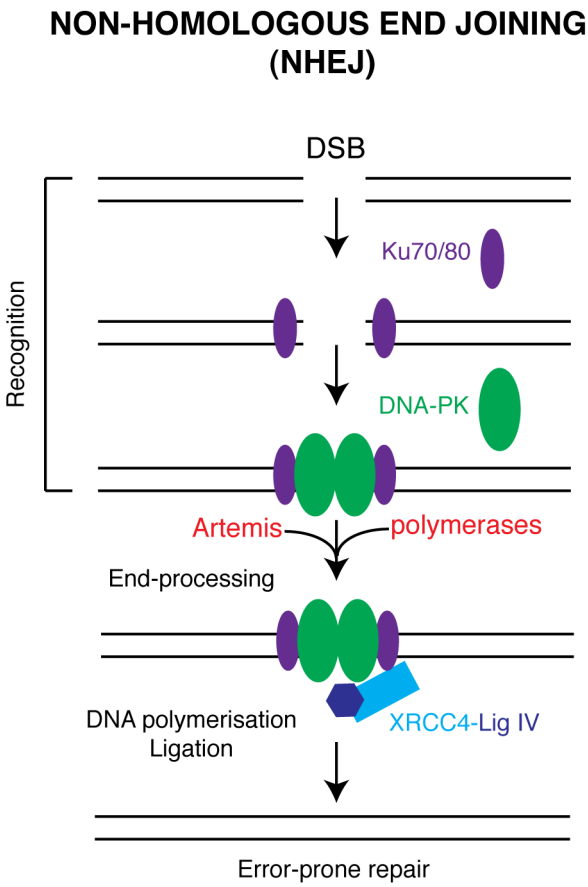

Figure 1.6 Non-homologous end-joining (NHEJ)
Schematic of NHEJ: broken DNA ends are bound the Ku70/80 heterodimer, which recruit DNA-PK. DNA-PK recruits components required to process the DNA ends, followed by DNA ligases to seal the break.

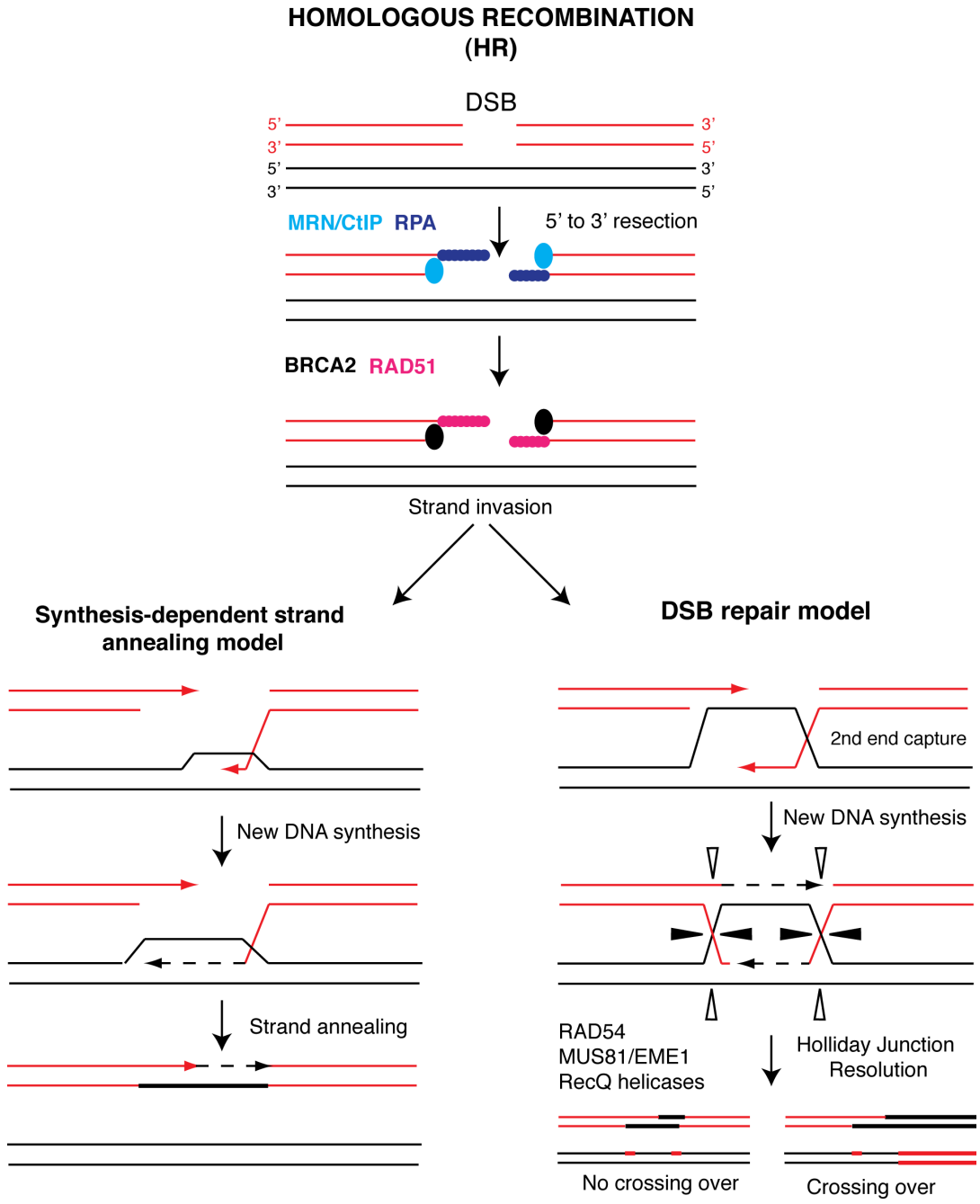

Figure 1.7 Homologous recombination mediated repair (HR)
Schematic of two different models for HR, adapted from (Paques and Haber, 1999). The DSB is resected by MRE11 and CtIP, generating ssDNA tracts, which are coated in RPA. RPA is exchanged for RAD51, which creates a nucleoprotein filament capable of mediating strand invasion into the homologous sister molecule. In the SDSA model, the second DSB end is not captured by the homologous template, and the invading strand is displaced as it is synthesised. In the DSB repair model, both ends are captured by the homologous template, resulting in the formation of a double Holliday junction, which must then be resolved, generating products with or without crossing over between homologous DNA molecules.

and others with roles in processing DNA ends or mediating DNA repair. Other recruited factors have no apparent direct role in either repair or DNA damage checkpoint responses, but instead affect chromatin structure, and may play a role in regulating the interaction between DNA damage/repair and both transcription and replication (Lukas et al., 2011b).

Upon generation of a DSB, histone H2A family member X (H2AX) is both phosphorylated at Serine-139 (Rogakou et al., 1998), and dephosphorylated at tyrosine 142 (Xiao et al., 2009, Cook et al., 2009). Phosphorylated H2AX is referred to as gamma-H2AX (γH2AX), and the major kinase responsible for this phosphorylation is ATM (ataxia telangiectasia mutated), the master regulator of the response to DSBs (Kastan and Bartek, 2004, Kastan et al., 1992). ATM is recruited to DSBs primarily by the MRN complex (Williams and Tainer, 2005, Lukas et al., 2011b), illustrated in Figure 1.8. γH2AX is then recognised by a central coordinator of DNA damage foci formation, MDC1 (mediator of DNA damage-checkpoint 1)(Shang et al., 2003, Goldberg et al., 2003, Stewart et al., 2003). MDC1 anchors ATM at the DSB, through interaction with NBS1, allowing ATM to further phosphorylate H2AX and other substrates at the DSB, including MDC1 itself (Lukas et al., 2011b). Through phosphorylation of MDC1, two ubiquitin ligases, RNF8 and RNF168 are recruited, resulting in ubiquitylation of a number of substrates, including H2AX (Mailand et al., 2007) and the accumulation of the proteins TP53 binding protein-1 (53BP1) and BRCA1 at sites of DNA damage (Doil et al., 2009). The mechanisms of 53BP1 recruitment to DSBs are not fully understood. Activated ATM is also able to phosphorylate further ATM homodimers, generating active monomers that are able to transduce the DNA damage checkpoint activating signal, through phosphorylation of CHK2 (see section 1.8.5), as well as amplifying the local response to the DNA break (Hartlerode and Scully, 2009, Lukas et al., 2011b).

ssDNA breaks during S or G2 phases of the cell cycle result in activation of the ATM- and Rad3-related kinase, ATR. ssDNA coated with the ssDNA-binding protein RPA recruits ATR in complex with its interacting partner ATRIP, resulting in ATR activation and phosphorylation of downstream effector kinase CHK1 (Zou and Elledge, 2003). ssDNA may be generated directly at stalled replication forks, following uncoupling of polymerase and helicase activities (MacDougall et al., 2007), or

indirectly, following processing of stalled replication forks and double strand breaks (Bryant et al., 2009, Davies et al., 2007). Activation of ATR also involves a number of other factors including Claspin (Kumagai et al., 2004), TOPBP1 and the RAD9-HUS1-RAD1 (9-1-1) clamp (Sancar et al., 2004). Claspin is associated with replication forks during normal replication, and when phosphorylated by ATR binds CHK1 to facilitate its activation by ATR (Smith et al., 2010).

Failure to detect, and thus respond to, DNA damage, results in genome instability, and dependent on the specific defect, gross chromosome rearrangements. For example, cells harbouring mutations in NBS, which is essential for ATM recruitment to chromosome breaks (Falck et al., 2005), are defective in the response to DSBs and show gross chromosomal rearrangements (Taalman et al., 1983).

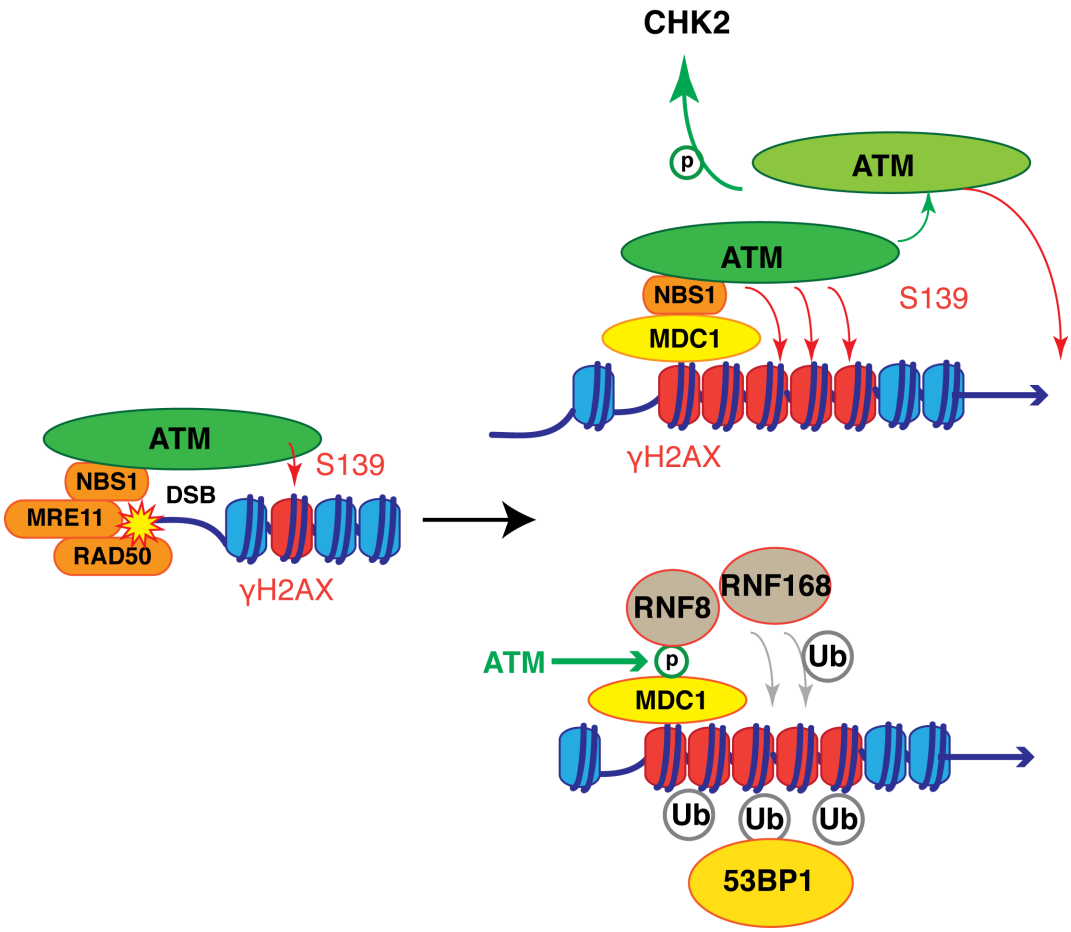

Figure 1.8 Recognition of double strand breaks
Adapted from (Lukas et al., 2011b). Schematic of the molecular events triggered by DSB formation.

1.8.4 Replication fork stalling – restart and repair

Replication forks may stall when they encounter bulky DNA lesions, nicked DNA, ssDNA gaps, DSBs, or at particularly challenging sequences in the genome. In addition, depleted cellular nucleotide pools, and impaired replisome activity can cause replication fork stalling, conditions which can be induced by treatment with the ribonucleotide reductase inhibitor hydroxyurea, or with the DNA polymerase inhibitor Aphidicolin. The replication fork must employ one of a number of pathways to restart after stalling or else collapse, requiring firing of alternative origins to complete replication of the genome (Petermann and Helleday, 2010). There are several models to explain how restart of stalled replication forks may be achieved: 1) through re-annealing of ssDNA generated during fork stalling (Figure 1.9) (Byun et al., 2005, Petermann and Helleday, 2010, Cheok et al., 2005) 2) through fork regression, followed by Holliday junction formation, recombination and dissolution (Petermann and Helleday, 2010) or 3) through processing of the replication fork into a double strand break, which is then repaired through homologous recombination (Hanada et al., 2007, Constantinou et al., 2002, Trenz et al., 2006). Processing and repair of stalled forks is illustrated in Figure 1.9.

One-ended DSBs are generated when a stalled fork persists for many hours, at which point it is cleaved by MUS81-EME1 (Hanada et al., 2007, Petermann and Helleday, 2010, Constantinou et al., 2002). One-ended DSBs are also formed when replication forks stall at a nicked template or ssDNA tract. These replication associated DSBs are repaired by homologous recombination (see Figure 1.9) and it is possible that repair creates a new origin of replication and restarts replication in a model known as ‘break-induced replication’, which is observed in bacteria (Llorente et al., 2008). Alternatively, the firing of alternative latent origins that are usually passively replicated may enable completion of replication. In this latter scenario, a replication fork coming from the other direction would generate a two-ended DSB (Figure 1.9), which can then be repaired by classical homologous recombination (see Section 1.8.2.2). Experiments in yeast indicate that following replication fork collapse at an irreparable DSB generated during G1, replication beyond the DSB is achieved by firing additional dormant origins of replication (Doksani et al., 2009).

Simple fork restart by ssDNA re-annealing is not possible where a physical obstacle, such as modified bases or DNA adducts, blocked fork progression. Therefore

mechanisms exist for bypassing DNA lesions during DNA replication, collectively known as DNA damage tolerance (Sale et al., 2012, Branzei, 2011). In one pathway, error-prone translesion DNA polymerases may be employed which are able to replicate past the obstruction (Sale et al., 2012). The lesion is then repaired after replication. However, translesion synthesis is mutagenic, and must be tightly regulated. In a second pathway, the homologous sister template may be used to replicate past the lesion, in a mechanism similar to homologous recombination mediated repair of double strand breaks (see section 1.8.2.2). This is known as template switching, and occurs commonly at repetitive sequence elements, at which replication fork slippage occurs (Colnaghi et al., 2011). Template switching involves many of the same proteins as homologous recombination (which arises from a double strand break) and likely requires similar factors to resolve intermediates (Branzei, 2011).

Recombination between sister DNA molecules at the correct genomic locus is error free, although can result in gene conversion. However, recombination between similar sequences on different chromosomes or between inverted repeats on the same chromosome can result in gross chromosomal rearrangements, including translocations, inversions and deletions, as shown in Figure 1.5. As a consequence of these rearrangements, dicentric and acentric chromosomes may be generated, that are likely to missegregate during mitosis. In addition incomplete resolution of replication intermediates and DNA catenanes can result in chromosome missegregation at mitosis (Cimini et al., 1997, Chan et al., 2007). Template switching has been implicated in complex genomic rearrangements in human cells (Lee et al., 2007, Liu et al., 2011, Colnaghi et al., 2011); and defects in fork stabilisation, restart or repair, or in the fidelity of these processes, also result in genome instability (Branzei and Foiani, 2010, Davies et al., 2004, Schlacher et al., 2011). Alternatively, an increased frequency of fork stalling and therefore of recombination-mediated repair of replication forks and fork-associated DSBs would also contribute to chromosomal rearrangements (Colnaghi et al., 2011).

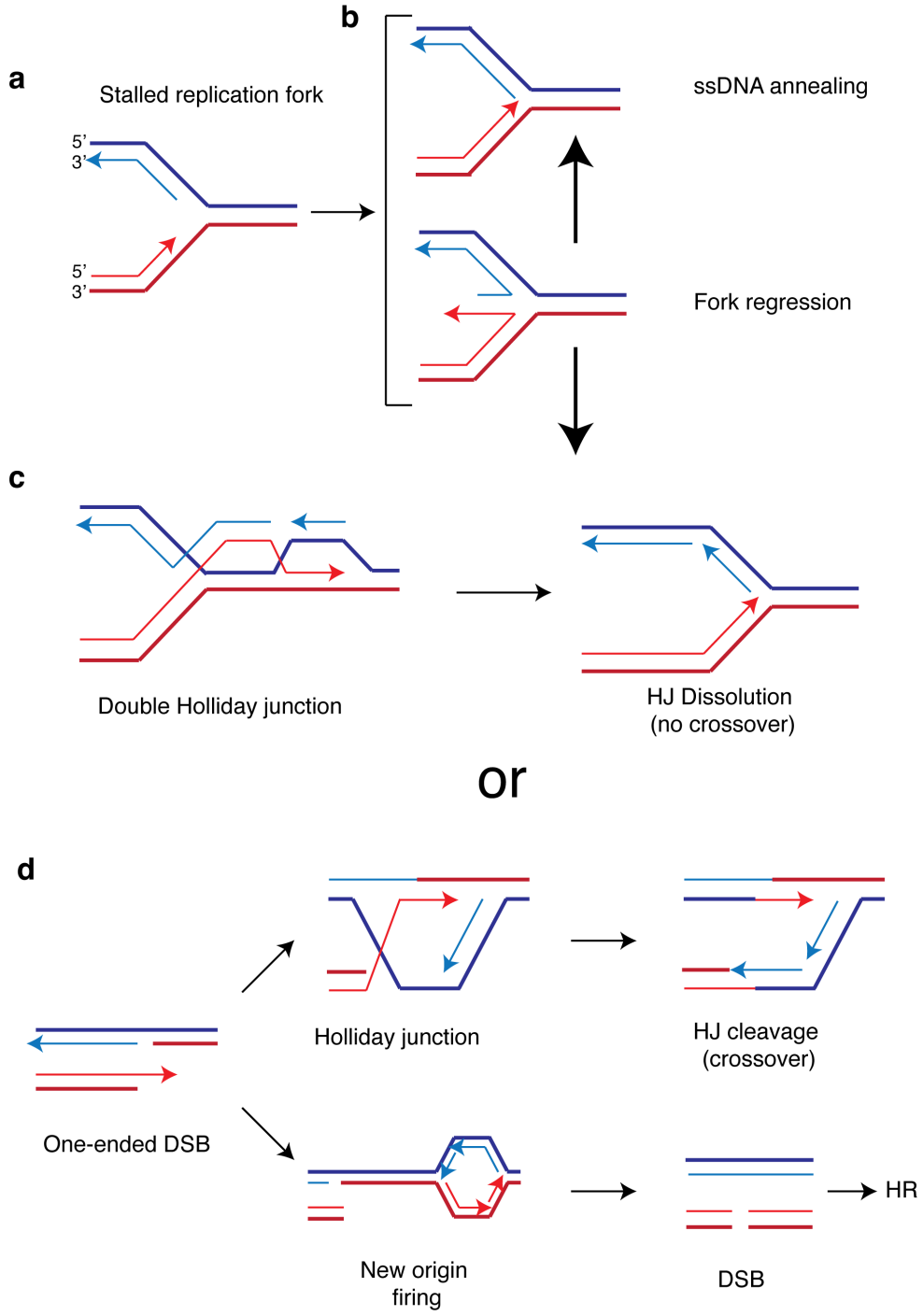

Figure 1.9 Restart and repair of stalled replication forks
Adapted from (Petermann and Helleday, 2010) a) Stalled replication fork with tracts of ssDNA generated by uncoupling of the polymerase and helicase activities b) reannealing of the ssDNA to promote fork restart c) reversal of the replication fork to generate a four way 'chicken foot' structure that can then be processed for resolution by c) Holliday junction formation and dissolution without crossing over d) The stalled fork may be cleaved to form one-ended DSB, which is then repaired by HR and fork progression may restart. Alternatively replication may be completed by another fork coming the opposite direction, generating a two-ended DSB.

1.8.5 The cell cycle checkpoint response to DNA damage

In response to DNA damage, cell cycle transitions are blocked at G1-S and in G2-M, and progression through S phase is halted or slowed for cells that are actively replicating their DNA (the intra-S checkpoint). Activation of ATM/ATR by DNA damage results in the phosphorylation and subsequent activation of the effector kinases CHK1 and CHK2, which, together with ATM/ATR, mediate the cellular checkpoint responses to DNA damage (Stracker et al., 2009). CHK1 is primarily phosphorylated by ATR, while ATM activates CHK2. In addition, ATM activates a number of other cellular pathways including the p38 MAP-kinase and NF-kappaB pathways (Wu et al., 2006). This downstream response is important to prevent the proliferation and propagation of cells with damaged genomes. In addition, ATR and CHK1 both have constitutive functions in DNA replication (Petermann et al., 2010, Sorensen et al., 2004, Beck et al., 2010).

CHK1/2 mediated phosphorylation represses the activity of the regulatory phosphatases CDC25A and CDC25C, which control activation of CDKs at the G1-S and G2-M boundaries, thus preventing cell cycle progression (Kastan and Bartek, 2004, Mailand et al., 2000). In addition both CHK1 and CHK2 promote the degradation of an ubiquitin ligase that targets p53 for degradation (MDMX) (Chen et al., 2005, Jin et al., 2006). P53 accumulation results in transcription of p53 target genes, including the cyclin-dependent kinase inhibitor p21, which binds and inhibits CDK-cyclin complexes, preventing cell cycle progression from G1-S or G2-M phases (Kastan et al., 1992, Kastan and Bartek, 2004). Checkpoint signalling pathways at G1-S and in S-G2 are illustrated in Figure 1.10.

The G1-S checkpoint is primarily mediated by ATM-CHK2, and is dependent upon the function of both P53 and the Retinoblastoma protein (Rb), which is the gatekeeper of entry into S-phase. Therefore P53 and Rb mutant tumour cells display defective G1-S checkpoint function (Kuerbitz et al., 1992, Bunz et al., 1998). However, P53 mutant tumour cells still accumulate in G2 in response to DNA damage, indicating that p53-independent mechanisms are able to sustain a G2 arrest (Kastan and Bartek, 2004). The G2 checkpoint appears to be less stringent than the G1-S checkpoint, requiring around 20 DSBs for activation, compared to activation of the G1-S checkpoint by a single DSB (Deckbar et al., 2007, Krempler et al., 2007, Huang et al., 1996).

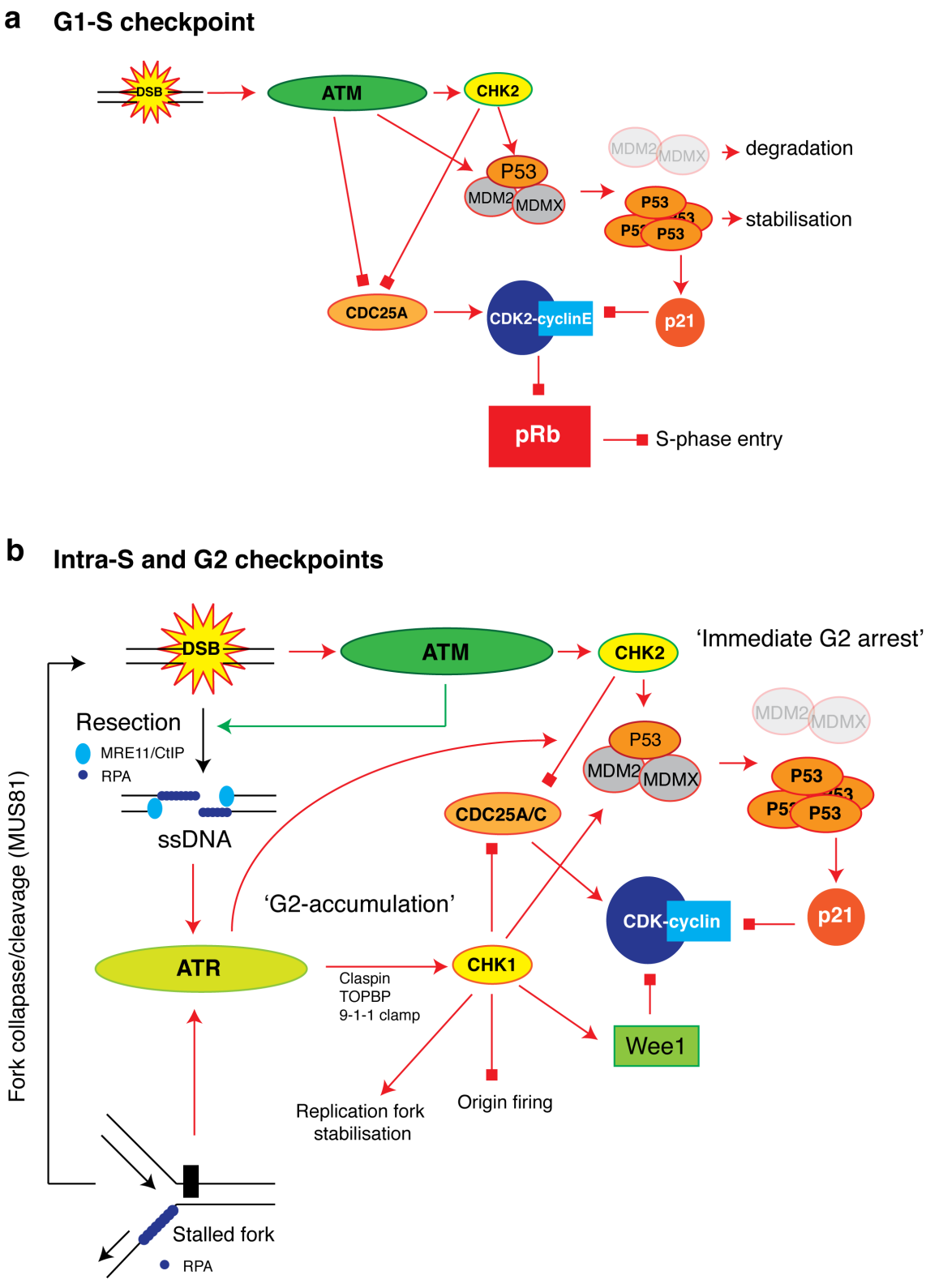

Figure 1.10 DNA damage checkpoint signalling
Schematic of DNA damage checkpoint signalling in a) G1 and b) S and G2.

In S and G2, ATM and ATR are usually activated together. ATM-CHK2 is activated by DSBs as in G1, but when DSBs are resected to facilitate DNA repair by homologous recombination, ssDNA tracts are generated, which activate ATR and subsequently CHK1 (Jazayeri et al., 2006, Stracker et al., 2009, Smith et al., 2010). During S phase, stalled replication forks also activate ATR, which is important in both preventing the firing of late origins of replication, and stabilising existing replication forks (Smith et al., 2010, Bartek et al., 2004). Paradoxically, it appears origin firing may actually be increased locally around a DSB (Doksani et al., 2009), suggesting that the repression of new origin firing only occurs beyond a certain threshold of DNA damage/fork stalling, or that there is local regulation of origin firing in the vicinity of DNA damage.

Defects in checkpoint activation may result in failure to repair DNA damage or stabilise DNA replication forks, leading to an increased likelihood of chromosome rearrangements, and the propagation of damaged genomes.

1.9 DNA damage and CIN

Clearly cells possess multiple pathways to maintain the stability of the genome. Disruption of one pathway may be compensated for by another, which may or may not be sufficient to maintain genome instability. DNA damage can result in the formation of chromosome fusions, translocations or acentric fragments (Richardson and Jasin, 2000, Richardson et al., 1998, Gisselsson, 2008, Acilan et al., 2007), which are then unstable during mitosis, as was described in section 1.2.1. In support of the involvement of DNA damage in cancer development, an active DNA damage response is observed in both pre-malignant and malignant tumours (Bartkova et al., 2005, Gorgoulis et al., 2005), and cancers show complex karyotypic changes (Roschke et al., 2003, Liu et al., 2011, Bardi et al., 1993). Elevated DNA damage may arise through defects in cellular capacity to respond to endogenous levels of damage, or alternatively through increased generation of DNA lesions, including the uncapping of telomeres.

1.9.1 Defective DNA damage response and chromosomal abnormalities

Defects in the DNA damage response, whether in detection, repair or checkpoint signalling, can result in genome instability (Buis et al., 2008, Celeste et al., 2002, Savitsky et al., 1995, Brown and Baltimore, 2000, Chan et al., 2007). The same protein can have multiple roles in the DNA damage response, for example MRE11, as part of the MRN complex, is involved in DNA damage detection, checkpoint activation and DNA repair, and MRE11-null cells exhibit gross chromosome abnormalities (Buis et al., 2008, Garcia et al., 2011, Bryant et al., 2009). Deficiencies in these key regulators can result in broad DNA damage response defects. In addition, proteins like ATR and CHK1 have constitutive roles in DNA replication, in the absence of DNA damage. Consequently, defects in ATR/CHK1 result in catastrophic genome instability, and early embryonic lethality is observed in mice lacking either ATR or CHK1 (Brown and Baltimore, 2000, Liu et al., 2000).

Unrepaired DSBs may require a checkpoint defect in order for the cell to enter into mitosis, but given the proposed relative insensitivity of the G2-M checkpoint (Lobrich and Jeggo, 2007), it is likely that low levels of unrepaired damage would persist into mitosis, as has been demonstrated following low dose irradiation (Deckbar et al., 2007). Improperly repaired DNA damage, for example chromosome translocations or telomere fusions, circumvents the requirement for altered checkpoint control to enter mitosis, as there is no longer a checkpoint-activating DNA lesion (Richardson and Jasin, 2000, Stewenius et al., 2005, Acilan et al., 2007).

In addition, defects in one DNA repair pathway may result in inappropriate repair by other pathways. For example, tumours harbouring mutations in BRCA1 or BRCA2 exhibit defective homologous recombination, and thus DSBs are inappropriately repaired by non-homologous end joining, and gross chromosomal abnormalities are observed (Wang et al., 2001, Moynahan et al., 2001, Xia et al., 2001). Similarly, individuals with mutations in the Bloom's syndrome RECQ helicase, *BLM*, a key player in homologous recombination and DNA replication, also exhibit chromosomal fragility, and chromosome segregation errors during mitosis (Chan et al., 2007, Wu and Hickson, 2003, Bachrati and Hickson, 2008). Due to the various roles of BLM in both replication and repair, chromosomal fragility in Bloom's syndrome results at least in part from DNA replication stress (Chan et al., 2009, Chabosseau et al., 2011).

Patients harbouring germline mutations in a number of DNA damage response genes show marked cancer predisposition, summarised in Table 1.2. A subgroup of these syndromes are described as chromosome breakage syndromes, reflecting the genome instability observed in patients cells, both normal and cancerous (German, 1980). Mutations in components of the DNA damage response, most notably ATM and p53, are also observed in sporadic cancers.

Gene	Inheritance	Chromosome location	Disease association	Cancer predisposition
Ku70	AR	22q11-13		T-cell lymphomas
Ku80	AR	2q35		Pro-B cell lymphomas
DNA ligase IV	AR	13q22-24	LIG4 syndrome	Lymphoid malignancies
BRCA1	AD	17q21	Hereditary breast cancer	Breast and ovarian cancer
BRCA2 (FANCD1)	AD (AR)	13q12.3	Hereditary breast cancer (AD), Fanconi Anaemia (AR)	Breast and ovarian cancer
MRE11	AR	11q21	Ataxia-telangiectasia like disorder	
RAD50	AR	5q31		Increased breast cancer risk
NBS1	AR	8q21	Nijmegen breakage syndrome	Haematologic malignancies
ATM	AR	11q22.3	Ataxia telangiectasia	Haematologic malignancies
ATR	AR	3q22-24	Seckel syndrome	
FANCD2	AR	3p25.3	Fanconi anaemia	Acute myeloid leukaemia, squamous cell carcinoma
BLM	AR	15q26.1	Bloom's syndrome	Various (leukaemia, lymphoma, carcinoma)
PALB2 (FANCN)	AR	16p12	Fanconi anaemia	Breast and ovarian cancer
BACH1 (FANCJ)	AR	17q22	Fanconi anaemia	Breast cancer
CHK2	AR	22q12.1	Li-Fraumeni syndrome 2	Sarcoma, breast, cancer, brain tumours
TP53	AD	17p13.1	Li-Fraumeni syndrome	Various. Sarcoma at young age
WRN	AR	8p12-11.2	Werner's syndrome	Sarcoma

Table 1.2 Hereditary syndromes caused by mutations in components of the DNA damage response
Adapted from (Hartlerode and Scully, 2009). Abbreviations: AR – autosomal recessive; AD – autosomal dominant

1.9.2 Increased generation of endogenous DNA damage

Elevated DNA damage, in the absence of a defect in the DNA damage response, may also lead to chromosomal aberrations. Endogenous damage may be generated through an increased level of oxidative stress, arising due to perturbations of cellular metabolism (see section 1.8.1); induction of mitochondrial oxidative stress in kidney and colon cells resulted in chromosomal instability (Mishra et al., 2009a, Mishra et al., 2009b). Alternatively, telomere uncapping may result in chromosomal fusions and bridge-fusion-breakage cycles (Gisselsson, 2008, Gisselsson et al., 2000). Finally defects in replication, termed replication stress, may generate double strand breaks and erroneous recombination between chromosomes, as described in section 1.8.4.

1.9.3 Telomere Uncapping

To avoid erosion of essential genetic material during DNA replication, the ends of chromosomes (the telomeres) consist of 9-15 kb of tandem TTAGGG repeats, preceded by approximately 100-300 kb of telomere-associated repeats. The protein complex Shelterin, which assembles on telomeres, together with a 3'-overhang of 50-300 nucleotides, appears to shield against inappropriate DNA repair (O'Sullivan and Karlseder, 2010). In stem cells, telomere length is maintained by the RNA-directed DNA polymerase telomerase, endowing them with limitless replicative potential. In somatic cells, which do not express telomerase, the telomeres are progressively shortened such that cells can only undergo a defined number of cell divisions before the induction of replicative senescence, when telomere length becomes too short.

Critical telomere shortening, or alteration of telomere structure, can result in activation of the DNA damage response, resulting in erroneous repair and the generation of chromosome fusions (Gisselsson et al., 2001, Artandi et al., 2000). Telomerase deficient mice display chromosomal abnormalities and aneuploidy (Blasco et al., 1997) and silencing the Shelterin component TRF2 results in gross chromosome fusions, mediated through non-homologous end joining, within just a few rounds of the cell cycle (Smogorzewska et al., 2002). Uncapped telomeres can also engage in inappropriate homologous recombination (Laud et al., 2005), which may actually be

exploited as an alternative mechanism to avoid excessive telomere erosion and achieve immortalisation, without telomerase expression.

However, by virtue of their drive to proliferate, cancer cells almost invariably reactivate telomerase (Shay and Wright, 1996). As telomerase expression will prevent telomere erosion, it remains unclear whether telomere dysfunction plays a role in ongoing CIN, once a tumour is established. However, there is evidence that telomere attrition may play a role in promoting transformation, generating a transient high level of genome instability at the pre-malignant stage, before reactivation of telomerase expression and loss of p53 (O'Sullivan and Karlseder, 2010). Non-reciprocal translocations observed in tumours formed in telomerase deficient p53-mutant mice are reminiscent of chromosomal abnormalities observed in some tumours (Artandi et al., 2000, Gisselsson et al., 2001), and telomere fusion events may also mediate whole chromosome losses during anaphase (Pampalona et al., 2010b). Reactivation of telomerase following this period of gross genomic rearrangement both immortalises the cells, and restores relative genome stability (Gisselsson et al., 2001, Counter et al., 1992).

Intriguingly, it appears that even in cells with telomerase reactivation, a degree of telomere dysfunction can still occur, mediating ongoing chromosomal instability (Gisselsson et al., 2001). A study of five colon cancer cell lines indicated that anaphase bridging could be telomere-mediated in SW480 CIN+ cells (Stewenius et al., 2005). However, the mechanism for this dysfunction is not clear. One possible mechanism is through replication defects, as telomeres possess properties of fragile sites, and are late replicating regions (Sfeir et al., 2009, Barefield and Karlseder, 2012). Alternatively, persistent cohesion between sister telomeres can result in eventual fusion by non-homologous end joining (Hsiao and Smith, 2009). Nevertheless, the majority of chromosome fusions observed in tumours do not contain telomeric sequences, and instead breaks are located at centromeres or interstitially on chromosome arms, suggesting that telomere fusions are not the sole driver of chromosome aberrations in CIN cancers (Gisselsson et al., 2001, Martinez and van Wely, 2011).

In summary, telomere dysfunction may play a role in genomic instability during tumour development, which is rescued once telomerase is activated. However, low-

level telomere dysfunction, generated through unknown mechanisms, may participate in on going chromosomal instability.

1.9.4 DNA replication stress

During DNA replication, the genome is at its most vulnerable. A host of enzymes must unwind the DNA, cut and re-ligate DNA helices in order to relieve topological strain, negotiate collisions with the transcription machinery and complex secondary structures and resolve recombination intermediates, to name just a few of the complex processes that must be undertaken to accurately copy the genome. Interference with any of these processes can destabilise the genome. However, defects in replication cannot be too profound otherwise viability will be compromised (Brown and Baltimore, 2000, Liu et al., 2000).

'Replication stress' is a summary term for a number of processes affecting the fidelity and completion of DNA replication. Replication stress may be induced in multiple ways, including oncogene activation and tumour suppressor loss (Tort et al., 2006, Bartkova et al., 2006), direct defects in the replication machinery (Barkley et al., 2009, Davies et al., 2007, Chan et al., 2009) and conditions that impede the normal progress of the replication fork. These may include nucleotide deficiency (Bester et al., 2011), DNA lesions (Heller and Marians, 2006, Furuta et al., 2003, Groth et al., 2010), and abnormal secondary DNA structures, or challenging DNA sequences (Ozeri-Galai et al., 2011, Glover, 2006, Branzei and Foiani, 2010, Schwartz et al., 2006). Experimentally, replication stress is often induced using low concentrations of the DNA polymerase inhibitor Aphidicolin, which dramatically slow but do not completely block DNA replication, and allow cell cycle progression at normal speeds (Glover et al., 1984). In low concentrations of Aphidicolin, and in the conditions listed above, regions of the genome known as fragile sites are particularly susceptible to DNA damage (Glover et al., 1984).

Fragile sites represent a challenge to DNA replication, due to either inherent difficulty replicating certain sequence elements, for example AT-dinucleotide-rich sequences, or alternatively due to secondary structures which may alter the chromatin environment surrounding the fragile site (Schwartz et al., 2006). These sequence elements may disrupt replication fork progression during a normal S phase, resulting in

the firing of all available origins around the fragile site under unperturbed conditions. Consequently, under conditions of replication stress, for example in the presence of Aphidicolin, no extra origins are available to aid in replication restart after fork stalling, or to compensate for slow replication fork progression (Courbet et al., 2008, Ozeri-Galai et al., 2011). Alternatively, paucity of available origins within a given genomic locus, in which the sequence does not pose an obvious challenge to replication under normal conditions, may suffer preferential fragility in conditions of replication stress (for example, nucleotide deficiency) due to the lack of additional origins to fire (Letessier et al., 2011). Furthermore, genomic loci that mark a transition zone between early and late replicating regions may also be particularly susceptible to slow replication fork rates (Palumbo et al., 2010).

Cells cultured in conditions of replication stress exhibit DNA damage and chromosome breaks (Glover et al., 1984). In addition replication stress results in chromosome segregation errors in mitosis (Ichijima et al., 2010, Kawabata et al., 2011). Further evidence supporting a possible association between chromosomal instability and replication stress comes from genome wide studies of break points in cancer. A recent analysis of common deletions in the genomes of 746 cancer cell lines identified frequent homozygous deletions at fragile sites (Bignell et al., 2010), and other studies have also identified genomic alterations suggestive of replication stress in human cancers (Dereli-Oz et al., 2011, Arlt et al., 2009, Lee et al., 2007). However, it is important to note that while fragile sites are the most susceptible loci to chromosome breakage and loss of heterozygosity (LOH) under replication stress, the copy number changes that would result from replication stress in the context of the selective pressures of tumorigenesis are not clear. Indeed, it has been shown that while fragile sites are preferentially affected early on in tumorigenesis, in advanced tumours the whole genome is susceptible to copy number changes and LOH (Bartkova et al., 2005, Gorgoulis et al., 2005). Intriguingly, a recent study found that longer-term culture of cells after oncogene activation resulted in copy number alterations similar to those observed in CIN+ cancers, including loss of 8p and gain of the short arm of chromosome 20 (Bester et al., 2011).

1.9.4.1 Oncogene-induced replication stress

The DNA damage response has been found to be active in both pre-malignant and malignant tumours (Bartkova et al., 2005, Gorgoulis et al., 2005), and it has been proposed that this may be explained by oncogene activation (Halazonetis et al., 2008). Several lines of experimental evidence provide support for this model. Overexpression of cyclin E resulted in increases in various markers of DNA damage, including generation of tracts of RPA-coated ssDNA, and also caused altered replication dynamics, including premature fork termination (Bartkova et al., 2005, Bartkova et al., 2006). In addition, overexpression of cyclin E correlated with DNA damage checkpoint activation in colon adenomas (Bartkova et al., 2005). Tumour suppressor loss can also result in replication stress, as inactivation of the retinoblastoma protein has similarly been shown to result in activation of the DNA damage response (Tort et al., 2006).

A recent study found that oncogene activation results in depletion of cellular nucleoside levels, and subsequent decreased rates of replication fork progression, asymmetry between sister replication forks, increased origin firing and DNA damage (Bester et al., 2011). After prolonged oncogene activation, loss of heterozygosity (LOH) was observed at fragile site loci, and cells exhibited chromosome gains and losses. The replication defects and DNA damage could be rescued by supplementing cells with an exogenous supply of nucleosides, or by forcing expression of c-Myc, which controls the expression of many genes involved in nucleoside biosynthesis. Hence amplification and overexpression of c-Myc, observed in many cancers, could help compensate for oncogene-induced replication stress. This may explain previous observations of elevated, rather than depleted, deoxyribonucleotide (dNTP) pools in transformed cells (Mathews, 2006, Traut, 1994).

In an alternative model, oncogene-induced replication stress is thought to arise as a consequence of disordered origin firing, through deregulation of CDK activity; cells may enter S phase without sufficient licensed origins of replication, or re-license origins that have already fired during a given S phase (Blow and Gillespie, 2008). Mouse cells harbouring a mutation in MCM4, a component of the MCM2-7 complex that is essential for origin licensing, have decreased numbers of licensed origins of replication and exhibit structural chromosome aberrations and anaphase segregation

errors (Kawabata et al., 2011), linking defective origin licensing to chromosomal instability.

1.9.4.2 Cellular phenotypes associated with replication stress

Replication stress results in an array of cellular phenotypes, both evident during S phase, and downstream of aberrant DNA replication, shown in the schematic in Figure 1.11. As described above, replication stress will result in activation of the DNA damage response, namely phosphorylation of H2AX, and activation of ATM and CHK2 (Bartkova et al., 2005, Gorgoulis et al., 2005, Bester et al., 2011). In addition, more specific DNA damage phenotypes are also observed.

Replication stress induced by Aphidicolin induces a high level of DNA damage in early mitosis (Chan et al., 2009, Lukas et al., 2011a, Ichijima et al., 2010). Intriguingly, this DNA damage is generated even in the presence of a functional G2-M checkpoint (Lukas et al., 2011a). It is proposed that the DNA damage foci observed in these mitotic cells result from rupture of under-replicated genomic loci during chromosome condensation (shown in Figure 1.11), as silencing the condensin subunit SMC2 reduces the level of prometaphase DNA damage induced by Aphidicolin treatment (Lukas et al., 2011a). Generation of DSBs from unresolved replication intermediates upon entry into mitosis has also been reported in cells with defects in origin licensing (Kawabata et al., 2011). Chromosomal rupture may result in acentric chromosomes at anaphase, or the formation of chromosome fusions and translocations in the next cell cycle, through NHEJ mediated repair.

Replication stress also results in the formation of ultra-fine anaphase DNA bridges (Chan et al., 2009). These structures are not visible with DNA dyes, but stain positively for two DNA helicases, BLM and PICH, and the single-stranded DNA binding protein RPA, among other proteins (Chan and Hickson, 2009). The first reports of these structures were in Bloom's syndrome cells (Chan et al., 2007) and as DNA threads between sister centromeres that were exacerbated by topoisomerase inhibition (Baumann et al., 2007). Ultra-fine bridges appear to represent either catenated DNA, or unresolved replication intermediates (Chan and Hickson, 2009, Chan et al., 2007, Chan et al., 2009). DNA catenation between sister chromatids occurs under normal circumstances, and resolution requires the removal of cohesin, which may explain why

most ultra-fine bridges arise from centromeres, as cohesion is maintained at the centromere until immediately prior to anaphase onset (Wang et al., 2008). Catenation-associated ultra-fine bridges provide an explanation for the observation of ultra-fine bridges in early anaphase cells under normal conditions (Chan et al., 2007). Induction of replication stress, however, results in a marked increased frequency of ultra-fine bridges, which persist later into anaphase (Chan et al., 2007, Chan et al., 2009, Lukas et al., 2011a). The recruitment of helicases BLM and PICH, along with topoisomerase IIIa, indicates that the formation of ultra-fine bridges may be a mechanism for resolving late replication intermediates and DNA catenanes (Chan and Hickson, 2011), although the fate of these structures is not well understood at present.

After passage through mitosis, cells under replication stress exhibit large nuclear bodies marked by 53BP1, which disappear on entry into S phase (Lukas et al., 2011a, Harrigan et al., 2011). The function of these 53BP1 nuclear bodies is incompletely understood, but they appear to be transcriptionally inactive, and may function to shield the lesion from further damage or inappropriate DNA repair (Lukas et al., 2011a, Harrigan et al., 2011). Hence it is possible that post-replication repair, and the response to replication stress, extends into the next cell cycle, following transmission through mitosis. 53BP1 bodies appear to localise to the same genomic loci that rupture during chromosome condensation upon entry into mitosis, as silencing the condensin subunit SMC2 reduces both mitotic DNA damage and 53BP1 body formation in cells under replication stress (Lukas et al., 2011a). Interestingly, silencing BLM (which results in elevated ultra-fine bridge formation (Chan et al., 2009)) also increases the frequency of these nuclear bodies, despite only a small increase in prometaphase DNA damage. This suggests a role for BLM in the resolution or processing of ultra-fine bridges during anaphase to prevent breakage and 53BP1 body formation at fragile sites (Lukas et al., 2011a).

All these phenotypes, while intimately associated with replication stress, are indirect measures. To directly assess DNA replication, single DNA molecules can be analysed using DNA combing, following sequential labelling with two different labelled thymidine analogues (Bensimon et al., 1994). This technique allows the direct assessment of multiple facets of DNA replication, including replication fork progression rate, inter-origin distance, fork stalling, termination, restart and sister fork asymmetry.

Replication stress may perturb any or all of these measures (Ozeri-Galai et al., 2011, Bester et al., 2011, Davies et al., 2007, Bartkova et al., 2005).

Replication stress therefore results in a range of cellular phenotypes, manifesting throughout the cell cycle, from direct evidence of replication defects in S-phase, chromosomal aberrations and ultra-fine bridges in mitosis, and 53BP1 nuclear bodies in G1 cells. Increased reliance on recombination mediated repair of damaged replication forks in cells under replication stress, as well as the generation of DSBs following replication fork collapse, is likely to generate structurally abnormal chromosomes at an increased rate, leading to chromosome missegregation at anaphase (see Figure 1.5).

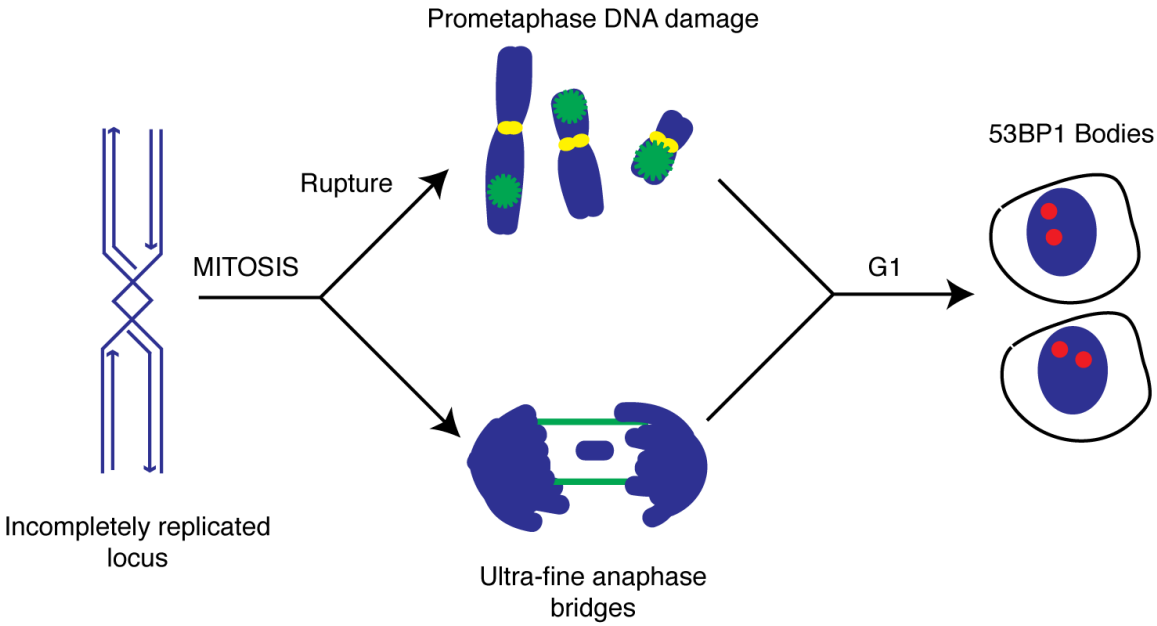

Figure 1.11 Replication stress associated phenotypes
Schematic showing the manifestation of genomic loci under replication stress in mitosis as prometaphase DNA damage foci and ultra-fine bridges, and then in G1 as 53BP1-positive nuclear bodies.

1.10 Defects in chromosome assembly

As described above, defects in maintaining the structural integrity of DNA may result in gross chromosomal rearrangements after DNA damage. However, chromosomes may also be rendered unstable if the assembly of compacted chromosomes, which are necessary for accurate segregation in mitosis, is disrupted.

Cohesion is established during S phase, behind the replication fork, and functions to hold sister chromatids in close apposition. The cohesin complex has pleiotropic functions in transcription, DNA repair, replication, telomere maintenance and in mitosis (Mannini et al., 2010, Sherwood et al., 2010, Hsiao and Smith, 2009). Cohesion between sister chromatids is essential for accurate formation of kinetochore-microtubule attachments during mitosis (Ng et al., 2009, Jaqaman et al., 2010). Defects in sister chromatid cohesion result in chromosome missegregation and mutations in various cohesin components have been identified in multiple tumour types (See section 1.16.1.2) (Solomon et al., 2011, Barber et al., 2008). However, it is not yet clear which functions of cohesin are implicated in the CIN phenotype, nor whether the identified mutations have any functional consequences. An interesting study in yeast, in which the amount of cohesin subunits was decreased in a graded fashion, has indicated that chromosome condensation, DNA repair and the stability of repetitive DNA elements such as telomeres are more easily perturbed by cohesin disruption than chromosome attachment in mitosis (Heidinger-Pauli et al., 2010). CIN may also be generated by failure to remove cohesin, as persistent cohesion at telomeres can result in sister chromatid fusions by non-homologous end joining (Hsiao and Smith, 2009) (see section 1.9.3). Hence cohesin defects might primarily result in structural chromosome defects rather than defective chromosome attachment during mitosis through defective chromosome assembly (Gordon et al., 2012).

Upon entry into mitosis, DNA is compacted into chromosomes. Defects in this process result in elevated DNA catenation, and chromosome segregation errors (Lukas et al., 2011a). Persistent catenation induced by topoisomerase inhibition results in chromosome segregation defects in human cells, which may explain anaphase bridges and lagging chromosomes observed in cells depleted of condensin subunits (Samoshkin et al., 2009, Lukas et al., 2011a, Cimini et al., 1997). Similarly, defects in the catenation checkpoint result in chromosome abnormalities and missegregation (Deming et al., 2001). Alternatively, condensation defects may provoke the formation of improper kinetochore-microtubule attachments through defective centromere specification (Samoshkin et al., 2009).

Hence, in addition to pre-mitotic generation of structurally abnormal chromosomes through DNA damage, defects in chromosome assembly may also cause

chromosome segregation errors, generating both lagging chromosomes and anaphase bridges. It is unclear whether condensin or decatenation defects would generate acentric chromosomes.

1.11 Pre-mitotic mechanisms of CIN – summary

From the above discussion, it is evident that there are multiple different pathways through which structural chromosome aberrations may arise, affecting DNA repair, replication and telomere maintenance. Aberrant DNA replication or repair of DNA damage may result in the generation of chromosome fusions and acentric chromosome fragments that may then go on to missegregate during mitosis, in addition to generating rearrangements that do not affect the accuracy of chromosome segregation at anaphase.

1.12 Can one mechanism explain structural and numerical CIN?

Both SNP array and spectral karyotyping based measures indicate a highly significant correlation between structural and numerical chromosomal complexity in CIN+ tumour cells (Roschke et al., 2003, Lee et al., 2011). This co-occurrence implies that rather than being driven by distinct mechanisms, structural and numerical CIN might reflect the same underlying mechanism. One possibility is that structural and numerical CIN are driven simultaneously by the same molecular defect, but occur independently of one another. A second possibility is that structural chromosome defects result in numerical CIN or vice versa. These mechanisms are not mutually exclusive, and indeed it is likely that both might occur in CIN+ cells.

Single gene defects can independently affect both chromosome number and structure, as some proteins have roles in both DNA replication and repair as well as in mitosis. In addition, delays in interphase or defects in DNA damage repair can affect the centriole duplication cycle, simultaneously generating structural chromosome abnormalities and extra centrioles that may provoke missegregation of chromosomes during mitosis (Nigg and Stearns, 2011, Shimada et al., 2009, Shimada et al., 2010, McDermott et al., 2006). For example, loss of the retinoblastoma protein (Rb) can result in both structural alterations and mitotic defects, as Rb has a role in both the G1-S DNA

damage checkpoint and in regulating centriole duplication (Tort et al., 2006, Meraldi et al., 1999). Similarly, CHK2 and BRCA1 are reported to have roles in maintaining mitotic fidelity as well as in DNA damage signalling and repair (Stolz et al., 2010). In these situations, one mutation or gene deletion could result in the generation of structural chromosome defects during interphase, as well as whole chromosome missegregation during mitosis, independently of structural defects.

However, structural aberrations generated during interphase result in chromosome segregation errors, and furthermore these errors can lead to whole chromosome non-disjunction and numerical chromosomal instability (Baxter and Diffley, 2008, Pampalona et al., 2010b, Stewenius et al., 2005, Pampalona et al., 2010a, Gisselsson et al., 2001). Kinetochore-microtubule attachments of anaphase bridges may detach during anaphase, resulting in chromosome non-disjunction (Pampalona et al., 2010b, Stewenius et al., 2005), while experiments in both mammalian cells and yeast have demonstrated that persistent DNA catenation resulting from topoisomerase dysfunction results in lagging chromosomes (Baxter and Diffley, 2008, Cimini et al., 1997).

Conversely, it has recently been shown that segregation errors may be subject to DNA damage if trapped in the cytokinesis furrow or if they form micronuclei (Crasta et al., 2012, Janssen et al., 2011). Cytokinesis-mediated damage to drug-induced lagging chromosomes resulted in chromosome translocations in RPE1-hTERT cells (Janssen et al., 2011). However, these translocations occurred in less than 6% of cells, despite a chromosome segregation error frequency of 80%, suggesting that this mechanism of generating structural aberrations may occur relatively rarely. In a second study, it was demonstrated that micronuclei resulting from lagging chromosomes may be incompletely replicated prior to the next mitosis, resulting in massive chromosome fragmentation (Crasta et al., 2012). In this study, no chromosome translocations were identified, despite use of the same cell line, further supporting the contention that translocations as a result of cytokinesis-induced damage are rare.

It is yet to be examined whether this post-mitotic DNA damage contributes to CIN in cancer cells. Both of the described mechanisms (cytokinesis-mediated damage and micronucleus fragmentation) would presumably affect segregation errors of all origins, both mitotic and pre-mitotic. Indeed this mechanism of damage might be predicted to be more likely to affect acentric chromosome fragments and anaphase

bridges, which are more likely to remain in the cytokinesis furrow than lagging chromosomes, and which also form micronuclei (Pampalona et al., 2010a, Baxter and Diffley, 2008, Acilan et al., 2007, Stewenius et al., 2005, Pampalona et al., 2010b).

1.13 Mechanisms of CIN – summary

CIN can clearly be generated through a range of mechanisms, affecting DNA integrity and chromosome structure during interphase or chromosome attachment to the spindle in mitosis. It is unclear whether mitotic or pre-mitotic dysfunction drives the majority of segregation errors in CIN+ cells, or even if there is a consistency in the pattern of CIN observed between different tumours of the same tissue type. To date, most investigations of mechanisms driving CIN have been in small numbers of cell lines, of mixed tissues of origin, probably leading to undue extrapolation about the mechanisms responsible for CIN in cancer. Consistent patterns of genomic change between cancers of the same subtype, and indeed across all cancers suggest that there may be common mechanisms, but to establish this will require in depth analysis of CIN and associated defects in cancer cells, rather than experimentally-induced chromosomal instability. Colorectal cancer has been used widely to study CIN, and therefore represents an ideal subtype in which to examine the array of possible driving mechanisms.

1.14 Genetic instability in colorectal cancer

Colorectal cancers can be broadly subdivided into two classes according to the type of genetic instability observed. The majority (80-85%) display chromosomal instability, while between 15-20% display defective mismatch repair and consequent microsatellite instability (MSI/MIN). Microsatellite instability only rarely co-occurs with CIN (Grady and Carethers, 2008, Lengauer et al., 1997). The molecular basis for MSI is well understood, but mechanisms and genetic changes responsible for CIN in CRC remain unclear. In a meta-analysis of 10,126 colorectal cancer patients, tumour aneuploidy was used as a surrogate measure for CIN and found to be associated with a worse prognosis (Walther et al., 2008). In addition, CIN predicted colon cancer recurrence, independently of tumour stage (Mettu et al., 2010). Therefore, as in other cancer types, CIN is associated with poor patient outcome in colorectal cancer.

1.15 Microsatellite instability

The 15-20% of colorectal tumours displaying microsatellite instability achieve this through either mutational inactivation of mismatch repair (MMR) components (MSH2, MLH1, MSH6, PMS2) or by gene-silencing through promoter methylation (MLH1). Microsatellite instability is responsible for an inherited form of colon cancer (hereditary non-polyposis colon cancer, also called Lynch syndrome) in which affected individuals harbour heterozygous germline mutations in components of the mismatch repair machinery. The genomic alterations causing Lynch syndrome, and their relative frequencies, are summarised in Table 1.3. Loss of the wild-type allele unleashes microsatellite instability, elevating the mutation rate and promoting carcinogenesis in a range of organs, including the colon. Microsatellite instability is also observed in sporadic colorectal cancer, through hyper-methylation of the *MLH1* promoter, resulting in lack of expression of this key component of the mismatch repair machinery (Herman et al., 1998, Veigl et al., 1998, Kane et al., 1997).

Microsatellite instability is evident as heterogeneous expansions and contractions of repetitive sequence elements (microsatellites) across the cell population, as well as an elevated frequency of point mutations. The mutation rate at the *HPRT* locus was measured in MSI versus microsatellite stable colorectal cancer cell lines, and was found to be up to 100-fold higher in MSI cell lines (Eshleman et al., 1995). Clinically, tumours with MSI are identified through immunohistochemical staining for MMR components, and through the observation of instability over at least two of a panel of five different microsatellites across the genome, defined in the revised Bethesda guidelines (Umar et al., 2004).

MMR Gene	Chromosomal Location	MMR Partners	Lynch Syndrome germline mutation (%)
MSH2	2p15	MSH6, MSH3	31-45
MSH6	2p15	MSH2	5-8
MLH1	3p21	PMS2, MLH3, PMS1	32-49
PMS2	7p22	MLH1	0-2

Table 1.3 Mismatch repair genes commonly mutated in Lynch Syndrome
(Adapted from (Grady and Carethers, 2008))

1.16 CIN in colorectal cancer

1.16.1 Is there a mutational basis for CIN in colorectal cancer?

A genetic basis for CIN in colorectal cancer has remained elusive, despite the observation of aneuploidy in greater than 80% of colorectal tumours (Grady and Carethers, 2008). As described in Section 1.8, staining for markers of DNA damage is observed in both pre-malignant colorectal adenomas and in adenocarcinoma, suggesting that genome instability occurs relatively early in cancer development (Bartkova et al., 2005, Gorgoulis et al., 2005, Grady and Carethers, 2008). Whether mitotic or pre-mitotic mechanisms account for CIN in colorectal cancer has not been resolved. Mutations have been identified at low frequencies in genes encoding components of the mitotic checkpoint, cohesin complex, and DNA damage response, which are discussed below.

1.16.1.1 MRE11A mutations

Mutations have been identified in the *MRE11A* gene, although all but one tumour in this study harboured only heterozygous mutations (Wang et al., 2004b). MRE11 loss or silencing results in structural chromosomal abnormalities and aneuploidy (Buis et al., 2008, Barber et al., 2008) but mouse embryonic fibroblasts with only one copy of MRE11 behave similarly to wild-type fibroblasts, implying that MRE11 does not act in a haploinsufficient manner (Buis et al., 2008). Intronic splice-site mutations, which reduce MRE11 expression levels, have also been reported in MSI colorectal cancer (Giannini et al., 2004). These mutations are incompletely penetrant, and wild-type transcript is still produced, albeit at lower levels. Mutations were identified in 84% of MSI tumours, and 38% harboured biallelic mutations (Giannini et al., 2004). However, as there is residual expression of wild-type MRE11 in the context of either monoallelic or biallelic mutation, the functional implications of these mutations in MSI tumours are unclear (van der Heijden et al., 2006).

1.16.1.2 Cohesin Subunit mutations

A study that sequenced the human homologues of genes identified as potential CIN genes in yeast identified mutations in cohesin subunits (*SMC1L1, SMC3, NIPBL*

(homologue of yeast Scc2), *STAG3* (homologue of yeast Scc3) (Barber et al., 2008). Mutation in one of these subunits was identified in 10/132 colorectal tumours sequenced (7.5%). Again, however, these mutations were heterozygous, and the functional consequences of the single amino acid changes (which constituted 9 of the 10 mutations identified) are not known. Furthermore, the tumours were not classified according to CIN status prior to sequencing. Recently mutations in the cohesin subunit *STAG2* were found in a diverse range of tumours (Solomon et al., 2011). As *STAG2* is on the X chromosome, only one mutational event is required for inactivation. However, in this study, just 2/74 (3%) colorectal cancers were identified that lacked STAG2 protein by immunohistochemistry (Solomon et al., 2011).

1.16.1.3 Mutations in mitotic checkpoint components

As described in section 1.3.3, heterozygous mutations in checkpoint gene *BUB1* have been identified in two CIN+ colorectal cancer cell lines, which act in a dominant negative fashion (Cahill et al., 1998). Later work from the same laboratory found mutations in genes encoding the ZW10, ROD and ZWILCH proteins, which localise to the kinetochore and function in the mitotic checkpoint by anchoring MAD1 (Wang et al., 2004b, Kops et al., 2005). However, the majority of CIN+ cell lines examined thus far appear to have a functional mitotic checkpoint (Tighe et al., 2001, Gascoigne and Taylor, 2008), suggesting that mutations in mitotic checkpoint components may be rare events.

1.16.1.4 APC mutations

The *APC* (Adenomatous Polyposis Coli) gene is one of the most frequently mutated genes in colorectal cancer. The APC protein regulates Wnt signalling, which controls the ordered growth of colonic crypts. Mutant APC deregulates this ordered growth (Wasan et al., 1998). The C terminus of APC interacts with the microtubule plus-end binding protein EB1 (Su et al., 1995), and a number of *in vitro* studies have implicated mutant APC in chromosomal instability (Tighe et al., 2001, Smith et al., 1994, Kaplan et al., 2001, Green and Kaplan, 2003, Fodde et al., 2001, Bakhoum et al., 2009a, Rusan and Peifer, 2008). In one mouse study, evidence of tetraploidy and abnormal mitosis was found in the small intestines of *APC* mutant mice (Caldwell et al., 2007). However,

CIN was not observed in another study of mice carrying various different *APC* mutations, including a C-terminal mutation that abrogates microtubule binding (Lewis et al., 2012). Furthermore, analysis of the relationship between *APC* mutations and CIN does not support a role for *APC* mutation in driving CIN in human tumours (Sieber et al., 2002, Rowan et al., 2005, Jallepalli and Lengauer, 2001), and in addition, a substantial proportion of MSI colorectal tumours also harbour *APC* mutations (Homfray et al., 1998). Together these data suggest that CIN associated with *APC* mutation may be an *in vitro* phenomenon.

1.16.1.5 FBXW7 (CDC4) mutations

FBXW7 is a ubiquitin ligase responsible for cyclin E degradation, among other substrates (Welcker and Clurman, 2008). *FBXW7* mutations were identified in 22 of 190 colorectal tumours (11.6%) and six tumours showed biallelic inactivation (Rajagopalan et al., 2004). Upon targeted disruption of *FBXW7* in diploid CIN- HCT-116 and DLD1 colorectal cancer cells, the authors observed nuclear atypia and micronucleation, as well as mitotic delay, effects that seemed to be mediated through cyclin E over-expression. The same group subsequently found that sister chromatid cohesion was affected by *FBXW7* loss (Barber et al., 2008). However, these phenotypes were not observed in cells with only one allele disrupted and it is unclear what the consequences of the specific mutations would be for genome stability (Barber et al., 2008, Rajagopalan et al., 2004). It has been suggested that mutations identified in *FBXW7* may act in a dominant negative fashion, hence heterozygous mutations may be sufficient to drive loss of function (Welcker and Clurman, 2008). However, in another study, in which 18/284 (8%) tumours harboured mutations in *FBXW7,* no association was found between these mutations and CIN (determined by DNA index) (Kemp et al., 2005). Recently, it has been shown that double *Fbw7/Tp53* knockout mice develop tumours that display CIN, suggesting that Fbw7 (FBXW7 in mice) loss may only cause CIN in the context of P53 mutation (Grim et al., 2012).

1.16.1.6 TP53 Mutations

TP53 encodes the p53 protein, a key component of the cellular response to DNA damage (see section 1.8.3)(Bunz et al., 1998), which is also implicated in aneuploidy

tolerance (Thompson and Compton, 2010, Andreassen et al., 2001). P53 is mutated in approximately half of colorectal cancers (Katkoori et al., 2012, Lopez et al., 2012, Rodrigues et al., 1990). However, inactivation of p53 does not result in aneuploidy or chromosomal instability (Bunz et al., 2002), and P53 mutations occur in some MSI cancers (Lee et al., 2011, Katkoori et al., 2012), indicating that TP53 mutations may be involved in the tolerance of CIN/aneuploidy rather than in driving instability itself.

The relationship between the majority of the mutations described above and CIN in colorectal cancer is not clear; many mutations were heterozygous (Wang et al., 2004b, Barber et al., 2008), and there are conflicting reports concerning the association of these mutations with CIN in vivo (Sieber et al., 2002, Kemp et al., 2005, Giannini et al., 2002). In addition, in the two largest studies seeking to identify mutations in 'CIN genes' (Wang et al., 2004b, Barber et al., 2008), it is not clear whether the tumours were classified according to MSI/CIN status prior to sequencing. However, if these mutations do contribute to CIN *in vivo*, they account for only a minority of tumours and hence the molecular basis for CIN in the majority of tumours remains elusive (Wang et al., 2004b, Barber et al., 2008, Rajagopalan et al., 2004, Kemp et al., 2005, Grady and Carethers, 2008). Recently exome sequencing, DNA copy number, mRNA expression and promoter methylation data were published for 276 colon and rectal tumours, which were classified as either hyper-mutated (with microsatellite instability) or non-hypermutated (and likely to harbour CIN) (TCGA, 2012). Table 1.4 shows the frequency of mutations in the genes described above, which have been linked to CIN in CRC, in both hyper-mutated and non-hypermutated colon and rectal cancers from this study. In addition, frequencies of mutations in other genes with known roles in colorectal tumorigenesis are included.

1.16.2 Recurrent copy number changes in CIN colorectal cancer

Numerous studies have identified recurrent copy number gain and loss events in CIN+/aneuploid CRCs, with recurrent gains in chromsomes 7, 8, 13 and 20q, and losses in 4, 8p, 14q, 17p, and 18q (Sheffer et al., 2009, Diep et al., 2006, Nakao et al., 2004, Tsafrir et al., 2006, Watanabe et al., 2001, Jen et al., 1994). The two most frequent genomic losses are on 17p and 18q. 17p is the genomic location for TP53. Chromosome

18q encodes two tumour suppressor genes SMAD4 and DCC, and multiple other genes whose expression is downregulated following copy number loss, which may have roles in colorectal cancer (Bacolod and Barany, 2011, Fearon et al., 1990, Vogelstein et al., 1988). SMAD4 regulates transcription downstream of TGF-beta (transforming growth factor) signalling. Mutations in SMAD4 occur in only a minority of tumours and SMAD4 has not been implicated in the suppression of CIN (Takagi et al., 1996, Bass et al., 2011). Similarly, DCC mutations occur only in a minority of tumours, and DCC loss has not been implicated in CIN. DCC is a dependence receptor that induces apoptosis in the absence of its ligand netrin-1; it appears that the tumour suppressive effect of DCC is dependent on the ratio of ligand to receptor (Goldschneider and Mehlen, 2010). Genetically silencing the pro-apoptotic activity of DCC in the context of APC mutation leads to increased tumour formation and more aggressive tumours (Castets et al., 2012).

18q loss has been associated with poor prognosis in multiple studies in CRC and other tumour types, including esophageal, gastric, breast, head and neck, prostate and pancreatic cancers (Popat and Houlston, 2005, Sheffer et al., 2009, Watanabe et al., 2001, Jen et al., 1994, Pasello et al., 2008, Furuya et al., 2000, Bauer et al., 2008, Yatsuoka et al., 2000, Huiping et al., 1998, Tsuda et al., 1998, Latil et al., 1994). Loss of 18q has been previously implicated in CIN and aneuploidy in CRC, leading to suggestions that this chromosome arm harbours genes that encode one or more aneuploidy suppressors (Rowan et al., 2005). It has been suggested that this association cannot solely be accounted for by loss of SMAD4 or DCC, as there are multiple genes whose expression correlates with both copy number and poor prognosis in CRC (Bacolod and Barany, 2011). Supporting the hypothesis that large copy number losses in tumour cells may arise through selection for repression of multiple genes (as opposed to just one tumour suppressor) a recently published study used RNA interference to identify a cluster of tumour-suppressive genes encoded on chromosome 8p, which is frequently lost in human cancers (Xue et al., 2012).

	% Hyper-mutated samples (n=35)	% Non-hypermutated samples (n=189)
DNA damage/ replication/repair		
MRE11A	9	0
FBXW7	46	11
TP53	20	60
ATM	40	6
Mitotic checkpoint		
ZW10	3	<1
KNTC1	11	<1
ZWILCH	11	0
BUB1	11	1
Cohesin subunits		
SMC1A	20	1
SMC3	9	0
NIPBL	37	1
STAG3	11	1
STAG2	11	1
Other		
APC	51	80
Other CRC genes		
SMAD4	20	10
DCC	23	2
CTNNB1	6	5
TCF7L2	31	9
EGFR	23	1
ERBB2	11	3
KRAS	31	44
NRAS	9	9
BRAF	46	3
PIK3CA	34	17
PTEN	17	1

Table 1.4 Mutations in CRC
Frequencies of mutations in the indicated genes in colon and rectal tumours subjected to exome sequencing (TCGA, 2012). Tumours were classified as hyper-mutated (of which >75% were MSI+) or non-hypermutated (MSS and therefore likely to be CIN). Genes shown in red are more frequent in non-hypermutated tumours. Genes were selected based on prior association with CIN in CRC or due to their prevalence in CRC in general (other CRC genes).

1.17 Conclusion

Cancer chromosomal instability is a high-risk clinical phenotype, associated with drug resistance and tumour relapse. CIN+ cancers exhibit highly complex karyotypes with both structural and numerical aberrations, and an elevated rate of chromosome segregation errors at anaphase. Chromosome segregation errors can arise as a consequence of interphase and mitotic dysfunction, both of which are able to generate structural and numerical chromosome abnormalities, although traditionally segregation errors have been perceived as a consequence of mitotic defects. However, which mechanisms are chiefly responsible for CIN in tumour cells has not been evaluated. The genomic basis for CIN in the majority of tumours also remains elusive.

This thesis explores the mechanistic basis for chromosomal instability in colorectal cancer. First, the causes of chromosome segregation errors in CIN+ colorectal cancer cell lines were examined, revealing a central role for replication defects that generate structural chromosome abnormalities in colorectal cancer CIN. Subsequently, genes encoded on chromosome 18q were investigated for a function in maintaining genome stability, as this locus is subject to frequent somatic copy number loss in CIN+ colorectal cancer. Through this approach, three novel regulators of genome stability were identified. The mechanisms by which silencing these genes induce chromosomal instability were explored, again revealing replication defects as the likely cause of chromosome segregation errors. Finally, using the mechanistic insights gained through this approach, a strategy to reduce instability in CIN+ colorectal cancer cell lines was tested.

Chapter 2. Materials & Methods

2.1 Cell lines

All cells were maintained at 37 ^{o}C with 5% CO_2. DLD1, GP2D, HCT116, HT29, HT55, LS174T, RKO, SW620, SW1116, SW1463, and T84 cells were cultured in Dulbecco's Modified Eagle Medium (D-MEM) (1X), liquid (High Glucose) with L-Glutamine (Gibco, Invitrogen). NCIH747 and NCIH508 cells were cultured in RPMI-1640 media with L-Glutamine (Gibco). RPE-1-hTERT cells were cultured in F-12 Ham Media (Sigma), supplemented with HEPES and sodium bicarbonate (Sigma). All media was supplemented with 10% foetal bovine serum (FBS – PAA laboratories, Austria) and 1/10000 units of Penicillin-Streptomycin (Sigma).

2.1.1 Cell line classification

Cell line ploidy had been previously assessed by flow cytometry (DNA index), in the laboratory of Professor Ian Tomlinson. Microsatellite instability status had also been determined previously, using microsatellite PCR and through assessment of mutation/methylation status of mismatch repair genes. It has previously been shown that ploidy correlates with numerical and structural karyotypic complexity, two karyotypic features indicative of chromosomal instability (Lee et al., 2011, Roschke et al., 2003). Thus cell lines with a DNA index of <1.2 were all MSI+, and were classified as CIN-. Cell lines with a DNA index >1.2 were classified as CIN+. One CIN+ cell line (LS411N) was also MSI+. Flow cytometry ploidy values were corroborated by median copy number estimates from SNP array analysis ((Lee et al., 2011) and see Section 2.11.2). A number of the cell lines included in the panel have also been previously characterised for CIN status using clonal FISH (see section 2.4) and these were correctly classified as CIN+ or CIN- using DNA index and MSI status (Lengauer et al., 1997, Roschke et al., 2003, Thompson and Compton, 2008). Table 3.1 in Chapter 3 summarises the key characteristics of the cell lines used in this thesis.

2.2 Transfections

2.2.1 Plasmid preparation

Plasmids were incubated with ultra-competent XL-10^{TM} gold bacteria (Agilent) on ice for 30 minutes, heat-shocked at 42^{o}C for 45 seconds and then put on ice for 2 minutes. Bacteria were then incubated in a shaking incubator at 37^{o}C for 1 hour in SOC medium. Bacteria were then spread onto agar containing the appropriate antibiotics and incubated at 37^{o}C overnight to allow colony growth. Colonies were picked and amplified in L-broth for DNA preparation using the Qiagen Cartridge Midi/Maxi Kit, according to the manufacturer's instructions. DNA quality and concentration was assessed using a NanoDrop®.

2.2.2 Plasmid transfections

HCT116, DLD1, RKO, SKCO1, HT29 and SW620 cells were transfected with pH2B-mRFP (gift from Anne Straube) using Fugene 6.0 (Promega). Per 10 cm^2 dish of 70% confluent cells to be transfected: 9 µl of Fugene was incubated with 300 µl optiMEM (Gibco) for 5 minutes, before addition of 3 µg of DNA and further incubation for 15 minutes. Transfection mix was then added to cells in 6 ml of culture media. After two days, cells were split into 4 dishes and placed under selection with 1 mg/ml G418 for 2-3 weeks. Cells were then harvested and flow-sorted for mRFP expression using a MoFlo1 cell sorter (top 10% of cells expressing mRFP, excluding the brightest 5% of cells, as these are likely to be dead or dying cells). All stable cell lines expressing H2B-mRFP were maintained long-term in 500 µg/ml G418.

2.2.3 SiRNA transfections

All siRNAs were siUPGRADE SMARTpools of 4 distinct siRNA sequences, from Dharmacon (Thermo Scientific). SiRNA stocks were dissolved in 1 x siRNA buffer (Thermo Scientific) at 20 µM. All transfections were performed by reverse transfection at 40 nM, using Lipofectamine RNAi-max (Invitrogen). For 1 well of a 6-well plate: 3 µl siRNA was diluted in 197 µl optiMEM (Gibco) and incubated for 5 minutes. Simultaneously, 4 µl of Lipofectamine RNAi-max was added to 196 µl optiMEM, and incubated for 5 minutes. The two solutions were then combined in a 1:1 ratio, and

incubated for a further 25 minutes, before adding to cells and culture media up to a final volume of 1.5 ml. Cell seeding densities were as follows: 1.5 x 10^5 cells/well (HCT-116 and DLD1), 2 x 10^5 cells/well (RKO), 4 x 10^5 cells/well (NCIH508).

2.3 Immunostaining

2.3.1 Immunofluorescence on coverslips

Cells were grown on coverslips (22 x 22 mm) coated with poly-L-lysine. Media was removed, coverslips were washed in 1 x PBS and then simultaneously fixed and permeabilised in PTEMF buffer for 10 minutes at room temperature. Coverslips were then washed in 1 x PBS, and blocked in 3% BSA in PBS for 1 hour at room temperature or overnight at 4^{o}C. Coverslips were then transferred, cells facing upwards, onto glass plates covered in Nescofilm (Nesco). Cells were incubated with 150 µl/coverslip of primary antibodies diluted in 3% BSA-PBS for 1 hour at room temperature. Primary antibodies used in this thesis are summarised in Table 2.1. Coverslips were washed 3 x in PBS, before incubation with fluorescently-labelled secondary antibodies and 4',6-diamidino-2-phenylindole (DAPI - to stain DNA), diluted in 3% BSA-PBS for 1 hour at room temperature. Secondary antibodies (Molecular probes, used at 1:500): Goat anti-mouse conjugated to AlexaFluor(AF)488 (A11017), goat anti-rabbit AF594 (A11012), goat anti-human AF647 (A21445). DNA was stained with DAPI (Roche). Coverslips were then washed 3 x in PBS, mounted onto glass slides in Vectashield (Vector H-1000), and sealed with nail varnish.

PTEMF:
4% formaldehyde
20 mM PIPES
10 mM EGTA
1 mM $MgCl_2$

Antibody target	Supplier/Catalogue number	Species	Dilution	Notes
α-tubulin	Sigma T6074	Mouse	1:1000	
Hec1	Abcam Ab3613	Mouse	1:1000	
Centrin3	Abcam Ab54531	Mouse	1:1000	
Cyclin A1	Santa Cruz sc-56299	Mouse	1:350	
Phosphorylated histone H2A.X (Ser 139)	Millipore 05-636	Mouse	1:500	Use 1:1000 on chromosome spreads
RPA (p34)	Neomarkers MS-691	Mouse	1:500	Discontinued by supplier
IdU	BD Clone B4 347580	Mouse	1:1000	DNA fibres
MAD2	Covance PRB-452C	Rabbit	1:500	
53BP1	Santa Cruz sc-22760	Rabbit	1:500	
β-tubulin	Abcam ab6046	Rabbit	1:1000	
CldU	Oxford Biotech BU1/75	Rat	1:1000	DNA fibres
Centromere/ CREST	Antibodies Incorporated	Human	1:1000	

Table 2.1 Antibodies used for immunofluorescence

2.3.2 Immunofluorescence on chromosome spreads

Cells at 70% confluency were treated with 100 μg/ml Colcemid for 1 hour prior to trypsinisation and centrifugation (1000 rpm, 5 minutes). After washing in PBS, cells were resuspended in hypotonic buffer for 5 minutes (HCT116, SW620) or 10 minutes (HT29, HT55, SW1116). Cells were cyto-centrifuged onto glass slides at 2200 rpm for 10mins, in a CytoTek cytospinner. Slides were fixed in 4% formaldehyde in PBS for 10 minutes, followed by permeabilisation in KCM buffer for 10 minutes at room temperature. Slides were blocked for 15 minutes at 37^{o}C in antibody dilution buffer with 100 μg/ml RNase A (Sigma). Slides were then incubated with primary antibodies diluted in antibody dilution buffer, for 1 hour at room temperature, in a humidified chamber. Slides were washed in 1xPBS 0.1% Tween-20 (PBS-T) and then incubated with secondary antibodies and DAPI, diluted in antibody dilution buffer, for 30 minutes at room temperature in humidified chamber. Slides were rinsed in PBS-T and fixed for 10 minutes in 4% formaldehyde. Slides were then dehydrated through an ethanol series (70% - 3 minutes, 90% - 2 minutes, 100% - 1 minutes) and allowed to air dry, before mounting in Vectashield under a coverslip, and sealing with nail varnish.

Hypotonic buffer:
0.2% KCl
0.2% Tri-Sodium Citrate

KCM buffer:
120mM KCl
20mM NaCl
10mM Tris (pH 7.5)
0.1% Triton X-100

Antibody dilution buffer:
20mM Tris
2% BSA
150mM NaCl
0.1% Triton x-100

2.3.3 DNA fibre assays

DNA fibre assays were performed by Dr Petra Groth and Marie-Christine Weller in the laboratory of Professor Thomas Helleday, as described in (Groth et al., 2010).

Briefly, cells were plated 72 h before harvesting for fibre analysis. To measure replication rates, cells were pulse-labelled with 25 μM CldU (Sigma, C6891-100MG) diluted in media for 30 minutes followed by a 30-minute pulse of 250 μM IdU (Sigma I7125-5G). Cells were scraped and harvested in cold PBS, spun down, counted, and diluted to a concentration of 1×10^6 cells/ml. 2 μl of cell suspension, together with spreading buffer (200 mM Tris–HCl, pH 7.4, 50 mM EDTA and 0.5% SDS) was put on a microscope slide and incubated for a few minutes to lyse the cells. The slide was then tilted to spread the DNA fibres over the slide. Slides were then air-dried and the fibres were fixed on the slides with methanol/acetic acid (3:1). Immuno-staining of DNA fibres was done with the following antibodies: monoclonal rat anti-BrdU (Oxford Biotechnologies) for CldU and monoclonal mouse anti-BrdU (Becton Dickinson) for

IdU. Secondary antibodies used were goat anti-rat AlexaFluor 555 and goat anti-mouse AlexaFluor 488 (Molecular probes).

2.4 Fluorescence *in-situ* hybridization (FISH)

2.4.1 Sample preparation

2.4.1.1 Metaphase spreads

Cells were treated with 100 ng/ml Colcemid (GIBCO: cat #: 15210-040) for 1 hour prior to trypsinisation, centrifugation (1000 rpm, 5 minutes unless otherwise stated) and washing in PBS. Cells were resuspended in a small volume of PBS (100 µl) swelled with hypotonic KCl (0.4%) pre-warmed to 37^{o}C for 7 minutes, before centrifugation and fixation in 3:1 Methanol:Acetic acid. Centrifugation and resuspension in fixative were repeated until the fixative solution was clear of debris. Cells were dropped from height onto glass slides using a Pasteur pipette and aged for approximately 2 weeks prior to FISH.

2.4.1.2 Clonal FISH

500 cells were seeded in 1 ml media onto glass slides in 10 cm^2 dishes. After cells attached, 15 ml of media was added to the dish. Colonies of 30-60 cells were allowed to grow. Slides were treated with 0.4% KCl pre-warmed to 37^{o}C for 7 minutes, and fixed in 3:1 Methanol:Acetic acid for 30 minutes at room temperature. Slides were air-dried.

2.4.1.3 Cytokinesis block assay

0.5 x 10^5 HCT-116 cells were transfected at 40 nM in a final volume of 500 µl, and seeded onto glass slides in 10 cm^2. After 16 hours (to allow the cells to attach), 10 ml media was added. At 36 hours, cells were treated with 100 µM Blebbistatin (to block cytokinesis) or DMSO for 12 hours. Cells were then fixed in the same way as clonal FISH slides.

2.4.2 Probe hybridisation and analysis:

2.4.2.1 Clonal FISH

Slides were denatured at 70°C in 2X saline-sodium citrate (SSC)/75% Formamide for 2 minutes. After 2 minutes, slides were immediately quenched in ice-cold 70% Ethanol, and dehydrated through 85% and 100% Ethanol (1 minute in each solution). Per slide: 1 µl of each of two directly labelled centromere-specific DNA probes (Abbott Molecular probes) was added to 8 µl of hybridisation buffer (Abbott Molecular probes). Probes were denatured at 90°C for 6 minutes in a 1.5 ml eppendorf tube on a hot block. Slides were then hybridised to the probe solution under coverslips sealed with rubber cement (WeldTite) for 16 hours at 37°C in a humidified chamber. Slides were then washed in 50% Formamide/2X SSC and 2X SSC at 42°C (5 minutes per wash, 3 washes per solution), followed by 4X SSC (with 0.1% Tween20) and PBS washes for 5 minutes each at room temperature. Slides were dehydrated through an Ethanol series (70%, 90%, 100%, 1 minute each) and mounted in Vectashield hard set plus DAPI mounting medium (H-1500).

DNA probes directly labelled with fluorescent dyes were used to label the centromeres of chromosomes 2 and 15. Probes used were: CEP2 (D2Z1) Spectrum orange, CEP15 (D15Z1) Spectrum green (Abbott Molecular Probes). Chromosomes 2 and 15 were selected due to an analysis previously conducted in the laboratory, which found that these two chromosomes exhibited infrequent copy number changes in tumours, suggesting that they are good marker chromosomes for the background instability rate (Roylance et al., 2011).

2.4.2.2 Population FISH and Cytokinesis block assay

Metaphase spread slides (population FISH) or cytokinesis block assay slides were processed as described above for clonal FISH.

2.4.2.3 Metaphase Spreads (all human centromere probe):

Slides were pre-treated in 2X SSC plus 0.5% Tween20 for 15 minutes at 37°C, before dehydration through an Ethanol series (70%, 85% and 100%, 1 minute each). Slides

were air-dried at room temperature. Slides and probe (All human centromere alpha-satellite DNA probe labelled with FITC, Poseidon) were co-denatured under a 22 x 22 mm coverslip, sealed with rubber cement, at 75^{o}C for 10 minutes on a hot block. Hybridisation took place overnight in a humidified chamber at 37^{o}C. After hybridisation, rubber cement was removed, and slides rinsed in wash buffer II for 2 minutes at room temperature, to remove coverslips. Slides were then washed in Post-Wash buffer for 2 minutes at 72^{o}C, and then wash buffer II for 1 minute at room temperature. Slides were then dehydrated through an Ethanol series (70%, 85%, 100%) for 1 minute each, and allowed to air dry. Slides were then mounted in Vectashield hard set with DAPI.

Post-wash buffer
0.4X SSC
0.3% Tween20

Wash buffer II
2X SSC
0.1% Tween20

2.5 Microscopy

2.5.1 Image Acquisition

3D-image stacks were acquired in 0.2 μm steps using an Olympus Deltavision RT microscope (Applied Precision, LLC) equipped with a CoolSnap HQ camera. Deconvolution of image stacks and quantitative measurements was performed with SoftWorx Explorer (Applied Precision, LLC). Deconvolution was conservative, and ran for 8 cycles.

2.5.2 Image analysis

2.5.2.1 Segregation error classification

Cells were stained with antibodies against β-tubulin and with anti-centromere antibodies (see Table 2.1 Anaphase cells were identified according to tubulin staining pattern, to exclude telophase cells (see Introduction, Figure 1.2). Images (A stack of 100 images,

taken every 0.2 μM in order to capture the whole cell at high resolution) were acquired of cells with segregation errors. Segregation errors were then classified according to the following criteria, illustrated in Figure 2.1:

1. Lagging chromosomes were defined as chromosomes with one centromere signal that remained in the spindle midzone and were separated from the main body of segregating anaphase chromosomes (Figure 2.1i)
2. Acentric chromosome fragments were identified by a lack of centromere staining (Figure 2.1ii)
3. Anaphase bridges were identified as chromatin bridges connecting both bodies of segregating anaphase chromosomes (Figure 2.1iii)
4. Any segregation error that could not be classified according to the above criteria was classified as other. Segregation errors classified as 'other' included pairs of lagging chromosome linked by a DNA bridge, conglomerates of multiple chromosomes, and dicentric lagging chromosomes (Figure 2.1 iv-vi)

To quantify kinetochore distortion on lagging chromosomes, which indicates merotelic attachment, slides were stained with antibodies for NDC80, in addition to CREST serum and anti- β-tubulin antibodies. NDC80 signal was then scored as spherical or distorted. Monastrol washout was used as a positive control.

2.5.2.2 Structural chromosome abnormalities

Structural abnormalities identified on high-resolution images of metaphase spreads were classified as follows, illustrated in Figure 2.2:

1. Acentric – any chromosome lacking alpha-satellite probe signal, with signal clearly evident on surrounding chromosomes within the same chromosome spread, acting as an internal probe hybridisation control (Figure 2.2a)
2. Dicentric – any chromosome displaying two spatially-separated centromere signals. Some cell lines had conserved dicentric chromosomes across all metaphases, but one centromere signal did not display cohesion (Figure 2.2b). These constitutive events were not classified as dicentric chromosomes (see page 97)

3. Double strand breaks – any chromosome with an interstitial gap in a chromosome arm, or which had discrepant chromosome arm lengths (Figure 2.2c)
4. DNA strand linkage – chromosomes connected by a clear DNA strand linkage (Figure 2.2d)
5. Other – any chromosome abnormality not encompassed by above descriptions. These were primarily multivalent chromosome configurations, fragmented (or pulverised) chromosomes, chromosomes with appendages and paired homologous chromosomes (Figure 2.2e)

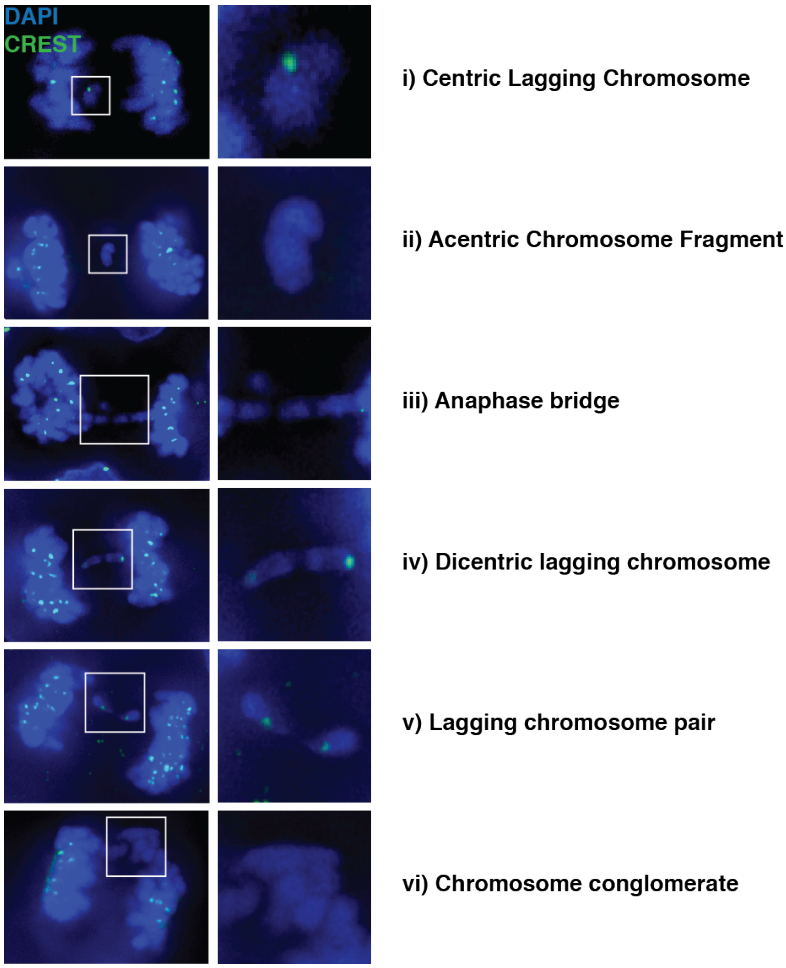

Figure 2.1 Segregation error classification
Anaphase cells exhibiting different types of segregation errors. Cells are stained with DAPI and anti-centromere antibodies (green). Right-hand panels are enlarged images of the boxed areas in the left-hand panels.

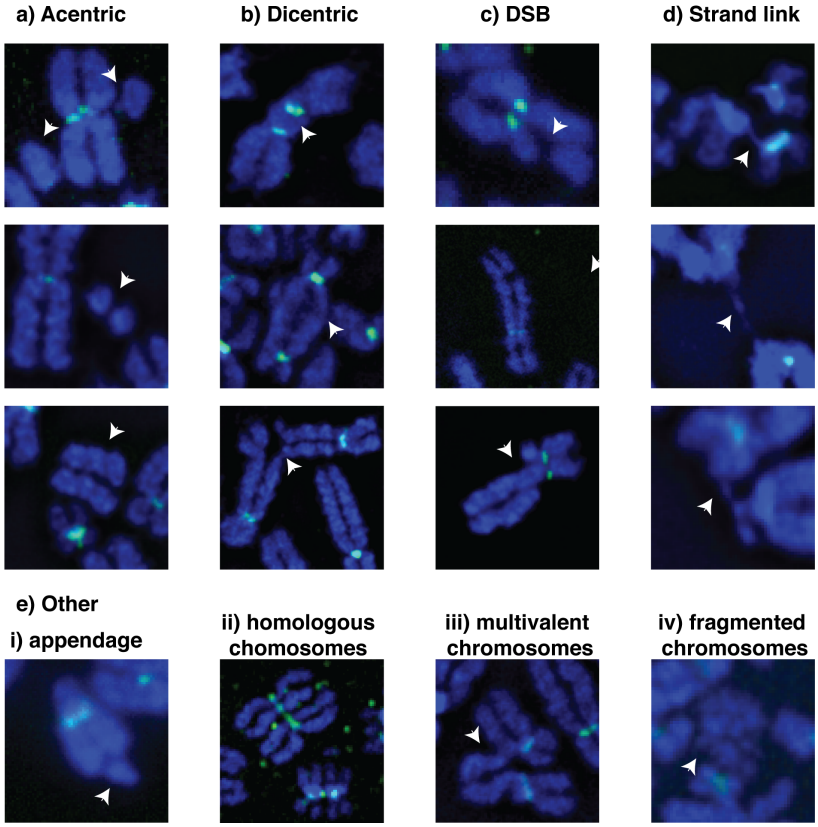

Figure 2.2 Structural abnormalities in metaphase chromosomes
Chromosome spreads hybridised to an All-centromere probe (green). Examples of different chromosome structural aberrations are shown, indicated by white arrowheads

2.5.2.3 Sister chromatid cohesion

The inter-centromere distance was measured manually in SoftWorx Explorer. This measurement has been previously used to assess sister chromatid cohesion (Rajesh et al., 2011). 5 chromatid pairs were measured per metaphase. 100 metaphases per cell line were then inspected for premature chromatid separation, visible as a gap between the two sister chromatids at the centromere (Solomon et al., 2011).

2.5.2.4 DNA damage on chromosome spreads

To assess telomere damage, chromosome spreads were identified that stained positively with both anti-γH2AX and anti-centromere antibodies (as an internal immuno-staining control). γH2AX foci were then scored for their location on chromosome arms. Foci were scored as either being interstitial along the chromosome arms, or being at the

termini of chromosome arms. Foci on acentric chromosomes were classified as interstitial. Equally, chromosomes with discrepant arm lengths displaying γH2AX on the end of the shortened arm were classified as interstitial. Foci on very short chromosome arms were not scored, as it was not possible to determine whether this damage was telomeric or interstitial.

2.5.2.5 DNA Fibres

Analysis was performed by Petra Groth and Marie-Christine Weller as described previously (Groth et al., 2010).DNA fibres were imaged by confocal microscopy. The lengths of CldU and IdU tracks were measured using ImageJ software and values were converted into kilobase pairs using the conversion factor 1 μm = 2.59 kb.

2.5.3 Time-lapse microscopy

Cells were seeded into 8- or 2-well chamber slides (Lab-Tek II) 24 to 48 hours prior to imaging. Imaging was performed with a Olympus Deltavision Personal microscope (API) equipped with a mCherry/eGFP filter set and environmental chamber, maintaining the cells at 5% CO_2 and 37^{o}C. Cells expressing H2B-mRFP were imaged using a using a 40x oil NA 1.3 objective, at 10% neutral density, 0.1 second exposure. Seven stacked images were acquired in 2 μm steps at each point.

2.5.3.1 Mitotic progression movies

0.25 x 10^5 cells were seeded (with or without siRNA reverse transfection) 48 hours prior to imaging. For transfected cells, media was changed after 24 hours. Cells were then imaged every 3 minutes for 6 to 8 hours. When imaging the central four wells of an 8-well chamber slide, a maximum of 9 geographical locations per well (39 points per experiment) could be imaged during the 3 minute time-lapse. Movies were analysed using SoftWorx Explorer. Mitotic cells were analysed for the timing of mitotic progression. Nuclear envelope breakdown was designated as the beginning of mitosis and anaphase onset was designated as the end of mitosis. The timing of chromosome congression and the delay between chromosome congression and anaphase onset were also scored (see page 103 for examples).

2.5.3.2 Mitotic checkpoint movies

0.25 x 10^5 HCT-116 H2B-mRFP cells were reverse transfected 48 hours prior to imaging. Cells were treated with Nocodazole (50 ng/ml) immediately prior to imaging. Cells were then imaged every 10 minutes for 8.5 hours. Only cells that entered mitosis within the first two hours were analysed, to ensure that mitotic arrest could be assessed for at least 6 hours.

2.6 Flow cytometry

2.6.1 Mitotic index:

Cells were trypsinised, harvested, and washed in phosphate-buffered saline (PBS) before fixation in 70% Ethanol. Cells were stained with mouse anti-MPM2 antibody (3:500 Millipore 05-368) overnight at 4^{o}C in 0.2% BSA-PBS prior to washing and incubation with secondary antibody (goat anti-mouse AF647, Molecular probes A21463) and DAPI. Samples were analysed using a BD LSR-II benchtop cytometer, and processed using FlowJo software. Cell cycle profiles were analysed by fitting to the Watson-Pragmatic model (Watson et al., 1987).

2.6.2 Mitotic checkpoint

CIN+ and CIN- cells were treated with 100 ng/ml Nocodazole or vehicle control for 8 hours and then harvested, fixed, stained and analysed as described in section 2.6.1.

2.6.3 G2-M Checkpoint

Cells were exposed to irradiation (20 Gy or 10 Gy) using a Cs137 Gamma Irradiator, and then incubated in Nocodazole for 16 hours prior to harvesting and staining as described in section 2.6.1. 50ng/ml Nocodazole was used for experiments confined to HCT-116 cells, while 100ng/ml for experiments comparing CIN+ and CIN- cell lines. As a positive control, control-transfected HCT-116 cells were treated with caffeine (5 mM) for 2 hours prior to exposure to irradiation and throughout the 16-hour recovery period.

2.6.4 Intra-S phase checkpoint

4 x 10^5 cells were reverse transfected in 6 cm^2 dishes. 48 hours after transfection, cells were pulsed labelled with EdU (10 μM - Invitrogen) for 30 minutes, prior to 30 minutes exposure to 1 μM Camptothecin (Sigma) or vehicle control. Samples were fixed at 0, 4, 6 and 8 hours, in 4% formaldehyde. EdU was detected using the Click-IT™ imaging kit (Invitrogen) according to the manufacturer's instructions, and DNA was stained with DAPI. Samples were analysed using a BD LSR-II benchtop cytometer and data was processed and analysed using FlowJo software. CHK1 inhibitor AZD7762 treatment was at 10 nM. AZD7762 was added simultaneously with the EdU labelling, and maintained throughout the rest of the experiment.

2.7 Miscellaneous cell treatments

2.7.1 Monastrol washout

Cells were treated with 100 μM Monastrol for 1 hour, to transiently block bipolar spindle formation and increase the formation of merotelic attachments. Cells were then gently rinsed in PBS (3 x 5 minutes), followed by a recovery period of 45 minutes in normal media, prior to fixation.

2.7.2 Irradiation

Irradiation was performed at the desired dose using a Cs137 Gamma Irradiator. 20 Gy and 10 Gy were used to assess G2-M DNA damage checkpoint, while 2 Gy was used to assess DNA damage foci formation.

2.7.3 Aphidicolin

Low concentration Aphidicolin treatment was at 0.2 μM for 24 hours, which slows but does not completely block replication, and induces expression of common fragile sites (Glover et al., 1984). To completely block replication in HCT116 cells, Aphidicolin was used at 2 μM.

2.7.4 Blebbistatin

Cells were treated with Blebbistatin (Sigma) at 100 μM. For the cytokinesis block FISH assay cells were treated for 12 hours and processed as described in section 2.4.1.3. For the 53BP1 body rescue assay, cells were treated for 4 hours, before PTEMF fixation and staining with antibodies for cyclin A1 and 53BP1.

2.8 Characterisation of genes encoded on chromosome 18q

2.8.1 siRNA transfections

The segregation error screen was performed in 12 well plates, using siRNA transfection conditions as described in section 2.2.3. HCT-116 cells were seeded at a density of 0.5 x 10^5 cells per well, onto poly-L-lysine (Sigma) coated coverslips. Dharmacon scrambled control no.2 was used as a negative control for the screen, and there was one control well per plate. After 48 hours cells were fixed in PTEMF and stained with antibodies for alpha tubulin and Anti-centromere antibodies (as described in section 2.3.1. 30 anaphases per siRNA pool were scored manually for the presence of segregation errors. SiRNA sequences for PIGN, RKHD2, ZNF516, as well as CCDC68 and CCDC102B, are shown in Table 2.2.

2.8.2 RNA extraction and RT-qPCR

RNA was extracted using the Qiagen RNeasy kit according to the manufacturer's instructions. Reverse transcription was performed using the First strand cDNA synthesis kit (Amersham). Quantitative reverse-transcription PCR (qRT-PCR) was performed in 96 well plates using pre-designed TaqMan® probe/primers on an ABI 7900HT system (Applied Biosystems) following the manufacturer's instructions. All reactions were performed in duplicate within each biological replicate. The relative amount of mRNA was calculated using the comparative CT method after normalisation to GAPDH. Probes used for qRT-PCR are shown in Table 2.3.

Target	siRNA/ shRNA		Sequence	Vector	Cat. No.
CCDC68	siRNA	1	TACTTCATTCTCTTTGTTC		MU-014610-00
		2	TCGGTCTTCAATTCACTTG		
		3	ATTTCCGTAACCTAATCAA		
		4	AATAATGTGAGCGGACGTA		
	shRNA	1	AAAGTTATACACTAGAGAG	pGIPZ	V2LHS_137441
		2	TCAAGGATTACAGTACTTG	pGIPZ	V2LHS_137443
		3	TATCTTCCATCTTATCCCT	pGIPZ	V3LHS_386245
CCDC-102B	siRNA	1	AATCTCTCTAGCTCTGCTC		MU-014445-01
		2	TATTGCCTGACAGTTCTTG		
		3	CCACTCGTAATCTAGTTT		
		4	TGATCCACTCGGTTGTTTG		
	shRNA	1	TACTGTAGAAATGTCTATC	pGIPZ	V2LHS_157777
		2	TTCACATAACCACAATTTC	pGIPZ	V2LHS_157778
		3	TATTCTGAGTTGTCTTCCT	pGIPZ	V3LHS_318543
		4	TCAACACCATCTAGATTGG	pGIPZ	V3LHS_318547
PIGN	siRNA	1	TATGTATAAACGTGGTCTC		MU-012463-01
		2	TAACTGAGTAGTCAACTGA		
		3	AATTCGTAAAGTGCATCTG		
		4	TAATACTTCAATTCCCAGG		
	shRNA	1	TATGTATAAACGTGGTCTC	pGIPZ	V2LHS_244784
		2	AATTCGTAAAGTGCATCTG	pGIPZ	V2LHS_246658
		3	TCATCTAATTCGTAAAGTG	pGIPZ	V2LHS_50417
RKHD2	siRNA	1	AAAGCAGGGATATATATTG		MU-006989-01
		2	AACTAGGGCAGCAATAACC		
		4	TAACCCTCCGAGCAAGTGG		
		17	TATACGTGTTTGTCTTGGC		
	shRNA	1	TTGGATATCATTCTTGCGC	pGIPZ	V2LHS_235038
		2	ATGCATTTCTATTTCTTCC	pGIPZ	V2LHS_135328
		3	AATTGGATATCATTCTTGC	pGIPZ	V2LHS_234137
ZNF516	siRNA	1	TTTGTAAACAGGTTCCCGC		MU-006909-01
		2	TAACCATTGGGCTGAATCC		
		3	AACGACTAAAGCCGCCTGC		
		4	TTTCCGAGGCGTTATCTCC		
	shRNA	1	TTAAGTAAACTGTTGCTCTCGC	pSM2c	V2HS_79666
		2	TATTCTTAGGCATGCTAGCGG	pSM2c	V2HS_79668
		3	TAACAAGGAGAGGCATCTGCC	pSM2c	V2HS_79671

Table 2.2 siRNA and shRNA sequences used in this study
Antisense sequences are shown for both si- and shRNAs

GENE	PROBE
CCDC68	Hs00228732_m1
CCDC102B	Hs00227117_m1
PIGN	Hs00202443_m1
RKHD2	Hs00535127_s1
ZNF516	Hs00206187_m1
GAPDH	Hs01554513_g1

Table 2.3 Taqman Probe catalogue numbers used for qRT-PCR

2.8.3 Western blotting

Cells were washed once in PBS, and then harvested on ice by cell-scraping in ice-cold lysis buffer. Lysates were kept on ice for 15 minutes, before centrifugation at 13000 rpm for 15 minutes at 4^{o}C. Supernatant was then transferred to fresh, pre-chilled eppendorf tubes, and protein concentration was determined using the Bradford assay (BioRad). Samples were then mixed at a 1:1 ratio with 2X sample buffer and boiled at 95^{o}C for 10 minutes on a hot block. Protein was separated on pre-cast NuPAGE 4-12% Bis-Tris gels (Invitrogen), in 1 X MES buffer (Invitrogen). Protein was transferred to poly-vinylidene fluoride membrane (GE healthcare, Amersham Biosciences) by semi-dry transfer at 150 mA for 1.5 hours in 2X Transfer buffer with 20% Methanol. Gel and membrane were pre-incubated in 2X transfer buffer for 10 minutes prior to transfer. After transfer, membranes were washed once in 1X Tris-buffered saline with 0.1% Tween20 (TBS-T). Membranes were then incubated with 5% milk in TBS-T for 1 hour, before overnight incubation at 4^{o}C with primary antibodies diluted 5% milk in TBS-T. Membranes were washed in TBS-T (3 x 5 minutes followed by 3 x 15 minutes), then incubated with HRP-conjugated secondary antibody (1:10000 Dako) dissolved in 5% milk in TBS-T for 45 minutes. Membranes were washed as before, rinsed in H_2O and HRP was detected by chemiluminescence (ECL, Amersham Biosciences). Loading was quantified with an HRP-conjugated anti-β-actin antibody (1:100000, Sigma).

Lysis buffer

20 mM Tris (pH 7.5)

150 mM NaCl

5 mM EDTA
50 mM NaF
1% Triton
Protease inhibitors (1 tablet per 10 ml lysis buffer) (Roche)

2X Sample buffer
200ul NuPage 4X buffer (Invitrogen)
80ul DTT 1M (Sigma)
120ul lysis buffer

Antibodies used for Western blots
MAD2 (mouse 1:1000 BD Biosciences 610678)
RAD51 (mouse 1:500 Abcam ab213).
pS824-Kap1 (1:1000 A300-767A-1, Bethyl Laboratories)
Kap1 (1:1000 A300-274A, Bethyl Laboratories)
pS966-SMC1 (1:1000 A300-050A, Bethyl Laboratories)
SMC1 (1:1000 AB9262, Abcam)
Beta-catenin (1:1000 BD Transduction Laboratories 610154)

2.8.4 shRNA cell lines

HCT-116 cells were transfected with small-hairpin RNA (shRNA) plasmids (pGIPZ or pSM2c, Open Biosystems, see Table 2.2) using Fugene 6.0 (Promega) in 6 well plates. Transfections were at the same ratios as described in section 2.2.2, but the final volume was 2 ml. After 2 days, cells were trypsinised, seeded into 10 cm^2 dishes, and placed under selection with 0.5 μM Puromycin for 2-3 weeks. A maximum of 3 colonies per shRNA plasmid were amplified, then RNA was extracted and qPCR performed to determine gene silencing. Colonies with knockdown were selected for analysis of segregation error rate. Two clones representing two distinct shRNA sequences, with equivalent levels of mRNA depletion, were then chosen for clonal FISH. shRNA cell lines were maintained in 0.5 μM Puromycin.

2.9 Nucleoside supplementation

Nucleosides (Adenosine (A4036), Cytidine (C4654), Guanosine and Uridine – all from Sigma-Aldrich) were dissolved in media at a total nucleoside concentration of 3 mM on the day of the experiment. The nucleoside solution was then filtered, and supplemented to cells at 0.3 μM for 48 hours prior to assay readout.

2.9.1 Segregation error and mitotic DNA damage quantification

After 48 hours of nucleoside supplementation cells were fixed and stained according to the protocol described in section 2.3.1. Cells were stained with antibodies to γH2AX and β-tubulin, and anti-centromere antibodies, to enable quantification of segregation errors and prometaphase γH2AX foci from within the same sample. Images of 100 prometaphases were acquired for manual quantification per sample per experiment. 30 anaphases per sample per experiment were scored for the presence of segregation errors.

2.9.2 Proliferation assays

Cells were seeded into 96 well plates at 4000 cells per well (8000 cells per well for SW1116), and after 24 hours, supplemented with nucleosides at 0.3 μM. After nucleoside addition, plates were imaged using an IncuCyte Long-term *in-situ* Cell Imaging System, located within an incubator. Phase contrast images were acquired every 2 hours for 72 hours, and the IncuCyte software estimated the percentage cell monolayer confluence automatically. Experiments included six technical replicates. Outlying wells were excluded manually, and growth curves were then constructed. Growth rates were calculated by measuring the gradient of the linear growth phase.

2.9.3 Cellular ATP measurement

Cells were seeded in 50 μl of media into 96 well plates (4000 cells/well HT29 and SW620, 8000 cells per/well HT55 and SW1116). After 24 hours cells were supplemented with 50 μl 2X nucleoside solution, to give a final concentration of 0.3 μM. Following 48 hours of nucleoside supplementation, cells were treated with Cell Titer Glo reagent (thawed and brought to room temperature). First, plates were removed from the incubator and cooled to room temperature for approximately 30 minutes. 95 μl

of Cell Titer Glo was added to each well. Plates were then agitated for 2 minutes at room temperature, before reading on the Envision plate reader (Wallac). Control measurements were taken from wells with media only, with and without nucleosides. ATP levels were then normalised to the biomass value for the well.

Biomass values reflect the total protein of both viable and non-viable cells. After plate-reading, cells were fixed with 50% trichloroacetate for 1 hour at 4^{o}C. Cells were then rinsed twice with deionised H_2O and air dried overnight. 50 µl TOX6 stain (In Vitro Toxicology assay kit Sulforhodamine B solution – Sigma) was then added to each well, and plates rocked gently at room temperature for 1 hour. The stain was then removed and cells washed twice quickly with 1% acetic acid. Plates were then air dried until no moisture was visible (approximately 1 hour). Dye was then solubilised with 10 mM Tris at a volume equal to the original volume of tissue culture medium (100 µl), and plates incubated at room temperature for 5 minutes. Dye absorbance at 490-530nm wavelength was measured using a spectrophotometer. Background readings were taken from the wells that had contained media only, with and without nucleosides.

2.10 Tumour specimen analysis

2.10.1 Ploidy analysis - flow cytometry

Flow cytometry of tumour samples, and BAC array-CGH data was performed in the laboratory of Professor Ian Tomlinson

BAC array-CGH data was obtained for 26 aneuploid tumours. Aneuploidy status was determined previously by flow cytometry. Briefly, 50µm scrolls of formalin fixed paraffin embedded tumour tissue were placed in a microfuge tube and deparaffinised in xylene. The tissue was then serially rehydrated through 100%, 95%, 70% and 50% ethanol for 5 minutes at room temperature then washed twice with distilled water. A suspension of nuclei was made by incubating the tissue at 37^{o}C for 30 minutes in a 0.5% pepsin solution (Sigma) prepared in 0.9% saline pH 1.5. The nuclei were washed once with PBS, stained with propidium iodide and analysed using a Calibur 1 benchtop cytometer and CellQuest software.

2.10.2 Carcinoma-in-adenoma Patient samples

Processing and analysis of Carcinoma-in-adenoma tissue samples was performed by Dr Enric Domingo, in the laboratory of Professor Ian Tomlinson.

Twenty archival formalin-fixed paraffin-embedded tumours showing adjacent but discrete colorectal carcinoma and adenoma were identified. Samples and records were used in accordance with UK research ethics approval (MREC06/Q1702/99). Hematoxylin and eosin slides of the samples were reviewed and regions marked as normal (if present), adenoma or carcinoma accordingly. These were used as a guide to take tissue from each region from unstained slides by needle microdissection. DNA was extracted with a standard proteinase K digestion followed by purification with the DNeasy kit (Qiagen).

2.10.2.1 Image cytometry

Ploidy analysis was performed using an automated image-based cytometry technique (Fairfield Imaging, Nottingham, UK) as previously described (Dunn et al., 2010, Leedham et al., 2009). Briefly, a 40μm section was cut from a paraffin-embedded block, mounted on slide and de-waxed. Adenomatous and carcinomatous portions of lesions were needle-dissected separately from toluidine blue-stained slides with a hematoxylin and eosin slide as a guide and disaggregated with protease, spun down to a monolayer and stained with Feulgen reagent. Nuclei were scanned using a Zeiss Axioplan microscope coupled to a high-resolution digital camera model C4742-95 (Hamamatsu Photonics, Japan) and integrated optical density histograms were generated using Histogram Draftsmen 1.4 software (Fairfield Imaging). The average of scanned nuclei from epithelial cells per sample was 1126±434. Histograms were analysed and the number of nuclei between 1.6c and 2.4c fraction and over 2.5c were counted separately to calculate the percentage of aneuploid nuclei in each sample.

2.10.2.2 LOH analysis for Carcinoma-in-adenoma cohort

SNP arrays: The Illumina Sentrix Beadarray human linkage mapping panel version IVb containing 5,861 markers distributed evenly over the genome, with an average

physical distance of 482 kb, was used according to the Goldengate genotyping assay instructions (Illumina, San Diego, USA). Briefly, DNA was amplified, fragmented and hybridized to the Beadchip, followed by single-base extension. Then Beadchips were stained, dried and scanned using a Beadarray reader (Illumina, San Diego, USA). Image data were visualised using Genomestudio (Illumina, San Diego, USA). All samples had call rates above 0.97. Adenomas and carcinomas were marked as having LOH or no LOH in 18q according to the absence or presence of heterozygous alleles respectively.
LOH analysis using microsatellites: Standard PCR conditions were used with the forward primer fluorescently labelled with HEX or FAM. At each marker, LOH was considered present when a peak area in the adenoma or the carcinoma was reduced to 50% of the other allele, relative to the normal paired DNA. Up to 5 microsatellites in 18q21 (D18S46, D18S1110, D18S35, D18S69 and D18S1407) were analysed. All PCRs were performed twice and all samples analysed with SNP arrays had concordant results.

2.11 Bioinformatics Analysis

2.11.1 Aneuploid tumour analysis

This analysis was designed in collaboration with David Endesfelder, Arne Schenk and Sarah McClelland and performed by DE and AS. Detailed description of relative contributions may be found in the relevant results chapters.

Data were segmented by circular binary segmention (R package *DNAcopy*). For the identification of regions of consistent gain and loss, we used the GISTIC algorithm (Beroukhim et al., 2007) with thresholds for gain of 0.1 and for loss of -0.1, and a q-value threshold of 0.25.

2.11.2 Defining Consistent Regions of Somatic Copy Number Loss – cell lines

Single nucleotide polymorphism comparative genomic hybridisation (SNP CGH) data (Affymetrix SNP 6.0) for 20 CIN+ and 9 CIN- cell lines was obtained from the Wellcome Trust Sanger Institute. Integer copy numbers were estimated for each SNP

probe using the PICNIC algorithm (Greenman et al., 2010). The following analysis steps were performed using R.

First, minimum consistent regions of genomic alteration were identified across all cell lines. Each region was then assessed for DNA copy number loss. To select for genomic regions altered specifically relative to the background ploidy of each cell line, ploidy status was estimated for each cell line using the median copy number over all SNP probes. Each region in each cell line was then defined as either lost (copy number > ploidy baseline) and normalised to the ploidy baseline of the cell line to give x_{norm}, or not lost (copy number ≤ ploidy baseline) and set to 0. To test for statistical significance between CIN+ and CIN- cell lines a d-score for each lost region was computed by calculating the mean normalised copy number x_{norm} across CIN+($\bar{x}_{norm,C}$) and CIN-($\bar{x}_{norm,M}$) cell lines, thereby accounting for both amplitude and frequency of genomic aberrations. A Significance Analysis of Microarrays (SAM – R package *siggenes*) was then performed with a modified two-sample t-statistic:

$$d(i) = \frac{\bar{x}_{norm,C}(i) - \bar{x}_{norm,M}(i)}{s(i) + s_0}$$

The parameter *s(i)* defines the region-specific standard deviation (Storey and Siegmund, 2001). In contrast to a standard two-sample t-statistic, SAM includes an additional parameter s0, which decreases the influence of high sample variance. This was empirically set to 0.5, which results in a balanced weighting of the frequency and amplitude of copy number losses. To detect significant regions, we randomly permuted (N = 10000) SNP probes for each sample separately. For each tested region, P-values were estimated by counting the percentage of permutation d-scores greater or equal than the observed d-score. To adjust for multiple testing, q-values were estimated with the R-package *qvalue* and genes with q < 0.25 were called significant. To ensure the selection of genes consistently altered across aneuploid tumours, any genomic change not seen across ≥ 50% of the tumours was excluded from further analysis. Genomic regions were then mapped to genes using the R package biomaRt (Durinck et al., 2005). Most CIN+ cell lines are near-triploid or near-tetraploid, so a loss of copy number relative to ploidy baseline can still result in a copy number of ≥ 2, with true genomic loss relative to diploidy/euploidy a rare event. We selected all genes that were present at 1 or 0 copies in at least 30% of CIN+ cell lines, and no more than 1 CIN- cell line.

2.11.3 TCGA (The Cancer Genome Atlas) data

Affymetrix SNP 6.0 Data was downloaded for 365 CRC samples. LogR ratios and allelic differences were estimated using the Affymetrix Genotyping Console™. Any samples that failed the Affymetrix quality control parameters were excluded. Pathological estimates were available of the percentage of tumour nuclei in an adjacent section from the same biopsy from which DNA was extracted for CGH. All tumours with <60% tumour nuclei were omitted from further analysis. To estimate copy number and LOH, the GAP algorithm, which accounts for stromal contamination levels as well as estimating the ploidy status of the tumour, was used (Popova et al., 2009). All regions with a minor allele copy number of zero were defined as LOH regions. DNA index was estimated by calculating the weighted mean copy number across all copy number segments, with weights equal to the segment length. Ploidy was estimated using the weighted median copy number. Copy number segments of loss and gain were defined relative to the ploidy status of each sample by subtracting the ploidy estimate from the estimated copy number. Agilent 244K custom gene expression (G4502A-07-3) data was downloaded for 154 CRC samples and was print-tip normalised with the R-package *marray*. Duplicated probes were averaged. Spearman's rank correlation coefficient was used for the correlation of copy number and expression data.

2.11.4 Structural/Numerical Complexity

To define a SNP array based structural complexity score (SCS), genomic regions with an integer copy number aberrant from the modal integer copy number of each chromosome were counted as one aberration. To avoid over-estimation, aberrations < 5% of the chromosome length were excluded. SCS was the sum of all structurally aberrant regions. A numerical complexity score (NCS) counted all whole chromosome gains or losses as one numerical aberration. All chromosomes where at least 75% of SNPs were present at a higher copy number than the ploidy of the sample were counted as whole chromosome gains and vice versa for losses. The NCS score was defined as the sum of all whole chromosome gains and losses. SCS and NCS scores were divided by 1.5 for triploid cell lines, and by 2 for tetraploid cell lines, to account for the increased probability of karyotypic abnormalities in polyploid genomes.

Chapter 3. Results 1 – CIN+ colorectal cancer cell lines display elevated replication stress

3.1 Introduction

CIN+ cancer cells make chromosome segregation errors during mitosis (Thompson and Compton, 2008, Lengauer et al., 1997). Segregation errors can be generated through defective attachments of chromosomes to the mitotic spindle, or as a consequence of structural chromosome aberrations (see Introduction, page 20). While numerous studies have identified possible causes of chromosome missegregation, it remains unclear which mechanisms are most prevalent in CIN+ cells; published studies have examined limited numbers of cell lines, of mixed tissue origins, which may mask any tissue-specific mechanisms sustaining CIN. As discussed in the introduction, CRC is a convenient cancer type in which to study CIN, as tumours can generally be classified as either CIN+/aneuploid or CIN-/microsatellite unstable. This subdivision enables comparison of the two tumour subtypes, which is not possible in other tumour types where CIN is observed more widely across all tumours. Therefore a panel of CIN+ colorectal cancer (CRC) cell lines were systematically characterised, in order to identify whether mitotic or pre-mitotic defects were responsible for the majority of chromosome segregation errors in this cancer type.

3.2 Classification of segregation errors in CIN+ CRC

Dr Sarah McClelland provided data in Figure 3.2a.

First, anaphase segregation error frequency was quantified in a panel of CIN+ cell lines, all of which show loss of chromosome 18q, a region of common copy number loss in CIN+ CRC (Sheffer et al., 2009). These cell lines were compared to MSI+/CIN- cell lines, and all lines used in this study are summarised in Table 3.1. Cells were grown on coverslips, fixed and visualised by indirect immunofluorescence. CIN+ CRC cells displayed an increased frequency of anaphase segregation errors compared to CIN- CRC cells (median = 38% versus 18%, p=0.0025, Figure 3.1a). This is consistent with studies examining segregation errors in small numbers of CIN+ versus CIN- cell lines

from mixed tissue backgrounds (Thompson and Compton, 2008, Silkworth et al., 2009, Ganem et al., 2009), and with cytogenetic quantifications of chromosome non-disjunction frequency in CIN+ and CIN- CRC cell lines (Lengauer et al., 1997).

Segregation errors driven by disordered chromosome structure, reflecting interphase defects, should consist predominantly of anaphase bridges and acentric chromosomes (Thompson and Compton, 2011b). In contrast, lagging chromosomes with centromeres (referred to as lagging chromosomes) are more likely to reflect mitotic defects (Ganem et al., 2009, Thompson and Compton, 2011b) (see Introduction, Section 1.2.1). The majority of segregation errors in CIN+ CRC cells consisted of anaphase bridges and acentric chromosomes (54-81%, median 70%, Figure 3.1b). Conversely, lagging chromosomes accounted for a median of 20% (range 10-43%, Figure 3.1b) of segregation errors. Taken together, CIN+ CRC cells exhibited significantly more segregation errors of pre-mitotic origins (acentric chromosomes and anaphase bridges) than lagging chromosomes (Figure 3.1c, $p=0.0018$). Examples of segregation errors from each of the CIN+ CRC cell lines analysed are shown in Figure 3.1d.

To ascertain that induction of improper kinetochore attachments in mitosis does not induce acentric chromosomes or anaphase bridges, CIN- HCT-116 cells were treated with the Eg5 inhibitor Monastrol for 1 hour to induce merotelic and syntelic attachments through transient inhibition of bipolar spindle formation (Thompson and Compton, 2008). Cells were then released into Monastrol-free media for 45 minutes prior to fixation and classification of segregation errors. Monastrol washout resulted in a 3–fold increase in the fraction of segregation errors that were lagging chromosomes, from 25.6% to 80.2%, and a corresponding reduction in the fraction constituted by acentric chromosomes and bridges (Figure 3.2a). Specific induction of lagging chromosomes after Monastrol washout was also observed in two CIN+ cell lines, HT55 and SW620 (Figure 3.2b). This result suggests that mitotic dysfunction does not commonly result in anaphase bridges or acentric chromosomes, but instead specifically induces lagging chromosomes.

Together with the analysis of endogenous segregation errors in CIN+ cell lines (Figure 3.2b), this indicates that pre-mitotic defects generating structurally abnormal chromosomes, rather than mitotic dysfunction, are likely to be the major cause of chromosome missegregation in this panel of CIN+ CRC cell lines.

Cell line	CIN status	Karyotype	Median copy number	MSI status	MMR Defect	wGII	SCS	NCS	TP53	APC	KRAS	SMAD4
COLO205	+	Hypertriploid (78)	3			0.45	12.0	6.0	Mutant	Mutant	WT*	Mutant
COLO320	+	Hyperdiploid (53)	2			0.31	15.0	3.0	Mutant	Mutant	WT	WT
COLO678	+	Hyperdiploid (54)	2			0.47	26.0	5.0	WT	Mutant	Mutant	Mutant
HT29	+	Hypertriploid (71)	3			0.55	16.0	4.7	Mutant	Mutant	WT*	Mutant
HT55	+	Hypertriploid (~72)	4			0.48	6.0	5.0	Mutant	Mutant	WT	WT
LS1034	+	Hypertriploid (77)	3			0.44	4.7	6.0	Mutant	Mutant	Mutant	WT
LS123	+	Hyperdiploid (63)	3			0.66	11.3	7.3	Mutant	Mutant	Mutant	Mutant
LS411N	+	Hypertriploid (75)	3	+	MLH1	0.44	8.0	4.7	Mutant	Mutant	WT*	WT
NCIH508	+	hypertetraploid (102)	4			0.49	5.0	5.0	Mutant	WT	WT*	WT
NCIH716	+	Hypotriploid (61)	3			0.70	13.3	7.3	Mutant	WT	WT	WT
NCIH747	+	Near-triploid (66)	3			0.59	10.7	6.0	Mutant	Mutant	Mutant	WT
SKCO1	+	Hypertriploid (~75)	3			0.53	27.3	4.0	WT	Mutant	Mutant	WT
SNUC1	+	Hypertriploid (78)	3			0.50	14.0	4.7	Mutant	WT	WT	WT
SW1116	+	Hypotriploid (63)	3			0.45	10.7	3.3	Mutant	Mutant	Mutant	WT
SW1417	+	Near-triploid (70)	3			0.52	12.0	4.0	Mutant	Mutant	WT*	WT
SW1463	+	Hypertriploid	3			0.57	6.0	8.0	Mutant	Mutant	Mutant	WT
SW403	+	Near-triploid (68)	2			0.35	21.0	4.0	Mutant	Mutant	Mutant	Mutant
SW620	+	Hyperdiploid (50)	2			0.32	18.0	4.0	Mutant	Mutant	Mutant	Mutant
SW948	+	Hypotriploid (67)	3			0.62	8.0	7.3	WT	Mutant	Mutant	WT
T84	+	Hyperdiploid (56)	3			0.55	12.0	4.7	Mutant	Mutant	Mutant	WT
GP2D		Diploid (46)	2	+	MLH1	0.02	0.0	0.0	WT	Mutant	Mutant	WT
GP5D		Diploid (46)	2	+	MLH1	0.02	0.0	0.0	WT	Mutant	Mutant	WT
HCT116		Near-diploid (45)	2	+	MLH1	0.07	0.0	0.0	WT	WT	Mutant	WT
HCT15/DLD1		Diploid (46)	2	+	MSH6	0.00	0.0	0.0	Mutant	Mutant	Mutant	WT
LOVO		Hyperdiploid (49)	2	+	MSH2	0.18	0.0	4.0	WT	Mutant	Mutant	WT
LS174T		Near-diploid (45)	2	+	MLH1	0.00	0.0	0.0	WT	WT	Mutant	WT
RKO		Diploid (46)	2	+	MLH1	0.13	11.0	1.0	WT	WT	WT*	WT
SNUC2B		Diploid (46)	2	+	Unknown	0.11	8.0	0.0	Mutant	WT	Mutant	WT
SW48		Near-diploid (47)	2	+	MLH1	0.09	0.0	2.0	WT	WT	WT^	WT

Table 3.1 Details of cell lines used in this study

* cell line has BRAF mutation, ^ cell line has EGFR mutation. Abbreviations: MSI (microsatellite instability), MMR (mismatch repair), wGII (weighted GII score), SCS (structural complexity score), NCS (numerical complexity score), WT (wild-type)

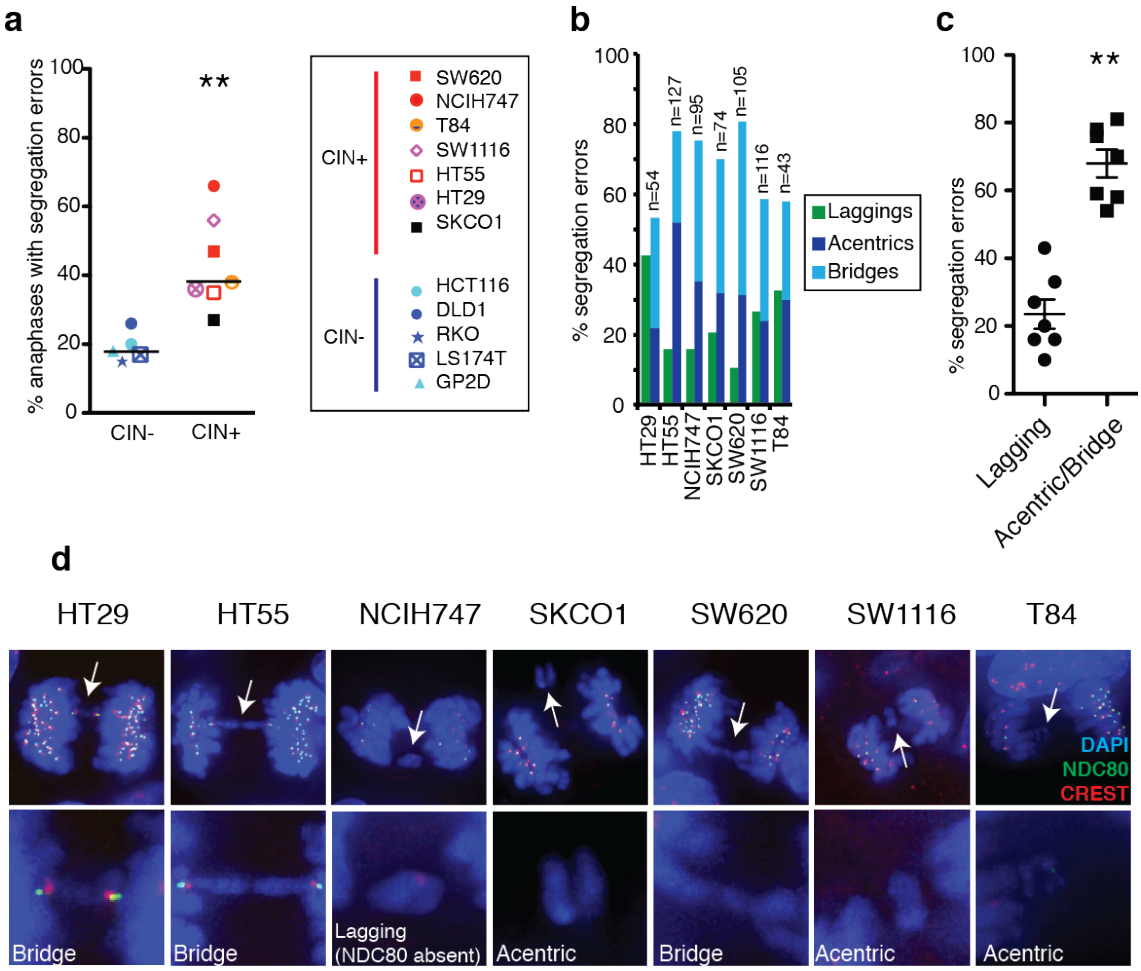

Figure 3.1 Anaphase segregation errors in CIN+ CRC cell lines
a) Percentage of anaphases exhibiting anaphase segregation errors in a panel of CIN+ and CIN- CRC cell lines, scored from fixed cell immunofluorescence. n>100 anaphases per cell line, sum of ≥2 experiments. Mann-Whitney test, p=0.0025.
b) Classification of segregation errors in 7 CIN+ cell lines, scored from cells stained with tubulin and CREST antibodies. Errors that did not fall into the categories were classified as 'other' and are not shown. The number of segregation errors classified for each cell line is shown above the bar for that cell line (sum of ≥2 experiments).
c) Comparison of frequencies of mitotic errors (lagging chromosomes) with pre-mitotic errors (acentric chromosomes and anaphase bridges) across 7 CIN+ cell lines (paired t-test, p=0.0018).
d) Example images of anaphases with segregation errors (indicated by arrows - first row images) in all 7 CIN+ CRC cell lines, with magnified panels showing the segregation error in the second row.

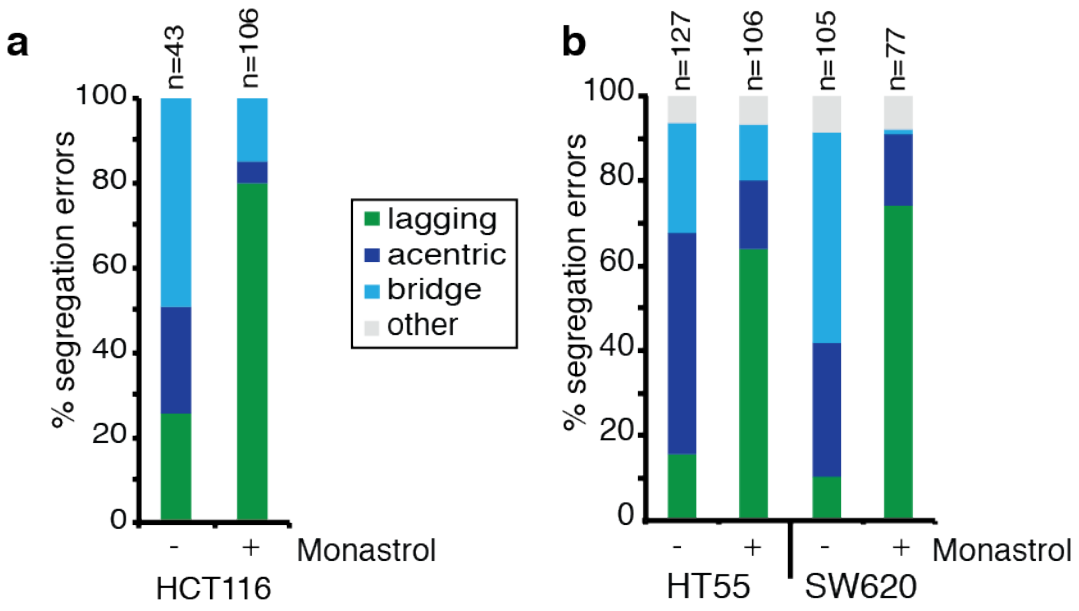

Figure 3.2 Monastrol washout specifically induces lagging chromosomes
Cells were treated with Monastrol (100 µM) for 1 hour and then released into Monastrol-free media for 45 minutes prior to fixation and staining with antibodies against NDC80, β-tubulin and anti-centromere antibodies. Shown is the segregation error classification in a) HCT-116 cells (n=no. of segregation errors, sum of 3 experiments) b) HT55 and SW620 cells (n=no. of segregation errors, one experiment)

3.3 Structural and numerical instability in CIN+ CRC

3.3.1 Structural and Numerical karyotypic complexity in CIN+ CRC cell line

The analysis in this section was done in collaboration with David Endesfelder. I conceived the complexity scores, the definitions of which were then refined together with DE, who then performed all analysis using R.

An expected consequence of CIN would be numerical and structural karyotypic changes that are conserved across a cell population, termed karyotypic complexity. The prevalence of acentric chromosomes and anaphase bridges at anaphase indicates that CIN+ cells should display structural as well as numerical karyotypic complexity. To assess this in CIN+ compared to CIN- cell lines, single nucleotide polymorphism (SNP) array data was used to derive indices for both structural and numerical karyotypic

complexity (see Chapter 2, Section 2.11.4). For this analysis an extended panel of 20 CIN+ cell lines and 9 CIN- cell lines was analysed (see Table 3.1)

To compute a structural complexity score (SCS), for each chromosome the number of regions showing copy number alteration relative to the median copy number of that chromosome were counted. The sum of the number of aberrations across all chromosomes was then normalised to the ploidy of the cell line, to account for the increased probability of structural alterations in polyploid genomes, due to the increased number of chromosomes. CIN+ cells collectively showed significantly higher SCS than CIN- cells, as would be expected in structurally unstable cells (Figure 3.3a, p=0.0003).

To investigate numerical karyotypic changes, a numerical complexity score (NCS) was derived. A chromosome was classified as showing numerical alteration if greater than 75% of the SNPs on that chromosome showed copy number alteration relative to cell line ploidy (defined as the median copy number across all chromosomes). SNPs had to be altered in the same direction (i.e. 75% gained or 75% lost, not a combination of both). The number of chromosomes showing numerical aberration was then normalised to cell line ploidy to give the NCS. As was observed for the SCS, CIN+ CRC cell lines exhibited significantly higher numerical complexity relative to CIN- CRC cell lines (Figure 3.3b, p<0.0001). Hence CIN+ cell lines exhibit both structural and numerical karyotypic complexity, as assessed using high-resolution SNP array data.

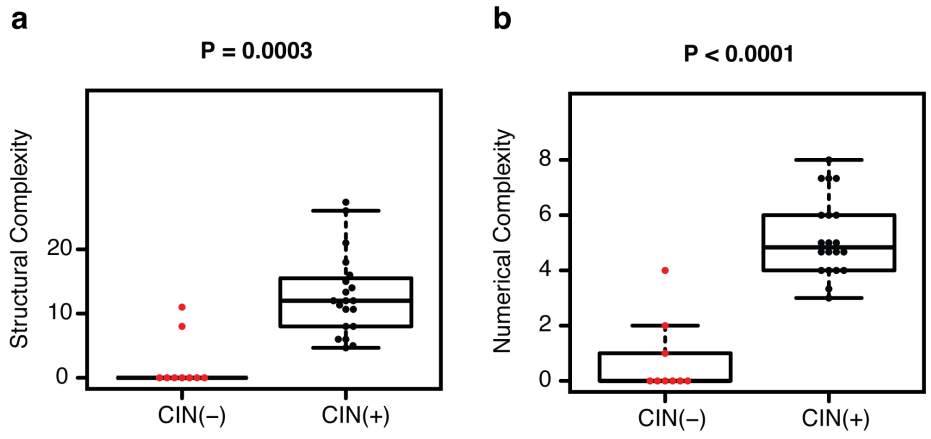

Figure 3.3 Karyotypic complexity in CRC cell lines
a) Structural and b) Numerical complexity scores for CIN- vs CIN+ cell lines. CIN+ and CIN- cell lines were compared using the Wilcoxon-Mann Whitney test.

3.3.2 Structural chromosome defects in CIN+ CRC

Elevated structural karyotypic complexity in CIN+ cells, together with the observation that the majority of segregation errors in CIN+ cell lines consist of acentric chromosomes or anaphase bridges suggests structurally abnormal chromosomes may be generated prior to mitosis, precipitating missegregation. To investigate this hypothesis, metaphase chromosome spreads were prepared from the seven CIN+ cell lines examined in Figure 3.1. Spreads were hybridised to a fluorescently labelled alpha-satellite DNA probe, which binds the centromere of every chromosome. Using this probe, acentric and dicentric chromosomes can be identified, in addition to DNA double strand breaks and multi-valent chromosome configurations. While this method detects structural chromosome changes that can affect chromosome segregation, it is likely to underestimate the frequency of structural events, as any event not affecting gross chromosome morphology (for example, translocations, inversions, deletions) will not be detected.

Examples of chromosomal abnormalities observed in each cell line are shown in Figure 3.4a. The most commonly observed chromosomal defects were acentric or dicentric chromosomes: 4-26% of metaphases (median 18%) displayed dicentric chromosomes, while 6-53% of metaphases (median 14%) displayed acentric chromosomes (Figure 3.4b). Double strand breaks were also observed, although at a lower frequency (1-10%, median 4%, of metaphases). Other abnormal morphologies, observed at very low frequencies, included multivalent chromosomes, ring chromosomes and fragmented chromosomes. Overall, 22-71% (median 36%) of CIN+ metaphases displayed structurally abnormal chromosomes (Figure 3.4c). The percentage of metaphases with structurally abnormal chromosomes correlated with segregation error frequency, although was not quite significant (Pearson's correlation co-efficient 0.72, $p=0.069$). These observations support the hypothesis that segregation errors in CIN+ cells frequently arise from structurally abnormal chromosomes. In two cell lines, HT55 and T84, particular structurally abnormal chromosomes (dicentric, but with one centromere not showing cohesion between the sister chromatids) were observed across the majority of metaphases, and were not scored as dicentric chromosomes (Figure 3.4d). These conserved abnormalities may reflect chromosome fusion events, with subsequent inactivation of one centromere, as has recently been

demonstrated in fission yeast (Sato et al., 2012). It is not clear whether a kinetochore would assemble on these ostensibly inactivated centromeres.

The observation of heterogeneous structural chromosome aberrations indicate that as well exhibiting conserved structural complexity, CIN+ cells display ongoing structural instability.

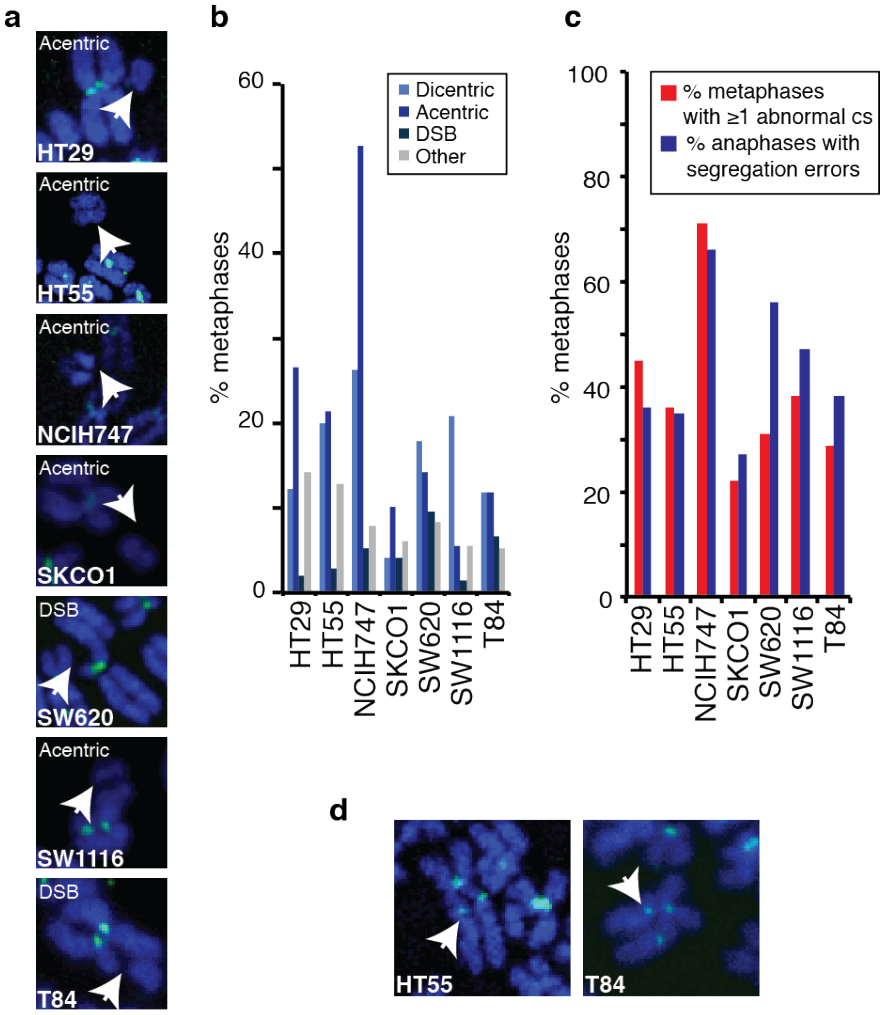

Figure 3.4 Structural chromosome aberrations in CIN+ CRC cells
a) Example images of structurally abnormal chromosomes from each of the 7 CIN+ cell lines. Arrows indicate the abnormalities, and the type of abnormality is labelled.
b) Percentage of metaphases with dicentric/acentric chromosomes, or with chromosomes displaying double strand breaks. Metaphases with more than one abnormal chromosome are scored independently for each class of abnormality. N=100 metaphases per cell line, across one or two experiments.
c) Percentage of metaphases with structurally abnormal chromosomes (red bars) compared to the frequency of anaphase segregation errors (blue bars). 100 metaphases were analysed per cell line, and only full metaphases included in the quantification.
d) Conserved structurally abnormal dicentric chromosomes in HT55 and T84 cells. Inactivated centromeres are indicated by arrows.

3.3.3 Numerical instability in CIN+ CRC

It was then necessary to confirm that these cell lines display numerical as well as structural instability, as suggested by the elevated NCS scores of CIN+ cell lines. To measure numerical heterogeneity, nuclei were hybridised to two fluorescently labelled specific centromere probes, for chromosomes 2 and 15, which do not commonly show copy number changes in colorectal cancer, and may therefore reflect stochastic changes more readily. An example of HT55 cells hybridised to both probes is shown in Figure 3.5a. The modal copy number of centromere 2 and 15 was quantified manually across at least 350 nuclei per cell line, and the percentage of cells with a copy number deviating from the mode determined. Deviation across the whole population was analysed as due to the growth pattern of some cell lines it was not possible to accurately measure deviation within clonal cell colonies. All CIN+ cell lines exhibited variation in chromosome copy number across the population, at a higher level than the variation observed in CIN- HCT116 cells (Figure 3.5 b,c). The percentage deviation from the mode observed for HCT-116 is consistent with a previous study in which 3 other CIN- cell lines were analysed (Lengauer et al., 1997). The three other CIN- cell lines (DLD1, RKO and SW48) exhibited a similar percentage deviation to HCT-116 (range 3-8%) (Figure 3.5 b,c). It is worth noting that normal lymphocytes displayed a 3% deviation in this assay, indicating a level of noise inherent to centromeric FISH analysis (Lengauer et al., 1997).

Cell lines exhibiting predominantly segregation errors of pre-mitotic origins (for example, HT55 and NCIH747) exhibit equivalent numerical heterogeneity relative to cell lines that exhibit a higher frequency of mitotic segregation errors (lagging chromosomes – for example T84 cells). This supports the hypothesis that structurally abnormal chromosomes can result in numerical chromosome copy number changes, consistent with other studies (Pampalona et al., 2010b, Stewenius et al., 2005). However, based on these experiments it not possible to exclude that missegregation of chromosomes is occurring through syntelic attachments, which segregate with the chromosome masses and do not lag at anaphase. It was therefore important to examine mitotic dysfunction in CIN+ cells more closely.

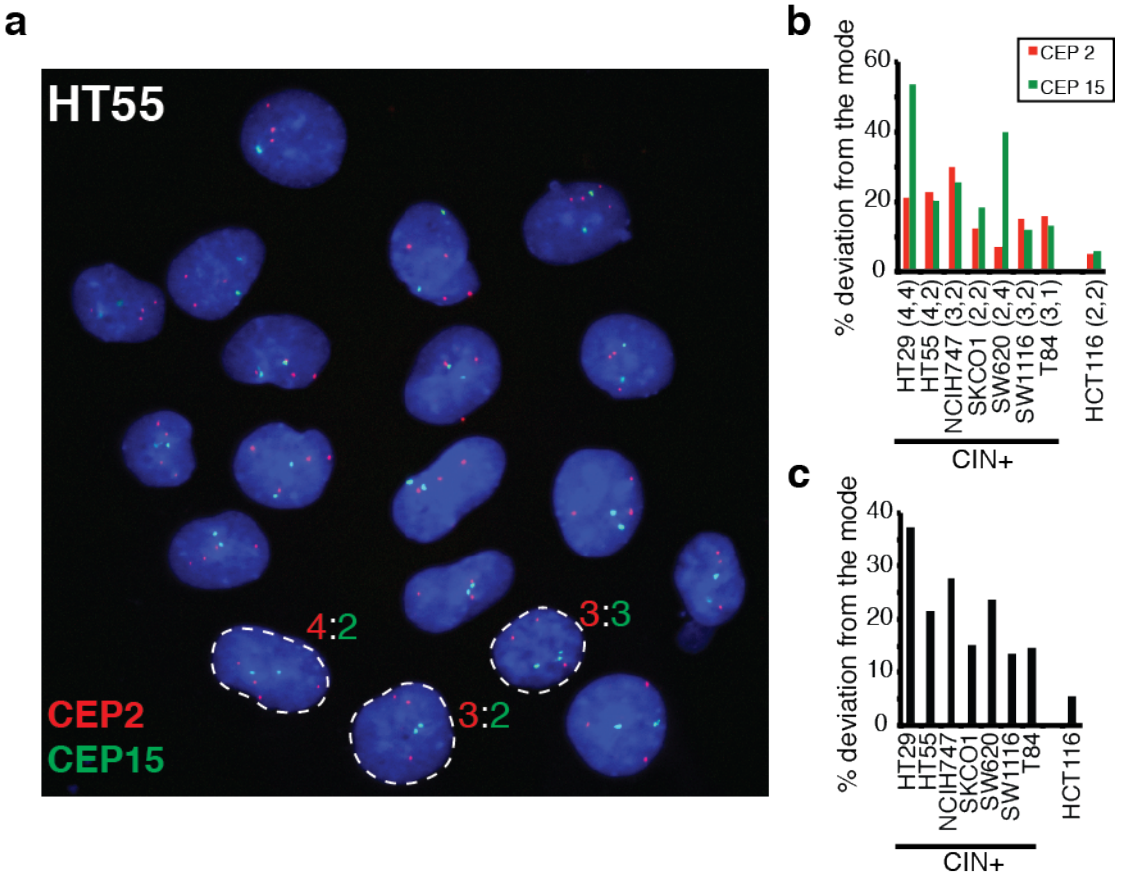

Figure 3.5 Numerical heterogeneity in CIN+ CRC cell lines
a) HT55 cells hybridised to two fluorescently labelled centromere probes (centromere 2 and centromere 15). Example nuclei with varying copy numbers of the chromosomes are outlined, and copy numbers indicated in the corresponding colours.
b) Percentage of cells deviating from the modal copy number of chromosomes 2 and 15 in CIN+ cells. CIN- HCT116 cells were measured for reference. n>350 nuclei, one experiment per cell line. Modal copy number for chromosomes 2 and 15 for each cell line is shown in brackets.
c) Average percentage deviation from mode across both probes

3.4 Mitotic defects in CIN+ CRC

In order to further test whether pre-mitotic or mitotic defects contribute to segregation errors in CIN+ CRC cells, a series of experiments to identify mitotic dysfunction were performed. Mitotic defects that have been linked to CIN include: mutations in mitotic checkpoint genes (Cahill et al., 1998, Tighe et al., 2001) and cohesin subunits (Solomon et al., 2011, Barber et al., 2008), multipolar spindle geometry (Ganem et al., 2009, Silkworth et al., 2009, Gisselsson et al., 2008), and hyper-stable mitotic spindle microtubules (Bakhoum et al., 2009a, Bakhoum et al., 2009b, Knowlton et al., 2006).

3.4.1 Mitotic progression

In order to assess whether there are any differences in the kinetics of mitotic progression between CIN+ and CIN- cells that might indicate mitotic dysfunction, time-lapse microscopy was used to measure the duration of different stages of mitosis. To visualise DNA, three CIN+ (HT29, SKCO1 and SW620) and three CIN- (DLD1, HCT116 and RKO) cell lines were transfected with a vector encoding histone-2B tagged with red fluorescent protein (pH2B-mRFP), and then flow-sorted for mRFP expression after antibiotic selection (see Materials and Methods). It was not possible to make H2B-mRFP cell lines of sufficient quality for time-lapse microscopy in the remaining CIN+ cell lines, in part due to low transfection efficiency. Therefore only three CIN- cell lines were examined in order to keep sample size consistent between CIN+ and CIN- groups. However, HT29, SW620, DLD1 and HCT116 cells represent some of the more widely used cell lines in studies of mitotic dysfunction in CRC, making them appropriate to use in this analysis (Thompson and Compton, 2008, Lengauer et al., 1998, Silkworth et al., 2009, Ganem et al., 2009).

Cell lines were imaged every three minutes for six hours in order to acquire high temporal resolution imaging of mitotic progression. The times of nuclear envelope breakdown (NEBD), the alignment of the last chromosome to the metaphase plate (LCC), and anaphase onset were noted for each cell undergoing mitosis. The appearance of these events is shown in the sequence of images in Figure 3.6a. The interval between NEBD and anaphase onset (the period monitored by the mitotic checkpoint, and during which CDK1-cyclin B activity is maintained) is the duration of mitosis, while the interval between NEBD and LCC is the time taken to congress all chromosomes before anaphase. A delay between chromosome congression (LCC) and anaphase onset might indicate subtle defects in kinetochore-microtubule attachments that result in sustained mitotic checkpoint activity and a metaphase delay.

No differences between CIN+ and CIN- cell lines were observed for any of these three intervals (NEBD-anaphase onset (Figure 3.6 b,c), NEBD-LCC (Figure 3.6 d,e), LCC-anaphase onset (Figure 3.6 f,g)). Individual cell lines showed cells with longer NEBD-LCC intervals (HCT116, SKCO1) or a longer metaphase delay (LCC-anaphase onset (RKO, SW620)). However, in each of these cases only one CIN+ cell line was affected, and a CIN- cell line was also affected by a similar delay. This

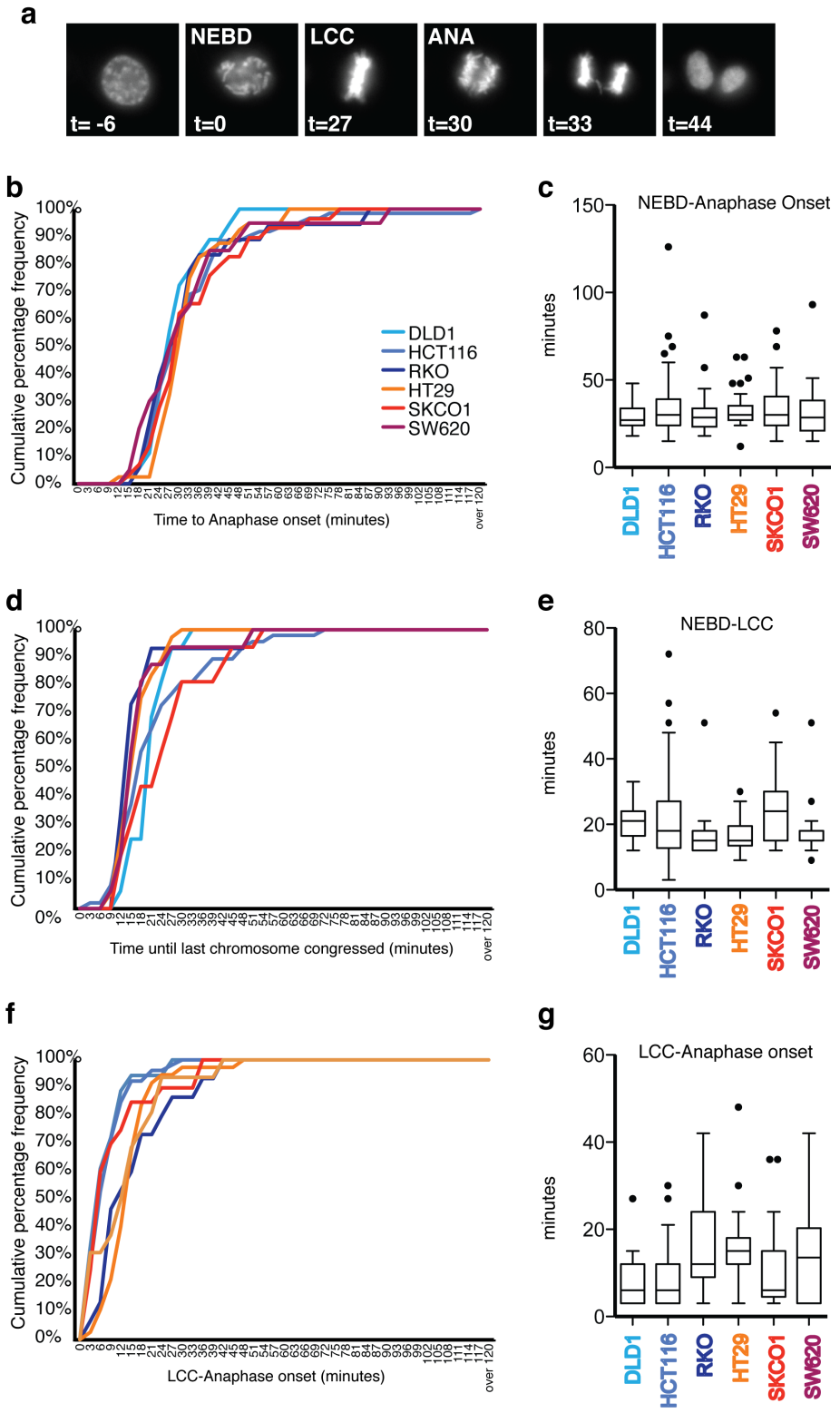

Figure 3.6 Mitotic progression in CIN+ versus CIN- CRC cell lines
a) Stills from time-lapse microscopy of SKCO1 H2B-mRFP cells showing the phases of mitosis and events noted during time-lapse quantification
b) Cumulative percentage frequency plot of time from NEBD (t=0) to anaphase onset

c) Box and whisker plot (Tukey) of NEBD-anaphase onset interval in CIN+ vs CIN- cells
d) Cumulative percentage frequency plot of time from NEBD (t=0) to chromosome congression (LCC)
e) Box and whisker plot (Tukey) of NEBD-chromosome congression in CIN+ vs CIN- cells
f) Cumulative percentage frequency plot of time from LCC (t=0) to anaphase onset
g) Box and whisker plot (Tukey) of LCC-anaphase onset in CIN+ vs CIN- cells
At least 20 cells were analysed per cell line for each parameter.

indicates that defective chromosome congression or metaphase arrest (indicating problems stabilising microtubule-kinetochore attachments) are unlikely to be a common feature of CIN+ cells, at least within this panel of cell lines.

3.4.2 Mitotic Checkpoint Function and sister chromatid cohesion

Time-lapse microscopy also reveals uncongressed chromosomes at anaphase, which are indicative of a checkpoint defect. The frequency of uncongressed chromosomes at anaphase was compared between CIN+ and CIN- cell lines. Two of the CIN- cell lines (HCT-116 and RKO) displayed rare uncongressed chromosomes (3% and 6% of anaphases respectively), while only one CIN+ cell line showed any uncongressed chromosomes at anaphase (SKCO1 – 5% of anaphases) (Figure 3.7a). Together with a previous study of CIN+ versus CIN- cell lines by time-lapse microscopy, this suggests that CIN+ cells rarely undergo premature anaphase, before all chromosomes are aligned and attached correctly to the mitotic spindle (Gascoigne and Taylor, 2008).

To further assess mitotic checkpoint proficiency, in a wider panel of cells, CIN+ and CIN- cells were exposed to a Nocodazole challenge. Nocodazole depolymerises microtubules resulting in sustained mitotic checkpoint signalling and mitotic arrest, reflected by an increased mitotic index (percentage of cells in mitosis). Cells were treated with either DMSO or 100ng/ml Nocodazole for eight hours, before fixation and analysis by flow cytometry (Figure 3.7b). Ideally time-lapse microscopy would have been utilised to assess the mitotic arrest in response to Nocodazole at a single cell level. However, due to the morphology of many of the CIN+ cell lines it was not possible to use phase-contrast imaging, which would have been necessary due to the limited number of available CIN+ H2B-mRFP cell lines. By flow cytometry, no significant difference in Nocodazole-induced mitotic arrest was observed between CIN+ and CIN-

cells (Figure 3.7c, p=0.54), consistent with previous studies examining mitotic checkpoint function in CIN+ versus CIN- CRC cell lines using both flow cytometry and time-lapse microscopy (Tighe et al., 2001, Gascoigne and Taylor, 2008). The three cell lines overlapping between this analysis and the published reports (CIN-: HCT116, DLD1 and CIN+: HT29) behaved similarly, confirming the utility of the assay. Through this analysis an additional eight CRC cell lines were profiled for mitotic checkpoint function.

The ability of CIN+ cells to establish and maintain sister chromatid cohesion was then assessed by measuring the inter-chromatid distance on metaphase-arrested chromosome spreads (Rajesh et al., 2011) (Figure 3.8a). Defects in sister chromatid cohesion can reflect either defects in the cohesin complex, or alternatively premature inactivation of the mitotic checkpoint, resulting in cohesin cleavage and sister chromatid separation. Silencing the cohesin subunit SCC1 in HCT-116 cells was used as a positive control, resulting in an increased centromere width indicative of decreased sister chromatid cohesion (Figure 3.8a,b). CIN+ cells did not display defective sister chromatid cohesion, relative to HCT-116 cells or HCT-116 cells depleted of cohesin. Defective cohesion also results in prematurely separated sister chromatids at metaphase (Solomon et al., 2011). Premature sister chromatid separation could be observed following SCC1 silencing (Figure 3.8c), but was not observed in CIN+ cell lines. In summary, no defects in either the mitotic checkpoint or sister chromatid cohesion were observed in this panel of CIN+ CRC cells.

3.4.3 Spindle defects and merotelic attachments

Dr Sarah McClelland provided data shown in Figure 3.9d and e.

Both abnormal spindle geometry and hyper-stable microtubules contribute to segregation errors through the formation of merotelic kinetochore-microtubule attachments (see Introduction, page 26) resulting in lagging chromosomes at anaphase. To examine spindle geometry, cells were stained with antibodies against centrin-3 (to mark centrioles) and beta-tubulin (to mark the mitotic spindle). Prometaphase cells were then scored for spindle morphology and centriole number, in order to determine whether multipolar spindle geometry, arising as a consequence of extra centrioles,

a

Uncongressed chromosomes at anaphase

CIN-			CIN+		
DLD1	HCT116	RKO	HT29	SKCO1	SW620
0%	3%	6%	0%	5%	0%

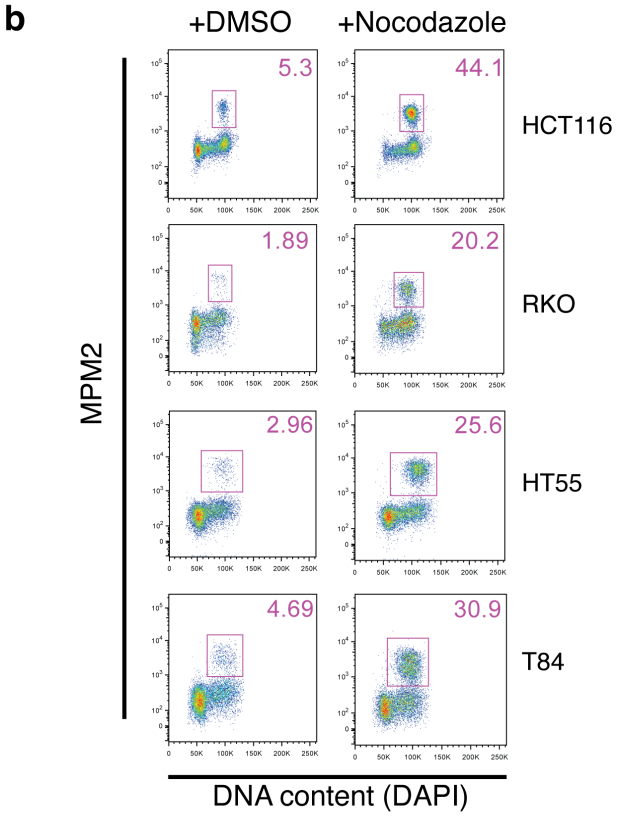

Figure 3.7 Mitotic checkpoint activity in CIN+ CRC cells
a) Table showing the percentage of anaphases with uncongressed chromosomes in CIN- versus CIN+ cells assessed from time-lapse microscopy n=25-75 cells per cell line
b) Flow cytometry data from a representative experiment showing an increase in MPM2 positive mitotic cells (boxed cell population) following incubation with 100ng/ml

Nocodazole for 8 hours. Shown are 2 CIN- cell lines (HCT-116 and RKO) and 2 CIN+ cell lines (HT55 and T84)
c) Fold change in mitotic index after 8 hours Nocodazole treatment for 8 hours across CIN- and CIN+ cell lines (average of at least 2 independent experiments, n=20000 cells per experiment) Statistical test: Mann-Whitney test

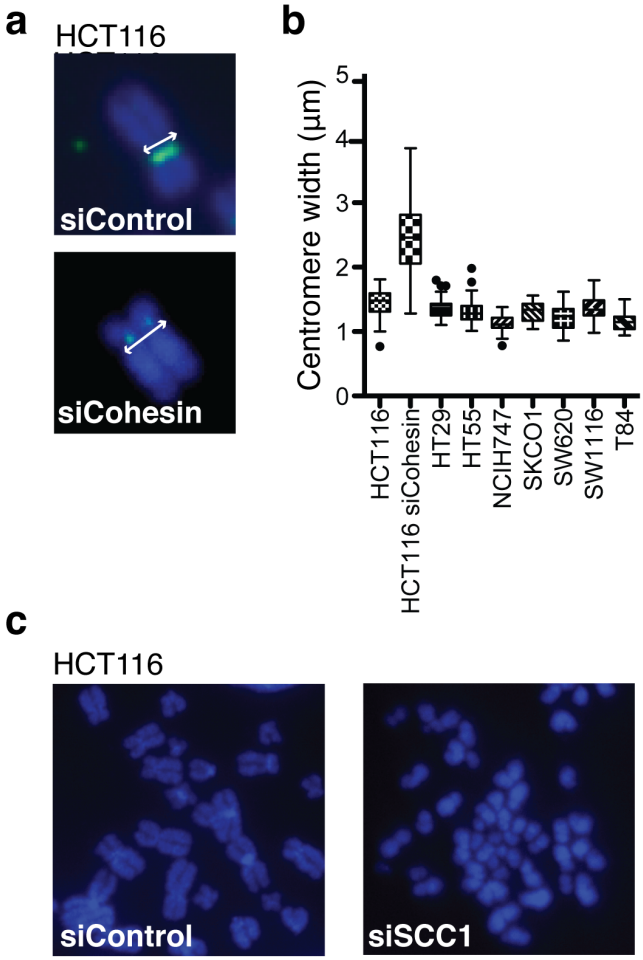

Figure 3.8 Sister chromatid cohesion in CIN+ CRC cells
a) Images illustrating inter-chromatid distance measurement of the centromere signal
b) Centromere signal width n=25 sister chromatid pairs across 5 metaphases, one experiment shown. HCT-116 cells were transfected with siRNA targeting SCC1 as a positive control
c) Images of HCT116 cells transfected with control or SCC1 siRNAs

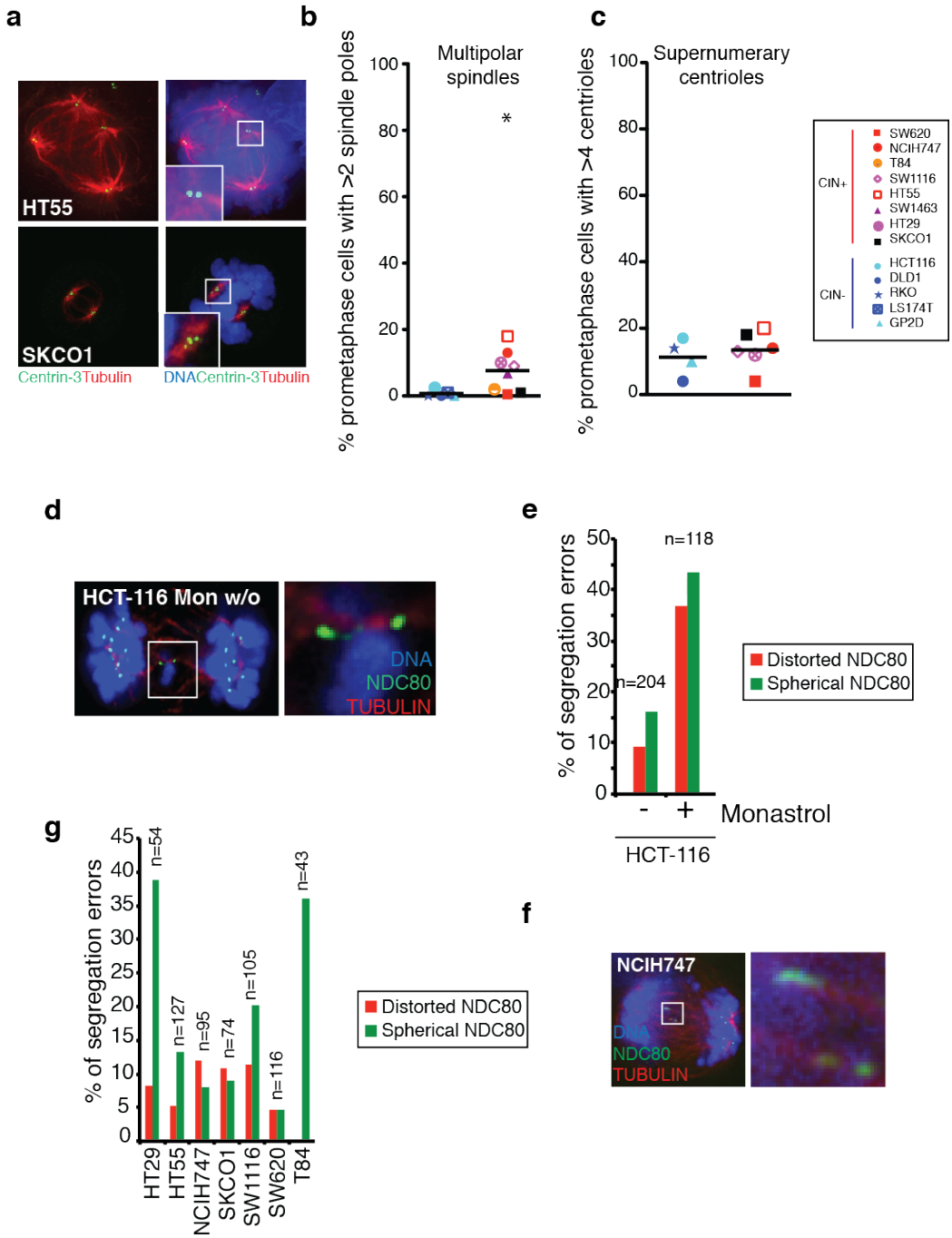

Figure 3.9 Spindle geometry and merotelic attachments in CIN+ CRC cell lines
a) Example images of (top) an HT55 cell with a multipolar spindle and extra centrioles and (bottom) a SKCO1 cell with a bipolar cell and extra centrioles (magnified panel).
b) Quantification of multipolar spindle morphology in CIN+ vs CIN- cells. N=100 cells per cell line, one experiment, Mann-Whitney test, p=0.027.
c) Quantification of the percentage of cells with >4 centrioles, corresponding to >2 centrosomes n=100 cells per cell line, one experiment, Mann-Whitney test, p=0.59. Cell lines omitted from this quantification could not be scored for morphological reasons.
d) A merotelic attachment with NDC80 distortion induced by Monastrol washout in HCT-116 cells. Image provided by Dr Sarah McClelland.

e) Quantification of the percentage of lagging chromosomes with and without kinetochore distortion in HCT-116 cells ± 100 μM Monastrol washout. Data provided by Dr Sarah McClelland.
f) A merotelic attachment in NCIH747 cells, showing NDC80 distortion
g) Quantification of the frequency of lagging chromosomes with and without kinetochore distortion in CIN+ cell lines. The number of lagging chromosomes scored is indicated above the bars. Data from two experiments.

---

might contribute to chromosome missegregation in CIN+ CRC cells. Examples of a prometaphase with i) a multipolar spindle and ii) a bipolar spindle with extra centrioles are shown in Figure 3.9a.

CIN+ CRC cells displayed a small but significant increase in the frequency of prometaphase cells with multipolar spindle morphology (median 8% vs 0% Figure 3.9b, p=0.027), consistent with two published studies examining a smaller panel of CRC cell lines (HCT-116, HT29 and SW620 cells)(Silkworth et al., 2009) and a cell line panel of mixed origins (Ganem et al., 2009). However, while almost all cells exhibiting multipolar spindles had greater than four centrioles (data not shown), there was no increase in the overall fraction of cells with extra centrioles in CIN+ compared to CIN- cells (Figure 3.9c, p=0.59).

This could indicate that CIN- cells are more proficient than CIN+ cells at clustering extra centrioles prior to spindle formation, as only CIN+ cells displayed multipolar spindle morphology in prometaphase despite an equivalent frequency of cells with extra centrioles between CIN- and CIN+ cell lines. This is contrary to the model proposed by the Pellman and Cimini laboratories (Ganem et al., 2009, Silkworth et al., 2009), which views centriole clustering as an acquired capability of CIN+ cells, to avoid deleterious multipolar divisions. However, direct evidence showing that multipolar spindle coalescence into bipolar spindles actually occurs (preventing lethal multipolar divisions) is lacking. Furthermore, the fate of daughter cells after mitoses with transient multipolar spindle intermediates is not known.

Both abnormal spindle geometry and hyper-stable microtubules result in the formation of merotelic kinetochore-microtubule attachments, and subsequent lagging chromosomes during anaphase (Ganem et al., 2009, Bakhoum et al., 2009a, Bakhoum et al., 2009b). To detect merotely, cells were stained with antibodies for the microtubule-binding kinetochore component NDC80, which is distorted in merotelic attachments (Hauf et al., 2003, Thompson and Compton, 2008). As a positive control to test the

ability of this assay to detect merotelic attachments, Monastrol washout treated HCT-116 cells were examined. After Monastrol-washout 80% of segregation errors were classified as lagging chromosomes, and 37% of segregation errors (46% of lagging chromosomes) were lagging chromosomes that displayed kinetochore distortion (Figure 3.9 d,e). As noted in section 3.2, in most of the CIN+ cell lines examined, only a minority of segregation errors comprised of lagging chromosomes (10-43%, median 20%). Further examination of these lagging chromosomes to identify evidence of merotely revealed that, in these cells, only 8% (range 0-12%, Figure 3.9 f,g) of segregation errors were comprised of lagging chromosomes with kinetochore distortion, suggesting that merotely may be a rare event.

These data indicate that mechanisms promoting improper kinetochore microtubule attachments, such as spindle multipolarity and hyper-stable microtubules, are unlikely to be the sole driver of chromosome segregation errors in CIN+ CRC. In addition, a recent study in HCT-116 cells (Thompson and Compton, 2011a) found that lagging chromosomes are usually ultimately segregated to the correct daughter cell. However, the authors propose that merotelic attachments could act as a surrogate marker for an elevated rate of formation of syntelic attachments, which are not visible at anaphase because they do not result in lagging chromosomes. Nevertheless, the relative rarity of lagging chromosomes and merotelic attachments in CIN+ cells suggests that syntelic attachments would also occur at low frequency in these cells.

3.5 Pre-mitotic defects in CIN+ CRC

A high frequency of anaphase bridges and acentric chromosomes, arising from structurally abnormal chromosomes, coupled with an absence of obvious mitotic defects, implicates pre-mitotic defects in the generation of chromosome segregation errors in CIN+ CRC. This is consistent with the *in vivo* observation of activation of the DNA damage response in both colorectal adenomas and carcinomas (Tort et al., 2006, Bartkova et al., 2005).

3.5.1 CIN+ cells display evidence of elevated DNA replication stress

DNA damage observed in colorectal adenomas and carcinomas is thought to reflect DNA replication stress (Bartkova et al., 2005, Lukas et al., 2011a, Gorgoulis et al., 2005, Chan et al., 2009). DNA replication stress results in a number of cellular phenotypes including DNA damage foci in early mitosis (prometaphase)(Chan et al., 2009, Ichijima et al., 2010, Lukas et al., 2011a), ultra-fine anaphase DNA bridges (Chan et al., 2009) and 53BP1-positive nuclear bodies in G1 cells (Lukas et al., 2011a) (See Introduction, page 54). An example of each of these phenotypes is shown in Figure 3.10a.

CIN+ CRC cells displayed elevated DNA damage in prometaphase cells (median 74% CIN+ vs 34% CIN- prometaphases with ≥3 γH2AX foci, Figure 3.10b, p=0.033). CIN+ cells also harboured more 53BP1 bodies in G1 cells compared to CIN- cells (Figure 3.10c, p=0.028). Concordant with the hypothesis that replication stress may drive chromosome segregation errors, ultra-fine bridges (visualised with antibodies for the single-stranded DNA binding protein RPA) were enriched in anaphases with segregation errors compared to anaphases without segregation errors (Figure 3.10d). Detection of ultra-fine bridges using validated antibodies against PICH or the BLM helicase, or quantification in early anaphase cells might reveal a greater number of these structures than were identified through staining for RPA.

A recent student found that cytokinesis-induced DNA damage of lagging chromosomes arising through merotely results in 53BP1 foci in G1 cells (Janssen et al., 2011). Inhibiting cytokinesis could reduce this DNA damage. However, the reversal of G1 53BP1 foci achieved by inhibiting cytokinesis in the one CIN+ CRC cell line examined in this study was minimal, and affected only cells with one 53BP1 focus (Janssen et al., 2011). In the analysis presented in Figure 3.10, only cells with greater at least three 53BP1 bodies were scored, which, based on the results of Janssen et al, are unlikely to have arisen from cytokinesis-induced DNA damage.

These observations suggested that elevated DNA replication stress could provide a mechanistic basis for chromosome segregation errors observed in CIN+ CRC cells.

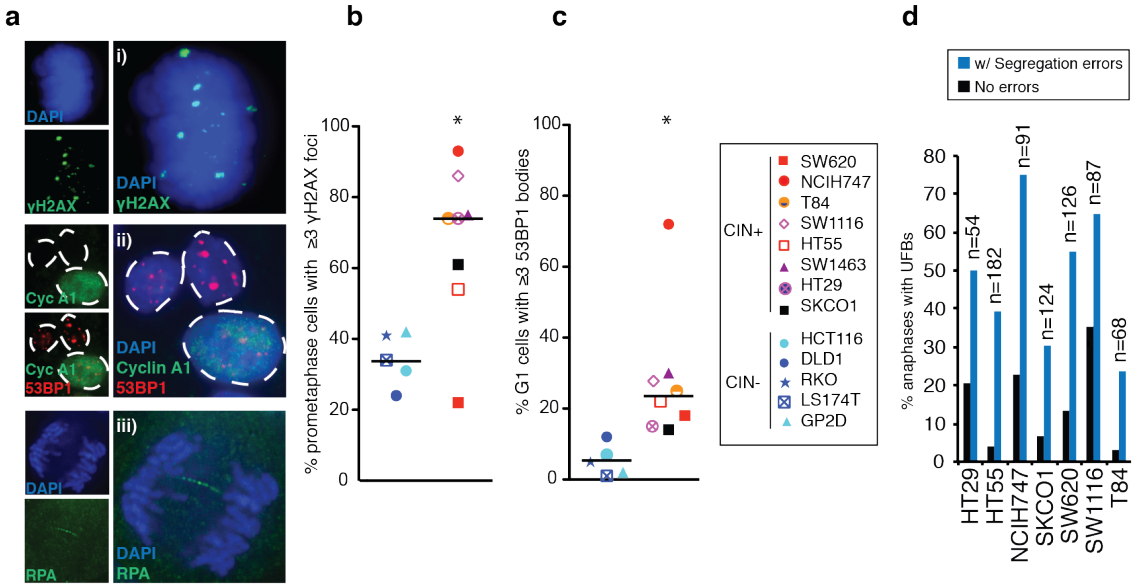

Figure 3.10 CIN+ cells display elevated DNA replication stress
a) NCIH747 cells exhibiting three hallmarks of DNA replication stress i) prometaphase γH2AX foci ii) 53BP1 bodies in G1 (cyclin A1 negative) cells and iii) ultra-fine anaphase bridges, stained with RPA
b) Quantification of prometaphase DNA damage in CIN- vs CIN+ cells n>100 cells per cell line, data from one experiment . Mann-Whitney test, p=0.033
c) Quantification of G1 53BP1 bodies in CIN- vs CIN+ cells n>200 cells per cell line, Mann-Whitney test, one experiment p=0.028
d) Quantification of ultra-fine bridges in CIN+ cells in anaphases with and without segregation errors. The number of anaphases scored is shown above each bar (sum of ≥2 experiments)

3.5.2 G2-M DNA damage checkpoint function

DNA double strand breaks activate a complex network of signalling events, which orchestrate DNA repair and halt the cell cycle in order to prevent transmission of DNA damage to daughter cells. The G2 checkpoint arrests cells in G2 in response to DNA damage and prevents entry into mitosis. Therefore double strand breaks observed in CIN+ prometaphase cells, and anaphase segregation errors characteristic of structural aberrations, could reflect a defective G2 checkpoint in CIN+ cells.

To assess G2-M checkpoint function, cells were exposed to 20 Gy of gamma-irradiation (see Materials and Methods), and incubated in either DMSO or Nocodazole (100 ng/ml) for 8 hours, to arrest any cells entering mitosis. The high level of irradiation

enables the examination of checkpoint function independent of cellular capacity to repair DNA damage, by generating an excess of double strand breaks. There was no significant difference between CIN+ and CIN- cell lines in terms of the ability to arrest in G2 following 20 Gy irradiation, although a subset of cell lines appeared to have a minor checkpoint defect (Figure 3.11), suggesting that this analysis may be underpowered to detect a difference in G2-M checkpoint function. Thus defective G2-M checkpoint function in a subset of CIN+ cells could facilitate chromosome missegregation by permitting cells with damaged DNA to enter mitosis.

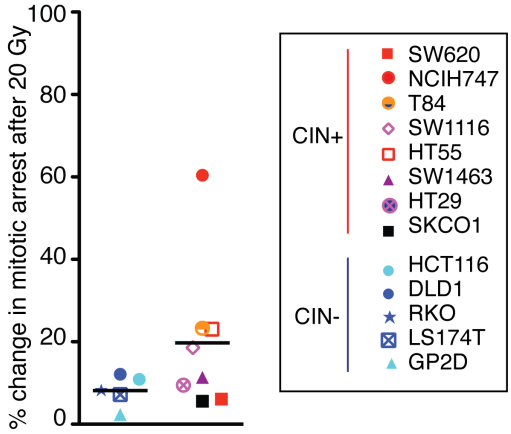

Figure 3.11 G2-M DNA damage checkpoint function in CIN+ CRC cell lines
Cells were exposed to 0 or 20 Gy irradiation, then incubated in Nocodazole 100 ng/ml for 8 hours. The mitotic index after 20 Gy irradiation is expressed as a percentage of the mitotic index in unirradiated cells. Representative experiment shown. Mann-Whitney test p=0.22

3.5.3 Telomere dysfunction does not account for CIN+ cell prometaphase damage

Telomere uncapping, followed by chromosome fusions and bridge-fusion breakage cycles, is an alternative possible source of DNA damage and segregation errors (Stewenius et al., 2005). DNA damage occurring as a consequence of telomere dysfunction is confined to the ends of telomeres, while DNA damage occurring through replication stress and other sources may affect anywhere along the length of the chromosomes (Stewenius et al., 2005, Chan et al., 2009, Lukas et al., 2011a), including the telomere.

To investigate whether DNA damage observed in CIN+ prometaphase cells was confined to the ends of chromosomes (indicating telomere dysfunction), chromosome spreads were prepared and stained by immunofluorescence with antibodies for γH2AX and anti-centromere antibodies. γH2AX foci were then classified as being either interstitial (along the length of the chromosome arm, Figure 3.12a) or terminal (on the end of chromosome arms, Figure 3.12a). Foci on short chromosome arms were not scored, as it could not be determined whether they were terminal or interstitial (Figure 3.12a). All four CIN+ cell lines analysed showed DNA damage both interstitially and at the termini of chromosome arms (Figure 3.12b). As DNA damage was not confined to telomeres, this indicates that telomere dysfunction is unlikely to be the sole source of DNA damage in these CIN+ cell lines. Furthermore, telomeres are fragile sites (Sfeir et al., 2009), so telomere damage might be expected in cells undergoing replication stress. In addition, DNA damage at the end of chromosomes can represent an interstitial double strand break with breakage of both chromosome arms and loss of the distal fragments, providing a further alternative explanation for the occurrence of DNA damage at chromosome ends.

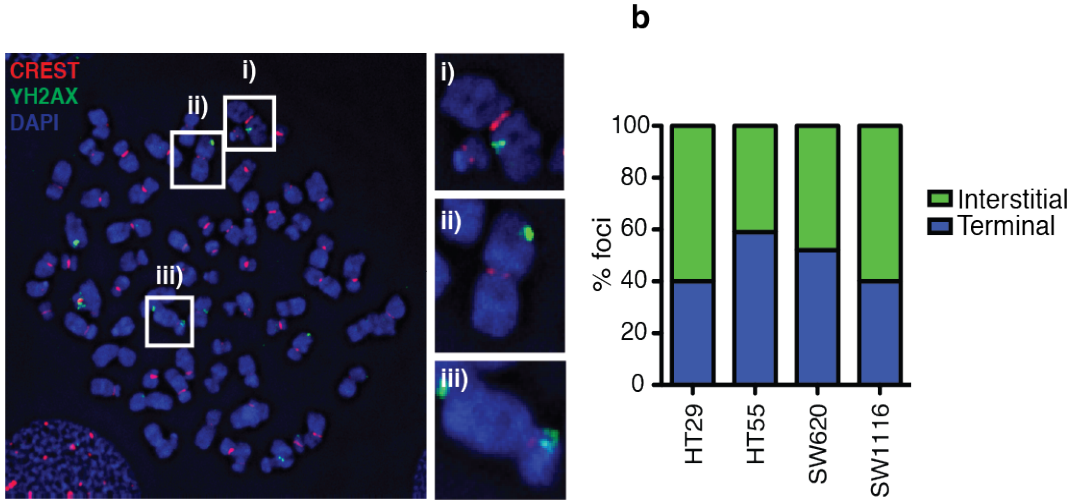

Figure 3.12 DNA damage are not confined to chromosome termini
a) An example of an HT29 metaphase spread stained with antibodies for γH2AX and anti-centromere antibodies, with inset i) interstitial γH2AX focus ii) γH2AX at the chromosome end (terminal DNA damage) and iii) γH2AX on a short chromosome arm (not scored)
b) Quantification of the percentage of foci that were interstitial or terminal across four CIN+ cell lines n>200 γH2AX foci per cell line. Data from one experiment.

3.6 Slow replication fork rates in CIN+ cell lines

DNA fibre assays and analysis were performed by Dr P Groth and M Weller. Data was interpreted together with PG, MW and Thomas Helleday.

To assess DNA replication directly, DNA fibre assays were performed on a panel of CIN+ cell lines (HT29, HT55, SW620 and SW1116), and in the CIN- cell lines, HCT-116 and RKO. Cells were sequentially pulsed with the thymidine analogues 5-chlorodeoxyuridine (CldU) and 5-iododeoxyuridine (IdU) for 30 minutes each, which are incorporated into replicating DNA. Cells were then fixed and DNA fibres prepared and stained to visualise the incorporated thymidine analogues. The lengths of tracts staining positively for CldU and IdU were then measured and the replication rate calculated. Representative DNA fibres are shown in Figure 3.13a. This revealed a slower replication rate in CIN+ cell lines relative to the two CIN- cell lines, and cell lines in other published studies (Figure 3.13 a,b and see Table 3.2). HCT-116 cells had an average replication fork rate (CldU measurement) of 1.11±0.16 kb/min while the fastest CIN+ cell line (HT29) had a replication fork rate of 0.83±0.05 kb/min. HT55 cells were the slowest at 0.55±0.06 kb/min, while SW620 and SW1116 had fork rates of 0.72±0.09 kb/min, and 0.65±0.05 kb/min respectively. Only 4-26% of forks in the CIN+ cell lines exceeded a rate of 1 kb/min, compared to greater than 50% of forks in both HCT-116 and RKO cell lines (Figure 3.13c). The distribution of replication fork rates is shown in Figure 3.13d.

Importantly, polyploidy cannot explain the slow replication rate in CIN+ cells as SW620 cells are near-diploid, HT29 and SW1116 are near-triploid, and HT55 cells are near-tetraploid (Table 3.1). The same pattern was observed for IdU measurements (see Figure 3.13b). The rate of replication fork progression seen in CIN+ cell lines is similar to that observed at fragile sites in an perturbed S phase, and genome-wide under conditions of replication stress (Ozeri-Galai et al., 2011, Letessier et al., 2011, Palakodeti et al., 2010), indicating that the slow replication rate may signify replication stress in CIN+ cells. However, it should be noted that absolute DNA replication rates determined by converting fibre lengths into kilobase per minute replication rates may be inaccurate. For more accurate assessment of DNA replication rates, the DNA molecules

may be subjected to molecular combing, ensuring greater uniformity in the stretched state of the DNA molecules (Bensimon et al., 1994).

Replication fork structures were also assessed in the four CIN+ cell lines and CIN- HCT-116 cells (Figure 3.13 e,f). Structures were classified as being: 1) origins that fired during the CldU pulse (1st label origins); 2) progressing forks, which had already fired prior to addition of the first label, and which continued during the second labelling period); 3) stalled forks/forks that terminated during the first labelling periods (only labelled during the CldU pulse); 4) origins that fired during the IdU pulse (2nd label origin); 5) origins that terminated during the second labelling period. CIN+ cell lines showed more progressing forks and fewer newly firing origins than HCT-116 cells (Figure 3.13e). The frequency of stalled forks or 1st label terminations was slightly elevated in SW620 and HT55 cells (Figure 3.13e). However, reduced replication fork rates were the most notable and consistent difference between CIN+ cells and HCT-116 cells, which coupled with the other observed hallmarks of replication stress in these cell lines (Figure 3.10), provide support for the hypothesis that replication stress is a major driver of CIN in colorectal cancer.

3.7 Inducing replication stress in CIN- cells initiates chromosomal instability

Experiments in both yeast and mammalian cells have demonstrated that induction of replication stress results in DNA damage, and an elevated rate of structural chromosome abnormalities (Baxter and Diffley, 2008, Ichijima et al., 2010, Chan et al., 2009, Bartkova et al., 2006, Bartkova et al., 2005). More recently, it has been demonstrated that oncogene-induced replication stress can induce chromosome segregation errors in mitosis in mammalian cells (Ichijima et al., 2010). However, neither the type of segregation error generated, nor whether these segregation errors can also result in chromosome non-disjunction, was assessed in these studies.

To examine the effects of replication stress upon chromosome structural integrity and segregation fidelity, HCT116 cells were treated with a low concentration (0.2 μM) of the DNA polymerase inhibitor Aphidicolin. This concentration of Aphidicolin does not block replication completely, but result in altered rates of

replication fork progression and replication stress (Chan et al., 2009, Lukas et al., 2011a, Glover et al., 1984, Ozeri-Galai et al., 2011) (see Introduction page 54).

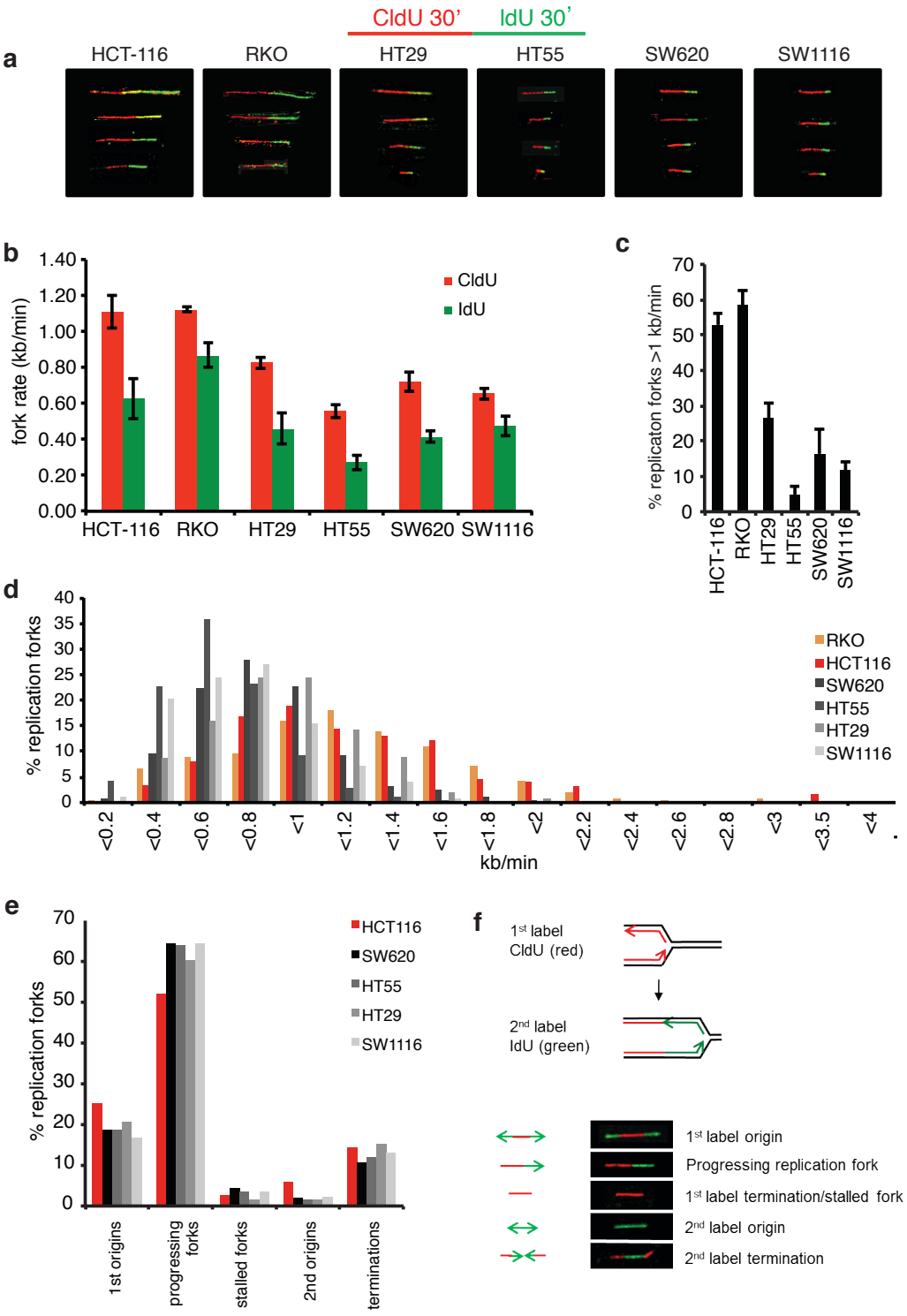

Figure 3.13 Slow replication fork rates in CIN+ CRC cell lines

a) Representative images of progressing replication forks labelled with CldU (red) and IdU (green) from each cell line
b) Mean fork rate ±s.e.m of 3 independent experiments, measured from both bidirectional and progressing forks. At least 50 fibres were analyased per cell line per experiment
c) % Forks progressing at >1 kb/min (mean±s.e.m of 3 independent experiments)
d) Distribution of fork rates for each cell line (sum of 3 independent experiments)
e) Types of replication fork structures observed in each cell line (sum of 3 independent experiments, n>600 fibres per cell line)
f) Schematic illustrating the different types of replication fork structures, with representative images

---

Cell type	DNA Combing/ DNA fibre	Reference	Fork rate (whole genome) kb/min	Fork rate (fragile site) kb/min
Lymphoblastoid	DNA combing	(Ozeri-Galai et al., 2011)	2.2 1 (+APH)	1.67 (FRA16C) 0.77 (+APH)
Keratinocytes	DNA combing	(Bester et al., 2011)	1.3 0.75 (+E6/E7)	
Foreskin fibroblasts (BJ)	DNA combing	(Bester et al., 2011)	1.5 1 (+cyclin E O/E)	
Primary fibroblasts	DNA combing	(Bester et al., 2011)	1.2 0.8(+cyclin E O/E)	
EBV-immortalised lymphocytes	DNA combing	(Letessier et al., 2011)	2.06	
Lymphocytes	DNA combing	(Palumbo et al., 2010)	1.91 0.47 (+APH)	1.2 (FRA6E) 0.45
U2OS osteo-sarcoma cell line	DNA fibre	(Petermann et al., 2010)	1.05	
HCT-116 (CIN-)	DNA fibre		1.11	
RKO (CIN-)	DNA fibre		1.12	
HT29 (CIN+)	DNA fibre		0.83	
HT55 (CIN+)	DNA fibre		0.55	
SW620 (CIN+)	DNA fibre		0.72	
SW1116 (CIN+)	DNA fibre		0.65	

Table 3.2 Replication fork rates of a range of cell lines
Fork rates (kb/min) measured by DNA fibre analysis of cell lines in published studies and of the cell lines in this thesis, over the whole genome, and at specific fragile sites

Aphidicolin-treated HCT-116 cells exhibited elevated prometaphase DNA damage (Figure 3.14 a,b), ultra-fine bridges (Figure 3.14 c,d) and G1 53BP1 bodies (Figure 3.14 e,f), consistent with responses to Aphidicolin treatment in other cell lines (Lukas et al., 2011a, Chan et al., 2009). Ultra-fine bridges were again enriched in cells with segregation errors, suggesting that the same defects that generate ultra-fine bridges also generate structural abnormalities and precipitate segregation errors. Interestingly, Aphidicolin-mediated induction of ultra-fine bridges that stained positively for RPA was more profound than the induction of ultra-fine bridges stained with PICH (83% of anaphases with RPA-positive versus 56% with PICH-positive ultra-fine bridges, Figure 3.15). Ultra-fine bridges may also represent persistent DNA catenation, which can be induced through inhibiting topoisomerases (Wang et al., 2008). In contrast to Aphidicolin treatment, treatment of cells with a specific inhibitor of topoisomerase-II alpha (ICRF193) resulted in a much weaker induction of RPA bridges (from 27 to 37% of anaphases) but an equivalent induction of PICH-positive UFBs (from 32 to 57% of anaphases, Figure 3.15). These data suggest that RPA is a good and reasonably specific marker for ultra-fine bridges induced by replication stress rather than DNA catenation. Discrepancies between the frequencies of PICH-positive ultra-fine bridges identified here and those in published studies (Chan et al., 2007, Chan et al., 2009) may be due to the fact that exclusively late anaphases were scored, in order to identify those with without segregation errors.

Following 24 hours of Aphidicolin exposure, 86% of HCT-116 anaphases exhibited segregation errors (Figure 3.16a), the majority of which were acentric chromosomes and anaphase bridges (Figure 3.16 b,c). Imaging Aphidicolin-treated HCT-116 H2B-mRFP cells revealed no delay in mitosis, despite an increased frequency of cells entering anaphase with uncongressed chromosomes (Figure 3.16 d,e). This indicates that the uncongressed chromosomes were not signalling to the mitotic checkpoint to delay anaphase onset. A likely explanation for this observation is that these uncongressed chromosomes are acentric, and in the absence of a centromere and kinetochore, they can neither attach to the mitotic spindle nor signal to the mitotic checkpoint.

In keeping with the types of segregation errors induced by Aphidicolin treatment, structurally abnormal chromosomes were present at high frequencies on metaphase

spreads; 3% of chromosomes displayed abnormalities, equating to greater than one abnormality per metaphase on average, versus 0.4% in untreated cells (Figure 3.17 a,b). 62% of metaphases displayed structural anomalies relative to 7% in control cells (Figure 3.17c). Hence, consistent with published reports, induction of replication stress results in structural chromosome aberrations.

To test whether replication stress-induced chromosome defects also lead to numerical chromosome segregation defects, similar to those observed in CIN+ cells, FISH was performed on interphase cells after 24 hours Aphidicolin treatment, as described in section 1.3. Deviation from the mode of both chromosomes was increased following Aphidicolin exposure (chromosome 2: from 5 to 11%, chromosome 15 from 5.8% to 8.4%, Figure 3.17 d,e), indicating that the structural instability resulting from replication stress can precipitate numerical instability.

In summary, pharmacological induction of DNA replication stress in CIN- HCT-116 cells results in a high frequency of anaphase segregation errors, chromosome structural defects and chromosome non-disjunction. Hence, induction of replication stress is able to recapitulate both structural and numerical chromosome aberrations that are observed in CIN+ CRC cells, further supporting the hypothesis that segregation errors in CIN+ cells may arise as a consequence of replication stress-induced structural defects.

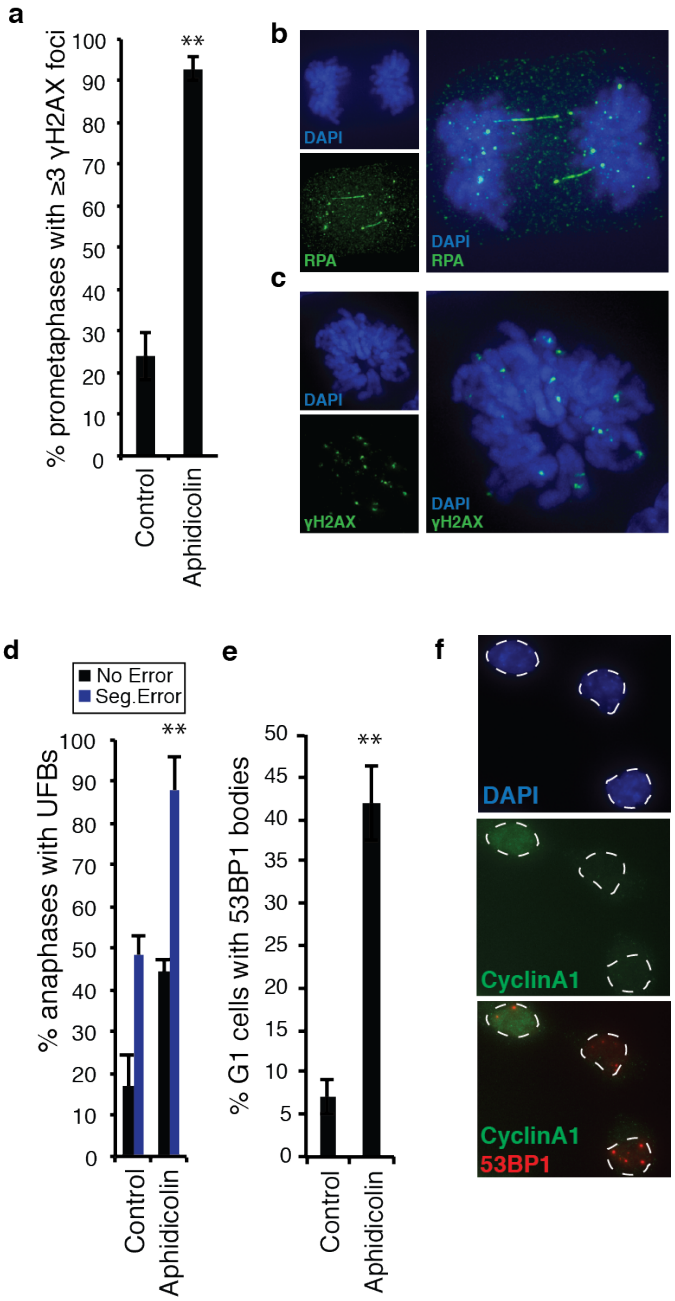

Figure 3.14 Pharmacological induction of replication stress in HCT-116
a) Quantification of prometaphase DNA damage in HCT-116 cells ± 0.2 μM Aphidicolin treatment for 24 hours (mean±s.e.m of 3 experiments, n=100 per experiment, ** $p<0.01$)
b) Prometaphase γH2AX foci in HCT-116 induced following Aphidicolin exposure
c) HCT-116 anaphase exhibiting ultra-fine bridges following Aphidicolin exposure
d) Quantification of ultra-fine bridges in anaphases with and without segregation errors ± Aphidicolin (mean±s.e.m of 3 experiments n=100 anaphases per experiment)
e) Quantification of G1 53BP1 bodies after Aphidicolin exposure (mean±s.e.m of 3 experiments n>150 cells per experiment)
f) Aphidicolin treated HCT-116 cells stained for cyclin A1 and 53BP1, exhibiting 53BP1 bodies in cyclin A1 negative cells. White lines show nuclear peripheries.

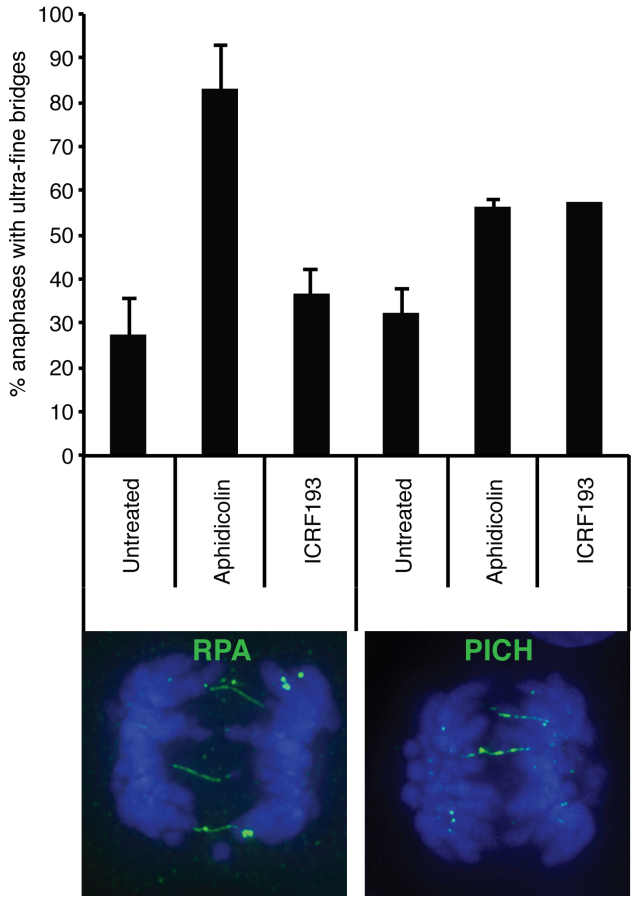

Figure 3.15 Comparison of PICH and RPA as markers of ultra-fine bridges
Percentage of HCT-116 anaphases with ultra-fine bridges marked with RPA or PICH, in untreated, Aphidicolin treated (0.2 μM, 24 hours), or ICRF193 treated (100nM, 2 hours before fixation) cells. Bars show mean and standard deviation of 3 experiments for untreated and Aphidicolin treated cells. ICRF193 experiments were performed twice. 100 anaphases were scored per condition per experiment.

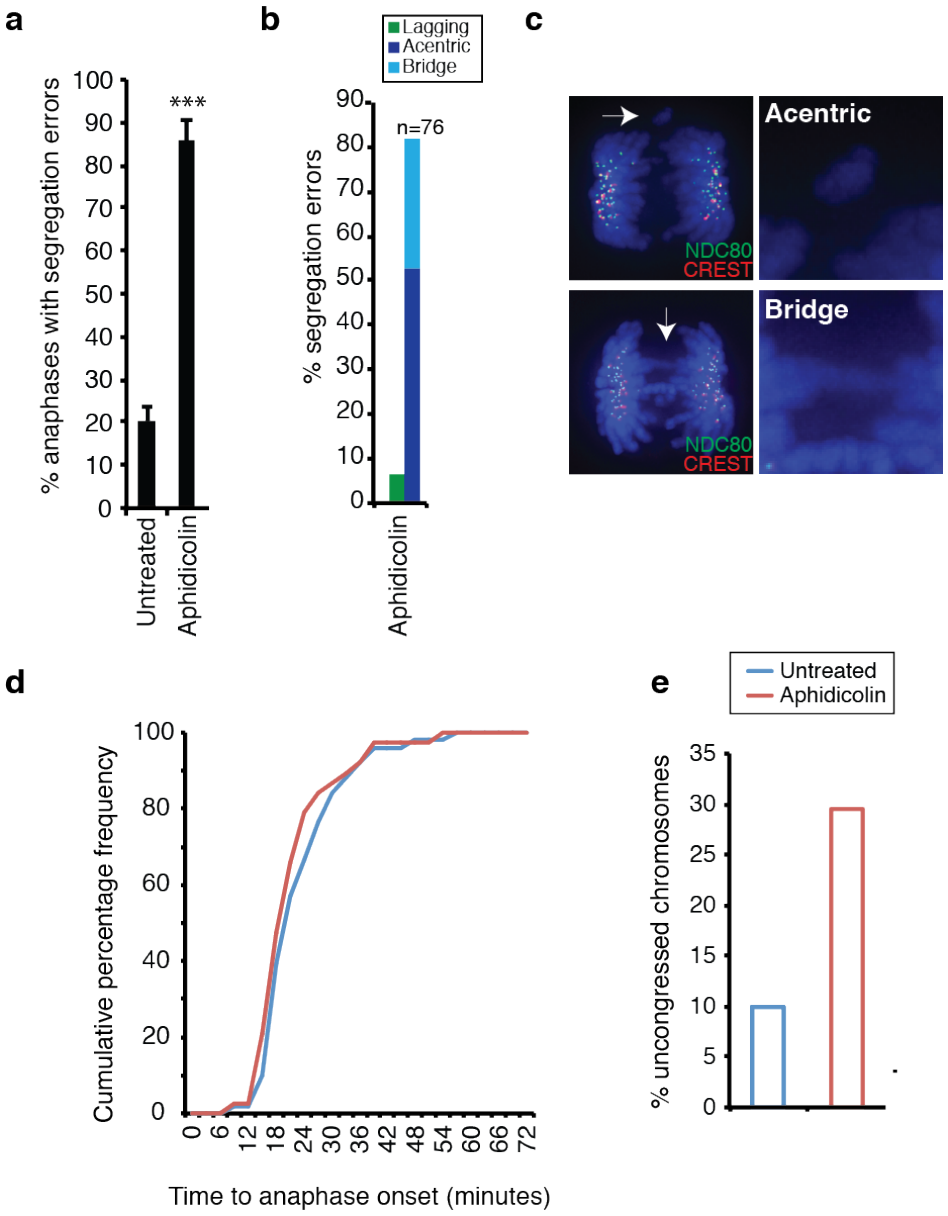

Figure 3.16 Pharmacological induction of replication stress induces chromosome segregation errors

a) Percentage anaphase segregation errors in HCT-116 cells ± Aphidicolin (0.2 μM 24 hours). Graph shows mean±s.e.m, 3 independent experiments, n>30 anaphases per experiment, student's t-test $p<0.001$

b) Segregation error classification of Aphidicolin treated cells (sum of 2 expts)

c) Examples of segregation errors in Aphidicolin treated cells, indicated by white arrows, with a magnified image of the segregation error

d) Cumulative percentage frequency plot of time from NEBD-anaphase onset ± Aphidicolin n=40 cells per condition

e) Percentage of cells entering anaphase with chromosomes that failed to congress to the metaphase plate n=40 cells per condition

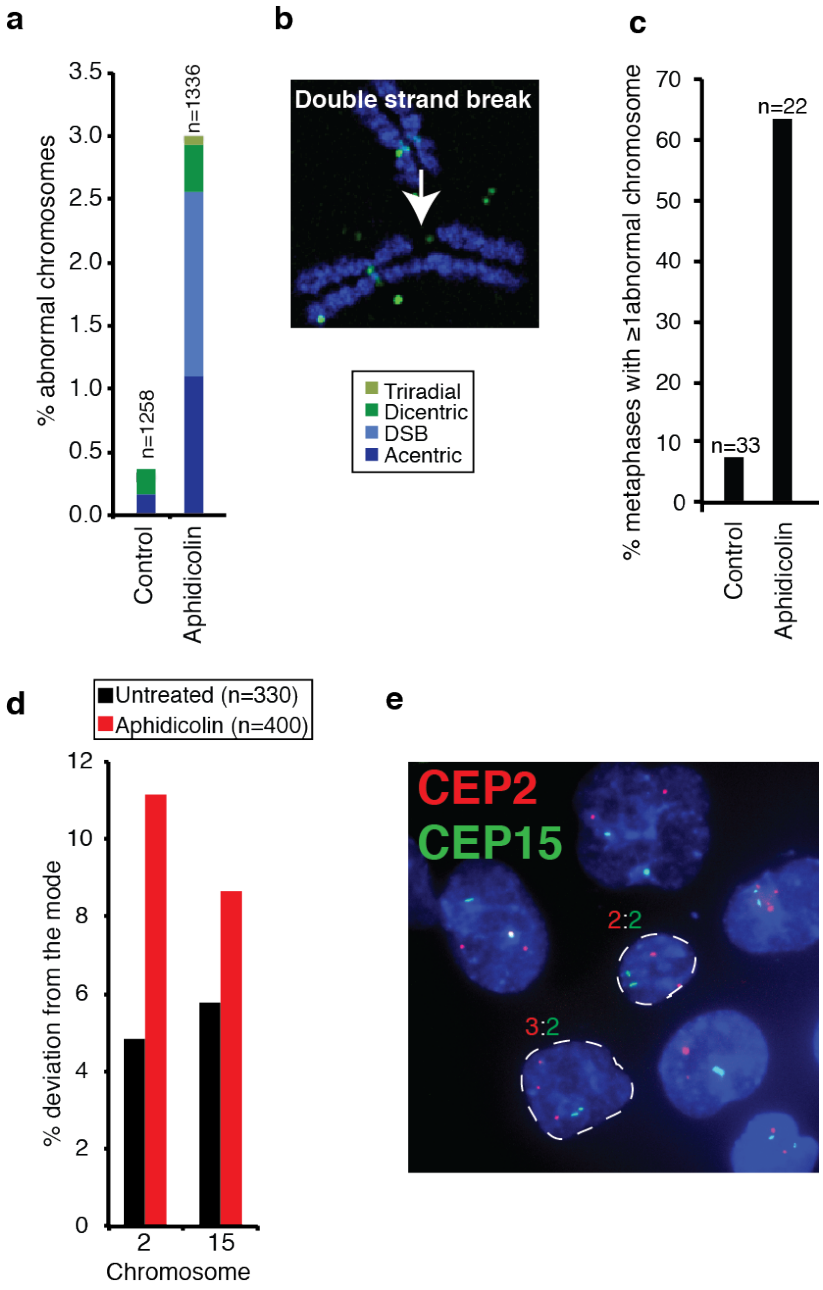

Figure 3.17 Pharmacological induction of replication stress results in structural and numerical instability

a) Percentage of chromosomes with structural abnormalities on HCT-116 metaphase spreads after Aphidicolin treatment (0.2 µM, 24 hours). Numbers of chromosomes scored are indicated above each bar. Data from one experiment.

b) Example image of a chromosome with Aphidicolin-induced DNA DSB

c) Quantification of percentage of HCT-116 metaphases with structural abnormalities. Numbers of metaphases scored are shown above each bar. Data from one experiment.

d) Percentage deviation from the modal centromere copy number of 2 for chromosomes 2 and 15, following Aphidicolin treatment. Numbers scored are indicated. Data from one experiment.

e) Aphidicolin-treated cells hybridised to fluorescently labelled centromere probes. Example nuclei are outlined and corresponding copy number indicated adjacently.

3.8 Conclusions and discussion

Having systematically examined anaphases in a panel of CIN+ cells it is evident that mitotic defects are not the sole cause of the chromosome segregation errors observed. The majority of segregation errors in CIN+ cells were acentric chromosomes and anaphase bridges (suggestive of pre-mitotic defects) rather than lagging chromosomes, which are suggestive of mitotic dysfunction. CIN+ cells exhibited hallmarks of DNA replication stress, namely elevated prometaphase DNA damage, and 53BP1 nuclear bodies in G1 cells. Furthermore, ultra-fine anaphase bridges were enriched in cells with segregation errors. Prometaphase DNA damage foci were not confined to the telomeres and hence are unlikely to be exclusively caused by telomere dysfunction. In keeping with these results, slow replication fork rates were observed in CIN+ cell lines. To test the hypothesis that replication stress can induce CIN, CIN- HCT-116 cells were treated with Aphidicolin, which resulted in both numerical and structural CIN. These data suggest that elevated replication stress could drive the structural aberrations and chromosome segregation errors observed in CIN+ cells.

Recent studies have revealed that lagging chromosomes, generated through experimental perturbation of mitosis, can precipitate structural chromosome defects (Crasta et al., 2012, Janssen et al., 2011). However, structural chromosome defects induced by mitotic dysfunction occur at low frequencies, despite induction of lagging chromosomes at very high frequencies (at least one lagging chromosome in 80% of anaphases). High frequencies of lagging chromosomes and evidence of obvious mitotic dysfunction would therefore be expected if mitotic dysfunction were the main driver of structural chromosome abnormalities in CIN+ cells. Contrary to this hypothesis, lagging chromosomes occur at relatively low frequencies in CIN+ CRC cell lines and there is an absence of gross mitotic dysfunction other than occasional multipolar spindles. This implies that the observed structural chromosome aberrations do not specifically arise as a consequence of DNA damage to lagging chromosomes. In addition the observation of slow replication fork rates alongside other hallmarks of replication stress, provides a possible direct mechanism for the generation of structural chromosome abnormalities during interphase, independent of mitotic dysfunction.

In summary, the evidence presented here indicates that pre-mitotic defects generating structurally abnormal chromosomes are likely to be the cause of the majority of segregation errors, at least in the panel in CIN+ CRC cells examined, and that these may be a consequence of elevated DNA replication stress relative to CIN- CRC cell lines. The cause of elevated DNA replication stress in CIN+ CRC is unclear. Neither mutations in known oncogenes nor *TP53* mutations can explain CIN, as these mutations also occur in CIN- cell lines, both as single mutations and in combination (see Table 3.1 (Lee et al., 2011, TCGA, 2012)). This suggests that alternative or additional mechanisms contributing to replication stress may be operating in CIN+ cells. In light of this efforts to identify novel suppressors of CIN in CRC will be described in the next chapter.

Chapter 4. Results 2 – Identifying CIN-suppressors encoded on chromosome 18q

CIN is a high-risk clinical phenotype. Therefore developing a greater understanding of mechanisms contributing to numerical and structural chromosomal instability in tumours is important to facilitate development of therapeutic approaches for targeting CIN. In Chapter 3, evidence was presented that suggests elevated replication stress is a prominent cause of CIN in colorectal cancer. However, the cause of the replication defect in CIN+ CRC is unknown.

In this chapter, the hypothesis that CIN could be driven by stable copy number changes is examined. While CIN+ tumours have complex karyotypes and ongoing instability, those copy number changes that occur recurrently, and which are observed specifically in CIN+ tumours, could result in repression or overexpression of genes that play a role in initating or sustaining CIN. Previous studies have identified common copy number gains and losses in CIN+ or aneuploid CRCs, with gains on chromosomes 7, 8, 13 and 20 , and losses in 4, 14, 17, and 18 (Sheffer et al., 2009, Diep et al., 2006, Nakao et al., 2004, Tsafrir et al., 2006, Watanabe et al., 2001, Jen et al., 1994). Studies in yeast have also lent support to the concept that aneuploidy-driven alterations in gene dosage can drive genomic instability (Pavelka et al., 2010, Sheltzer et al., 2011).

Therefore, high resolution genomic regions of copy number loss specific to CIN+ CRC were defined and the contribution of genes encoded in these loci to the maintenance of chromosomal stability was characterised using RNA interference. This analysis focussed on regions of copy number loss, as loss of chromosome 18q has long been viewed as a surrogate for CIN in colorectal cancer, provoking suggestions that it may encode suppressors of chromosomal instability (Rowan et al., 2005, Bacolod and Barany, 2011). In addition, gene-overexpression screening, which would have been necessary to investigate amplified regions in an unbiased fashion, is challenging as it is difficult to control protein expression levels, leading to substantial variation in the degree of overexpression between different vectors across a screen (Grimm, 2004). The screen examined cells for increased frequencies of chromosome segregation errors at anaphase, as the fidelity of this process is affected by defects in both interphase and mitosis. Through RNA interference-based examination of genes encoded in a region of

copy number loss on 18q, three candidate suppressors of CIN were identified on chromosome 18q, whose silencing promoted structural chromosomal aberrations and chromosome misegregation events, similar to those observed in CIN+ cancer cells.

In this chapter DNA copy number analysis and gene expression analysis were designed in collaboration with David Endesfelder, Sarah McClelland and Arne Schenk, with all analysis performed by David Endesfelder and Arne Schenk. Dr Enric Domingo undertook all analysis of the carcinoma-in-adenoma cohort. Methodology for the siRNA screen scoring and deconvolution was established with Dr Sarah McClelland, but all screening data presented here is my own.

4.1 A recurrent CIN-specific genome architecture

In order to identify CIN-specific regions of consistent copy number loss *in vivo*, comparative genomic hybridisation data (array CGH) was analysed for a cohort of 26 aneuploid colorectal tumours. Aneuploidy status was determined by flow cytometry. It is important to distinguish between aneuploidy and CIN; CIN results in aneuploidy, but tumours can also exhibit stable aneuploidy. Nonetheless, aneuploidy represents a reasonable surrogate measure for tumour CIN status, as analysing CIN in tissue specimens is challenging (see Introduction, Section 1.1.1). CGH data was analysed using the using the GISTIC algorithm (Beroukhim et al., 2007) (see Materials and Methods, Section 2.11.1), which identifies recurrent copy number changes. The most significant copy number losses ($q<0.25$) were observed on chromosomes 8p, 17p and 18q (Figure 4.1a).

In order to confirm that these copy number losses were specific to CIN+ CRC, rather than being observed in all colorectal cancers, SNP array data (Affymetrix SNP 6.0) was analysed for the panel of 29 CRC cell lines, both CIN+ and CIN-. Use of this platform also allowed high resolution mapping of regions of copy number loss. For consistency with the tumour analysis, cell lines with a DNA index of >1.2 were classified as CIN+ (CIN+ n=20, CIN- n=9). This threshold accurately classifies cell lines that have been previously characterised as CIN+ or CIN- by our and other groups using cytogenetics approaches (Lee et al., 2011, Thompson and Compton, 2008,

Roschke et al., 2003, Lengauer et al., 1997, Stolz et al., 2010, Abdel-Rahman et al., 2001, Melcher et al., 2002). Furthermore, as described in Chapter 3, 7 of the 20 cell lines displayed numerical and structural CIN measured directly by FISH. In addition, numerical and structural karyotypic complexity was demonstrated to be significantly higher in the 20 CIN+ cell lines than the 9 CIN- cell lines (Chapter 3, Figure 3.3). Details of the 29 cell lines are shown in Table 3.1 in Chapter 3.

An advantage of SNP array data is that it can be used to determine absolute integer copy number (Greenman et al., 2010), enabling the identification of regions of loss with a copy number of 1 or 0, which is not possible with conventional CGH. Analysis of the cell lines took into account both the amplitude and frequency of copy number loss across all cell lines. Genomic regions that showed significant copy number loss but were not lost in at least 50% of CIN+ cell lines were excluded. A more detailed explanation of the copy number analysis of the cell lines can be found on page 90.

Cell lines and aneuploid tumours shared strikingly similar patterns of copy number loss (Figure 4.1 a,b). The most commonly lost regions in both tumours and cell lines were 8p, 17p and 18q (Figure 4.1). A comparison between the genes encoded within regions of DNA copy number loss in aneuploid tumours (Figure 4.1a) with those most significantly lost in CIN+ cell lines (Figure 4.1b) revealed a highly significant overlap of 2015 genes (Fisher's exact test $p<2.2e-16$), indicating a consistent genomic architecture associated with CIN+ CRC. The significance of this overlap also indicates that CIN+ cell lines are genomically highly similar to aneuploid tumours. Genomic similarity between CIN+ cell lines and tumours is important, as it is currently only possible to study endogenous mechanisms of CIN *in vitro* using cell lines derived from CIN-tumours.

4.1.1 Recurrent loss of chromosome 18q in CIN+ Colorectal Cancer

Loss of the long arm of chromosome 18 (18q) was observed in 88% of aneuploid tumours and 80% of CIN+ cell lines, (Figure 4.1 and Table 4.1) consistent with published studies (Sheffer et al., 2009, Rowan et al., 2005, Jen et al., 1994, Vogelstein et al., 1988). The frequency of 18q loss is substantially higher than the frequency of mutations in either of the tumour suppressor genes SMAD4 or DCC (see Introduction Table 1.4). This suggests that selection for loss of heterozygosity due to mutations in

these genes cannot account for the high frequency of 18q loss in CIN+ CRC. As most CIN+ tumours tend to be near-triploid or tetraploid, a tumour can harbour relative

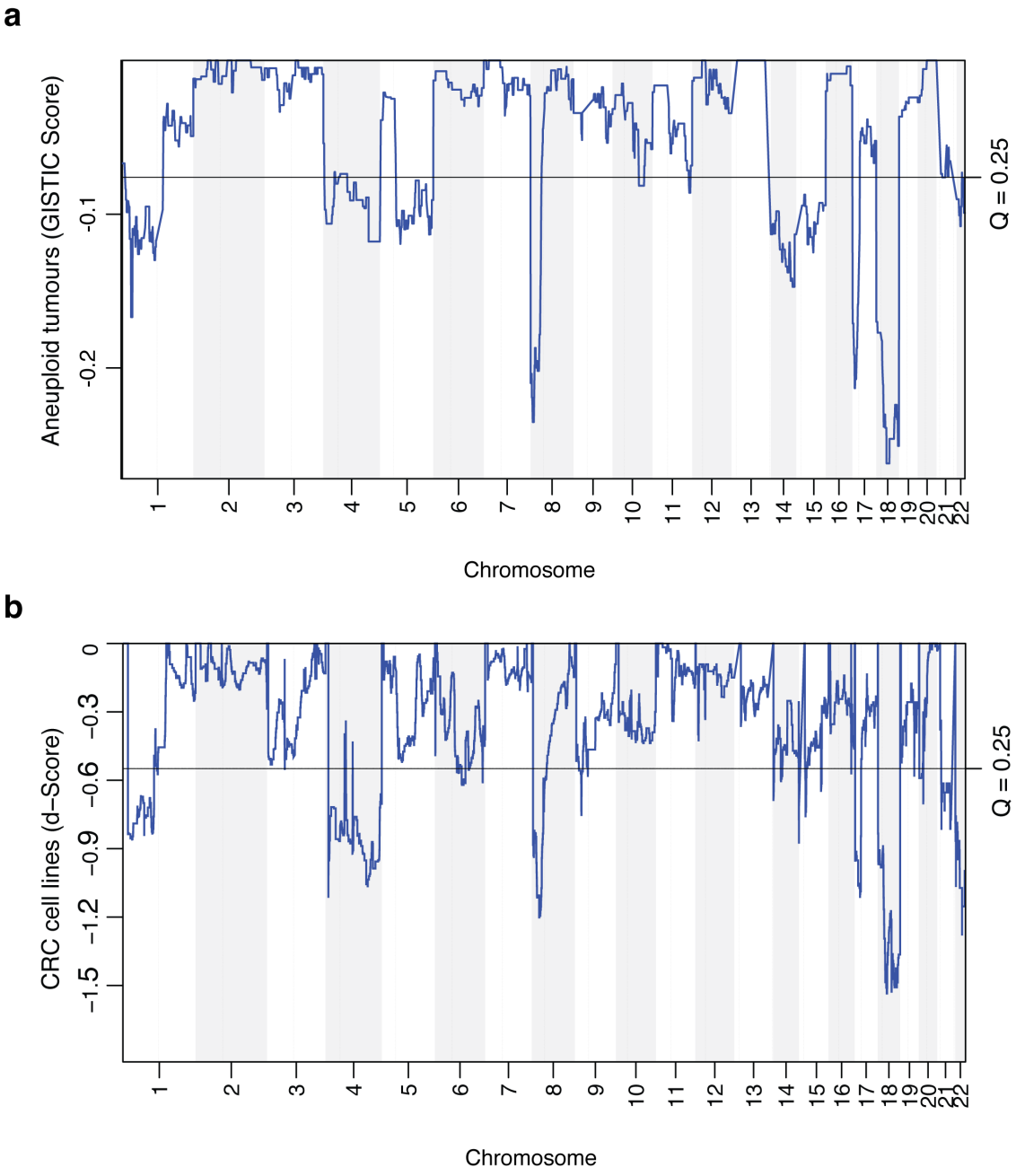

Figure 4.1 Somatic copy number losses in aneuploid/CIN+ colorectal cancer
a) GISTIC analysis of comparative genomic hybridisation data from 26 aneuploid colorectal tumours. Significant regions of somatic copy number loss were defined using a false discovery rate of 0.25, depicted by the black line.
b) Analysis of somatic copy number losses in CIN+ (n=20) versus CIN- (n=9) CRC cell lines. Significant regions of somatic copy number loss were defined using a false discovery rate of 0.25, depicted by the black line.

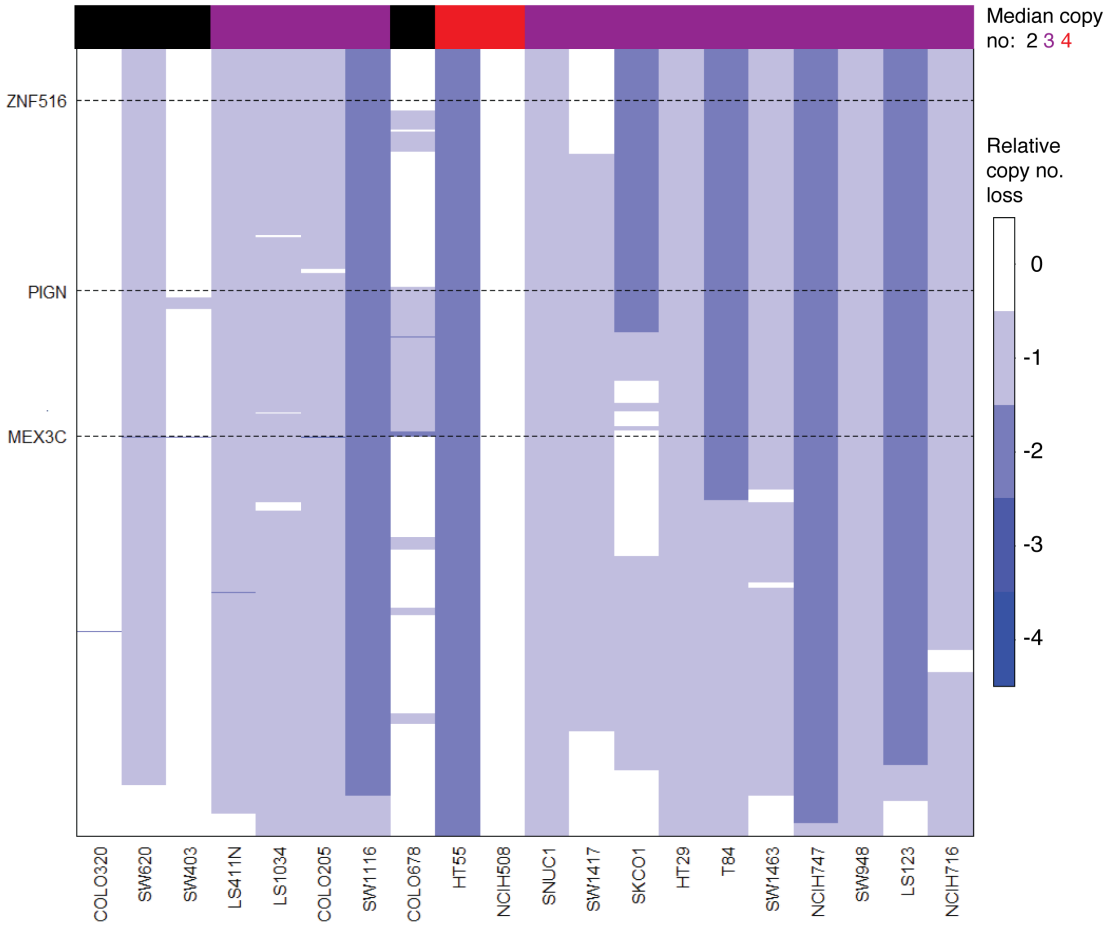

Figure 4.2 18q loss in CIN+ CRC cell lines
Heatmap of copy number loss over 18q 20 CIN+ CRC cell lines. Integer copy numbers were defined from SNP-CGH using the PICNIC algorithm(Greenman et al., 2010). Each column is a single cell line, with the y-axis representing the distance along 18q (centromere at the bottom). The bar along the top indicates cell line ploidy (median copy number). The key at the right hand side indicates the degree of copy number loss relative to median copy number.

copy number loss of two copies of 18q, and yet still retain one or two copies of 18q. This is illustrated in Figure 4.2, a heatmap of the relative copy number loss of 18q. 18q was the only region of the genome present at 1 or 0 copies in at least 30% of cell lines, and only one cell line had more than 2 copies of 18q (NCIH508 – Figure 4.2), despite the majority of CIN+ cell lines being polyploid. 18q loss was not confined to polyploid tumours, as near-diploid CIN+ cell lines also exhibited 18q loss (Figure 4.2).

	Sanger Cell Lines (CIN+, SNP 6.0) N = 20	Aneuploid Tumours (BAC Array) N = 26
18q loss (>50% of 18q)	80%	88%
18q loss (>75% of 18q)	70%	85%

Table 4.1 Frequency of 18q loss in CIN+ CRC cell lines and aneuploid colorectal tumours (BAC array and TCGA cohort)

4.1.2 A temporal association of 18q copy number loss with aneuploidy onset

All analysis of the carcinoma-in-adenoma cohort presented in this section was performed by Dr Enric Domingo. I conceived the analysis of 18q LOH in polyploid tumours, and interpreted data provided by David Endesfelder.

The temporal sequence of 18q loss in the development of CRC was then investigated, analysing a cohort of 28 adenomas (pre-invasive tumour) with adjacent carcinoma within the same specimen (Figure 4.3a). Hematoxylin and eosin slides of the samples were reviewed and regions marked as normal (if present), adenoma, or carcinoma accordingly. Then these were used as a guide to take tissue from each region from unstained slides by needle microdissection. DNA was extracted and assessed for 18q loss of heterozygosity (LOH), using either SNP array technology or microsatellite analysis (see Materials and Methods, section 2.10.2). 18q LOH is indicative of 18q somatic copy number loss.

10/28 (35.7%) of adenomas, and 21/28 (75%) of carcinomas from within the same specimens showed 18q LOH, indicating that 18q loss often occurs during the adenoma-carcinoma transition. This is consistent with the frequency of 18q LOH in adenomas and carcinomas reported in the landmark study by Vogelstein (Vogelstein et al., 1988). Interestingly, in Vogelstein's study, 18q LOH was observed at much higher frequencies in advanced than early adenomas. As the adenoma-carcinoma transition has already occurred in the 28-patient cohort analysed here, it can be inferred that the adenomas examined are advanced adenomas. Together with Vogelstein's observations, these data imply that 18q LOH occurs during the adenoma-carcinoma transition.

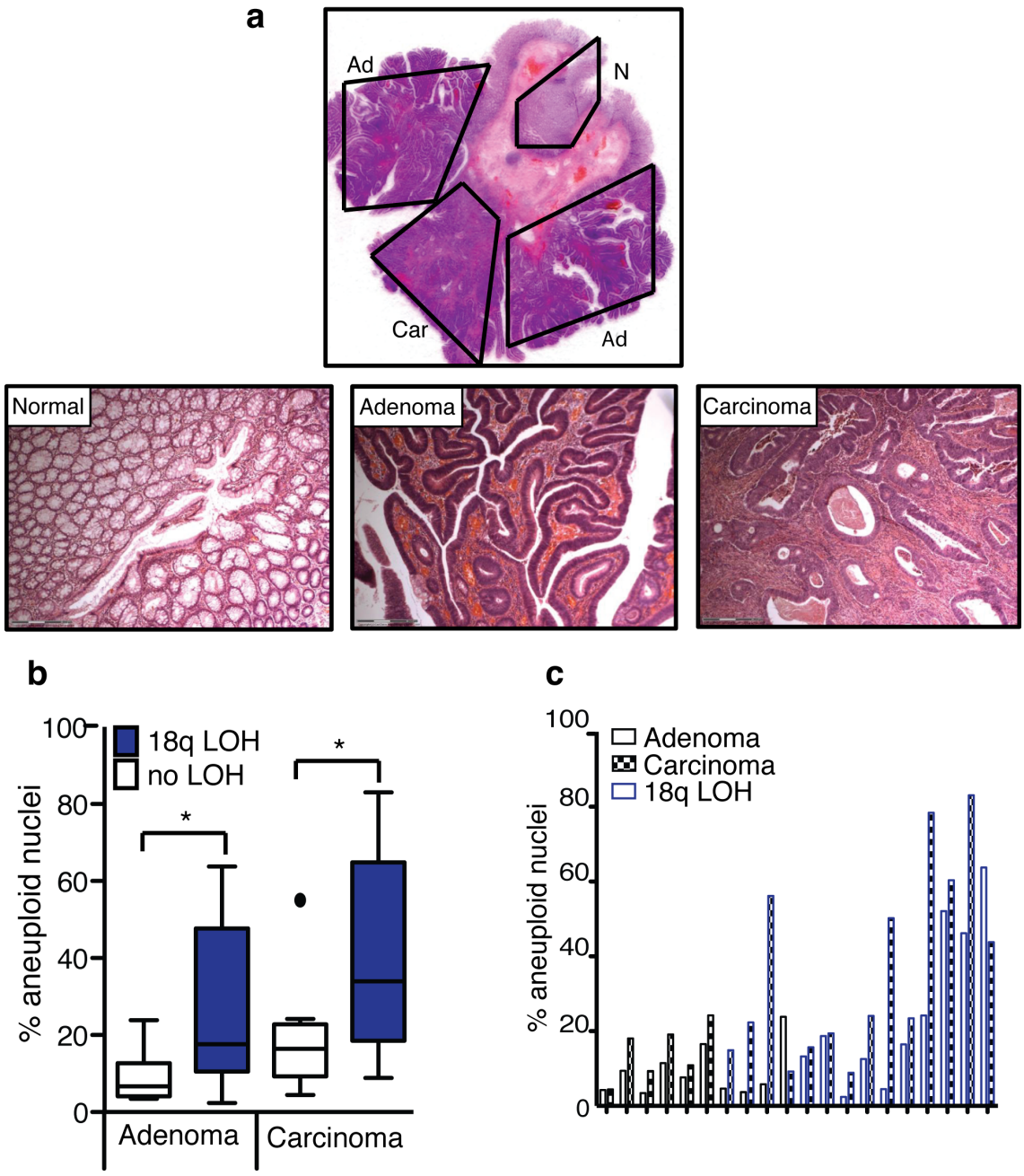

Figure 4.3 Temporal association of 18q loss and aneuploidy
a) Images of sections from a tumour specimen containing both carcinoma and adjacent adenoma
b) Paired adenomas and carcinomas (n=20) were classified according to 18q LOH status (see Materials and Methods) and the percentage of aneuploid nuclei determined by DNA image cytometry. The average of scanned nuclei from epithelial cells per sample was 1126±434. Tukey box and whiskers plot, students T-test * $p<0.05$
c) Percentage aneuploid nuclei in paired adenoma (blank bars) and carcinoma sections (patterned bars). 18q LOH is indicated by a blue bar outline.

Data provided by Enric Domingo.

To assess the relationship of 18q LOH with aneuploidy onset, suspensions of nuclei were then prepared from both adenoma and carcinoma, for a subset of 20 specimens and DNA image cytometry was used to determine ploidy status. 18q LOH was significantly associated with an increased percentage of aneuploid nuclei in adenomas ($p=0.03$) and in carcinomas ($p=0.05$) (Figure 4.3 b,c). These observations support the hypothesis that 18q loss precedes the onset of aneuploidy, during the adenoma to carcinoma transition (Thirlwell et al., 2010, Woodford-Richens et al., 2001).

To further explore the hypothesis that 18q loss precedes the onset of aneuploidy, 18q LOH was examined in tumours from an independent cohort of colorectal tumours from The Cancer Genome Atlas (TCGA). In polyploid tumours, 18q loss is rarely absolute and tumours often retain more than one copy of 18q. LOH may therefore indicate complete genomic deletion, the presence of only a single allele, or multiple copies of the same allele. In polyploid tumours retaining more than one copy of 18q, LOH implies that copy number loss occurred prior to polyploidisation, which often accompanies aneuploidy and CIN (Storchova and Pellman, 2004)(Figure 4.4a).

Of the polyploid TCGA tumours retaining more than one copy of 18q, 58.4% showed both LOH and copy number loss, for which the most likely explanation is copy number loss prior to polyploidisation. 7.6% showed LOH without copy number loss i.e. multiple copies of the same allele, at an equivalent copy number to the ploidy of the tumour. This indicates copy neutral LOH arising prior to polyploidy (Figure 4.4b). 23% of tumours showed 18q copy number loss without LOH, implying loss of 18q after polyploidisation, and the remaining 11% of tumours harboured neither 18q LOH nor 18q copy number loss (Figure 4.4b). The occurrence of polyploid tumours with multiple copies of the same allele of 18q, together with the observation of 18q LOH in adenomas, (Figure 4.3 and (Vogelstein et al., 1988)), support the hypothesis that 18q loss occurs before the onset of polyploidy in CRC tumorigenesis.

In summary, the long arm of chromosome 18 is recurrently lost in CIN+ CRC, and 18q loss appears to occur early during tumorigenesis, at the adenoma-carcinoma transition, coincident with the onset of aneuploidy. This raises the hypothesis that loss of 18q could have a role in initiating and maintaining chromosomal instability in CIN+ CRC, and might encode one or more CIN-suppressor genes, loss of which might initiate chromosome missegregation.

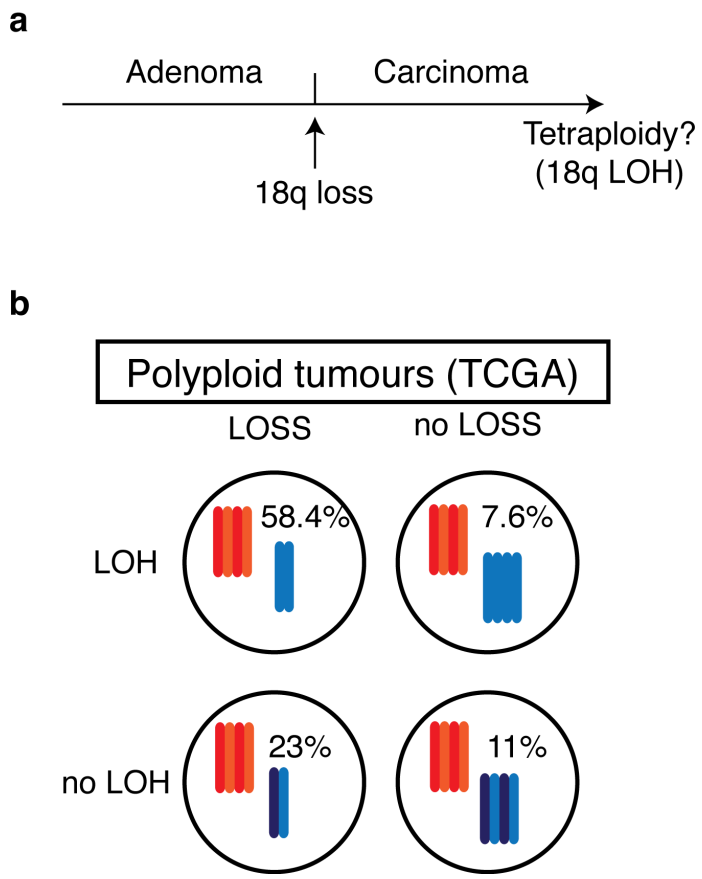

Figure 4.4 18q loss usually precedes polyploidy in CRC development
Schematic and percentage of polyploid tumours with >1 copy of 18q (TCGA cohort): LOH and copy number loss of 18q, LOH and no copy number loss, no LOH with copy number loss, and no LOH and no copy number loss. 18q loss was defined as >75% of 18q showing copy number loss relative to the ploidy of the tumour.

4.2 Screening for novel suppressors of chromosomal instability

4.2.1 Identification of candidate CIN-suppressor genes

To investigate the potential role of genes encoded on 18q in chromosome segregation fidelity, genes present at 0 or 1 copy in at least 30% of CIN+ cell lines were selected, identifying 94 genes encoded on chromosome 18q, and one gene on chromosome 15 (Appendix 1). Both genome-wide and on chromosome 18q, homozygous deletion was a rare event and is therefore unlikely to be a common genomic driver of CIN. These

genes represent the most frequently lost genes in this panel of CIN+ colorectal cancer cell lines, which are also lost in aneuploid colorectal tumours. These genes show copy number loss in 80% of CIN cell lines and 88% of aneuploid colorectal tumours analysed (Figure 4.1).

4.2.2 SiRNA screen for chromosome segregation error induction

CIN+ cells exhibit a high rate of chromosome segregation errors during anaphase, according to both published observations and data presented in Chapter 3 (Lengauer et al., 1997, Thompson and Compton, 2008). Segregation errors are associated with both mitotic and pre-mitotic defects that result in CIN. In order to identify previously uncharacterised regulators of CIN among the 95 genes identified above, a small-interfering RNA (siRNA) screen was performed in the near-diploid CIN- cell line, HCT-116 (Thompson and Compton, 2008, Lengauer et al., 1997, Roschke et al., 2003). HCT-116 cells have two intact copies of 18q (Gaasenbeek et al., 2006).

Dharmacon siGENOME smartpools of 4 different siRNA sequences were used to silence each putative CIN-suppressor gene. After 48 hours, indirect immunofluorescence was performed with antibodies for alpha-tubulin in order to distinguish anaphase from telophase cells (see Introduction Figure 1.2). The proportion of bipolar anaphase cells with one or more chromosome segregation errors was quantified manually for each gene (Figure 4.5a). Multipolar anaphases were noted but not included in the quantification of the segregation error frequency, as these divisions have been shown to generate non-viable cells and are considered unlikely to contribute substantially to ongoing CIN (Ganem et al., 2009, Stewenius et al., 2005). Hits were defined as genes whose depletion induced segregation errors to beyond three standard deviations above the mean segregation error frequency for control siRNA-transfected HCT-116 cells (>37%). Twelve genes exceeded this threshold, silencing of which resulted in segregation errors in 37-57% of anaphases (Figure 4.5b).

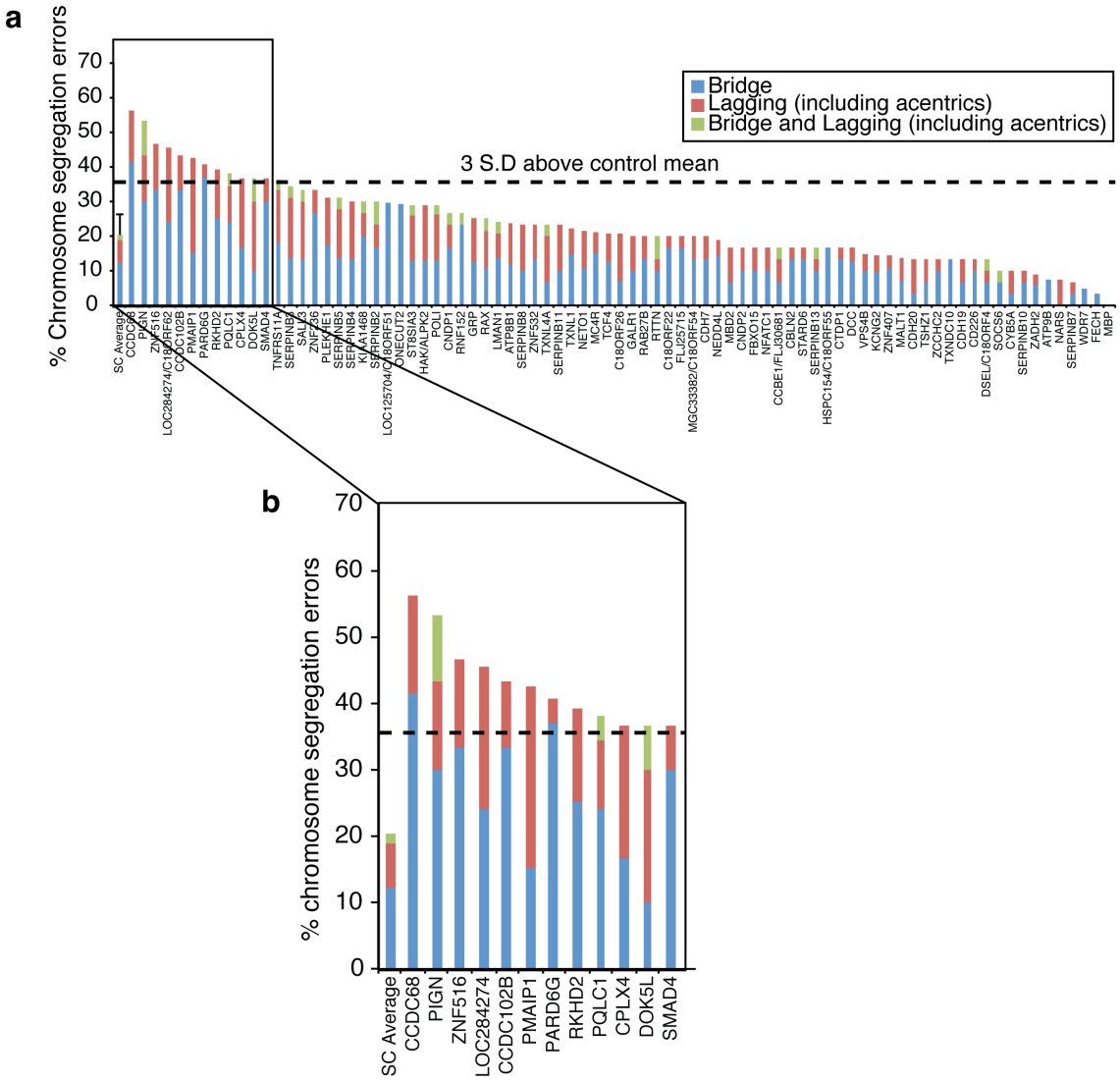

Figure 4.5 siRNA screen of 18q genes to identify suppressors of chromosome segregation errors

a) Percentage anaphases displaying chromosome segregation errors after 48 h silencing each of the 18q genes in HCT-116 cells, scored manually. N=30 anaphases per siRNA pool.

b) Zoomed in panel of the genes surpassing the screen threshold (>3 standard deviations above the mean segregation error frequency in control transfected cells =37% of anaphases)

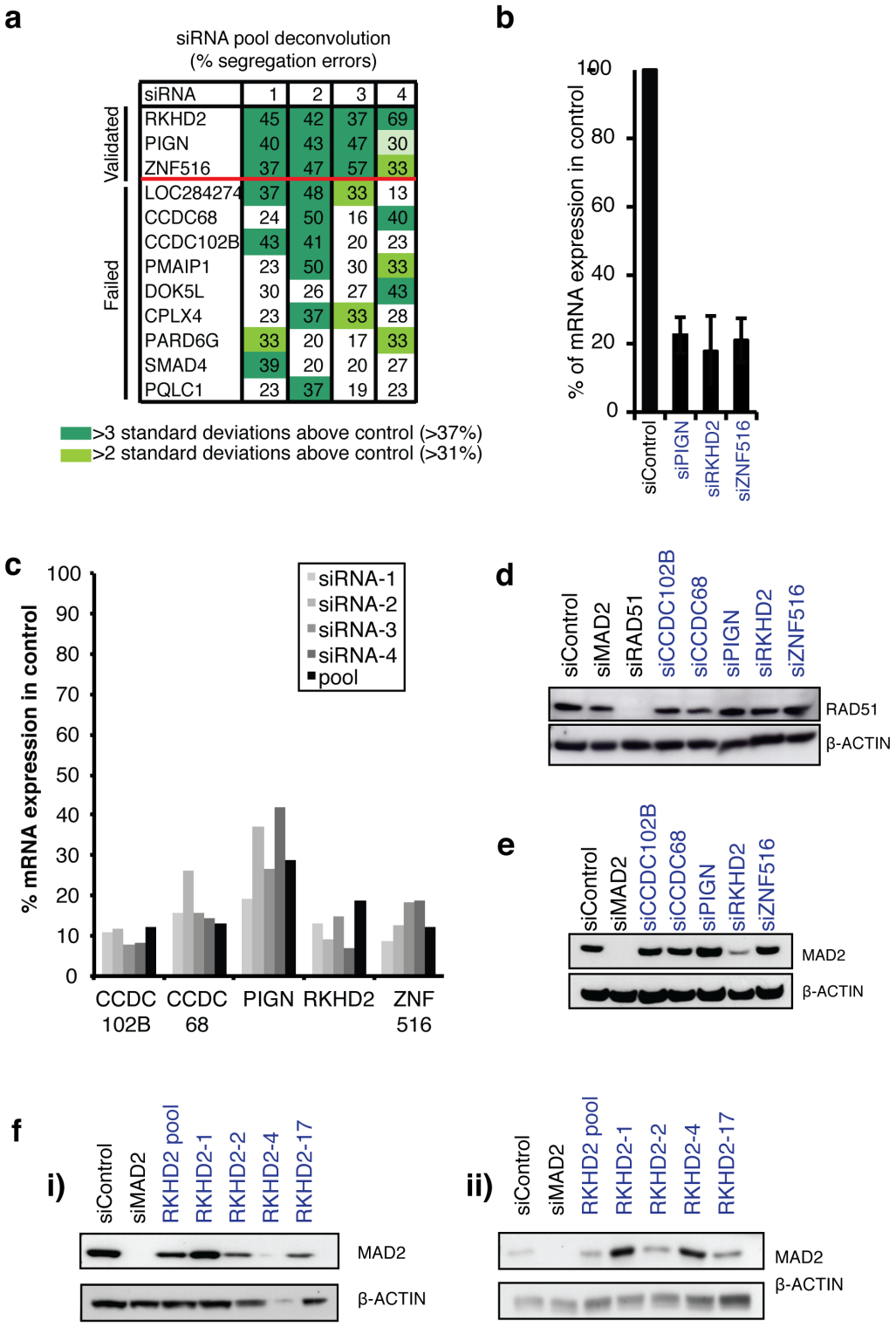

Figure 4.6 Screen deconvolution and validation
a) siRNA pool deconvolution: segregation error rates after transfection with the four individual siRNAs from the pool. Validation required at least two sequences to induce segregation errors in at least 37% of anaphases (dark green shading) n>30 anaphases per siRNA, one experiment.

b) mRNA expression in HCT-116 relative to expression in control-transfected cells for each validated siRNA pool. Bars depict the mean ± standard deviation of 3 independent experiments.
c) mRNA expression in HCT-116 relative to expression in control-transfected cells for individual sequences and siRNA pools.
d) RAD51 protein levels in HCT-116 after 48 h transfection with the indicated siRNAs
e) MAD2 protein levels in HCT-116 after 48 h transfection with the indicated siRNAs
f) MAD2 protein levels following transfection with individual RKHD2 siRNAs, MAD2 and RKHD2 siRNA pools, and scrambled control siRNA. Two western blots are shown due to under-loading of the RKHD2-4 sample in the first blot, and under-loading of the control sample in the second blot. This result was observed multiple times with at least two different batches of each siRNA sequence, although not with two batches of RKHD2-17 ordered within the last year.

4.3 SiRNA screen validation

4.3.1 siRNA pool deconvolution, silencing efficiency

The siRNA screen was performed with pools of four siRNA sequences targeting each of the 95 genes. To exclude siRNA pools that acted through off target effects, hit gene silencing was then repeated with the four individual siRNA sequences comprising the original siRNA pool. Off-target effects are a major consideration in designing RNA interference based screening approaches (Sigoillot et al., 2012). Demonstrating reproducible phenotype induction between multiple different sequences targeting the same gene gives confidence that the phenotype is attributable to silencing the targeted gene, rather than a consequence of off-target effect. Therefore only siRNA pools for which four out of four siRNAs induced segregation errors were considered for further analysis (Figure 4.6a): PIGN, RKHD2, ZNF516.

Gene silencing efficiency was then measured by qPCR after transfection of the individual siRNA sequences and pools. In the assessment of the individual siRNA sequences, the genes that validated with at least two out of four siRNAs were also included (CCDC68, CCDC102B and LOC284274), to exclude the possibility that the failure of these sequences to validate was due to inadequate gene silencing by the siRNAs that failed to induce a phenotype. All siRNA pools effectively silenced target gene expression by more than 78% relative to control-transfected cells (Figure 4.6b,c). All individual sequences also effectively reduced gene expression, including those sequences that failed to validate for CCDC68 and CCDC102B (Figure 4.6c).

LOC284274 transcripts could not be detected in HCT-116 and thus no further analysis was conducted for this gene, as it was not possible to validate siRNA knockdown or exclude that this effect was off target. The observation of gene silencing without phenotype for siRNAs targeting CCDC68 and CCDC102B supports the application of a stringent threshold to define validated siRNA pools in this siRNA screen. Unfortunately, good antibodies were not available for any of these 5 genes, and thus it was not possible to assess protein knockdown.

It is important to note that on the basis of this analysis, it is not possible to exclude that other genes encoded on 18q have a role in suppressing chromosomal instability. SiRNA pools which scored below the screen threshold (for example those falling between 2-3 standard deviations above the mean level of segregation errors in control cells) may reproducibly increase segregation errors, although at a lower level than observed after silencing PIGN, RKHD2 and ZNF516. In addition not all proteins are equally amenable to siRNA-mediated depletion, due to for example, long protein half-life, high mRNA abundance or poor siRNA efficiency. Therefore it is not possible to exclude that there are other genes on 18q that might also have a role in suppressing chromosomal instability. However, as PIGN, RKHD2 and ZNF516 were the strongest validated hits from this screen, these genes were taken forwards for further validation.

4.3.2 Excluding common off-target effects

Publications in the last two years have reported frequent off-target effects on the core mitotic checkpoint component MAD2 (Hubner et al., 2010, Westhorpe et al., 2010, Tsui et al., 2009, Sigoillot et al., 2012), and more recently, the mediator of homologous recombination RAD51 (Sigoillot et al., 2012, Adamson et al., 2012). To ensure that the screen hits promoted chromosome segregation errors independently of such effects MAD2 and RAD51 protein levels were assessed following siRNA pool transfection. CCDC68 and CCDC102B pools were also included in this experiment. Levels of RAD51 were unaffected for every siRNA pool (Figure 4.6d). However, while PIGN and ZNF516 silencing had no effect, RKHD2 silencing reduced MAD2 levels (Figure 4.6e). Upon deconvolution it was evident that two RKHD2 oligonucleotides exhibited apparent off-target effects on MAD2 levels, while the other two sequences did not deplete MAD2 protein, but nevertheless induced segregation errors and depleted

RKHD2 expression (Figure 4.6 c,f). This indicates that MAD2 off-target effects were unlikely to explain the segregation error phenotype associated with RKHD2 depletion. In addition, MAD2 protein was still detectable after transfection with each of the four siRNAs and the pool, which might be sufficient to maintain checkpoint function (Figure 4.6 e,f). Nevertheless, siRNAs 2 and 17 for RKHD2 were excluded from any further experiments depleting RKHD2. The siRNA pool for RKHD2 therefore comprised only two sequences from this point onwards.

4.3.3 Validation in additional cell lines

To demonstrate that segregation error induction after silencing PIGN, RKHD2 and ZNF516 was not exclusive to HCT-116 cells, two additional CIN- diploid CRC cell lines, DLD1 and RKO, were transfected with siRNA pools targeting each of the CIN-suppressors. A significant increase in the frequency of segregation errors was observed following silencing of all three genes in both DLD1 and RKO cells, as was observed in HCT-116 cells (Figure 4.7 a,b, $p<0.05$). In addition, a CIN+ cell line, NCIH508, with no 18q loss (see Figure 4.2) showed significantly increased segregation error frequencies after transfection with all three siRNA pools (Figure 4.7c, $p<0.001$). The magnitude of segregation error induction was lower in NCIH508 cells, possibly due to the underlying high rate (48%) of anaphase segregation errors in these cells, which may result in an inability to tolerate relative induction to the degree observed in the three CIN- cell lines.

The observation of reproducible induction of segregation errors across four colorectal cancer cell lines after silencing PIGN, RKHD2 and ZNF516 suggests they are bona-fide suppressors of chromosomal instability. Furthermore, induction of segregation errors in NCIH508 cells suggests that the siRNA induced phenotype is independent of the microsatellite instability that characterises all three CIN- cell lines tested. However, as only colorectal cancer cell lines have been tested here, it remains unknown whether these genes have a role in suppressing CIN in other cell types. It also remains possible that the phenotypes observed upon silencing these genes are only evident in the context of cellular transformation, as only cancer cell lines have been tested.

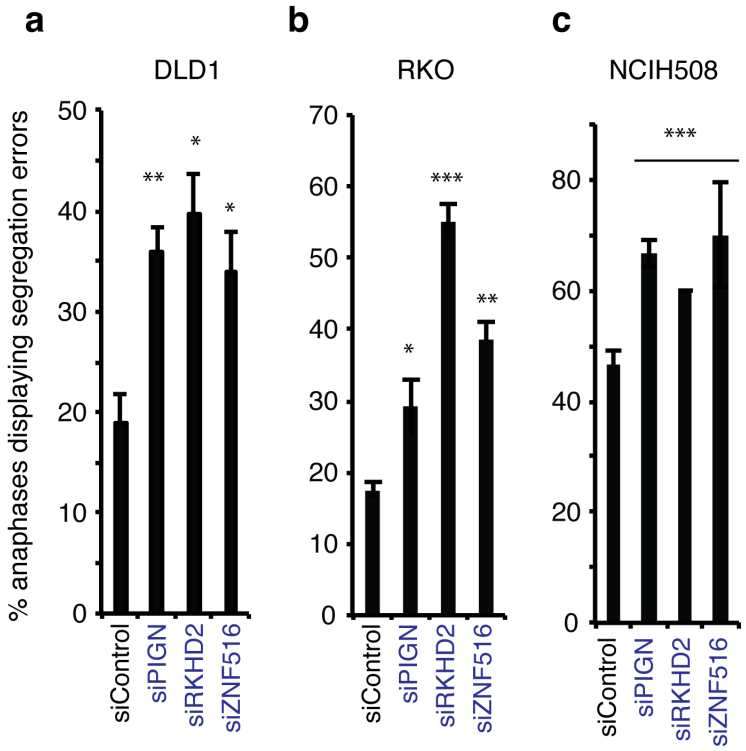

Figure 4.7 Validation in addition CRC cell lines
Percentage of anaphases with segregation errors following transfection with validated siRNA pools (n>30 anaphases per condition per experiment, 3 independent experiments). Bars are mean±S.E.M. statistical test: T-test (*p<0.05, **p<0.01, ***p<0.001) a) CIN- DLD1 b) CIN- RKO c) CIN+ 18q-normal NCIH508 cells.

4.4 Candidate CIN-suppressors are lost together in tumours, and copy number loss correlates with decreased expression

The three CIN-suppressor genes are all lost simultaneously in 70% of CIN+ cell lines (Table 4.2). 15% of cell lines showed loss of two out of the three of the CIN-suppressors. Consistent with this, in an independent cohort of colorectal tumours from The Cancer Genome Atlas (TCGA), 79% of aneuploid tumours (n=103) showed loss of all three genes, and just 5% showed loss of one or two of the genes. Therefore across both datasets, an average of 84.5% of tumours/cell lines showed loss of at least one of the three CIN-suppressor genes. The original cohort of aneuploid tumours was excluded from the analysis due to the comparatively low resolution of BAC CGH data, relative to SNP arrays.

Number of CIN-suppressors lost	Sanger Cell Lines (CIN+, SNP 6.0) N = 20	TCGA Tumours (CIN+, SNP.6.0) N = 103
Zero	15%	16%
One	0%	1%
Two	15%	4%
Three	70%	79%

Table 4.2 Frequency of CIN-suppressor loss
Percentage of cell lines and tumours losing all 3 CIN-suppressors, 1 CIN suppressor, 1-3 CIN suppressors, 0 CIN suppressors

Importantly, a highly significant correlation was observed between reduced copy number of the three genes and reduced mRNA expression in the TCGA cohort indicating that copy number loss is matched by reduced CIN-suppressor gene expression (Figure 4.8a). There were also significant correlations between decreasing copy number of 18q and decreasing expression for each of PIGN, RKHD2 and ZNF516 in CIN+ CRC cell lines (Figure 4.8b). This correlation supports the hypothesis that loss of 18q, resulting in lower expression of these genes, could contribute to CIN in colorectal cancer.

4.5 CIN-suppressors: background

The functions of the gene-products of the three CIN-suppressor proteins are not well characterised and none of them has a described function in maintaining genome stability. Studies of orthologues in lower eukaryotes have shed light on some aspects of the function of RKHD2 and PIGN, and ZNF516 may have a role in transcriptional regulation. This section will outline briefly what is known about each of the three proteins.

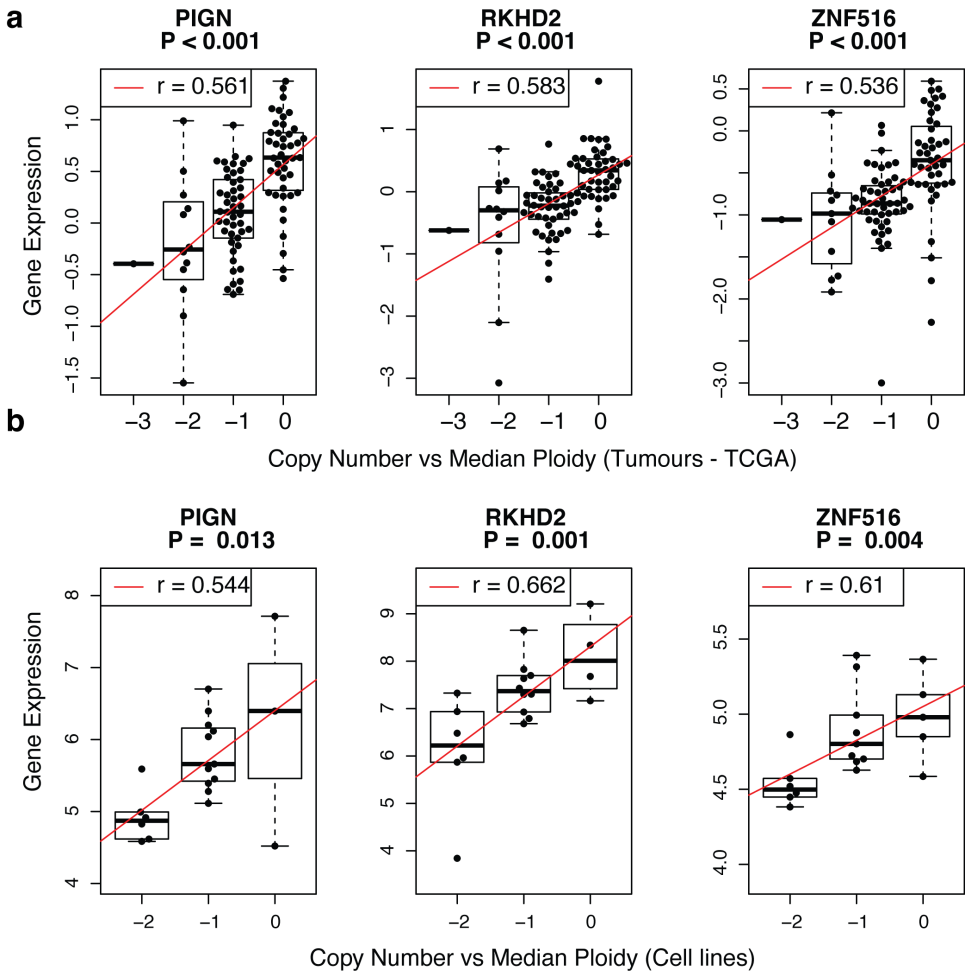

Figure 4.8 Gene expression correlates with copy number loss in tumours and cell lines
Expression of CIN-suppressor genes in relation to copy number loss, in a) colorectal tumours (TCGA cohort and b) CIN+ CRC cell lines. Significant correlations were observed for all genes in the tumour cohort, and for PIGN, RKHD2 and ZNF516 in cell lines ($p<0.001$, Spearman's Rank Correlation coefficient).

4.5.1 PIGN

PIGN (phosphatidylinositol glycan anchor biosynthesis, class N) is a multi-pass membrane protein involved in the synthesis of glycosylphosphatidylinositol (GPI) anchors. GPI anchors are important in the attachment of proteins to the external leaflet of the plasma membrane, and GPI-anchored proteins have a wide range of different cellular functions (Paulick and Bertozzi, 2008). PIGN is responsible for modifying the first mannose in GPI precursors, but deletion of PIGN in murine embryonal carcinoma

cells did not impair GPI anchor synthesis and only partially affected protein surface expression (Hong et al., 1999). PIGN has orthologues in both budding and fission yeast (Mcd4p and Its8 respectively), which appear to be primarily localised to the endoplasmic reticulum (Hong et al., 1999, Yada et al., 2001). Its8 mutant and knockout fission yeast have septation defects, although as this is a consequence of altered cell wall properties, it is unclear whether this role in cell division would be conserved in higher eukaryotes (Yada et al., 2001). Budding yeast Mcd4p has been reported to have a role in adenosine triphosphate (ATP) transport both at the Golgi apparatus, and for extracellular release (Zhong et al., 2003). In humans, germline mutations in PIGN are associated with multiple congenital anomalies-hypotonia seizures syndrome (Maydan et al., 2011).

4.5.2 RKHD2

RKHD2 (RING finger and KH domain-containing protein 2), also known as MEX3C, is an RNA binding protein with two K homology (KH) domains and a C-terminal RING finger motif, as well as a nuclear export signal sequence. RKHD2 binds RNA via the KH domains (Buchet-Poyau et al., 2007) and is the orthologue of *Caenorhabditis elegans* mex-3 (muscle excess 3), which does not possess the C-terminal RING motif. *C. elegans* MEX-3 localises to germline-specific cytoplasmic granules, and promotes mitotic proliferation of germline stem cells, essential for continuous gametogenesis (Ariz et al., 2009). Mammalian RKHD2 is primarily located in the cytoplasm, but shuttles between nucleus and cytoplasm via the CRM1-dependent nuclear export pathway (Buchet-Poyau et al., 2007). RKHD2 interacts with Argonaute proteins 1 and 2, both components of the RNA-induced silencing complex (RISC), which is central in siRNA and micro-RNA mediated mRNA silencing (Buchet-Poyau et al., 2007). RKHD2 may also interact with 14-3-3η, which has been implicated in the response to DNA damage (Courchet et al., 2008, Wanzel et al., 2005).

4.5.3 ZNF516

ZNF516 is part of the zinc finger domain family of proteins, and forms part of a multi-protein transcriptional repressor complex, potentially through interaction with C-terminal binding protein (CtBP) (Quinlan et al., 2006, Malovannaya et al., 2010, Lee et

al., 2005, Shi et al., 2003). In addition to ZNF516 and CtBP, this complex contains the histone demethylase KDM1, histone deacetylase 1/2, BRCA2-associated factor BRAF35 (Lee et al., 2005) and the CoREST transcription factor. The specific role(s) that ZNF516 plays within this complex is not yet clear.

4.6 Silencing candidate CIN suppressors results in structural instability

CIN+ cell lines and tumours are characterised by both numerical and structural instability. As described in Chapter 3, CIN+ CRC cell lines predominantly exhibited acentric chromosomes and anaphase bridges, pointing towards pre-mitotic, rather than mitotic, defects being the major driver of CIN in the cell lines examined. The type of segregation errors induced by silencing each of the three CIN-suppressors was therefore also determined.

Inducing improper attachments in mitosis with Monastrol specifically induced lagging chromosomes (Chapter 3, Figure 3.2). In contrast, inducing replication stress with Aphidicolin treatment induced acentric chromosomes and anaphase bridges (Chapter 3, Figure 3.16). Silencing each of the CIN-suppressors in HCT-116 cells primarily resulted in acentric chromosomes and anaphase bridges (Figure 4.9a), rather than lagging chromosomes. This is similar to Aphidicolin treatment and the profile of segregation errors observed in CIN+ cell lines. Hence, the segregation errors observed after silencing PIGN, RKHD2 and ZNF516 indicate the occurrence of pre-mitotic defects that generate structurally abnormal chromosomes.

In order to identify structurally abnormal chromosomes that might result in missegregation, such as chromosomes with double strand breaks (DSBs) or acentric and dicentric chromosomes, metaphase chromosome spreads were prepared after siRNA-mediated CIN-suppressor silencing and hybridised to a fluorescently labelled pan-centromeric probe, as described in Chapter 3. Structurally abnormal chromosomes were identified at increased rates following silencing of all three CIN-suppressors (Figure 4.9 b,c), with PIGN and RKHD2 depletion in particular resulting in a high frequency of chromosome abnormalities. A variety of different abnormal chromosome architectures were observed: acentric and dicentric chromosomes, double strand breaks, and triradial

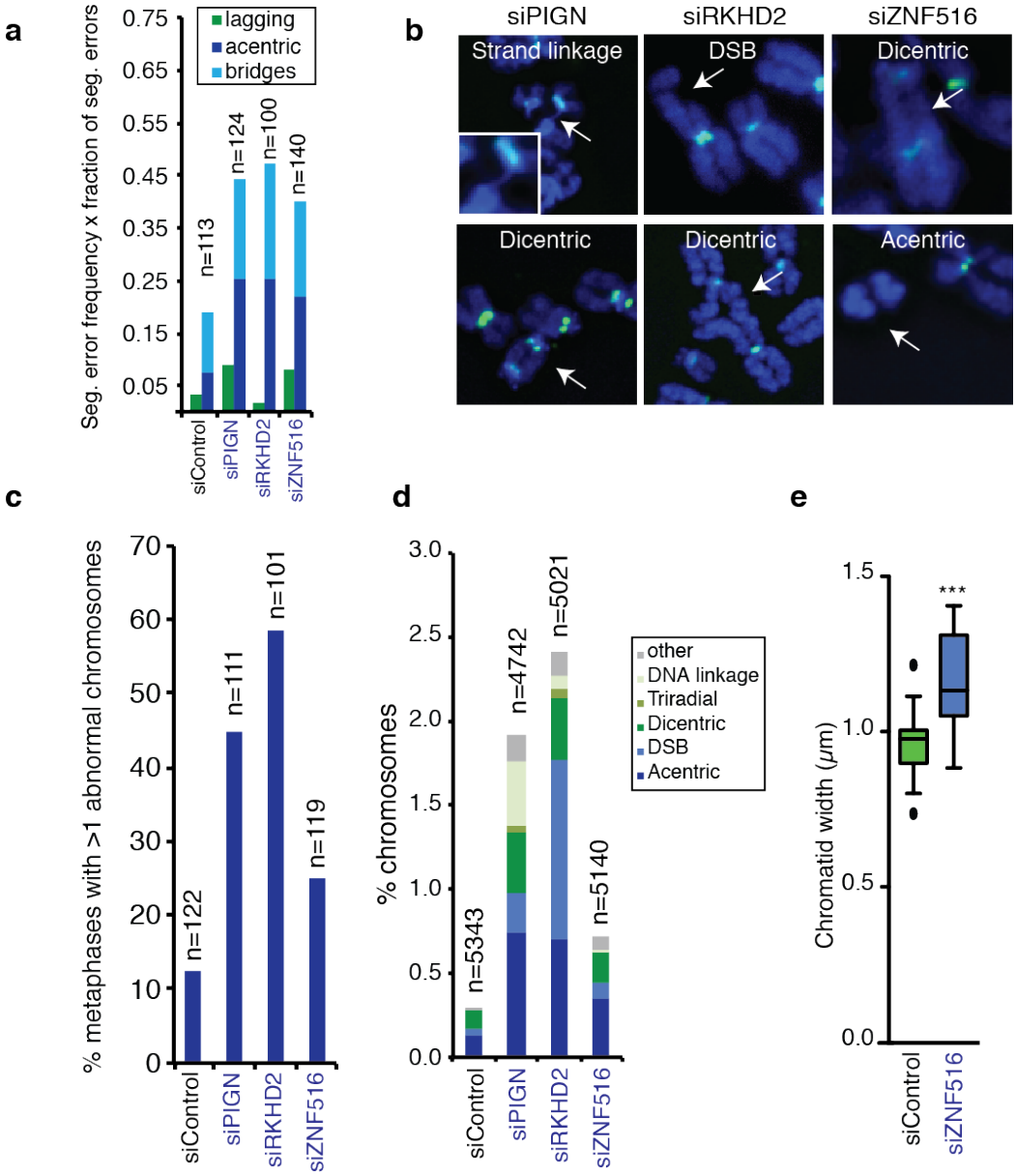

Figure 4.9 Structural aberrations after CIN-suppressor silencing

a) Segregation error classification after CIN-suppressor silencing in HCT-116 cells. Number of errors counted indicated above each bar, sum of 3 experiments.

b) Examples of structurally abnormal chromosomes observed following CIN-suppressor silencing. Abnormalities indicated by arrows. Magnified panel (siPIGN) demonstrates a fine DNA strand linkage.

c) Percentage of metaphases displaying structurally abnormal chromosomes measured from chromosome preparations hybridised to an all-centromere FITC labelled probe. Number of metaphases counted indicated above each bar, sum of 2 experiments.

d) Percentage of structurally abnormal chromosomes. Number of chromosomes scored indicated above each bar, sum of 2 experiments.

e) Chromatid width measured from un-denatured control and siZNF516 colcemid-arrested metaphase spreads stained with DAPI (inset) (Box: median, upper and lower quartile, Whiskers: Tukey) n=250 chromatids per condition, across 2 experiments, t-test $p<0.001$

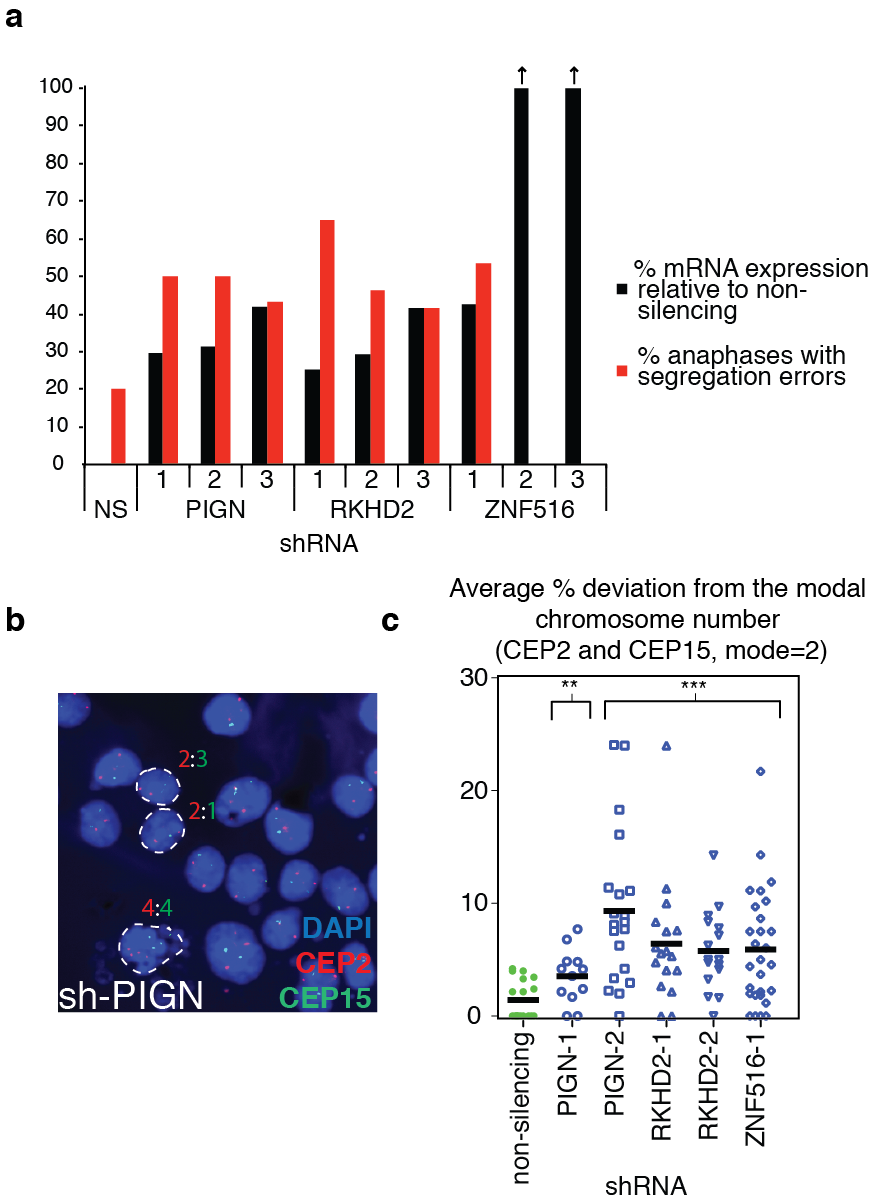

Figure 4.10 Chromosome non-disjunction initiated by CIN-suppressor silencing
a) shRNA cell lines: black bars are mRNA expression levels of the indicated gene as a percentage of expression in cells expressing a non-silencing shRNA (NS); red bars are percentage segregation error frequencies in anaphase cells. Data from one experimental time-point is shown for both segregation error frequency and mRNA expression. Expression levels for the two ZNF516 shRNAs exceeded levels in control cells, and thus cells were not scored for anaphase segregation errors.
b) shPIGN cells probed for centromere 2 and centromere 15
c) HCT-116 cell lines stably expressing shRNAs against the CIN-suppressor genes were seeded at low density on glass slides and allowed to form colonies. Slides were then hybridised to fluorescently labelled centromeric probes to chromosomes 2 and 15 and stained with DAPI. Each point is the mean percentage deviation from the modal centromere copy number for the two centromeric probes for an individual colony. Lines are median values, statistical test: one-way ANOVA ($p<0.01$). At least 12 colonies of >30 cells were assessed per shRNA sequence. Data from one experiment.

chromosomes (Figure 4.9c). Following PIGN silencing, fine DNA strand links were observed between distinct chromosomes (Figure 4.9 b,d). RKHD2 silencing resulted in a high frequency of double strand breaks, as well as acentric and dicentric chromosomes. Silencing ZNF516 resulted in a smaller increase in the rate of structural abnormalities (Figure 4.9 c,d). However, ZNF516 silencing also resulted in apparent partial chromosome de-condensation and an increased chromatid width (Figure 4.9e, $p<0.001$), which may potentially obscure other structural chromosome abnormalities. Given that ZNF516 forms part of a histone-modifying protein complex, it is possible that chromosome de-condensation after ZNF516 silencing could reflect altered methylation or acetylation status of chromatin (Lee et al., 2005).

4.7 CIN-suppressor silencing results in numerical instability

Chromosome losses and gains (chromosome non-disjunction/numerical CIN) are a logical consequence of anaphase chromosome segregation defects. Chromosome non-disjunction was therefore quantified following silencing of the CIN-suppressor genes, by performing fluorescence *in-situ* hybridisation on clonal cell colonies (clonal FISH).

For colonies to grow to a sufficient size, longer-term knockdown of CIN-suppressor genes was required and therefore cell lines stably expressing small-hairpin RNAs (shRNAs) against each gene were constructed. Three shRNA sequences were tested against each gene. In general the sequences were distinct from the siRNA sequences, although for PIGN two of the three shRNA sequences overlapped with the siRNAs (Table 2.2). All genes were efficiently silenced by shRNAs except for ZNF516, which was only silenced by one shRNA (Figure 4.10a). Consistent with siRNA-mediated induction of segregation errors, shRNA-mediated silencing increased the segregation error rate for all genes (Figure 4.10a), validating the use of these cell lines for long term knockdown experiments. Therefore for each gene, between 5 and 7 independent sh/siRNA sequences reproduced the segregation error phenotype, further rendering the possibility of off-target effects less likely.

Two cell lines per gene with equivalent knockdown levels were then chosen for clonal FISH analysis. Only one cell line was assessable for ZNF516. Cells were seeded

at low density onto glass slides and allowed to form colonies, before fixation and hybridisation to two fluorescently labelled centromere probes (Figure 4.10b). Next, the percentage of cells with a centromere copy number deviating from the mode for each colony was quantified. There was significantly increased intra-colony deviation in modal chromosome copy number for each cell line (Figure 4.10c), indicating that substantial chromosome non-disjunction occurs following CIN-suppressor gene silencing, leading to numerical chromosomal changes, in addition to structural chromosome aberrations.

To further verify this result, chromosome non-disjunction was also measured after siRNA mediated silencing, using a cytokinesis-block assay. 48 hours after transfection, cells were incubated with 100 µM Blebbistatin to block cytokinesis, resulting in the formation of binucleate cells. Non-disjunction was then quantified between paired sister nuclei in binucleate cells (see Figure 4.11a for example images). Non-disjunction between sister nuclei was increased after silencing all three genes (Figure 4.11b).

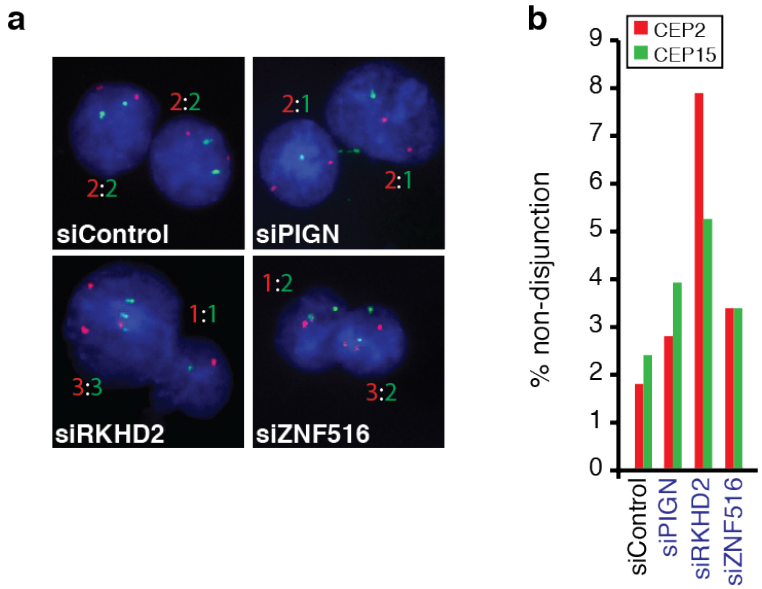

Figure 4.11 Cytokinesis block chromosome non-disjunction assay
48 h post-transfection HCT-116 on were treated with Blebbistatin (100 µM), to inhibit cytokinesis and generate binucleate cells, for 16 hours prior to fixation and hybridisation to two centromeric probes (for chromosomes 2 and 15). Non-disjunction was then scored between paired daughter nuclei (n=100 pairs of sister nuclei per condition). a) Percentage of binucleates displaying balanced non-disjunction (i.e. loss of a probe signal from one nucleus is reflected by gain in the sister nucleus). Data from one experiment. b) Examples of binucleate cells after silencing each of the CIN-suppressor genes.

4.8 Conclusions and discussion

In summary, three novel suppressors of CIN have been identified (PIGN, RKHD2 and ZNF516), encoded on chromosome 18q, a region of frequent somatic copy number loss in CIN+ CRC. Silencing these genes resulted in segregation error induction in four different CRC cell lines, including a CIN+ cell line without 18q loss. The pattern of segregation errors and chromosomal abnormalities initiated following CIN-suppressor silencing suggested that pre-mitotic defects rather than mitotic defects were likely to be responsible for increased segregation error frequency, similar to the observations in CIN+ cells. The possible mechanisms underlying these defects will be explored in the next chapter.

Chapter 5. Results 3 – Depletion of CIN-suppressors is associated with pre-mitotic rather than mitotic defects

In chapter 4, three novel CIN-suppressor genes were identified that are encoded on chromosome 18q, a region of recurrent copy number loss in CIN+ colorectal cancer. In order to characterise the defects causing the chromosomal instability observed after silencing these three genes, a series of experiments examining both pre-mitotic and mitotic defects were undertaken. Classification of segregation errors induced by CIN-suppressor silencing revealed high frequencies of acentric chromosomes and anaphase bridges, which was coupled with the detection of structural aberrations in metaphase chromosomes. These results indicated that pre-mitotic defects were likely to explain the segregation errors observed following CIN-suppressor silencing (Gisselsson, 2008). However, as mitotic dysfunction has also recently been implicated in the initiation of structural chromosome defects (Janssen et al., 2011, Crasta et al., 2012), cells were examined for both pre-mitotic and mitotic dysfunction following CIN-suppressor silencing. All experiments were performed in the CIN- cell line HCT-116.

5.1 Assessment of DNA replication stress following CIN-suppressor silencing

As discussed previously, activation of the DNA damage response has been observed in both colorectal adenomas and carcinomas, thought to be a consequence of DNA replication stress (Tort et al., 2006, Bartkova et al., 2005). In addition, data presented in Chapter 3 indicated elevated DNA replication stress in CIN+ CRC cells, relative to CIN- cells. As CIN-suppressor silencing induced primarily acentric chromosomes and anaphase bridges (Figure 4.9), this implicated pre-mitotic defects as the cause of observed segregation errors. Therefore the hypothesis that CIN-suppressor silencing might lead to the induction of DNA replication-stress was examined.

5.1.1 DNA damage induction

Western blots for ATM signalling were performed by Dr Nnennaya Kanu

First, DNA double strand breaks were visualised using antibodies for γH2AX and 53BP1, following depletion of CIN-suppressor genes. As discussed in Chapter 3, DNA damage in mitosis can reflect DNA replication stress (Lukas et al., 2011a, Chan et al., 2009). Alternatively, DNA damage in mitosis may reflect a G2-M checkpoint defect. Silencing the CIN-suppressors (PIGN, RKHD2 and ZNF516) resulted in a significantly increased fraction of prometaphase cells with ≥3 γH2AX foci (69-73% of cells, relative to 24% in control transfected cells, Figure 5.1 a,b, $p<0.05$).

Interphase DNA damage may also be induced by DNA replication stress, as well as DNA repair defects, oxidative damage and telomere uncapping (Bester et al., 2011, Bartkova et al., 2005)(see Introduction Section 1.9). As γH2AX signal in interphase cells can be more diffuse, to assist in the scoring of interphase DNA damage, γH2AX was co-localised with 53BP1, which is only recruited to double strand breaks during interphase and not during mitosis (Giunta et al., 2010, Schultz et al., 2000). PIGN and RKHD2 silencing resulted in an increased frequency of interphase cells with ≥3 co-localising γH2AX/53BP1 foci (Figure 5.1 c,d, $p<0.05$), while ZNF516 silencing resulted in only a slight increase in interphase DNA damage.

The observation of γH2AX/53BP1 foci suggests that recognition of DNA double strand breaks is proficient after silencing all three CIN-suppressors. However, to further verify this, cells were exposed to 2 Gy of gamma-irradiation (IR) and fixed for immunofluorescence after 15 minutes (Figure 5.1 e,f). This confirmed proficient double strand break recognition, as cells depleted of each of the three CIN-suppressors showed high levels of γH2AX/53BP1-positive foci formation in response to IR. ATM is the major kinase responsible for phosphorylating γH2AX and orchestrating foci formation at DSBs. Therefore the formation of foci marked by γH2AX suggests that ATM is activated proficiently after DNA damage in the context of CIN-suppressor silencing. In addition, phosphorylation of two other downstream targets of ATM, SMC1 (phospho-S966) and KAP1 (phospho-S824), was observed following irradiation (5 Gy) of CIN-suppressor depleted cells (Figure 5.1g), indicating that ATM signalling in response to double strand breaks is broadly intact.

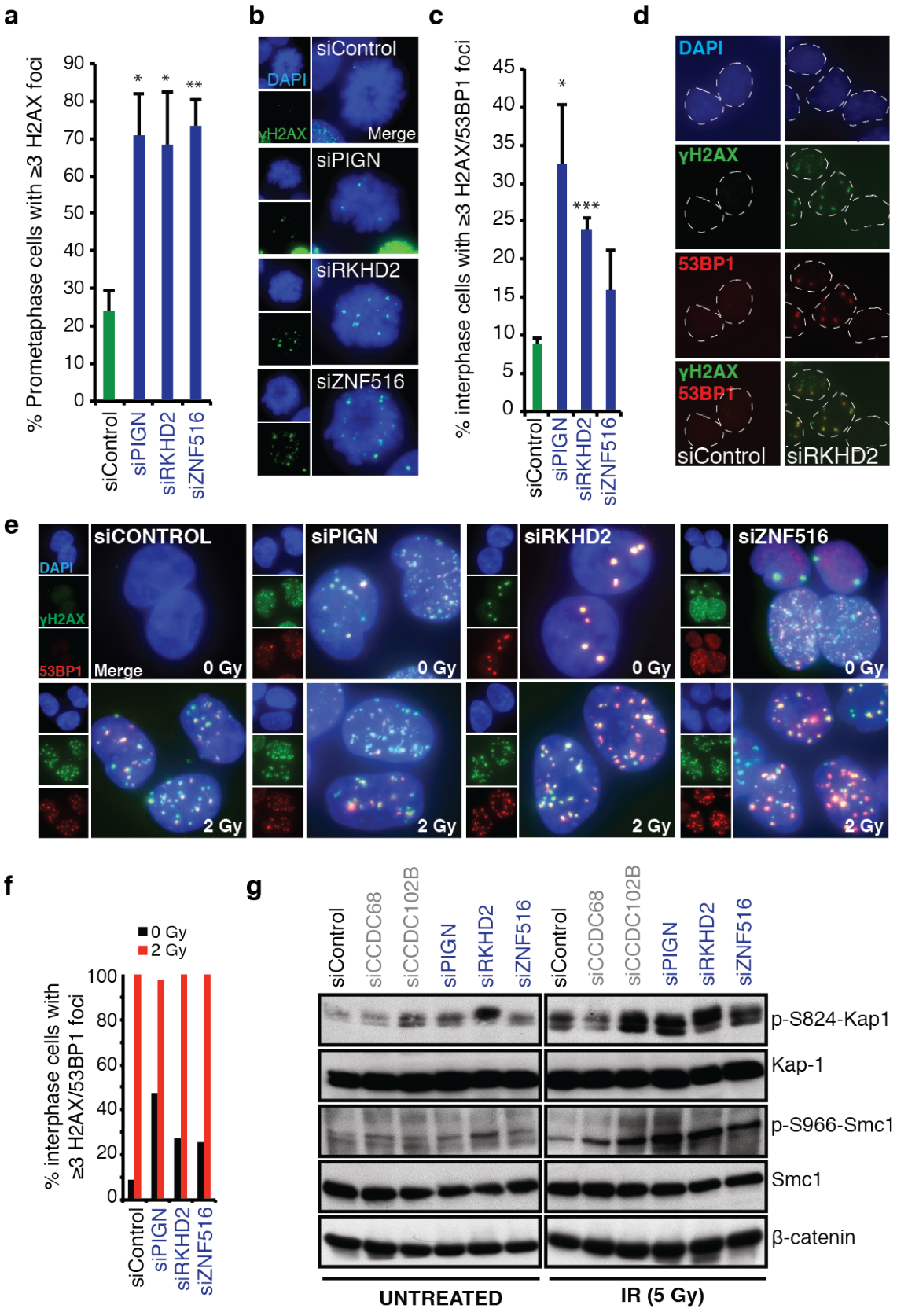

Figure 5.1. CIN-suppressor silencing results in DNA damage

a) % of prometaphase cells with ≥3 γH2AX foci (mean±s.e.m of three independent experiments, n=100 cells per experiment) Two-tailed t-test, $p<0.05$
b) Example images of prometaphase cells with γH2AX foci following CIN-suppressor silencing.
c) % Interphase cells with ≥3 γH2AX/53BP1 co-localising foci (mean±s.e.m of three independent experiments, n=100 cells per experiment), Two-tailed t-test, $p<0.05$
d) Example of interphase DNA damage foci induced by RKHD2 silencing. White dotted lines indicate nuclear boundaries.
e) Cells transfected with the indicated siRNAs were exposed to 2 Gy IR, fixed after 15 minutes and stained for γH2AX (green) and 53BP1 (red). Clear induction of colocalising γH2AX /53BP 1 foci was observed in all conditions.
f) Quantification of e) n>150 cells per condition
g) Immunoblot of proteins extracts made 1 hour after exposure of transfected cells to 0 or 5 Gy IR. Western blot performed by Nnennaya Kanu

---

5.1.2 Ultra-fine bridges

To further investigate whether CIN suppressor silencing results in replication stress, the percentage of anaphases with ultra-fine bridges was quantified. Silencing PIGN and ZNF516 significantly increased the percentage of cells with ultra-fine bridges (Figure 5.2 a,b, $p<0.05$). Similarly to CIN+ CRC cells, and cells treated with Aphidicolin (see Chapter 3), this increase in ultra-fine bridges specifically affected anaphases with segregation errors (Figure 5.2a), suggesting a link between the aetiology of the ultra-fine bridges and anaphase segregation errors.

RKHD2 silencing did not induce ultra-fine bridges, but conversely reduced the frequency of these structures relative to control cells, although this reduction was not statistically significant (Figure 5.2a, $p=0.14$). One explanation for this could be that RKHD2 depletion results in the formation of ultra-fine bridges that are not marked by RPA (but which might be visualised through staining for alternative markers such as PICH or BLM), and suppresses the formation of ultra-fine bridges that are RPA-positive. Alternatively, this reduction could indicate that RKHD2 silencing destabilises the structures that generate ultra-fine bridges upon entry into mitosis. Prometaphase DNA damage foci are thought to arise through rupture of under-replicated genomic loci during chromosome condensation, and the same loci are thought to contribute to ultra-fine bridges (Lukas et al., 2011a, Chan and Hickson, 2009, Chan et al., 2009). Rupture of loci under replication stress could be exacerbated in RKHD2-depleted cells, resulting in fewer ultra-fine bridges, but elevated prometaphase DNA damage relative to

interphase cells (Figure 5.1a-c). A third possibility is that RKHD2 silencing reduces the formation of structures that generate ultra-fine bridges prior to entry into mitosis. Ultra-fine bridges are thought to represent unresolved replication intermediates or DNA catenanes (Chan and Hickson, 2009). If the frequency of replication fork collapse, which generates double-strand breaks, is increased in RKHD2-depleted cells then this might result in a decrease in the frequency of ultra-fine bridges, whilst generating interphase DNA damage (Figure 5.1c) and, through improper repair, structurally abnormal chromosomes.

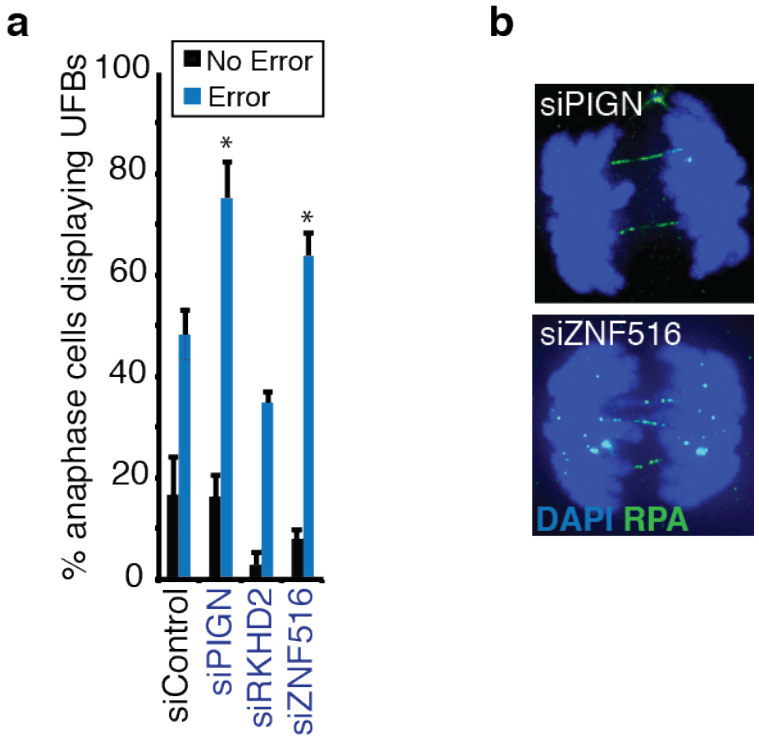

Figure 5.2 Induction of ultra-fine bridges after CIN-suppressor silencing
a) % Anaphases with ultra-fine bridges (identified by RPA staining), subdivided into cells with and without segregation errors (mean±s.e.m of three independent experiments, n=100 cells per experiment, T-test *p<0.05). Only anaphases that could be clearly scored for the presence or absence of segregation errors were included, which excludes all early anaphases.
b) Examples of PIGN and ZNF516-depleted cells displaying ultra-fine bridges

5.1.3 53BP1 bodies in G1 cells

In addition to prometaphase DNA damage and ultra-fine bridges, replication stress also results in the formation of 53BP1 nuclear bodies in G1 cells, following the mitotic passage of chromosomes under replication stress (Lukas et al., 2011a, Harrigan et al., 2011). Consistent with the presence of ultra-fine bridges and prometaphase DNA damage, silencing PIGN and ZNF516 increased the frequency of cyclin-A1 negative G1 cells with 53BP1 bodies (Figure 5.3 a,b, $p<0.05$). An increase in the fraction of G1 cells with 53BP1 bodies was also seen following RKHD2 depletion (Figure 5.3a, $p<0.05$). This observation supports the hypothesis that RKHD2 silencing results in replication stress, even though an increase in ultra-fine bridges is not observed.

This hypothesis is further supported by data presented in the study that first identified the connection between replication stress and 53BP1 nuclear bodies (Lukas et al., 2011a). Silencing the condensin complex component SMC2 reduces the number of prometaphase DNA damage foci induced by Aphidicolin treatment, and also reduces 53BP1 body formation, thought to be due to reduced rupture of under-replicated genomic loci during chromosome condensation. However, SMC2 silencing results in a marked increase in the rate of formation of ultra-fine bridges, thought to represent unresolved replication intermediates (Lukas et al., 2011a, Chan and Hickson, 2009). Therefore prometaphase DNA damage foci and ultra-fine bridges, observed after replication stress, appear to be intimately related, and may originate from the same DNA lesions. However, from these data, it appears that it is mainly loci that have ruptured to form prometaphase DNA damage foci that result in 53BP1 body formation, rather than ultra-fine bridges. Hence, the appearance of raised prometaphase DNA damage and 53BP1 bodies following RKHD2 silencing, in the absence of ultra-fine bridges, is still consistent with a replication stress phenotype.

5.1.4 53BP1 bodies induced by CIN-suppressor silencing are not a consequence of chromosome damage during cytokinesis

53BP1 foci in G1 cells can also result from lagging chromosomes that were damaged during cytokinesis (Janssen et al., 2011). DNA damage foci were observed in cells that underwent anaphase with segregation errors induced by Monastrol washout or treatment

with an inhibitor of the mitotic checkpoint. The degree of DNA damage could be significantly reduced by treatment with a cytokinesis inhibitor (Janssen et al., 2011). The scoring threshold utilised here (≥3 53BP1 bodies) should eliminate the majority of cells with foci attributable solely to lagging chromosomes, which tend to number between one and three foci per cell (Janssen et al., 2011). Nonetheless, it was important to formally test whether 53BP1 bodies induced by CIN-suppressor gene silencing were cytokinesis-dependent or independent. Cells were treated with a cytokinesis inhibitor (Blebbistatin) or DMSO for four hours prior to fixation and staining for cyclin A1 and 53BP1. In Blebbistatin treated samples, only binucleate cells were scored for 53BP1 bodies, to ensure that cells had gone through mitosis in the presence of the cytokinesis block (Figure 5.3c).

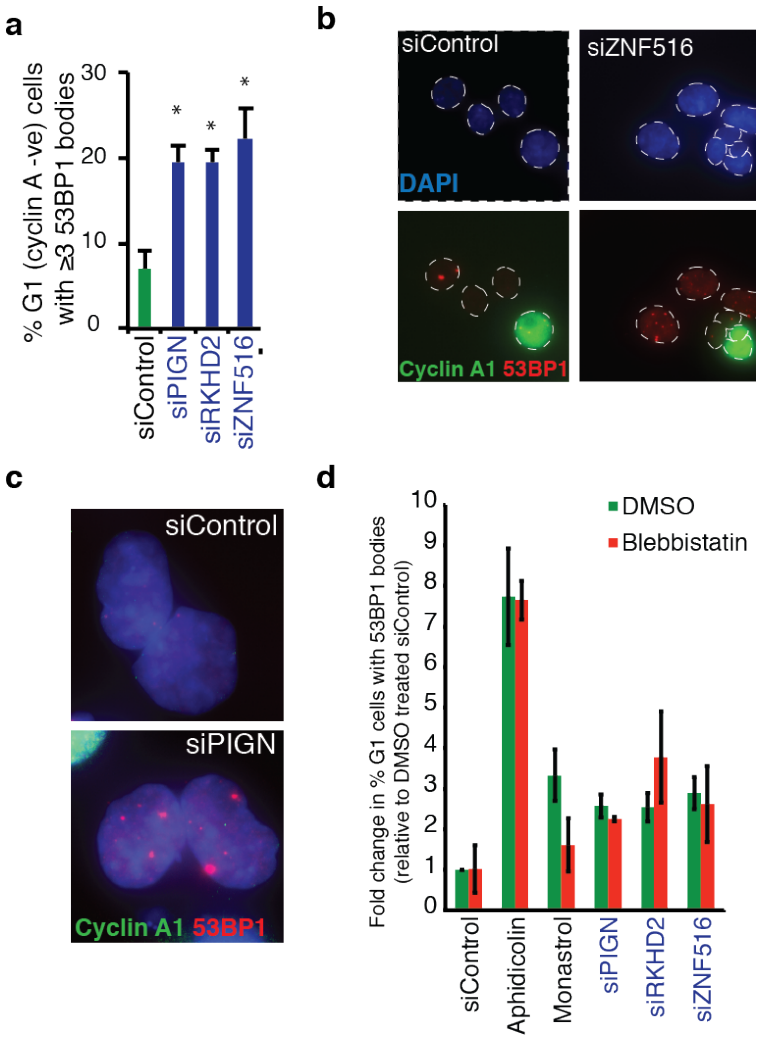

Figure 5.3 Induction of 53BP1 bodies in G1 cells

a)% G1 cells (cyclin A1 negative) with ≥3 53BP1 bodies (mean±s.e.m, 3 experiments, n>150 cells per experiment). 53BP1 bodies were comparable in size to those induced by Aphidicolin treatment.
b) Examples of 53BP1 bodies in cyclin A1 negative cells after ZNF516 silencing. Nuclear peripheries indicated by white dotted lines.
c) Cells were treated for 2 h with 100 μM Blebbistatin to block cytokinesis. Shown are binucleate cells stained for cyclin A1 and 53BP1. 53BP1 bodies are still evident in the PIGN-depleted cells, despite inhibition of cytokinesis.
d) Quantification of 53BP1 bodies after CIN-suppressor silencing ± 100 μM Blebbistatin treatment. Values are normalised to DMSO treated control-transfected cells (mean ± s.d. of two independent experiments, n>200 cells per condition per experiment).

As a positive control for cytokinesis-induced 53BP1 foci, cells were treated with Monastrol for one hour, generating improper kinetochore-microtubule attachments and lagging chromosomes (Janssen et al., 2011). Cells were then released into media containing either Blebbistatin or DMSO. Monastrol washout resulted in a 3.3-fold increase in the percentage of cells with 3 or more 53BP1 bodies, whereas in the presence of Blebbistatin this increase was reduced to 1.6-fold. As a positive control for replication stress-induced 53BP1 bodies, which have been shown not to be affected by cytokinesis inhibition (Lukas et al., 2011a), cells were treated with Aphidicolin for 24 hours before addition of either Blebbistatin or DMSO. There was no reduction in Aphidicolin-induced 53BP1 body formation after cytokinesis inhibition (Figure 5.3d). Likewise, 53BP1 bodies induced by PIGN, RKHD2 or ZNF516 silencing were not appreciably affected by cytokinesis inhibition (Figure 5.3d). This experiment indicates that the 53BP1 bodies observed after CIN-suppressor silencing are not a consequence of chromosome missegregation-induced DNA damage (Janssen et al., 2011, Lukas et al., 2011a), suggesting that that these nuclear bodies reflect DNA replication stress.

5.1.5 DNA fibre analysis reveals slow replication rates after CIN-suppressor silencing

DNA fibre analysis was performed and analysed by Dr Petra Groth and Marie-Christine Weller. Data was interpreted together with PG, MW and Thomas Helleday.

In order to more directly examine DNA replication DNA fibre analysis was performed, comparing control-transfected cells, to cells depleted of each of the three CIN-suppressor genes. 48 hours post-transfection, cells were pulsed for 30 minutes with 5-chlorodeoxyuridine (CldU), followed by a 30-minute pulse with 5-iododeoxyuridine (IdU), before DNA fibre analysis. CIN-suppressor-depleted cells showed a greater proportion of slow progressing replication forks relative to control transfected cells (Figure 5.4 a,b**)**. PIGN and ZNF516-depleted cells exhibited mean fork rates of 0.5 and 0.58 kb/min respectively, relative to 0.8 kb/min in control-transfected cells (CldU fork rates, Figure 5.4c). The slow replication rate observed following PIGN and ZNF516 silencing is similar to the slow replication rates observed in CIN+ cell lines, relative to HCT-116 cells (Chapter 3, Figure 3.13). The mean fork rate in RKHD2 depleted cell was similar to control-transfected cells, across the two experiments, reflecting the wide distribution of fork speeds in RKHD2-depleted cells (Figure 4b), although a reduction in mean fork speed of 5-10% was observed reproducibly between the experiments (Figure 5.4 c,d). One explanation for the wider distribution of fork rates after RKHD2 silencing is a mixed population of cells with differing levels of RKHD2 depletion.

Quantification of the observed replication structures after CIN-suppressor silencing revealed no gross differences compared to control-transfected cells. Together these results indicate that silencing each of the CIN-suppressor impacts upon replication fork progression, most notably PIGN or ZNF516-silencing, which resulted in a 25-40% reduction in mean fork rate. These results are consistent with the other replication stress-associated phenotypes observed in cells depleted of each of the CIN-suppressors.

5.1.6 Pre-mitotic dysfunction following CIN-suppressor silencing

In summary, DNA replication stress has been assessed using three different measures: prometaphase DNA damage, ultra-fine bridges and G1 53BP1 bodies. Silencing PIGN and ZNF516 resulted in an increase in all three measures; evidence supporting that silencing these genes induced DNA replication stress. RKHD2 silencing led to increased interphase and prometaphase DNA damage and G1 53BP1 bodies, without an appreciable increase in ultra-fine bridges. In addition, DNA fibre analysis revealed altered fork progression following silencing of all three CIN-suppressors, particularly PIGN and ZNF516. These results suggest that CIN-suppressor silencing results in

segregation errors as a consequence of DNA replication stress. However, to exclude that mitotic dysfunction also contributes to segregation errors following CIN-suppressor silencing, possible defects in mitosis were also examined.

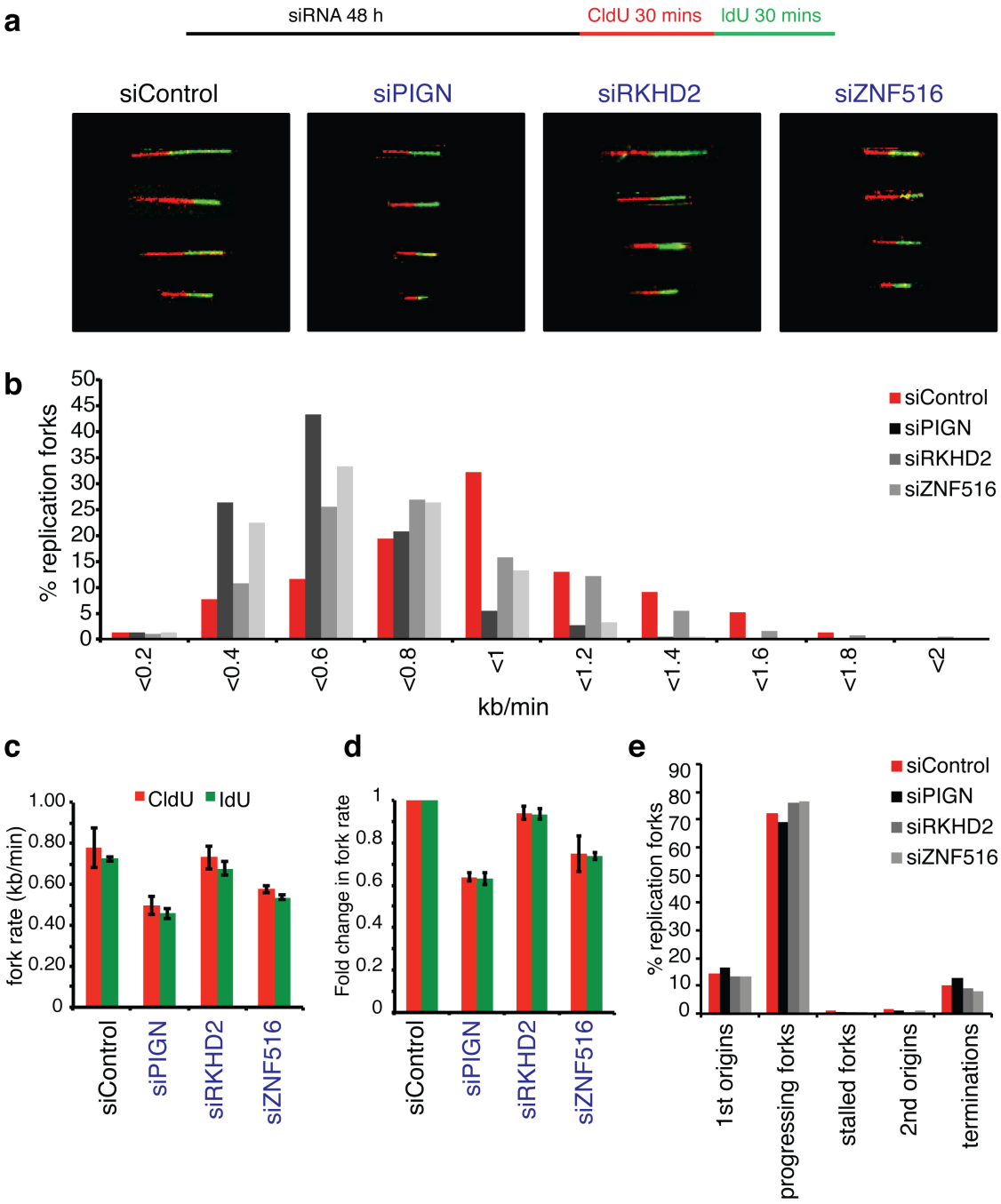

Figure 5.4 Reduced replication fork rates after CIN-suppressor silencing
48 hours after siRNA transfection, cells were pulsed with CldU, then IdU for 30 minutes each, before DNA combing was performed.
a) Representative images of DNA fibres after silencing the CIN-suppressors

b) Distribution of fork rates (CldU) (sum of two independent experiments, at least 50 fibres were measured per condition)
c) Mean fork rate (mean±s.d. of two independent experiments)
d) Fold change in fork rate (mean±s.d. of two independent experiments)
e) Quantification of fork structures after CIN-suppressor silencing (sum of two independent experiments, at least 400 structures were analysed per condition).

5.2 Examining mitotic dysfunction following CIN-suppressor silencing

As discussed previously, anaphase chromosome segregation errors can be induced directly by defects in mitosis, or indirectly through defects earlier in the cell cycle that generate mitotically unstable chromosomes (Cimini et al., 2001, Pampalona et al., 2010b, Chan et al., 2007, Stewenius et al., 2005). However, it has recently been shown that lagging chromosomes generated by improper attachments in mitosis can subsequently be affected by DNA damage (Crasta et al., 2012, Janssen et al., 2011), as discussed in Chapter 3, and Introduction Section 1.12. It is thus formally possible that a chromosome missegregated during the previous mitosis might be subject to DNA damage, generating a structurally abnormal chromosome that is then missegregated in the subsequent mitosis.

Cells depleted of the CIN-suppressors were therefore examined for evidence of mitotic dysfunction in order to exclude the possibility that acentric chromosomes and anaphase bridges observed in anaphase were a consequence of lagging chromosomes generated during a previous mitosis. The low frequency of lagging chromosomes after CIN-suppressor silencing suggests that extreme mitotic dysfunction is not occurring, but more subtle mitotic defects may nevertheless be occurring (Chapter 4, Figure 4.9a). Assessment of mitotic dysfunction was undertaken with a focus on mechanisms that can generate segregation errors: mitotic checkpoint defects, abnormal spindle geometry, and merotelic kinetochore-microtubule attachments.

5.2.1 Time-lapse microscopy following CIN-suppressor silencing reveals no alterations in mitotic progression following CIN silencing

To investigate whether silencing CIN-suppressors altered the kinetics of mitotic progression, CIN-suppressors were silenced in HCT116 H2B-mRFP cells, which were

then imaged by time-lapse microscopy. Elevated frequencies of anaphase segregation errors could be detected by time-lapse microscopy, confirming segregation error quantifications in fixed cells (Figure 5.5a, $p<0.05$). The kinetics of chromosome congression and alignment at metaphase were then quantified by measuring the interval between nuclear envelope breakdown (NEBD) and the completion of chromosome congression (LCC – last chromosome congressed). The time between completion of chromosome congression and anaphase onset was also measured, prolongation of which can indicate subtle defects in chromosome attachment leading to sustained mitotic checkpoint signalling and arrest in metaphase. MAD2 silencing (overriding mitotic checkpoint function), was used as a positive control for accelerated mitotic progression (Figure 5.5b). No alterations in the duration of mitosis or in the kinetics of chromosome congression (NEBD-LCC) and anaphase onset (LCC-anaphase onset) were observed following silencing of any of the CIN-suppressors (Figure 5.5 b-d).

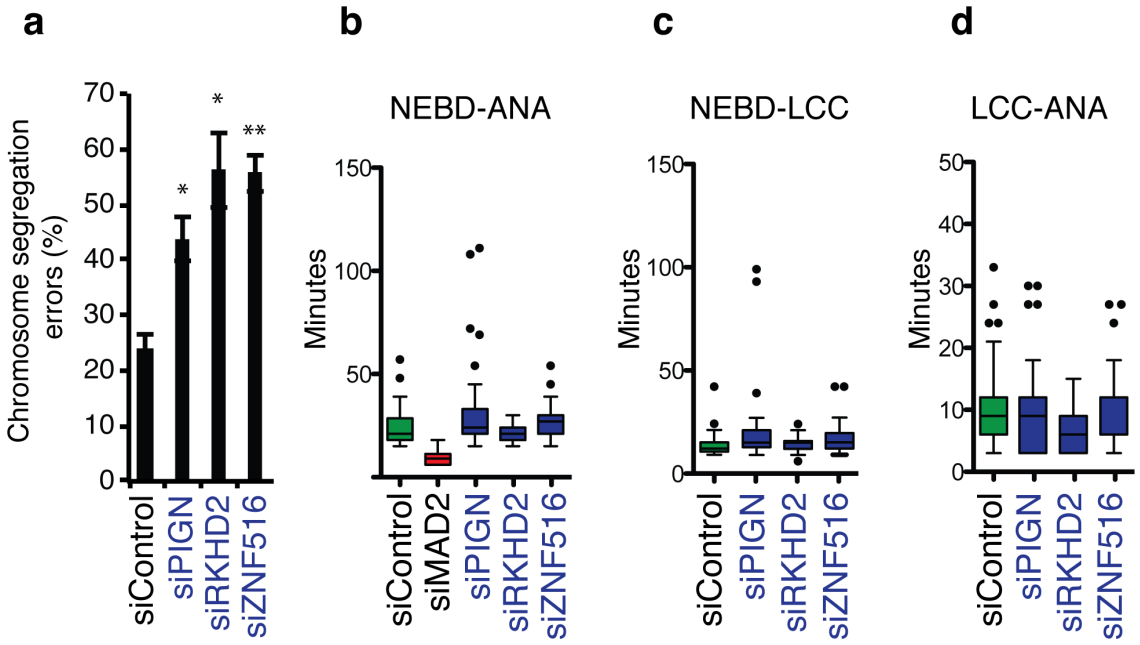

Figure 5.5 Time-lapse microscopy of HCT-116 H2B-mRFP cells after CIN-suppressor silencing

Cells transfected with the indicated siRNAs were imaged every 3 minutes for 6 hours to examine mitotic progression

a)% anaphases exhibiting segregation errors (mean±s.d. of two independent experiements, n>30 cells per experiment, two-tailed t-test

b) Duration of the interval between nuclear envelope breakdown (NEBD) and anaphase onset (ANA), which equates to the duration of mitosis n>50 cells per condition

c) Duration of the interval between nuclear envelope breakdown (NEBD) and completion of chromosome congression (LCC) n>50 cells per condition
d) Duration of the delay between chromosome congression and anaphase onset.

5.2.2 Segregation errors induced by CIN-suppressor silencing do not arise specifically from micronuclei

A recent study found that experimentally-induced lagging chromosomes that form micronuclei are incompletely replicated during the subsequent S-phase, which may undergo chromosome fragmentation upon entry of the cell into mitosis (Crasta et al., 2012). Hence, micronucleus formation and fragmentation following mitotic dysfunction could theoretically explain the structural abnormalities observed in metaphase chromosomes following CIN-suppressor silencing. Therefore, the relationship between chromosome missegregation and the presence of micronuclei was examined following CIN-suppressor silencing.

The presence of micronuclei was scored before and after segregation errors, following CIN-suppressor silencing in HCT-116 H2B-mRFP cells, using time-lapse microscopy. Of control cells that made segregation errors, just 27% were cells that had a micronucleus prior to mitosis (Figure 5.6a). In control cells that did not have a micronucleus prior to mitosis, 13% of segregation errors generated a micronucleus (Figure 5.6b). Segregation errors induced by CIN-suppressor silencing did not arise specifically in cells with micronuclei prior to mitosis (Figure 5.6a) and the fraction of segregation errors arising in cells with micronuclei was not increased after CIN-suppressor silencing, despite an increased frequency of micronucleus generation after segregation errors (Figure 5.6 a, b). Importantly, 81% of micronuclei examined, despite condensing during mitosis, did not reincorporate back into the nucleus. This indicates that cells without micronuclei were unlikely to have previously had a micronucleus, which had already reincorporated into the main nucleus.

In addition, HCT-116 cells are p53 wild type, and have previously been shown to arrest in G1 following segregation errors (Thompson and Compton, 2010). This suggests that structural alterations generated downstream of segregation errors would be less likely to manifest as segregation errors in the next mitosis, as cells would arrest in G1. This may explain the discrepancy between the fraction of cells that generate

micronuclei downstream of segregation errors and the fraction of cells that have micronuclei prior to making a segregation error (Figure 5.6 a,b). Therefore, these data indicate that structural chromosome abnormalities observed in mitosis following CIN-suppressor silencing are likely to have been generated *de novo* during interphase, rather than following segregation errors and micronucleus formation in the previous mitosis.

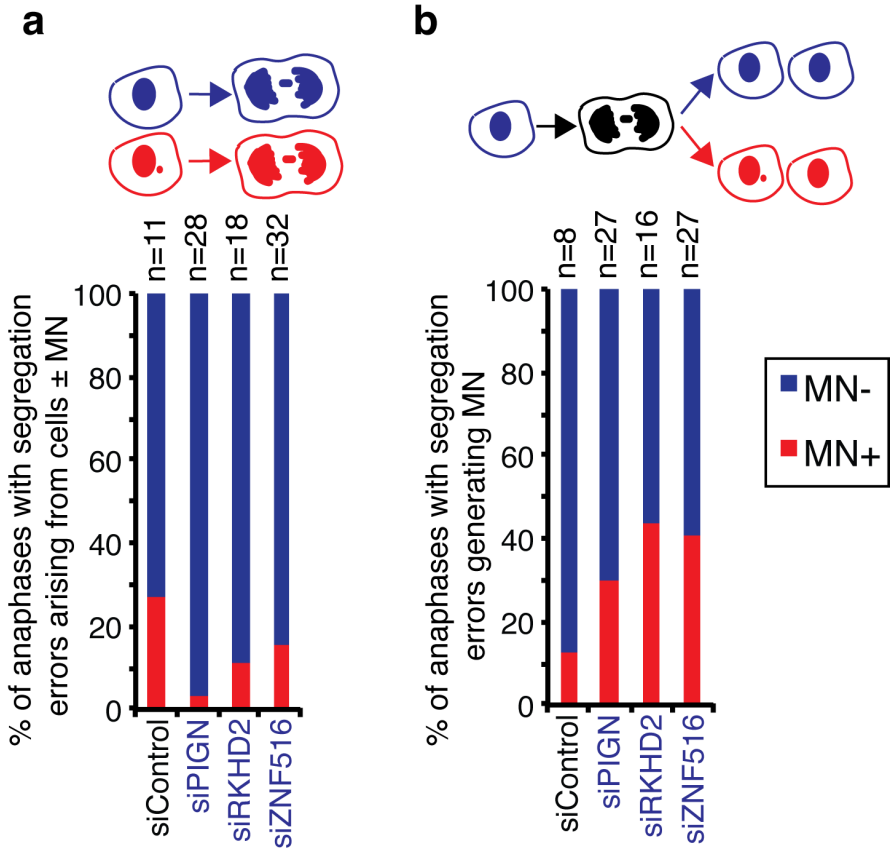

Figure 5.6 Segregation errors do not arise specifically in cells with micronuclei
HCT-116 H2B-mRFP cells were imaged every 3 minutes and anaphases exhibiting segregation errors scored for the presence of micronuclei (MN) both before and after mitosis. a)% anaphases exhibiting segregation errors classified according to the presence of MN prior to mitosis. A schematic illustrating the classification is shown above. b)% anaphases exhibiting segregation errors that resulted in the formation of MN after anaphase. Only cells that were MN- prior to mitosis were scored. A schematic illustrating the classification is shown above.

5.2.3 The mitotic checkpoint is not compromised after CIN-suppressor silencing

Dr Sarah McClelland provided images shown in Figure 5.7e.

Unaltered mitotic kinetics indicates that it is unlikely that the mitotic checkpoint is defective following CIN-suppressor silencing. However, to further test this, the efficiency of the mitotic checkpoint was tested using Nocodazole, to depolymerise mitotic spindle microtubules, promoting the accumulation of cells in mitosis due to sustained checkpoint activity. CIN-suppressor genes were silenced in HCT-116 H2B-mRFP cells, then the duration of mitosis monitored in individual cells by live-cell imaging following addition of 100ng/ml Nocodazole. This assay is deemed the gold standard for assessing mitotic checkpoint function (Khodjakov and Rieder, 2009). In the plots shown in Figure 5.7a each bar represents the fate of an individual cell, after mitotic arrest in Nocodazole. Figure 5.7b shows the duration of the mitotic arrest of each cell that was tracked in each condition.

Depletion of the mitotic checkpoint protein MAD2 was used as a positive control for mitotic checkpoint dysfunction, resulting in a complete failure of cells to arrest in mitosis (Figure 5.7 a,b). In contrast, silencing each of the CIN-suppressor genes did not attenuate a Nocodazole-induced mitotic arrest (Figure 5.7 a,b). This result could also be verified by flow cytometry following silencing of each of the three genes (data not shown). Furthermore, there was no evidence for premature cleavage of cohesin between sister chromatids following CIN-suppressor gene depletion, as seen by normal inter-chromatid distance of metaphase chromosomes (Figure 5.7c).

Checkpoint function was then ascertained in untreated cells. By live-cell imaging there was no increase in the frequency of anaphases with uncongressed chromosomes following PIGN and ZNF516 silencing, and only a small increase of 2% after RKHD2 silencing (Figure 5.7d). By contrast 100% of MAD2-depleted cells failed to congress their chromosomes before anaphase onset (data not shown). To further exclude the possibility that checkpoint function was sufficient to detect multiple unattached kinetochores in the context of Nocodazole treatment, but unable to detect a single unattached kinetochore, it was confirmed that MAD2 was localised to single uncongressed chromosomes at prometaphase after silencing each CIN-suppressor gene.

Representative images are shown in Figure 5.7e. This suggests that the checkpoint is sufficiently functional to detect a single unattached chromosome. Therefore any uncongressed chromosomes at anaphase (Figure 5.7d) may be acentric chromosomes, similar to those observed after Aphidicolin treatment (Chapter 3 Figure 3.16 a,b).

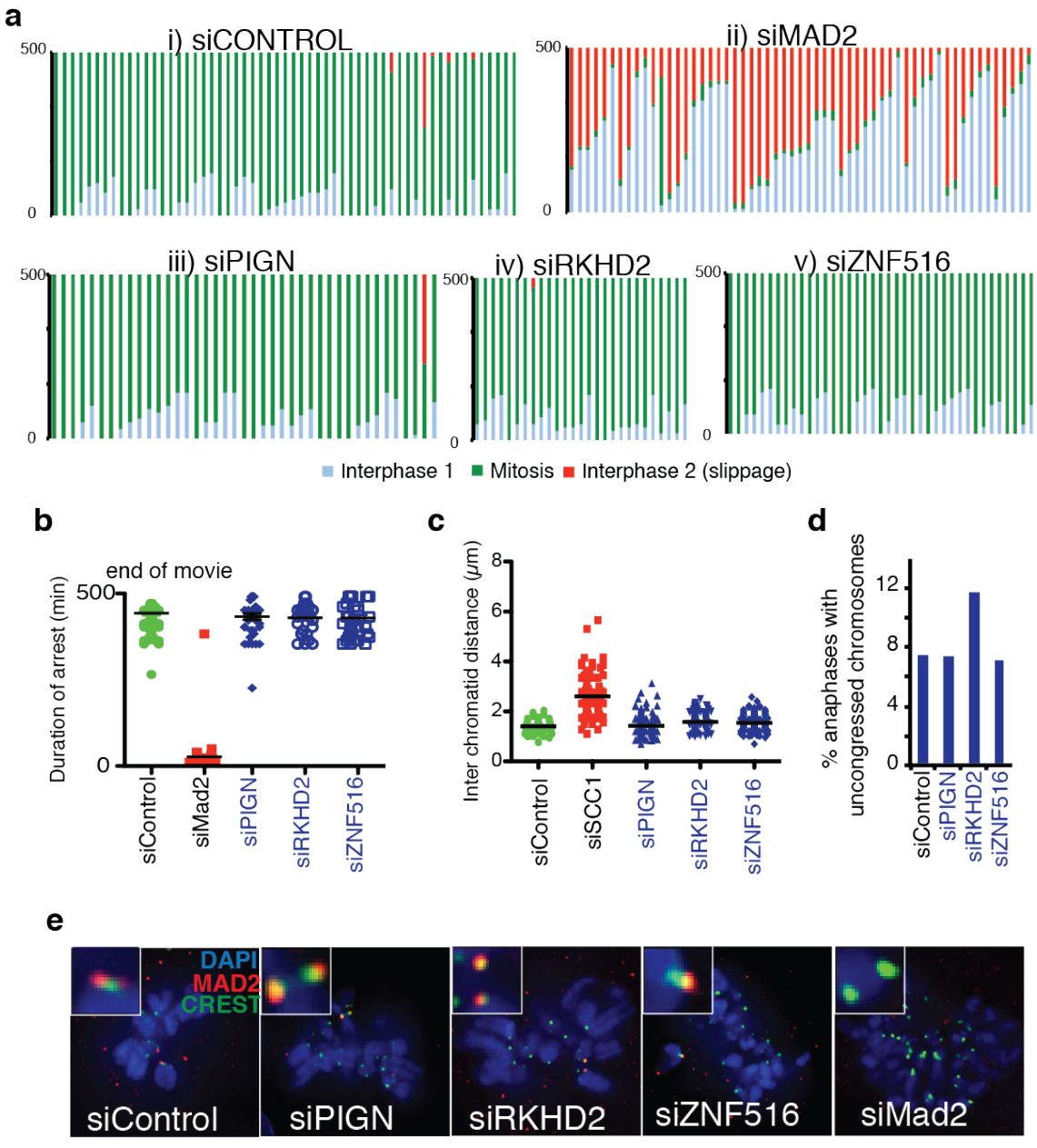

Figure 5.7 The mitotic checkpoint is functional after CIN-suppressor silencing
a) 48h post-transfection HCT-116 H2B-mRFP cells were treated with 50 ng/ml Nocodazole and imaged every 10 minutes for 8.5 hours. Individual cells were tracked for their entry into mitosis, and whether they maintained a mitotic arrest, exited mitosis

or died from mitosis. Bars represent individual cells. Only cells entering mitosis within the first two hours of the movie were tracked. Data from one experiment.
b) Duration of mitotic arrest of the cells from a)
c) Inter-chromatid distance (sister chromatid cohesion) measured from metaphase spreads hybridised to an all-centromere probe. 5 chromatid pairs per metaphase were measured across 25 metaphases. Silencing the cohesin subunit SCC1 was used as a positive control. Data from one experiment.
d)% HCT-116 H2B-mRFP cells (untreated) entering anaphase with uncongressed chromosomes after CIN-suppressor silencing. Cells were imaged every 3 minutes for 6 hours (n>50 cells per condition).
e) Representative images of MAD2 localisation to centromeres of uncongressed chromosomes after CIN-suppressor silencing. Centromeres were visualised with CREST serum. Images provided by Sarah McClelland.

5.2.4 Defective spindle geometry

Since the mitotic checkpoint appeared to be unaffected after CIN-suppressor gene depletion, cells were examined for causes of checkpoint-independent mechanisms of chromosome missegregation. Merotely can be induced by transient spindle multipolarity (Ganem et al., 2009, Silkworth et al., 2009). Therefore the percentages of prometaphases with multipolar spindles and extra centrioles were quantified following depletion of CIN-suppressor genes. Silencing ECT2, which results in cytokinesis failure, tetraploidy and spindle multipolarity, was used as a positive control (Figure 5.8 a,b).

RKHD2 and ZNF516 silencing did not affect spindle geometry or centriole number (Figure 5.8 a,b). However, PIGN silencing led to an increase in multipolar spindles in prometaphase cells (15% versus 2% in control cells, Figure 5.8a, $p<0.01$) and in the percentage of cells with supernumerary centrioles (from 17% to 54%, Figure 5.8b, $p<0.01$). Example images are shown in Figure 5.8c. Unlike ECT2 or MAD2 depletion, PIGN silencing did not result in induction of polyploidy, as measured by FACS-based analysis of DNA content (Figure 5.8 d,e). Furthermore, the majority of PIGN-depleted cells with extra centrioles had fewer than eight centrioles, the number expected in a polyploid cell. As predicted, ECT2-depleted cells primarily had 8 or more centrioles (Figure 5.8b).

These observations suggest that the increased frequency of multipolar spindle geometry after PIGN could be attributable to defects in centriole duplication and

integrity, rather than polyploidisation. Alternatively, extra centrioles could simply reflect the replication defects observed after PIGN silencing, as DNA damage and problems during DNA replication can affect centriole duplication and integrity (Nigg and Stearns, 2011). In keeping with this latter hypothesis, when centrioles were quantified in anaphase cells there appeared to be no relationship between the number of centrioles and the appearance of segregation errors after PIGN silencing (Figure 5.8f). This is in contrast to the observation of an increase in ultra-fine bridges specifically in cells with segregation errors after PIGN silencing (Figure 5.2a), implying there is no causal relationship between extra centrioles and segregation errors. However, it is possible that extra centrioles and multipolar spindle geometry contribute to segregation errors at very low frequencies, reflected in the low frequency of lagging chromosomes induced by PIGN-silencing (Chapter 4, Figure 4.9).

5.2.5 Merotelic kinetochore-microtubule attachments

Data shown in Figure 5.9b was provided by Dr Sarah McClelland.

One explanation for the absence of an increased frequency of segregation errors in cells with extra centrioles after PIGN-silencing is that cells with extra centrioles generally undergo multipolar division. However the rate of multipolar divisions was not elevated following PIGN depletion (Figure 5.9a), which indicates that cells were able to cluster extra spindle poles to form a pseudo-bipolar spindle prior to anaphase, a process that may promote merotelic attachments (Ganem et al., 2009). It is also possible that cells could have arrested in early mitosis and subsequently died, although this was not observed by time-lapse microscopy (Figure 5.5).

Therefore, cells depleted of the CIN-suppressor genes were examined for evidence of merotelic attachments. As described in Chapter 3, lagging chromosomes with distortion of NDC80, the microtubule-binding component of the kinetochore, are an indicator of merotely (Thompson and Compton, 2008). The percentage of lagging chromosomes with NDC80 distortion was therefore scored after silencing the CIN-suppressors. Monastrol washout was used as a positive control, as shown in Chapter 3. An increase in the fraction of merotelic attachments was observed in PIGN-depleted cells (17% of segregation errors versus 9% in control-transfected cells). The absence of

an increase in merotelic attachments following silencing of RKHD2 and ZNF516 indicates that hyper-stable microtubules or spindle defects are unlikely to contribute to segregation errors in the RKHD2- or ZNF516-depleted cells, as these should also result in the formation merotelic attachments.

The increase in merotelic attachments observed in PIGN-depleted cells is in keeping with coalescence of multipolar spindles into a bipolar spindle prior to anaphase (Ganem et al., 2009). However, this finding appears to conflict with the lack of enrichment of segregation errors in cells with extra centrioles (Figure 5.8f). A possible explanation that reconciles both observations is that cells with extra centrioles arise stochastically at relatively low frequency due to defects in interphase. Merotelic attachments generating lagging chromosomes might then occur as in cells with extra centrioles, through multipolar spindle coalescence. However, due to the interphase defects, these cells simultaneously exhibit acentric chromosomes and anaphase bridges, which are also observed in cells without centriole amplification. In this way, the fraction of segregation errors constituted by merotelically-attached lagging chromosomes would be increased but the overall percentage of anaphases with segregation errors would not be increased in cells with extra centrioles.

5.3 Summary – pre-mitotic versus mitotic defects after CIN-suppressor silencing

In summary, mitotic defects were not generally apparent following CIN-suppressor silencing, the exception being an increase in multipolar spindles in PIGN-depleted cells, discussed above. This may explain the low frequencies of lagging chromosomes induced following PIGN silencing, but does not appear to contribute substantially to overall segregation error induction. Cells depleted of each of the three CIN-suppressors exhibit phenotypes associated with DNA replication stress, similar to CIN+ CRC cell lines with 18q loss. Together these phenotypes suggest replication stress as a possible mechanism for the structural chromosome abnormalities and high frequencies of pre-mitotic segregation errors observed following CIN-suppressor silencing. Below, preliminary experiments further addressing roles for the three genes in structural chromosome maintenance are described.

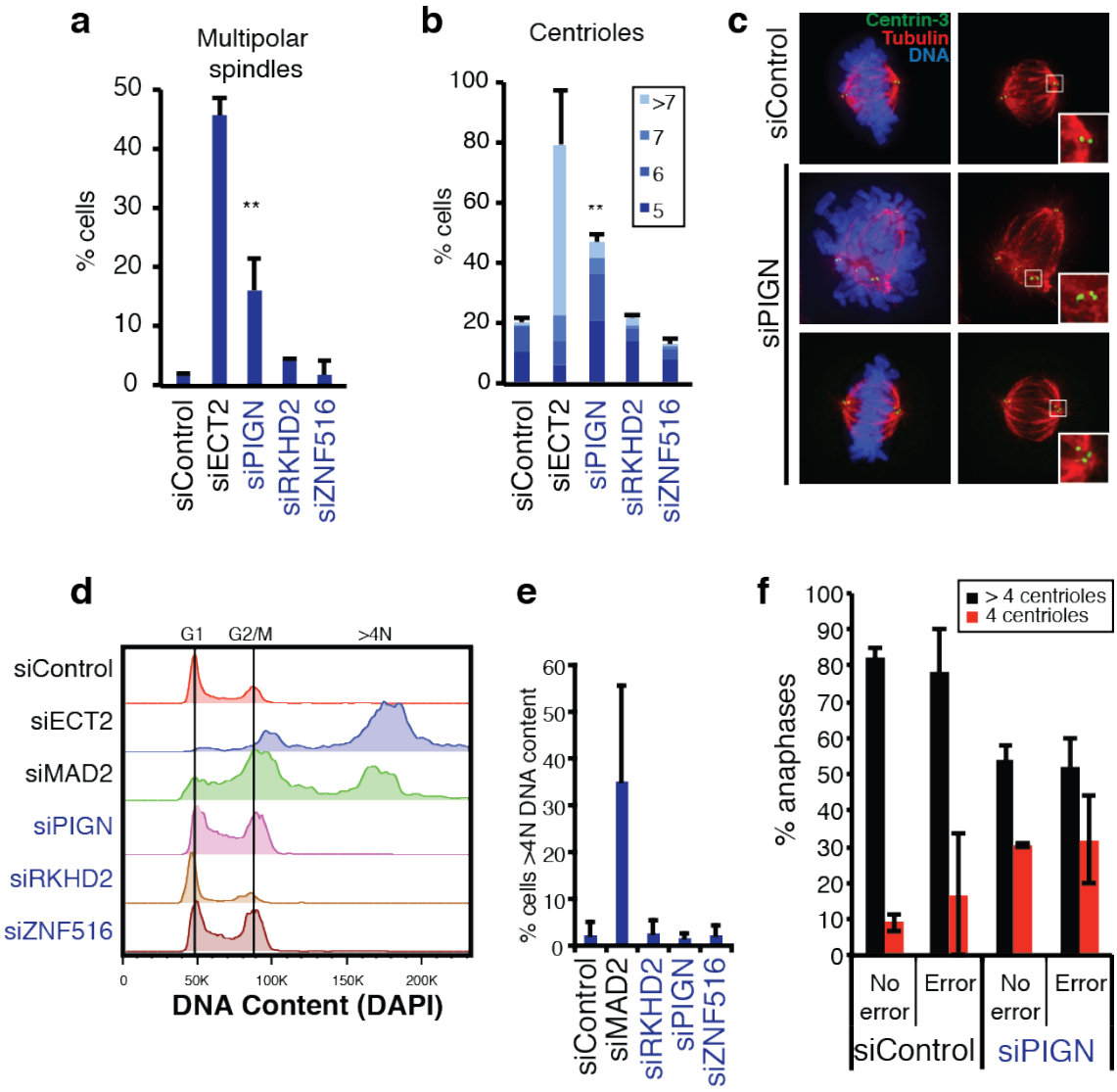

Figure 5.8 Examining spindle geometry after CIN-suppressor silencing
a) % Prometaphase cells with multipolar spindles (>2 poles). Spindles and centrioles were visualised with antibodies for centrin-3 (centriolar component) and β-tubulin. (mean±s.e.m of three independent experiments, n=100 cells per experiment).
b) % prometaphase cells with >4 centrioles (2 centrioles per centrosome) (mean±s.e.m of three independent experiments, n=100 cells per experiment).
c) Example images of mitotic spindles and centrioles in siControl and siPIGN cells, with magnified panels showing extra centrioles in siPIGN cells.
d) Representative flow cytometry profiles of DNA content after silencing each of the CIN-suppressors (n=10000 cells).
e) % cells with >4N (cycling polyploid cells) DNA content (mean±s.d. of two independent experiments, n=10000 cells per condition).
f) % anaphases with 4/>4 centrioles after control or PIGN silencing. Anaphases were categorised into those with and without segregation errors. (mean±s.d. of two independent experiments, n>30 cells per experiment).

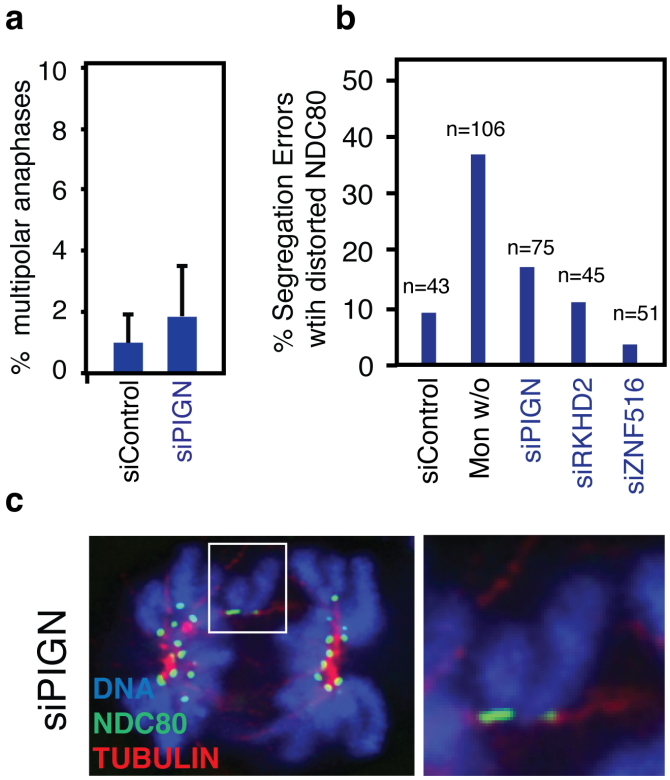

Figure 5.9 Evaluation of kinetochore-microtubule attachments after CIN-suppressor silencing
a) % Multipolar anaphases after control or PIGN silencing.
b) Cells were stained with antibodies for NDC80, β-tubulin and anti-centromere antibodies. Segregation errors were classified as lagging chromosomes, acentric chromosomes or anaphase bridges. Shown is the percentage of segregation errors that were lagging chromosomes with NDC80 distortion.
c) An example of a lagging chromosome with distorted NDC80 signal (merotelic attachment) in a PIGN-depleted cell.

5.4 Further characterisation of pre-mitotic defects induced by CIN-suppressor silencing

5.4.1 G2-M DNA damage checkpoint function

As outlined in the introduction, cells can arrest cell cycle progression in response to DNA damage. Defects in the DNA damage checkpoint at the G2-M transition could explain structural abnormalities observed in metaphase chromosomes following CIN-suppressor silencing. It was therefore important to check the function of the G2-M

checkpoint in response to irradiation-induced DNA damage, in order to exclude the possibility that prometaphase γH2AX foci observed after PIGN, RKHD2 and ZNF516 silencing were a result of a defective G2-M checkpoint. In Figure 5.1 e-g, it was demonstrated that ATM activation by DNA damage, determined by phosphorylation of downstream substrates, remained intact following CIN-suppressor silencing. This suggests that checkpoint function should be normal.

Cells were exposed to either 0 or 20 Gy IR and then incubated over night in 100ng/ml Nocodazole, to capture cells entering mitosis. 20 Gy IR used in this assay induces a level of DNA damage high enough to allow the efficiency of the DNA damage checkpoint to be studied relatively independently of double strand break repair. The percentage of cells arrested in mitosis (mitotic index) after 20 Gy was then expressed as a percentage of the mitotic index in un-irradiated cells. Silencing PIGN and ZNF516 did not affect irradiation-induced G2 arrest (Figure 5.10a), supporting the hypothesis that increased prometaphase γH2AX foci observed after silencing PIGN and ZNF516 is a consequence of replication stress rather than checkpoint dysfunction. Unexpectedly, RKHD2 silencing resulted in greatly reduced irradiation-induced G2 arrest, with a reduction in mitotic entry of only 20% after irradiation compared to 80% in control cells (Figure 5.10 a,b). The magnitude of this G2-M checkpoint defect was similar to that observed after inhibiting DNA damage checkpoint signalling with 5mM Caffeine (Figure 5.10a). A dose dependent increase in G2 arrested cells could be observed after control but not RKHD2 silencing (Figure 5.10b). Furthermore, the checkpoint defect induced by RKHD2 silencing could also be verified by time-lapse microscopy of HCT-116 H2B-mRFP cells after 10 Gy irradiation (Figure 5.10c).

The checkpoint defect observed following RKHD2 depletion is not mediated through defective activation ATM signalling. Phosphorylated ATM (pS1981) localises to nuclear foci in RKHD2-depleted cells in response to irradiation, indicating normal ATM activation and recruited to sites of DNA damage (Figure 5.10 c,d). In addition, it has already been shown (Figure 5.1 e,f) that γH2AX and 53BP1 localise to foci normally after irradiation in RKHD2-depleted cells, and downstream ATM signalling is clearly activated in response to irradiation (Figure 5.1g).

This observation suggests that defective G2-M checkpoint function might contribute to prometaphase γH2AX foci induced by RKHD2 silencing, although not

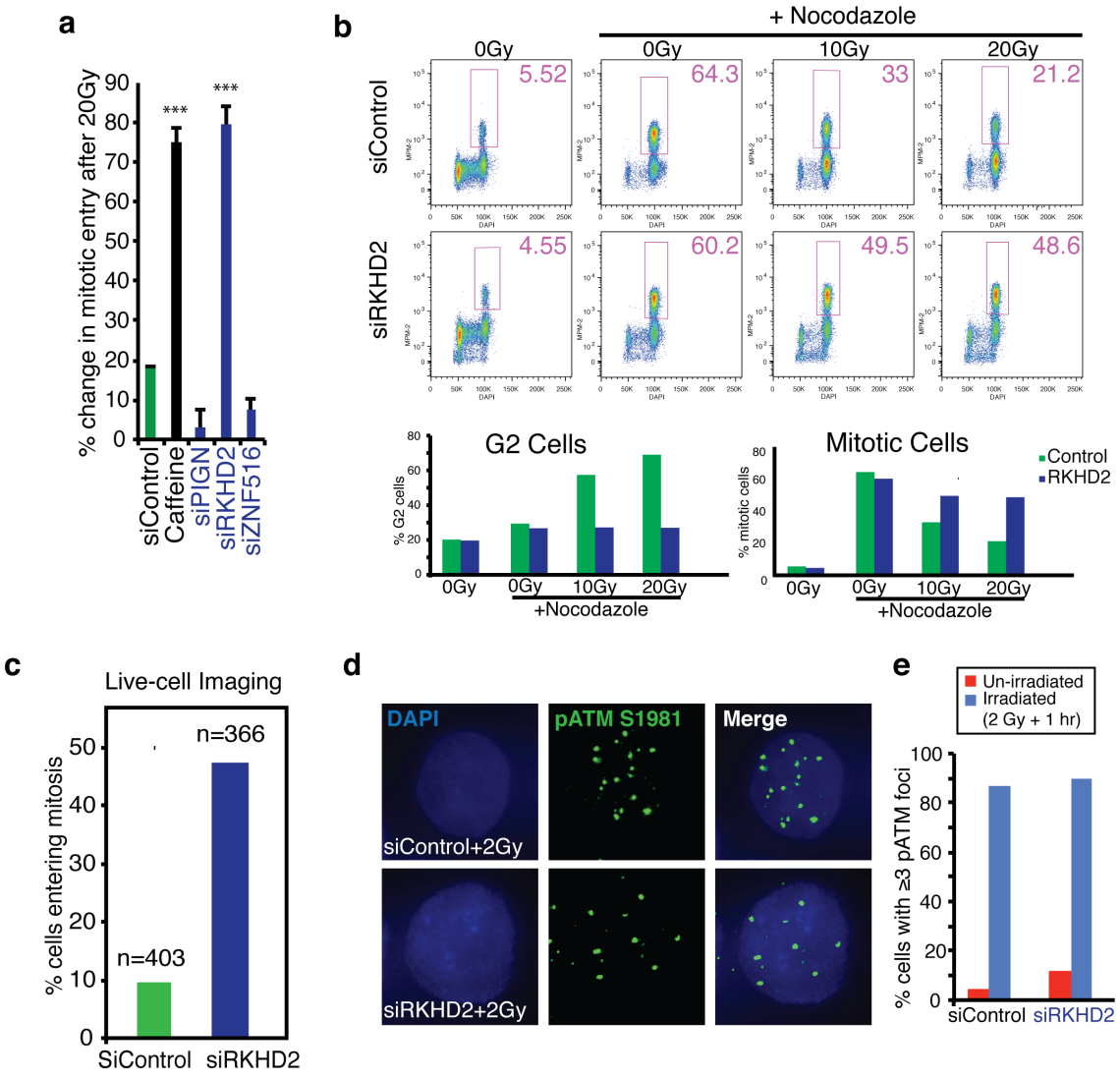

Figure 5.10 RKHD2 depletion leads to a defective G2/M DNA damage checkpoint
a) 48h post-transfection, cells were exposed to 0 or 20 Gy IR, then incubated for 16 hours in 50 ng/ml Nocodazole. The mitotic index was then measured by flow cytometry. The mitotic index of irradiated cells is expressed as a percentage of the mitotic index in un-irradiated cells. Caffeine treatment was at 5mm for 2 hours prior to irradiation and then throughout the Nocodazole block.
b) Representative flow cytometry plots showing the mitotic index of control and RKHD2-depleted cells to 0, 10 and 20 Gy IR. Graphs below show quantifications of the % of cells in G2 and mitosis. N=20000 cells per condition
c) 48h post-transfection HCT-116 H2B-mRFP cells were exposed to 10 Gy IR, then immediatedly imaged every 10 minutes for 24 hours. The percentage of cells that entered mitosis over the 24 hours was scored manually. Data from one experiment.
d) Control and siRKHD2-transfected cells were exposed to 2 Gy IR, fixed after 1h and stained with antibodies for phosphorylated ATM. Representative images are shown.
e) Quantification of d) n=100 cells per condition. Data from one experiment.

those observed following PIGN or ZNF516 silencing. However, defective checkpoint signalling does not induce DNA damage per se, so this defect does not provide an explanation for the elevated DNA damage observed after RKHD2 silencing, both in interphase and in mitotic cells. Furthermore, this defect does not explain either the observation of increased G1 53BP1 bodies (Figure 5.3a), or decreased replication fork rates (Figure 5.4 b-d) in RKHD2-depleted cells. It is also noteworthy that the frequency of RKHD2-deficient prometaphase cells with three or more γH2AX foci is greater than the percentage of interphase cells with an equivalent number of foci (Figure 5.1 a-d), which supports the hypothesis that γH2AX foci are generated upon entry into mitosis, potentially as a consequence of rupture of genomic loci under replication stress.

Depletion of another DNA damage checkpoint kinase, ATR, synergises with Aphidicolin treatment in the induction of 53BP1 bodies in G1 cells (Lukas et al., 2011a). If RKHD2 played a role in checkpoints responsive to replication stress, in addition to the G2-M checkpoint, then this might explain 53BP1 bodies and prometaphase DNA damage observed following RKHD2 silencing. If RKHD2 is involved in the response to DNA damage during S phase, then this could also explain elevated interphase DNA damage observed following RKHD2 silencing (Figure 5.1 c,d). Furthermore, activation of ATR in response to DNA damage in S phase, rather than ATM activation in G2, is thought to be responsible for durable G2 accumulation, as was measured in the assay shown in Figure 5.10a (Smith et al., 2010).

5.4.2 Intra-S checkpoint function

To explore whether RKHD2-depleted cells also exhibited defective intra-S phase checkpoint function, cells were pulse-labelled with EdU, to mark S phase cells (see Materials and Methods), and then exposed to Camptothecin for half an hour. Camptothecin stabilises topoisomerase I cleavage complexes, which may block the unwinding of DNA ahead of the replication fork, or prevent the resolution of topoisomerase-induced nicked DNA, which results in replication fork stalling (Takemura et al., 2006). Cells were released from Camptothecin and then harvested at regular intervals and analysed by flow cytometry (Aarts et al., 2012). Cells treated with a CHK1 inhibitor (AZD7762) were used as a positive control to abrogate intra-S checkpoint function (Figure 5.11 a, b). EdU labelled control-transfected cells were still

arrested in S-phase at 4 and 8 hours after Camptothecin treatment, while AZD7762-treated cells were already entering G2/M by 4 hours, and almost all EdU labelled cells were in G2/M by 8 hours (Figure 5.11b).

No defect in intra-S checkpoint function was observed after PIGN or ZNF516 silencing (Figure 5.11 c,d). However, RKHD2-depleted cells, like AZD7762-treated cells, were faster to recover from a Camptothecin-induced S-phase arrest compared to control cells (Figure 5.12 a-c), suggesting a possible role for RKHD2 in the intra-S phase checkpoint response. In keeping with the hypothesis that RKHD2 depleted cells may have intra-S checkpoint defects, a 4 hour 2 μM Aphidicolin exposure (which completely blocks S phase progression in HCT-116 cells, data not shown) results in double strand break formation in RKHD2-depleted cells, but not in control-transfected cells (Figure 5.13). A caveat of this experiment is that it has not been excluded that this result could reflect cell cycle arrest; if DNA damage is highest in G1 and S-phase cells, then an Aphidicolin block could enrich for these cells and thereby for DNA damage. Alternatively, increased DNA damage could reflect failure to stabilise stalled replication forks as a result of defective activation of the intra-S checkpoint in RKHD2-depleted cells, leading to fork collapse and generation of double strand breaks. Further experiments are needed to verify this result.

5.5 Conclusions and discussion

Evidence presented in this chapter further bolsters suggestions from the previous chapter that silencing the CIN-suppressor genes results primarily in pre-mitotic defects. Phenotypes associated with replication stress were observed after silencing each of the three CIN-suppressor genes, including altered replication fork rates. Particularly slow replication fork rates were observed after silencing PIGN and ZNF516. Observation of these replication-associated defects is concordant with the observation of structural chromosome aberrations that result in anaphases displaying acentric chromosomes and chromatin bridges in CIN-suppressor depleted cells. In contrast, only PIGN silencing resulted in any appreciable mitotic dysfunction, which appears not to contribute substantially to chromosome missegregation.

Nevertheless, it is not possible to completely exclude that RKHD2 or ZNF516 silencing results in subtle mitotic dysfunction based on the results presented above. In addition, other causes of DNA damage and structural chromosome aberrations, such as oxidative DNA damage and telomere damage, have not been assessed following CIN-suppressor silencing. However, the observation of clear replication defects following CIN-suppressor silencing implicates replication stress as a likely cause of structural chromosome aberrations and chromosome segregation errors. These results further emphasise the contribution of pre-mitotic defects to chromosome missegregation at anaphase.

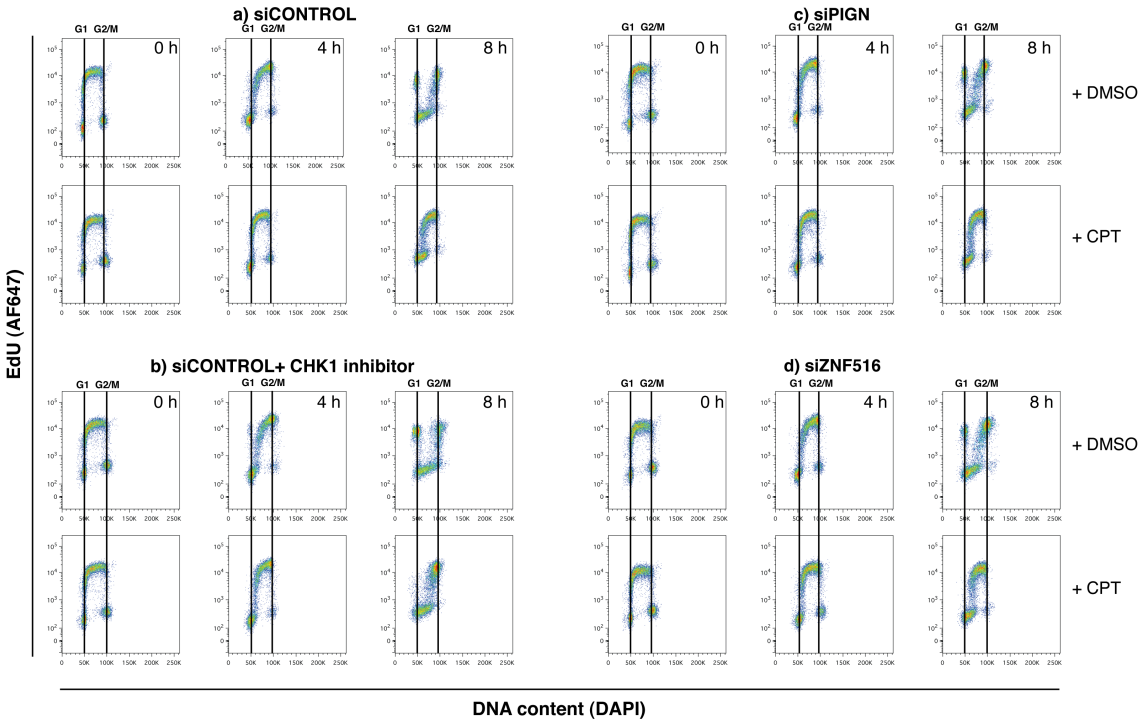

Figure 5.11 Intra-S phase checkpoint function after CIN-suppressor silencing
48 hours post-transfection cells were pulse-labelled with 10 µM EdU for 30 minutes. EdU was removed, cells washed and then treated for 30 minutes with 1 µM Camptothecin (CPT) or DMSO. CHK1 inhibitor (AZD7762) was added simultaneously with the EdU pulse, and was present throughout the rest of the experiment. Cells were then fixed at the indicated time points, EdU detected, and samples analysed by Flow Cytometry to assess the alterations in the DNA content of the EdU-labelled S phase cells. To aid the interpretation of the data, G1 (2N) and G2/M (4N) DNA content is indicated by lines. These lines are located based on the EdU-negative G2 and G1 cell populations. Representative flow cytometry profiles (from one of three independent experiments) are shown for a) siControl b) siControl+AZD7762 c) siPIGN and d) siZNF516.

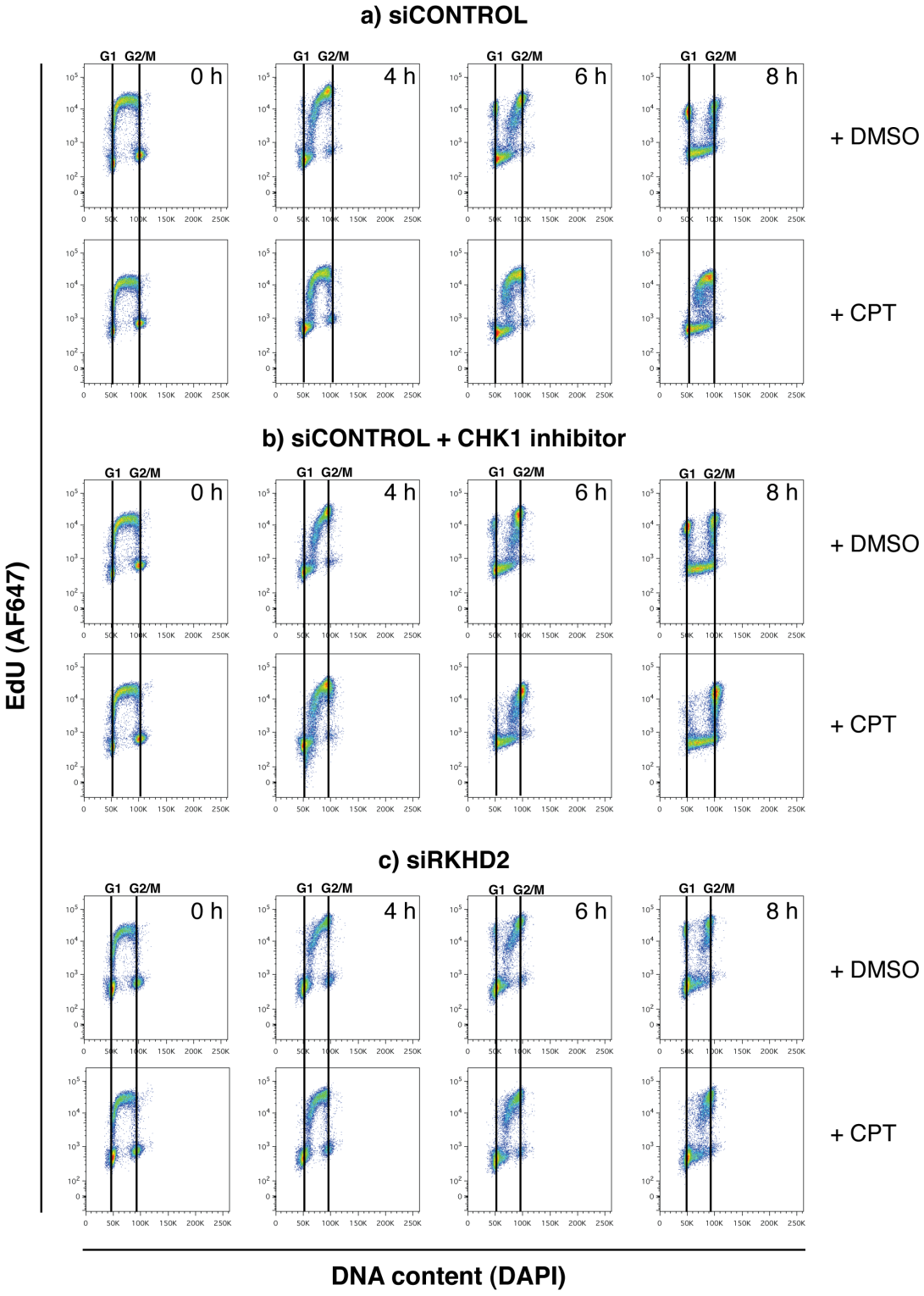

Figure 5.12 Intra-S phase checkpoint dysfunction after RKHD2 silencing
The same experiment was performed as for figure 5.11. An additional 6h timepoint is shown. Representative flow cytometry plots from one of four independent experiments are shown a) siControl b) siControl + AZD7762 c) siRKHD2

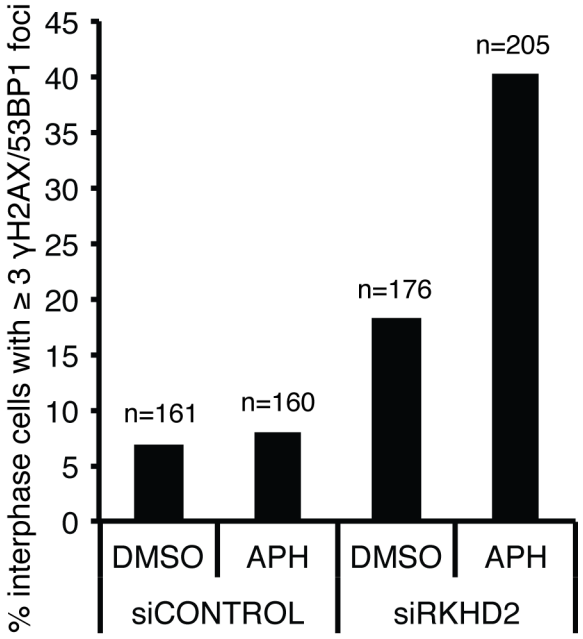

Figure 5.13 Replication block induces double-strand breaks in RKHD2-depleted cells
Control and RKHD2-depleted cells were treated with 2 μM Aphidicolin for 4 hours. This completely blocks DNA replication and induces replication fork stalling. Cells were then stained with γH2AX and 53BP1 antibodies, and DNA damage foci scored. The numbers of cells scored are indicated on the plot. NB This experiment has only been performed once.

5.5.1 CIN-suppressor gene function

Understanding exactly how silencing these genes are inducing replication defects will require further study, and at present can only be the subject of speculation. Preliminary experiments examining the localisation of GFP tagged RKHD2 and ZNF516 protein revealed that RKHD2 localises to the cytoplasm, in occasional granule structures, while ZNF516 localises to discrete nuclear domains (Figure 5.14). The limited amount already known about the function of these proteins does not necessarily indicate a direct role in DNA replication or the response to DNA damage, perhaps with the exception of ZNF516, which forms part of a histone-modifying complex. It is possible that the effect of CIN-suppressor silencing on genome stability could be mediated indirectly, via modifications or altered expression of other proteins. Interestingly, all of the genes have

putative ATM phosphorylation consensus sites (Table 5.1), although none of these has been experimentally verified (Matsuoka et al., 2007). Preliminary analysis of gene expression changes following silencing of each of the genes revealed an enrichment for pathways involved in the cell cycle, DNA replication and DNA damage, as well as DNA metabolism. However, based on what is known about the function of these proteins, it currently possible only to speculate about how their reduced expression might affect chromosomal stability.

PIGN has been suggested to have a role in ATP transport in the Golgi, which could have pleiotropic effects on the cell (Zhong et al., 2003). Alternatively, altered GPI-anchoring of various proteins could be responsible for the phenotype, although GPI anchoring was only minimally affected following PIGN silencing (Hong et al., 1999). Silencing PIGN appears to result in defects in S phase, including slow replication fork rates, but also infrequent defective mitotic spindle geometry. It is possible that the mitotic spindle defects arise as a result of delays during S phase, altering centriole duplication (Nigg and Stearns, 2011), or alternatively, S-phase and mitotic phenotypes may arise independently of each other, as a consequence of the potential diverse effects of PIGN silencing.

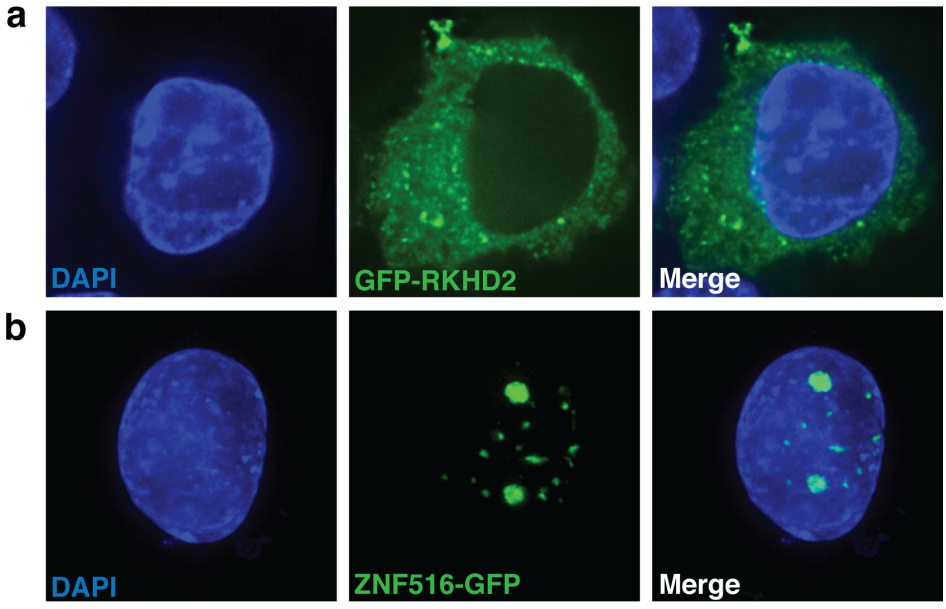

Figure 5.14 Preliminary localisation of GFP tagged RKHD2 and ZNF516
a) Representative HCT-116 cell expressing GFP-RKHD2
b) Representative HCT-116 cell expressing ZNF516-GFP

The role of RKHD2 in suppressing CIN could be directly mediated through a possible interaction with 14-3-3η, which has been shown to have a role in DNA damage responses (Wanzel et al., 2005, Courchet et al., 2008). Furthermore, RKHD2 has a ubiquitin ligase domain, so could play a role in ubiquitin modifications in response to DNA damage. Alternatively, as an RNA binding protein, RKHD2 could regulate the translation of a transcript important in the DNA damage response (Buchet-Poyau et al., 2007). Indeed a post-transcriptional response has previously been implicated in the DNA damage response (Reinhardt et al., 2010, Reinhardt et al., 2011). Immunoprecipitation followed by RNA sequencing would identify transcripts whose translation is regulated by RKHD2, and whether the identity or quantity of bound transcripts is altered by DNA damage. As RKHD2 has been shown to bind Argonaute proteins, which form part of the RNA interference machinery, it is also possible that the effects of RKHD2 silencing could be due to altered processing of cellular microRNAs, deregulating expression of multiple genes (Buchet-Poyau et al., 2007). Interrogation of gene expression analysis performed after RKHD2 depletion will assist in addressing this question.

Of the three genes, ZNF516 has the most obvious possible link to the maintenance of genome stability. ZNF516 is part of a complex with several histone modifiers (Lee et al., 2005, Hakimi et al., 2003), and directly binds the transcriptional regulator CtBP (Quinlan et al., 2006). This raises two possibilities for the role of ZNF516 in maintaining genome stability. First, the histone modifications executed by the complex in which ZNF516 resides could be necessary to coordinate DNA replication or the response to DNA damage. Secondly, the transcriptional regulatory function of this complex could affect the relative expression of other genes with important roles in DNA replication, damage or repair.

Further experiments will address the roles of these proteins in maintaining chromosomal stability.

Table 5.1 Predicted ATM phosphorylation sites in CIN-suppressor proteins
Data provided by Probir Chakravarty. Predicted phosphorylation sites using the group-based phosphorylation Scoring method. A GPS cut-off score of 2.6 was used to identify putative phosphorylation sites. [http://csbl.bmb.uga.edu/~ffzhou/gps_web/predict.php]

#	Protein_name	position	Peptide	kinase	GPS score
1	>PIGN_NP_789744.1	376	VKMTQKK	ATM	3.023
2	>PIGN_NP_789744.1	396	LSDSKQF	ATM	2.75
3	>PIGN_NP_789744.1	670	VYSTQSS	ATM	4.068
4	>MEX3C_NP_057710.3	88	AELSPEE	ATM	2.636
5	>MEX3C_NP_057710.3	152	ATASQTQ	ATM	6.114
6	>MEX3C_NP_057710.3	154	ASQTQQI	ATM	4.545
7	>MEX3C_NP_057710.3	241	VPSSEHV	ATM	3.477
8	>MEX3C_NP_057710.3	449	SSSSLGS	ATM	2.841
9	>MEX3C_NP_057710.3	537	RRGSQPS	ATM	4.205
10	>MEX3C_NP_057710.3	590	YSSSNGG	ATM	2.614
11	>MEX3C_NP_057710.3	596	GSTSSSP	ATM	3.045
12	>MEX3C_NP_057710.3	597	STSSSPP	ATM	3.227
13	>MEX3C_NP_057710.3	598	TSSSPPE	ATM	3.727
14	>MEX3C_NP_057710.3	652	TAVTQAI	ATM	3.591
15	>ZNF516_NP_055458.1	50	SSLSQHM	ATM	6.455
16	>ZNF516_NP_055458.1	72	HRASQKG	ATM	3.227
17	>ZNF516_NP_055458.1	108	MRASEGL	ATM	2.682
18	>ZNF516_NP_055458.1	132	NGASQAD	ATM	4.614
19	>ZNF516_NP_055458.1	144	NGASQAD	ATM	4.614
20	>ZNF516_NP_055458.1	258	QAFSQTW	ATM	3.773
21	>ZNF516_NP_055458.1	460	VLVSQEK	ATM	4.864
22	>ZNF516_NP_055458.1	560	GSLSEGD	ATM	4.159
23	>ZNF516_NP_055458.1	566	DSASQPS	ATM	7.136
24	>ZNF516_NP_055458.1	570	QPSSPGS	ATM	2.659
25	>ZNF516_NP_055458.1	657	ENSSRET	ATM	3.477
26	>ZNF516_NP_055458.1	851	KSGSSPL	ATM	2.636
27	>ZNF516_NP_055458.1	901	GAATQGP	ATM	3.295
28	>ZNF516_NP_055458.1	914	EASSKPV	ATM	3.75
29	>ZNF516_NP_055458.1	947	SANSKPV	ATM	3.341

Chapter 6. Results 4 – Nucleoside supplementation reduces segregation error frequency in CIN+ cell lines with 18q loss

As discussed in Chapter 3, CIN+ cells exhibit elevated replication stress relative to CIN- cell lines. These cells also display anaphase segregation errors characteristic of pre-mitotic defects that result in structural chromosome aberrations. CIN+ cells have slower replication rates, and exhibit signs of DNA replication stress. Chapters 4 and 5 described results showing induction of numerical and structural CIN upon silencing of three genes encoded on chromosome 18q, which is commonly lost in CIN+ colorectal cancer. More specifically, CIN- cells depleted of these genes exhibited replication stress, as well as structural chromosome aberrations and aneuploidy, phenocopying observations in CIN+ tumour cells.

In a recent study, slow replication rates were observed in the context of oncogene induced replication stress, which were attributed to cellular nucleotide deficiency (Bester et al., 2011). Accordingly, supplementing cells with exogenous nucleosides was able to ameliorate both slow replication rates and oncogene induced DNA damage, consistent with other studies that have rescued slow replication fork rates with nucleoside supplementation (Courbet et al., 2008, Anglana et al., 2003). An alternative explanation is that nucleoside supplementation augments DNA repair (Niida et al., 2010a, Niida et al., 2010b). Experimental data presented so far has shown that CIN+ cell lines with 18q loss, and also CIN- cells depleted of CIN-suppressor genes, display slow replication rates and other markers of replication stress. This raised the possibility that nucleoside supplementation might rescue segregation errors in both CIN+ cell lines, and those induced by CIN-suppressor silencing in CIN- diploid cells, if these errors and DNA damage were indeed caused by elevated replication stress.

6.1 Exogenous nucleosides reduce endogenous segregation error frequency in CIN+ cell lines

In this section, two experimental replicates of prometaphase γH2AX quantification were undertaken by Dr Nadeem Shaikh. Optimisation of nucleoside concentration was performed in collaboration with Dr Shaikh.

First, CIN+ cells were supplemented with nucleosides to investigate whether endogenous chromosomal instability could be reduced. To assess the effect of nucleoside supplementation upon replication stress, γH2AX foci were quantified in prometaphase cells after 48 hours exposure to exogenous nucleosides. A panel of four CIN+ cell lines (HT29, HT55, SW620 and SW1116) was used for this experiment. A reduction in the percentage of cells with more than three γH2AX foci was observed in all cell lines, although this was not significant in SW620 cells (Figure 6.1a, $p<0.05$). This suggests that nucleoside supplementation may rescue replication stress-induced DNA damage in CIN+ cells.

Next, it was determined whether the reduction in DNA damage after nucleoside supplementation also corresponded to a reduction in anaphase segregation error frequency. After 48 hours of nucleoside supplementation, segregation error frequency was significantly reduced in all cell lines, by 45-55% (Figure 6.1b $p<0.01$) from an average segregation error frequency of 49.2% across the four cell lines. Together with the data presented in Chapters 3 to 5, this observation supports the hypothesis that replication stress is a major driver of chromosome segregation errors in CIN+ cell lines.

6.2 Cell cycle distribution and mitotic entry after nucleoside supplementation

On the other hand, it was possible that the observed reduction in segregation errors could be explained by selective arrest of those cells that would have gone on to make segregation errors, without rescuing replication stress. To test this hypothesis, cell cycle distribution and the rate of mitotic entry were investigated after CIN+ cells received nucleoside supplementation.

Cells were treated with nucleosides for 48 hours before mitotic index was analysed by flow cytometry. No significant alterations in cell cycle distribution were observed in any of the cell lines, as illustrated by representative DNA histograms in Figure 6.2a, and cell cycle distributions in Figure 6.2b. In particular, there was no substantial change in mitotic index between untreated and nucleoside-treated cells (Figure 6.2c). While HT55 cells showed a slight reduction in mitotic index (4% decrease), HT29 and SW1116 cells showed a slight increase in mitotic index after nucleoside addition (13 and 6% increases respectively). The mitotic index of SW620 cells was unchanged after nucleoside addition.

Due to the observation of slight alterations in mitotic index after nucleoside addition, mitotic entry was assessed over 8 hours, in the presence of Nocodazole to capture cells in mitosis. After 48 hours of nucleoside supplementation, cells were treated with either DMSO or Nocodazole, while maintaining the presence or absence of exogenous nucleosides. The percentage of cells entering mitosis over 8 hours was then quantified by flow cytometry. The fold change in mitotic index after Nocodazole addition was similar in the presence of nucleosides compared to untreated cells (Figure 6.2d). Indeed, the increase in mitotic index in HT55 cells was equivalent between nucleoside-treated and untreated cells. Paradoxically, the two cell lines that showed a basal increase in mitotic index in the presence of nucleosides exhibited a slightly reduced Nocodazole-induced mitotic arrest when supplemented with nucleosides, relative to untreated cells exposed to Nocodazole. This may indicate that the increase in mitotic index after nucleoside addition reflects a longer duration of mitosis, rather than increased mitotic entry. A Nocodazole block eliminates the contribution of mitotic duration to the mitotic index as all cells are arrested in the early stages of mitosis. SW620 cells showed a greater increase in mitotic index in the presence of nucleosides, which could reflect an increased proliferation rate after nucleoside supplementation, but which does not result in an altered cell cycle distribution (Figure 6.2 a,b).

Overall, there is no consistent effect of nucleoside supplementation upon cell cycle distribution or mitotic entry. This suggests that decreased mitotic entry of cells cannot explain the reduction of segregation errors observed after nucleoside supplementation.

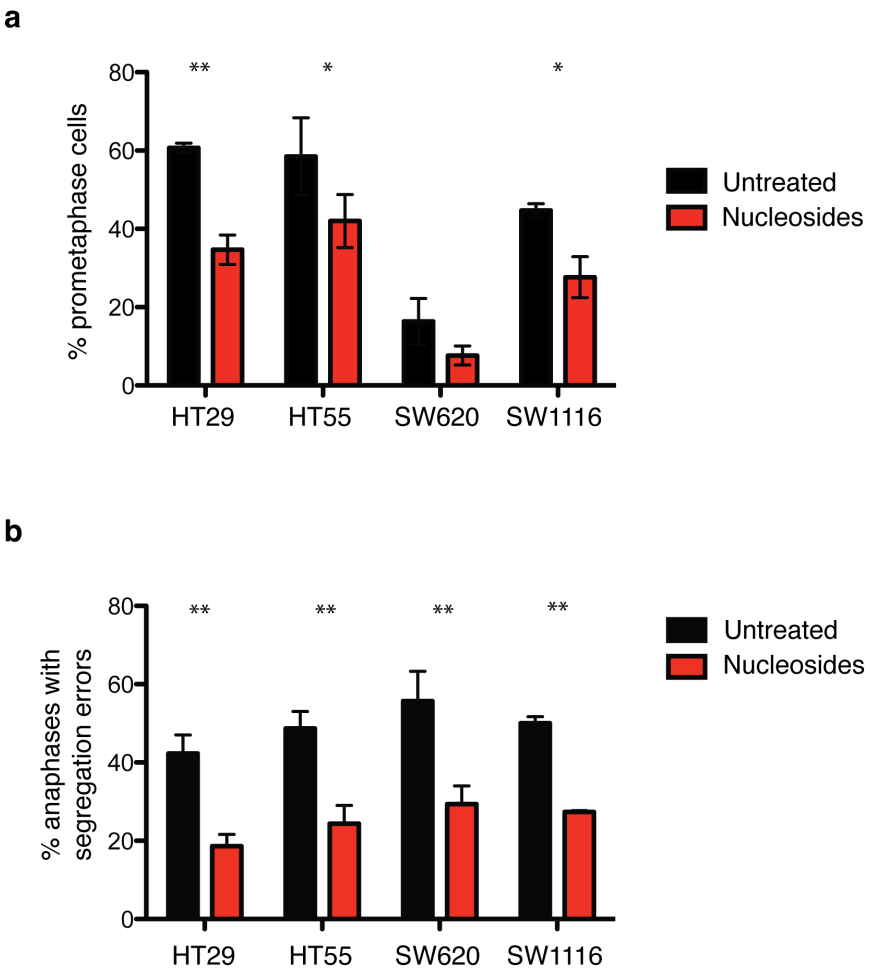

Figure 6.1 Nucleoside supplementation reduces segregation error frequency in CIN+ colorectal cancer cell lines

a) % prometaphase cells with ≥3 γH2AX foci ± 0.3 μM nucleosides (48h) (mean±s.e.m of 3 experiments, n=100 cells per cell line per experiment, statistical test: Two way ANOVA)

b)% anaphases with segregation errors ± 0.3 μM nucleosides (48h) (mean±s.e.m of 3 experiments, n=30 cells per cell line per experiment, statistical test: Two way ANOVA)

a

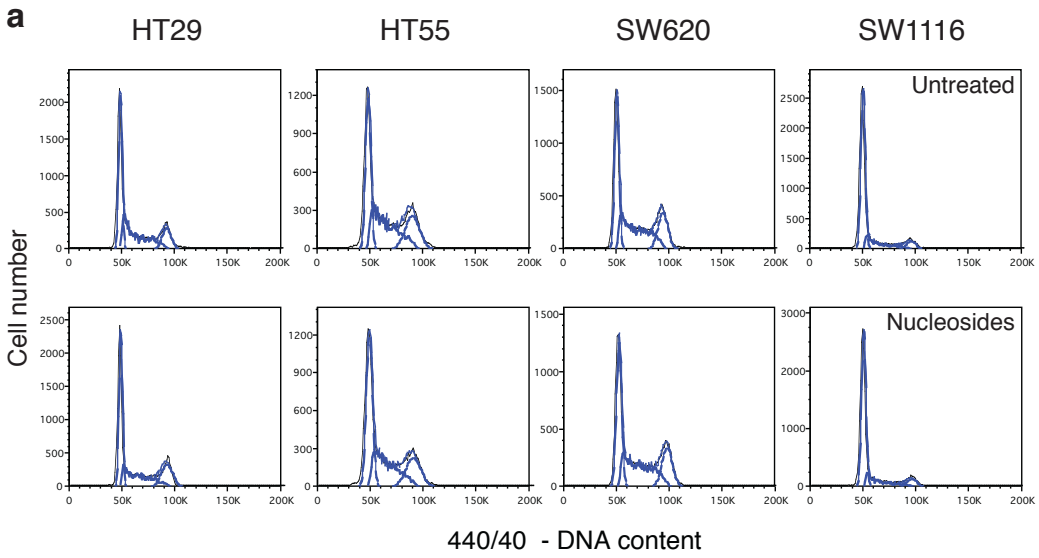

b

Cell line	G1		S		G2		M	
	Untreated	Nuc	Untreated	Nuc	Untreated	Nuc	Untreated	Nuc
HT29	43.4±0.6	47.2±0.6	35.5±1.7	32.6±0.9	17.6±1.9	20.3±0.4	2.5±0.3	2.9±0.2
HT55	39.5±3.9	43.2±1.6	38.3±1.3	35±1.4	20.6±2.3	20.0±0.6	2.9±0.3	2.8±0.2
SW620	38.2±1.3	39.7±0.6	40.4±0.7	37.6±1.2	19.6±1.6	20.7±1.9	3.4±0.4	3.3±0.2
SW1116	58.83±7.5	58.8±7.8	29.6±4.6	29.3±4.7	9.8±5.4	10.1±4.7	2.9±0.6	3.0±0.8

c

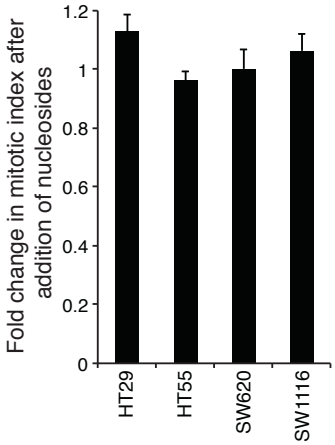

d

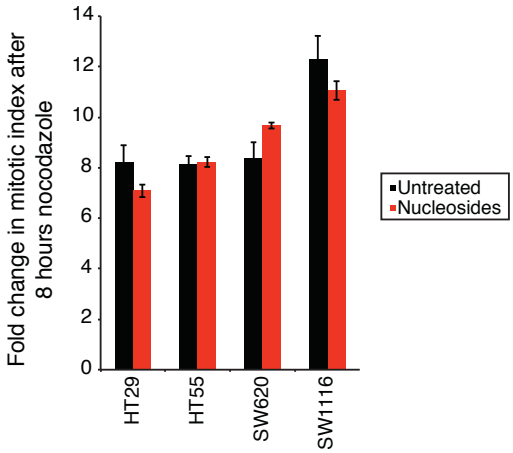

Figure 6.2 Nucleoside supplementation does not affect cell cycle distribution
a) Cells were grown ± 0.3 μM nucleosides (48h) and DNA content analysed by flow cytometry. Representative DNA histograms from one of three experiments are shown.
b) Proportion of cells in each stage of the cell cycle (mean±s.e.m of three independent experiments), measured by flow cytometry. Mitotic cells were identified by MPM2 staining. Cell cycle distribution was estimated using the Watson pragmatic algorithm.

c) Fold change in mitotic index after 48h nucleoside supplementation.
d) To assess mitotic entry rate, after 48h ± nucleosides, cells were incubated with Nocodazole (100 ng/ml) for 8 hours before harvesting and analysis by flow cytometry. Shown is the fold change in mitotic index induced by Nocodazole ± nucleosides (mean ± s.e.m of three independent experiments).

6.3 Nucleoside supplementation does not affect proliferation

A greater proportion of nucleoside-treated SW620 cells arrested in Nocodazole compared to untreated SW620 cells (Figure 6.2d), which could indicate an increased proliferation rate. Accelerated proliferation could reflect smoother passage through S phase, potentially indicative of reduced replication stress. Therefore, the effect of nucleoside supplementation upon the proliferation rates of the four cell lines was investigated.

Cells were seeded into 96 well plates and supplemented with nucleosides after 24 hours. Plates were then imaged every two hours for 72 hours, using the IncuCyte Long-term *in-situ* Cell Imaging System, which estimates the percentage of each well covered by the cell monolayer. Representative growth curves for each cell line are shown in Figure 6.3a. Figure 6.3b shows the average proliferation rates with and without nucleosides. There was no substantial change in proliferation rate upon addition of nucleosides, although SW620 cells showed a 13±5% increase in proliferation rate (Figure 6.3b,c). Increases in proliferation rate observed in HT29 and SW1116 cells were not reproducible between experiments (16±20 and 5±5% increases respectively).

In conclusion, nucleoside supplementation does not appear to cause an increase in proliferation rate, other than a slight increase in SW620 cells. This is consistent with the study by Bester et al, in which proliferation was not affected by nucleoside supplementation (Bester et al., 2011).

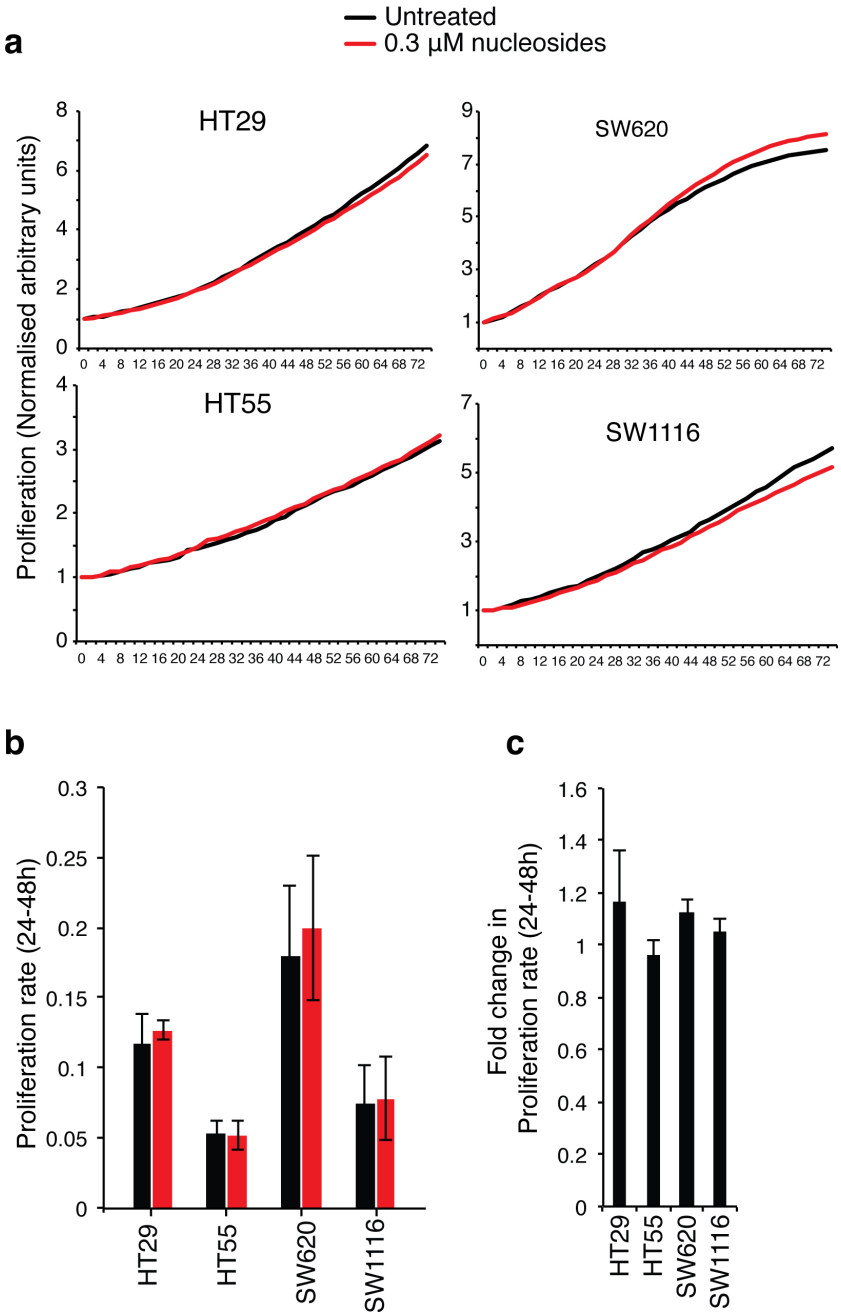

Figure 6.3 Nucleoside supplementation does not affect proliferation rate
Cells were seeded into 96 well plates, and imaged every 2 hours for 72 hours using an in-situ imaging system within the incubator. Confluency within the well was automatically estimated.
a) Representative proliferation curves for each cell line ± nucleosides. Each point is the average of 6 replicate wells. Outlier wells were excluded manually.
b) The gradient of the proliferation curve was measured between 24-48 hours, during the linear growth phase. Shown is the mean±s.e.m of three independent experiments
c) Fold change in the proliferation rate after nucleoside addition

6.4 Nucleoside supplementation does not increase ATP levels

Assessment and analysis of cellular ATP levels was conducted by Sally Dewhurst.

Another possible effect of nucleoside supplementation in cells is the improvement of cellular metabolic fitness by increasing the amount of available ATP, the substrate required for many enzymatic reactions. Increased availability of ATP might therefore increase the efficiency of replication or mitosis and reduce segregation errors indirectly.

To assess ATP levels, cells were seeded into 96 well plates, and supplemented with nucleosides after 24 hours. Following 48 hours, cells were incubated with Cell Titer Glo, which measures ATP levels, and values for each well were normalised to cell biomass. Cell biomass measurements were performed as due to morphological properties of the CIN+ cell lines, it was not possible to accurately estimate cell numbers within 96 well plates. There was no increase in cellular ATP levels after nucleoside supplementation (Figure 6.4). HT29 cells showed a relative decrease in cellular ATP levels, although this was not associated with altered proliferation or cell cycle distribution (Figures 6.2 and 6.3).

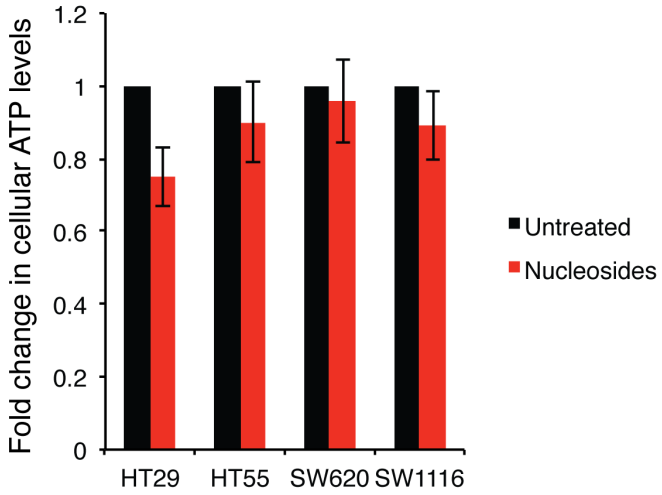

Figure 6.4 Nucleoside supplementation does not increase cellular ATP levels
ATP levels were measured using Cell Titer Glo (CTG). CTG values were then normalised to cell biomass (Sulforhodamine B solution). Fold-change in ATP levels was calculated for nucleoside treated cells by normalising the values to those of untreated cells. Mean ± s.e.m of three independent experiments.

In summary, other than the decreases in prometaphase DNA damage and anaphase segregation error frequency, no consistent effect of nucleoside supplementation was observed upon cell cycle distribution, mitotic entry, proliferation or cellular ATP levels. The results for each cell line are summarised in Table 6.1.

	HT29	HT55	SW620	SW1116
Prometaphase DNA damage	0.57	0.71	0.50	0.66
Segregation error frequency	0.44	0.50	0.52	0.54
Mitotic index (basal)	1.13	0.96	1.0	1.06
Mitotic entry (+Nocodazole)	0.87	1.00	1.17	0.90
Proliferation	1.16	0.96	1.13	1.05
ATP levels	0.74	0.90	0.96	0.89

Table 6.1 Summary of effects of nucleoside supplementation
Results are expressed as the fold change between nucleoside-treated and untreated cells.

6.5 Nucleoside supplementation does not reduce segregation error frequency in CIN- or 18q normal CIN+ cells.

While CIN+ cells displayed elevated levels of replication stress, CIN- cells also exhibited mitotic DNA damage and 53BP1 bodies, although at substantially lower levels (see Chapter 3, Figure 3.10). It was therefore possible that nucleosides might also reduce the lower frequencies of endogenous segregation errors in CIN- cells.

Four CIN- cell lines (DLD1, HCT-116, LS174T and RKO) were selected to investigate the effects of nucleosides upon segregation errors in CIN- cells. Unlike CIN+ cells (Figure 6.1b), nucleosides had no effect on segregation error frequency in any of the four CIN- cell lines tested (Figure 6.5a). This discrepancy could reflect different underlying defects causing replication stress in CIN+ relative to CIN- cells, with only the defect in CIN+ cells being attenuated by nucleoside treatment. This hypothesis is in accordance with the observation of normal replication fork rates in CIN- cells, while CIN+ cells had slow fork rates (Chapter 3, Figure 3.13).

The four CIN+ cell lines supplemented with nucleosides (Figure 6.1) have loss of one or more copy of 18q (Chapter 4 Figure 4.2). As almost all CIN+ cell lines and tumours harbour 18q loss, cell lines without 18q loss are rare. Nevertheless, NCIH508 CIN+ cells show neither loss of 18q nor complex rearrangements of this chromosome

arm (Figure 4.2). It was therefore tested whether supplementing NCIH508 cells with nucleosides was able to reduce the endogenous segregation error frequency. Interestingly, no change in segregation error frequency was observed in nucleoside-treated NCIH508 cells (Figure 6.5b). This raises the possibility that efficacy of nucleoside rescue could be related to 18q loss, although unfortunately the limited number of CIN+ cell lines without 18q loss means it has not been possible to formally test this hypothesis. It is also not possible to exclude that NCIH508 cells and the CIN- cell lines simply failed to take up the nucleosides from the media.

Nevertheless, to further investigate a possible link between loss of chromosome 18q and nucleoside-induced reduction of segregation error frequency, CIN- HCT-116 cells were transfected with siRNAs targeting the 18q-encoded CIN-suppressor genes PIGN, RKHD2 and ZNF516, and supplemented with nucleosides after 24 hours. It was determined previously in the laboratory that nucleoside supplementation does not affect the efficiency of gene silencing. Nucleoside supplementation reduced the frequency of segregation errors induced by CIN-suppressor silencing (PIGN: 62% to 32%, RKHD2: 57% to 36% and ZNF516: 43% to 34%, $p<0.05$, Figure 6.5c). Frequencies of segregation error in control-transfected cells, meanwhile, were unaffected. This result suggests that the frequency of segregation errors induced in NCIH508 cells by silencing PIGN, RKHD2 and ZNF516 (Chapter 4, Figure 4.7c) should also be reduced after nucleoside supplementation, a hypothesis that is yet to be tested.

Together these results indicate a possible link between the nucleoside-mediated reduction in segregation errors observed in four CIN+ cell lines, and loss of 18q. This may be more specifically linked to loss of the three CIN-suppressors, PIGN, RKHD2 and ZNF516, all of which are encoded on chromosome 18q. However, a larger cohort of 18q-normal CIN+ cell lines would be needed to conclusively test this hypothesis. Experiments are on-going to examine whether re-expressing these three genes can reduce segregation error frequency in CIN+ cells with 18q loss, as was observed in nucleoside supplementation experiments. Reduction of segregation errors by nucleoside supplementation, both in CIN+ cells and after CIN-suppressor silencing, provides further support for the hypothesis that replication defects are an important cause of CIN in colorectal cancer.

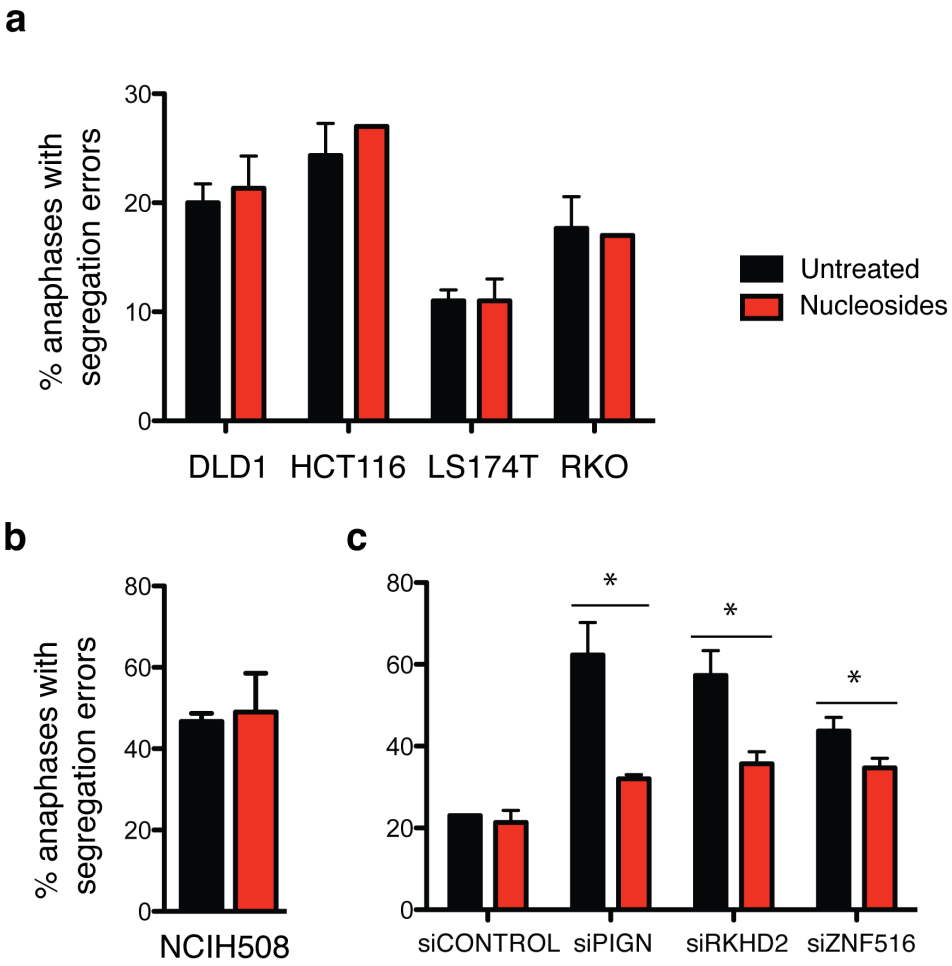

Figure 6.5 Nucleosides do not reduce segregation errors in CIN- or 18q normal CIN+ cell lines
Anaphase segregation error frequency was scored ± 0.3 μM nucleosides (48h) in a) 4 CIN- cell lines b) NCIH508 CIN+ cells, which do not have 18q loss c) HCT-116 depleted of CIN-suppressor genes (nucleosides added 24 hours post-transfection for 48 hours). Bars are mean±s.e.m of 3 independent experiments n>30 cells per cell line/siRNA per experiment, statistical test, paired T-test *p<0.05)

6.6 Conclusions and discussion

Data presented in this chapter have shown that nucleoside supplementation can reduce the frequency of endogenous segregation errors in CIN+ CRC cell lines. This is the first time that endogenous segregation errors have been rescued to any extent in CIN+ CRC cell lines. In contrast to four CIN+ cell lines with 18q loss, segregation errors were not reduced by nucleoside supplementation in a CIN+ cell line without 18q loss. Consistent with results in cell lines with loss of 18q, elevated segregation errors induced by CIN-

suppressor silencing were also significantly decreased by nucleoside supplementation. This raises the intriguing possibility of a link between loss of 18q and the reduction of segregation error frequency following nucleoside supplementation, and supports the hypothesis that 18q loss may elevate segregation error frequencies. However, a larger cohort of 18q-normal CIN+ cell lines would be needed to fully address this hypothesis. Examination of a panel of 18q-normal CIN+ cell lines might also uncover differences in the mechanisms responsible for chromosome segregation errors compared to CIN+ cell lines with 18q loss, which may reveal why nucleoside supplementation does not reduce segregation error frequency in NCIH508 cells.

The reduction in segregation errors after nucleoside supplementation was accompanied by a reduction in prometaphase DNA damage, supportive of an effect of nucleoside supplementation upon replication stress. Previous studies have reported that nucleoside supplementation rescues slow replication fork rates (Courbet et al., 2008, Bester et al., 2011, Anglana et al., 2003), and conversely that Aphidicolin induces slow fork progression (Ozeri-Galai et al., 2011, Palumbo et al., 2010). In Chapter 3 it was shown that treating CIN- HCT-116 cells with Aphidicolin induces structural chromosomal abnormalities, anaphase segregation errors and aneuploidy. Taken together these data point towards a link between slow replication fork rates and the genesis of structural chromosome aberrations in CIN+ cells, which may be ameliorated by nucleoside supplementation. Alternatively, it is possible that slow replication rates observed in CIN+ cells are not caused by insufficient nucleotide availability, and that nucleoside supplementation acts independently of DNA replication, by increasing the efficiency of DNA repair (Niida et al., 2010b). In support of a direct role of nucleoside supplementation on DNA structural integrity rather than general cellular fitness, no consistent effect was observed on proliferation rate, cell cycle distribution, or cellular ATP levels, indicating that the reduction in segregation errors was not mediated through increased viability of cells in the presence of nucleosides. It remains unclear exactly how nucleosides reduce segregation error frequency, but the decrease in prometaphase DNA damage following nucleoside supplementation suggests that the attenuating effect occurs in interphase, not mitosis. Further experiments are therefore needed to uncover the mechanism of action of nucleosides, and to examine the effects of nucleosides on structural chromosome aberrations and chromosome non-disjunction.

Chapter 7. Discussion

7.1 Mechanisms of CIN in colorectal cancer

7.1.1 Structural chromosome aberrations are the main cause of segregation errors in CIN+ CRC

In this thesis, a panel of genetically defined CIN+ colorectal cancer cell lines were examined to investigate the mechanisms driving chromosome missegregation at anaphase. The results of this analysis support published observations that CIN+ cancer cells are characterised by both structural and numerical instability (Roschke et al., 2003, Lee et al., 2011, Abdel-Rahman et al., 2001). However, contrary to the widely held view that CIN is primarily driven by mitotic dysfunction, CIN+ cell lines make high frequencies of acentric chromosomes and anaphase bridges, while lagging chromosomes are comparatively infrequent (Thompson and Compton, 2008, Thompson et al., 2010, Gregan et al., 2011, Pfau and Amon, 2012, Holland and Cleveland, 2012, Gordon et al., 2012).

Whether it is the structurally abnormal chromosomes or the low frequency lagging chromosomes that are the main drivers of numerical instability in CIN+ cells is not yet clear. However, as studies have indicated that merotelically attached chromosomes are usually ultimately segregated to the correct daughter cell, one could speculate that lagging chromosomes caused by merotely might not contribute substantially to chromosome non-disjunction (Cimini et al., 2004, Thompson and Compton, 2011a). In contrast, structural chromosome abnormalities and persistent DNA catenation have been shown result in chromosome non-disjunction and aneuploidy (Kawabata et al., 2011, Pampalona et al., 2010b, Pampalona et al., 2012, Stewenius et al., 2005, Baxter and Diffley, 2008). The frequency at which structural abnormalities are observed suggests that they do not generally arise as a consequence of DNA damage to chromosome segregation errors, as this causes only low frequency chromosome aberrations even after induction of segregation errors in almost every anaphase (Crasta et al., 2012, Janssen et al., 2011).

These results represent a shift from the perception that CIN is primarily driven by mitotic dysfunction (which results in lagging chromosomes) and instead suggest that

structurally abnormal chromosomes, generated prior to mitosis, are a central cause of both structural and numerical instability in CIN+ cancer cells.

7.1.2 CIN+ cells are characterised by elevated replication stress

Consistent with observations of acentric chromosomes and chromatin bridges at anaphase, which are indicative of pre-mitotic defects, CIN+ cells displayed evidence of elevated replication stress. CIN+ cells showed increased prometaphase DNA damage and 53BP1 bodies relative to CIN- cells, in addition to slower replication fork rates. Furthermore, ultra-fine bridges were enriched in CIN+ cells with segregation errors, an observation that implies that replication stress and segregation error induction are linked in CIN+ cells.

The exact mechanism through which the replication stress observed in CIN+ cells may result in structural chromosome abnormalities is not clear. Replication fork stalling, and subsequent collapse, is the most obvious mechanism through which replication defects may result in chromosome breakage and translocations. However, fork stalling was only marginally increased in three of four CIN+ cell lines analysed, relative to HCT-116 cells. Instead, CIN+ cells exhibited slow replication fork rates, similar to the effects of treating cells with drugs known to induce replication stress, such as Aphidicolin (Ozeri-Galai et al., 2011, Palumbo et al., 2010). In Chapter 3 it was shown that treatment of a CIN- cell line with Aphidicolin resulted in high frequencies of chromosome segregation errors, and aneuploidy. This suggests a possible causal link between the slow replication fork rate and chromosome abnormalities observed in mitosis. A demonstration of slow fork rates and only infrequent fork stalling after Aphidicolin treatment of the CIN- cell line would provide further support for this hypothesis. Alternatively, slow fork rates may reflect replication stress but are unconnected to the generation of structural chromosome aberrations.

Slow replication fork rates are usually coupled with an increase in origin firing (Anglana et al., 2003, Palumbo et al., 2010, Ozeri-Galai et al., 2011, Bester et al., 2011). Unexpectedly, however, CIN+ cells displayed decreased origin firing relative to CIN- HCT-116 cells, despite their slow fork rates. One possible explanation for this observation is unidirectional fork progression, where only one sister fork progresses from a given origin of replication. Unidirectional forks would have been classified as

progressing forks, due to the difficulty of distinguishing the two structures in genome-wide DNA fibre analysis (Palumbo et al., 2010). CIN+ cells displayed an increased proportion of progressing forks. In lymphocytes, the number of unidirectional forks is increased after a 24 hour 0.4 μM Aphidicolin treatment, while fork arrests were not detectable (Palumbo et al., 2010). Therefore one possibility is that an increase in asymmetric origin firing, compensating for the slow replication fork rates, might account for the increased proportion of progressing forks, and decreased origin firing in CIN+ cells. Alternatively, a decrease in origin firing could reflect inadequate origin licensing or constitutive activation of S phase checkpoint signalling in CIN+ cells (which prevents the firing of late origins) (Kawabata et al., 2011, Zegerman and Diffley, 2010). An attractive explanation for inadequate origin licensing is an imbalance between the levels of factors required for licensing and the number of origins in a polyploid genome. However, this does not explain the slow fork rate and decreased origin firing in SW620 cells, which are near diploid. While replication stress may directly result in CIN, another, not mutually exclusive, hypothesis remains possible; that replication of aneuploid (rather than polyploid) genomes inherently results in replication stress.

The ability of nucleosides to reduce both prometaphase DNA damage and segregation error frequency further supports the hypothesis that segregation errors arise through defects occurring prior to mitosis. Excess nucleosides have been shown to rescue slow fork rates in cells under replication stress (Bester et al., 2011, Anglana et al., 2003), which could indicate that nucleosides are ameliorating elevated replication stress in CIN+ CRC cells, and through this attenuation, reducing segregation error frequency. However, based on studies in both yeast and mammalian cells, it is also possible nucleosides may facilitate DNA repair (Niida et al., 2010a, Niida et al., 2010b), prevent hyper-recombination (Fasullo et al., 2010), or facilitate translesion polymerase activity (Niida et al., 2010b). Therefore, while the nucleoside-mediated reduction in segregation errors is supportive of the hypothesis that DNA damage during interphase drives CIN in CRC, further experiments are needed to understand the mechanism through which this reduction is mediated.

Hence, the CIN-associated replication defect uncovered in this thesis needs further characterisation, in order to fully understand whether or how it causes

chromosomal abnormalities observed at anaphase in CIN+ cells. In addition, it is also currently only possible to directly assess mechanisms underlying endogenous segregation errors in cell lines derived from CIN+ tumours. While copy number analysis revealed that the karyotypes of CIN+ CRC cell lines and aneuploid colorectal tumours are highly similar, it is still possible that culture conditions nevertheless alter mechanisms of on-going CIN. Therefore it will be important to validate the connection between replication stress and CIN in tumour specimens. In light of this, a study examining the relationship between CIN status, 18q LOH and γH2AX staining in a large cohort of colorectal tumours is currently underway.

It also remains to be seen whether CIN in other tumour types is driven by pre-mitotic dysfunction, and replication stress. Lagging chromosomes and numerical instability in U2OS osteosarcoma cells, and MCF7 breast cancer cells, were substantially reduced by overexpression of microtubule depolymerases (Bakhoum et al., 2009b). This suggests that mitotic defects might play a more prominent role in CIN in other cancer types. Classification of segregation errors, and examination of replication stress in CIN+ and CIN- cells of other cancer types will therefore be necessary to explore whether the relationship between replication stress and CIN is more widely observed. Reports documenting evidence of replication stress in tumour types other than CRC suggest that this could indeed be the case (Bartkova et al., 2010, Bartkova et al., 2005, Bartkova et al., 2006, Gorgoulis et al., 2005, Schlacher et al., 2012, Arlt et al., 2009, Hastings et al., 2009, Dereli-Oz et al., 2011). In this regard, preliminary investigations from our laboratory suggest that DNA replication stress plays a role in driving CIN in clear cell renal cell carcinoma cell lines.

7.1.3 CIN and oncogene-induced replication stress

The prevalence of CIN in tumours has led to suggestions that this phenotype can only be explained by common genomic aberrations, namely mutations in oncogenes and tumour suppressor genes, rather than mutations in genes involved in genome maintenance (Negrini et al., 2010). P53 mutations appear to occur after activation of the DNA damage response, and may arise through the selective pressure to override oncogene-induced senescence (Bartkova et al., 2005, Bartkova et al., 2006, Halazonetis et al., 2008, Negrini et al., 2010). This provides an attractive explanation for widespread

CIN in cancer, with P53 inactivation acting as a permissive factor allowing replication stress to drive CIN.

In the model described above, replication stress occurs in all tumours, through oncogene activation. Consistent with this model, of the cell lines summarised in Table 3.2, all the cancer cell lines exhibit slower fork rates than the non-transformed cell lines, irrespective of CIN status. In addition, all cell lines examined displayed some evidence of replication stress associated phenotypes, such as prometaphase DNA damage and 53BP1 bodies. This suggests that replication stress occurs in all cancer cell lines, consistent with the oncogene-induced replication stress model.

However, according to this hypothesis, the level of replication stress should be approximately equivalent between CIN- and CIN+ tumours, with permissive or restrictive factors (for example, P53 mutation or mismatch repair defects) representing the key difference between the two tumour types. This is not the case, as CIN+ cells examined in this thesis appear to have a more pronounced replication defect than CIN- cells. In addition, the combination of P53 mutation and oncogene activation in colon cancer cannot explain CIN, as CIN- cell lines and tumours exist that harbour both P53 mutations and oncogene-activation, for example KRAS mutation, both in colorectal cancer and in other cancer types (TCGA, 2012, Lee et al., 2011).

Therefore additional genomic changes may be required to drive the elevated replication stress observed in CIN+ cells, which either act in concert with oncogene activation or alternatively affect replication through independent mechanisms. The frequent loss of three putative suppressors of replication stress on chromosome 18q provides a possible explanation for the elevated DNA replication stress in CIN+ CRC. 18q loss occurs relatively late in colorectal cancer development, at the adenoma-carcinoma transition, probably after P53 mutation (D. Endesfelder, preliminary data). Based on the results presented in this thesis, 18q loss at the adenoma to carcinoma transition may cause an increase in replication stress beyond the level induced by oncogene activation, resulting in chromosomal instability. Whether the replication defect induced by CIN-suppressor loss is similar or distinct from oncogene-induced replication stress at a molecular level is not yet clear. Interestingly, 18q loss is more common in late stage metastatic disease (Paredes-Zaglul et al., 1998, Jen et al., 1994). One possible explanation for this observation is that elevated chromosomal instability

after 18q loss facilitates the development of aggressive disease and metastatic outgrowth.

7.2 18q and CIN in colon cancer

7.2.1 Using RNA interference to identify CIN-suppressor genes on 18q

PIGN, RKHD2 and ZNF516 were identified as CIN-suppressor genes using a targeted siRNA screen of genes encoded on chromosome 18q. Importantly, this approach was not biased towards genes with known functions in maintaining genome stability. However, an important consideration for RNA interference-based screens is off-target siRNA effects (Sigoillot et al., 2012, Adamson et al., 2012, Tsui et al., 2009). Multiple different si- or shRNA sequences for each of the three genes were demonstrated to induce segregation errors and furthermore, the siRNA phenotype was observed in four different cell lines, which suggests that segregation error induction is unlikely to be attributable to interaction with a specific genetic background. The gold-standard control for demonstrating that a phenotype is attributable to depletion of the siRNA target, rather than an off-target effect, is to re-express a siRNA resistant version of the protein and rescue the phenotype. These experiments are underway, and preliminary results show that re-expression of GFP-tagged RKHD2 rescues the phenotype of RKHD2-depletion.

It is important to note that loss of these three genes is unlikely to be the sole cause of instability in CIN+ CRC cell lines. Due to the false negative rate inherent to siRNA screens, discussed in Chapter 4, it is also not possible to exclude that other genes encoded on 18q may have a role in suppressing CIN. It is also probable that other genomic loci subject to copy number alteration encode either CIN-suppressors, whose loss promotes CIN, or CIN-drivers, gain of which promotes CIN.

The three genes identified on 18q are not obvious candidates for suppressors of chromosomal instability, perhaps with the exception of ZNF516. All three proteins have possible roles in regulating other proteins: through transcription (ZNF516), RNA interference (RKHD2), translation (RKHD2), or post-translational modifications (PIGN (GPI-anchors) and RKHD2 (ubiquitination)). This raises the possibility that the phenotypes observed after CIN-suppressor silencing might occur indirectly, through

altered expression, localisation or modification of other proteins, rather than directly, as would be expected if the proteins themselves have roles in genome maintenance.

Further work to investigate the localisation, interaction partners and post-translational modifications of the CIN-suppressors will be needed to understand how reduced expression of these genes results in replication defects and CIN. The diversity of function of the three CIN-suppressors suggests that endeavours to identify CIN genes should not be confined only to genes with predicted direct roles in genome maintenance and the cell cycle, as in previous studies (Barber et al., 2008, Wang et al., 2004b). The identification of CIN-suppressors within a region of copy number loss also suggests that efforts to identify CIN genes should not be limited to those harbouring mutations. Furthermore, this approach may be applicable to identifying potential drivers of CIN in other cancer types.

7.2.2 Copy number alterations as a cause of CIN

Copy number alterations are typically seen as a consequence of CIN, as the regions of genomic gain and loss often harbour tumour suppressors or oncogenes (Beroukhim et al., 2010, Bignell et al., 2010). However, copy number changes also occur in tumours that do not display CIN (Beroukhim et al., 2010, Abdel-Rahman et al., 2005), indicating that they do not necessarily reflect on going instability. These copy number changes may arise stochastically, through low-level instability, or through transient chromosome instability, such as is predicted to occur during telomere crisis. Therefore, chromosome gains and losses could occur prior to the onset of full CIN. These events may be selected for if they confer a proliferative or survival advantage, perhaps through altered dosage of a tumour suppressor or oncogene. However, all genes within the copy number-aberrant region are simultaneously subject to dosage changes, meaning that unselected phenotypes may be carried alongside the selected phenotype (proliferation or survival). This phenomenon has been documented in the development of multi-drug resistance in CIN+ cells (Duesberg et al., 2000), and provides a good rationale for screening genes encoded on chromosome 18q.

18q harbours two known tumour suppressor genes, SMAD4 and DCC. Therefore it is possible that loss of 18q is selected for, and maintained, on the basis of reduced expression of these tumour suppressor genes (Fearon et al., 1990, Bacolod and

Barany, 2011). It is also possible that the diversity fostered by CIN may provide an advantage during tumour growth, such that repression of the CIN-suppressors may also drive selection for the maintenance of 18q loss. Upon loss of 18q, multiple other genes are also repressed, in addition to the CIN-suppressors, SMAD4 and DCC, and it is therefore likely that reduced expression of other genes on 18q will also have a phenotypic impact on cells with 18q loss, independently of inducing chromosomal instability. For example, NOXA, a P53 target encoded on 18q, has been suggested to have role in promoting apoptosis in KRAS mutant tumours, so reduced expression of this protein might facilitate cell survival in KRAS mutant CIN+ tumours (de Bruijn et al., 2010). However, it is worth noting that not all genes on 18q show reduced gene expression in tumours with 18q loss, hence dosage compensation may occur for critical genes (Bacolod and Barany, 2011).

At present, the link between the chromosomal instability observed in cell lines with 18q loss and the phenotype observed following CIN-suppressor silencing remains associative. Loss of at least one of the three CIN-suppressors is observed in 84% of colorectal tumours in the TCGA cohort of tumours. In addition, decreasing copy number of the CIN-suppressors correlates significantly with a reduction in mRNA levels in both cell lines and tumours. Ideally, reduced or absent protein expression levels in CIN+ cancers with 18q loss should be demonstrated, however due to the lack of available antibodies this has not yet been possible. Furthermore, to prove a causal link, reduction in segregation error frequency should be demonstrated following re-expression of the CIN-suppressors in CIN+ cell lines that have lost 18q. These experiments are underway. As the majority (70%) of CIN+ cell lines have lost all three of the CIN-suppressors, and other independent factors are likely to contribute to CIN, re-expression of all three simultaneously may be necessary to have any significant effect on the level of CIN.

7.2.3 Clinical implications

If there is a causal link between the loss of 18q and CIN, then a better understanding of how segregation errors are induced upon silencing the three CIN-suppressors may shed light on the mechanisms of CIN in tumours with 18q loss, which may have clinical utility. Expression or copy number of the individual genes, or of 18q as a whole, could

be used as a prognostic marker, or as means of identifying tumours with CIN, which would be less technically challenging than other available methods of identifying CIN tumours. Loss of 18q is observed recurrently in colorectal cancer and in multiple other cancer types in addition to CRC including esophageal, gastric, breast, head and neck, prostate and pancreatic cancers (Popat and Houlston, 2005, Sheffer et al., 2009, Watanabe et al., 2001, Jen et al., 1994, Pasello et al., 2008, Furuya et al., 2000, Bauer et al., 2008, Yatsuoka et al., 2000, Huiping et al., 1998, Tsuda et al., 1998, Latil et al., 1994). This suggests 18q loss might be involved in the initiation of CIN in cancer types other than colorectal cancer.

18q LOH has long been proposed as a prognostic marker in CRC (Bacolod and Barany, 2011, Jen et al., 1994). Several studies have evaluated the relationship between 18q LOH and prognosis, with conflicting results (Jen et al., 1994, Popat and Houlston, 2005, Bertagnolli et al., 2011, Watanabe et al., 2001). In earlier studies, 18q LOH was found to be an independent predictor of poor prognosis in colorectal cancer. However, in the most recent and largest study, 18q LOH was not prognostic after MSI status was taken into account (i.e. assessing the impact of 18q LOH upon prognosis in only microsatellite stable tumours, of which the majority are likely to be CIN+) (Bertagnolli et al., 2011). This may be because 18q loss defines a subtype of CIN+ tumours, but it is CIN status rather than 18q status that determines poor prognosis. An alternative explanation is that 18q LOH was assessed rather than 18q copy number loss. Results presented in this thesis suggest that tumours with 18q loss may not show LOH at this locus, and conversely, that tumours with 18q LOH may not show genomic loss. Furthermore, a functional role is suggested for 18q copy number loss, which would not be fully accounted for by 18q LOH. In light of these observations, a study is underway to investigate the relative prognostic power of 18q copy number loss compared to 18q LOH.

7.3 Strategies to target CIN in tumours

Intra-tumour heterogeneity is a well-described contributor to the emergence of drug resistant disease in cancer patients (Ding et al., 2012, Yap et al., 2012, Burrell et al., 2010, Lee et al., 2011). Targeting mechanisms, such as chromosomal instability, that generate diversity within the tumour may therefore provide a tractable strategy to treat

heterogeneous tumours. The data presented in this thesis suggest that targeting replication stress might be effective in the treatment of CIN+ colorectal tumours. It remains unclear whether this replication stress confined to CIN+ tumours with 18q loss, but it is possible that loss of 18q could be used as a biomarker to identify tumours with elevated replication stress. Numerous chemotherapeutic drugs are already suggested to induce cytotoxicity through causing profound replication defects, including 5-Fluorouracil, topoisomerase inhibitors such as Epirubicin and Irinotecan and DNA crosslinking agents such as Mitomycin C. The efficacy of these agents could be based on their ability to drive CIN+ cells (already under substantial replication stress) over a threshold level of instability beyond which they cannot sustain viability. Such an effect has been documented with anti-mitotic agents; inducing excessive chromosome missegregation sensitises cells to paclitaxel treatment (Janssen et al., 2009). Furthermore, two recent publications from our laboratory have documented a paradoxical relationship between CIN and outcome; patients whose tumours exhibit extreme CIN have an improved prognosis relative to those whose tumours exhibit an intermediate level of CIN (Birkbak et al., 2011, Roylance et al., 2011). This suggests that for tumours with low levels of instability, drug treatment might enhance CIN to an intermediate level and thereby worsen prognosis.

The converse approach to exacerbating instability in CIN+ tumours would be strategies to stabilise CIN genomes, in order to limit further diversification. One might hypothesise that this would reduce both the likelihood of pre-existing drug resistant clone, but more particularly, reduce the capacity of the cells to adapt to altered selection pressures in the face of drug treatment. After surgery, the removal of the primary tumour reduces the number of tumour cells in the body, and therefore reduces the degree of heterogeneity (Yap et al., 2012). Speculatively, strategies to restrain the re-establishment of heterogeneity after surgery as the residual tumour cell population expands might then improve the efficacy of adjuvant treatment. Increasing cellular nucleoside levels might represent a possible means to accomplish this. However, an important caveat is that elevated nucleoside concentrations have been shown to result in mutagenesis in yeast (Kumar et al., 2011, Chabes and Stillman, 2007, Poli et al., 2012, Davidson et al., 2012), which might have deleterious effects. It is also possible that strategies to reduce the level of cellular DNA damage and chromosomal instability

might render cells *less* sensitive to treatment, by removing cells further from the threshold of tolerance of genomic instability at which genotoxic agents induce cell lethality. Reducing the level of instability could therefore have the undesired effect of converting tumours with a relatively favourable prognosis, due to extreme chromosomal instability, into tumours with poor outcome.

A third strategy to target CIN would be to sensitise cells to existing levels of replication stress. Various cellular adaptations are likely to be needed in order for CIN+ cancer cells to tolerate continuous extensive genome remodelling (McClelland et al., 2009, Gordon et al., 2012). Understanding the molecular basis for this tolerance is the subject of active research by a number of groups, including our own, as it is hypothesised that targeting these adaptations would selectively kill aneuploid cells (Tang et al., 2011, Williams et al., 2008, Torres et al., 2007, Storchova et al., 2006, Thompson and Compton, 2010). The tight connection between structural and numerical instability in CIN+ CRC suggests that efforts to understand and target mechanisms of CIN tolerance need to encompass both forms of instability, rather than purely whole chromosome aneuploidies, which have been the focus of studies published thus far.

7.4 Conclusion

The data presented in this thesis suggest that replication stress and CIN in cancer cells are intimately related, through the generation of structurally abnormal chromosomes during interphase that subsequently missegregate during mitosis, resulting in both whole chromosome and segmental aneuploidies. Surprisingly, the contribution of mitotic dysfunction to CIN in CRC cell lines appears to be relatively minor. Elevated replication stress in CIN+ cells may be caused in part by the loss of three suppressors (PIGN, RKHD2 and ZNF516) on chromosome 18q, which is recurrently lost in CIN+ CRC. Further work will address the nature of the replication defect in CIN+ cells, and how this may cause structural chromosome abnormalities, as well as characterising the three newly identified CIN-suppressor genes.

Chapter 8. Appendix

8.1 Appendix 1: List of genes screened by RNA interference

CS	ENSEMBL ID	Symbol	Description	Start	End
15	ENSG00000140386	SCAPER	S phase cyclin A-associated protein in the endoplasmic reticulum (S phase cyclin A-associated protein in the ER) (Zinc finger protein 291)	74427593	74984799
18	ENSG00000141646	SMAD4	Mothers against decapentaplegic homolog 4 (SMAD 4) (Mothers against DPP homolog 4) (Deletion target in pancreatic carcinoma 4) (hSMAD4)	46810611	46865413
18	ENSG00000176624	MEX3C	RNA-binding protein MEX3C (RING finger and KH domain-containing protein 2) (RING finger protein 194)	46954918	46977688
18	ENSG00000187323	DCC	Netrin receptor DCC precursor (Tumor suppressor protein DCC) (Colorectal cancer suppressor)	48121156	49311780
18	ENSG00000196628	TCF4	Transcription factor 4 (Immunoglobulin transcription factor 2) (ITF-2) (SL3-3 enhancer factor 2) (SEF-2)	51040560	51454183
18	ENSG00000206129		cDNA FLJ45743 fis, clone KIDNE2016464 (HCG2045177)	51821842	52009491
18	ENSG00000091164	TXNL1	Thioredoxin-like protein 1 (32 kDa thioredoxin-related protein)	52421053	52456874
18	ENSG00000091157	WDR7	WD repeat-containing protein 7 (TGF-beta resistance-associated protein TRAG) (Rabconnectin-3 beta)	52469614	52848040
18	ENSG00000177511	ST8SIA3	Sia-alpha-2,3-Gal-beta-1,4-GlcNAc-R:alpha 2,8-sialyltransferase	53170719	53187160
18	ENSG00000119547	ONECUT 2	One cut domain family member 2 (Transcription factor ONECUT-2) (OC-2) (Hepatocyte nuclear factor 6-beta) (HNF-6-beta)	53253915	53309527
18	ENSG00000066926	FECH	Ferrochelatase, mitochondrial precursor (EC 4.99.1.1) (Protoheme ferro-lyase) (Heme synthetase)	53366535	53404988
18	ENSG00000134440	NARS	Asparaginyl-tRNA synthetase, cytoplasmic (EC 6.1.1.22) (Asparagine-- tRNA ligase) (AsnRS)	53418894	53440175
18	ENSG00000081923	ATP8B1	Probable phospholipid-transporting ATPase IC (EC 3.6.3.1) (Familial intrahepatic cholestasis type 1) (ATPase class I type 8B member 1)	53464656	53550037
18	ENSG00000172186		Uncharacterized protein ENSP00000303812 (Fragment).	53835901	53837291
18	ENSG00000049759	NEDD4L	E3 ubiquitin-protein ligase NEDD4-like protein (EC 6.3.2.-) (Nedd4-2)	53862778	54216369

18	ENSG00000198796	ALPK2	Alpha-protein kinase 2 (EC 2.7.11.-) (Heart alpha-protein kinase)	54299459	54447169
18	ENSG00000172175	MALT1	Mucosa-associated lymphoid tissue lymphoma translocation protein 1 (EC 3.4.22.-) (MALT lymphoma-associated translocation) (Paracaspase)	54489598	54568350
18	ENSG00000074657	ZNF532	Zinc finger protein 532	54681041	54804663
18	ENSG00000166562	SEC11C	Signal peptidase complex catalytic subunit SEC11C (EC 3.4.-.-) (SEC11 homolog C) (SEC11-like protein 3) (Microsomal signal peptidase 21 kDa subunit)	54958105	54977041
18	ENSG00000134443	GRP	Gastrin-releasing peptide precursor (GRP) [Contains: Neuromedin-C (GRP-10)].	55038380	55048980
18	ENSG00000134438	RAX	Retinal homeobox protein Rx (Retina and anterior neural fold homeobox protein).	55085247	55091605
18	ENSG00000166569	CPLX4	Complexin-4 precursor (Complexin IV) (CPX IV).	55113634	55136861
18	ENSG00000074695	LMAN1	Protein ERGIC-53 precursor (ER-Golgi intermediate compartment 53 kDa protein) (Lectin mannose-binding 1) (Gp58) (Intracellular mannose- specific lectin MR60).	55148088	55177463
18	ENSG00000183287	CCBE1	Collagen and calcium-binding EGF domain-containing protein 1 precursor	55252129	55515554
18	ENSG00000141682	PMAIP1	Phorbol-12-myristate-13-acetate-induced protein 1 (PMA-induced protein 1) (Immediate-early-response protein APR) (NOXA)	55718172	55722518
18	ENSG00000166603	MC4R	Melanocortin receptor 4 (MC4-R)	56189323	56190988
18	ENSG00000101542	CDH20	Cadherin-20 precursor	57308755	57373345
18	ENSG00000176641	RNF152	RING finger protein 152	57633284	57711972
18	ENSG00000197563	PIGN	GPI ethanolamine phosphate transferase 1 (Phosphatidylinositol-glycan biosynthesis class N protein) (PIG-N) (MCD4 homolog)	57862440	58005269
18	ENSG00000134444	KIAA1468	LisH domain and HEAT repeat-containing protein KIAA1468	58005504	58125334
18	ENSG00000141655	TNFRSF11A	Tumor necrosis factor receptor superfamily member 11A precursor (Receptor activator of NF-KB) (Osteoclast differentiation factor receptor) (ODFR) (CD265 antigen)	58143500	58204482
18	ENSG00000141664	ZCCHC2	Zinc finger CCHC domain-containing protein 2	58342475	58396773
18	ENSG00000081913	PHLPP	PH domain leucine-rich repeat protein phosphatase) (Pleckstrin homology domain-containing family E protein 1) (Suprachiasmatic nucleus circadian oscillatory protein) (hSCOP)	58533897	58798646
18	ENSG00000215431		Uncharacterized protein ENSP00000383166 (Fragment).	58642403	58643704

18	ENSG00000171791	BCL2	Apoptosis regulator Bcl-2	58941559	59138341
18	ENSG00000119537	KDSR	3-ketodihydrosphingosine reductase precursor (EC 1.1.1.102) (3-dehydrosphinganine reductase) (KDS reductase) (Follicular variant translocation protein 1) (FVT-1).	59145951	59185486
18	ENSG00000057149	SERPINB4	Serpin B4 (Squamous cell carcinoma antigen 2) (SCCA-2) (Leupin)	59455474	59462482
18	ENSG00000206073	SERPINB3	Serpin B3 (Squamous cell carcinoma antigen 1) (SCCA-1) (Protein T4-A)	59473412	59480170
18	ENSG00000206072	SERPINB11	SERPINB11g	59521063	59542107
18	ENSG00000166396	SERPINB7	Serpin B7 (Megsin) (TP55)	59571257	59623584
18	ENSG00000197632	SERPINB2	Plasminogen activator inhibitor 2 precursor (PAI-2) (Placental plasminogen activator inhibitor) (Monocyte Arg-serpin) (Urokinase inhibitor)	59689906	59722100
18	ENSG00000166404	SERPINB10	Serpin B10 (Bomapin) (Proteinase inhibitor 10)	59726205	59754325
18	ENSG00000166401	SERPINB8	Serpin B8 (Cytoplasmic antiproteinase 2) (CAP-2) (CAP2) (Proteinase inhibitor 8)	59788238	59807585
18	ENSG00000179676	C18orf20	Uncharacterized protein C18orf20 precursor.	59898223	59967244
18	ENSG00000081138	CDH7	Cadherin-7 precursor	61568468	61703356
18	ENSG00000071991	CDH19	Cadherin-19 precursor	62322301	62422196
18	ENSG00000171451	DSEL	Dermatan-sulfate epimerase-like protein precursor	63324799	63335197
18	ENSG00000166479	TXNDC10	Protein disulfide-isomerase TXNDC10 precursor (EC 5.3.4.1) (Thioredoxin domain-containing protein 10) (Thioredoxin-related transmembrane protein 3)	64491907	64533342
18	ENSG00000150636	CCDC102B	Coiled-coil domain-containing protein 102B	64616297	64873406
18	ENSG00000206052	DOK6	Docking protein 6 (Downstream of tyrosine kinase 6)	65219271	65660357
18	ENSG00000150637	CD226	CD226 antigen precursor (DNAX accessory molecule 1) (DNAM-1)	65681175	65775140
18	ENSG00000176225	RTTN	Rotatin	65822025	66023942
18	ENSG00000170677	SOCS6	Suppressor of cytokine signaling 6 (SOCS-6) (Suppressor of cytokine signaling 4) (SOCS-4) (Cytokine-inducible SH2 protein 4) (CIS-4)	66107117	66148414
18	ENSG00000141668	CBLN2	Cerebellin-2	68354895	68362542
18	ENSG00000166342	NETO1	Neuropilin and tolloid-like protein 1 precursor (Brain-specific transmembrane protein containing 2 CUB and 1 LDL-receptor class A domains protein 1)	68565767	68685790
18	ENSG00000141665	FBXO15	F-box only protein 15	69891586	69965929
18	ENSG00000075336	C18orf55	TIM21-like protein, mitochondrial precursor	69966766	69977000
18	ENSG00000166347	CYB5A	Cytochrome b5	70071508	70110201

18	ENSG00000206043		Uncharacterized protein ENSP00000372122	70134090	70177398
18	ENSG00000187773	C18orf51	Uncharacterized protein C18orf51	70253944	70276159
18	ENSG00000133313	CNDP2	Cytosolic non-specific dipeptidase (CNDP dipeptidase 2) (Glutamate carboxypeptidase-like protein 1) (Peptidase A)	70314577	70339336
18	ENSG00000150656	CNDP1	Beta-Ala-His dipeptidase precursor (EC 3.4.13.20) (Carnosine dipeptidase 1) (CNDP dipeptidase 1) (Serum carnosinase) (Glutamate carboxypeptidase-like protein 2)	70352672	70403237
18	ENSG00000206029			70411054	70416040
18	ENSG00000215421	ZNF407	Zinc finger protein 407	70471907	70906616
18	ENSG00000180011	ZADH2	Zinc-binding alcohol dehydrogenase domain-containing protein 2	71039477	71050105
18	ENSG00000179981	TSHZ1	Teashirt homolog 1 (Serologically defined colon cancer antigen 33) (Antigen NY-CO-33)	71051719	71130886
18	ENSG00000206026	C18orf62		71250419	71268646
18	ENSG00000134046	MBD2	Methyl-CpG-binding domain protein 2 (Methyl-CpG-binding protein MBD2) (Demethylase) (DMTase)	49934573	50005156
18	ENSG00000101751	POLI	DNA polymerase iota (EC 2.7.7.7) (RAD30 homolog B) (Eta2)	50049847	50078600
18	ENSG00000174448	STARD6	StAR-related lipid transfer protein 6 (StARD6) (START domain-containing protein 6)	50104962	50134941
18	ENSG00000166845	C18orf54	Uncharacterized protein C18orf54 precursor	50139169	50162377
18	ENSG00000178690	C18orf26	Uncharacterized protein C18orf26	50409388	50417722
18	ENSG00000041353	RAB27B	Ras-related protein Rab-27B	50646706	50708124
18	ENSG00000166510	CCDC68	Coiled-coil domain-containing protein 68 (Cutaneous T-cell lymphoma- associated antigen se57-1) (CTCL tumor antigen se57-1)	50719792	50777635
18	ENSG00000119541	VPS4B	Vacuolar protein sorting-associating protein 4B (Suppressor of K(+) transport growth defect 1) (Protein SKD1)	59207407	59240732
18	ENSG00000206075	SERPINB5	Serpin B5 precursor (Maspin) (Protease inhibitor 5)	59295199	59323297
18	ENSG00000166634	SERPINB12	Serpin B12	59374373	59385224
18	ENSG00000197641	SERPINB13	Serpin B13 (Hurpin) (HaCaT UV-repressible serpin) (Proteinase inhibitor 13) (Headpin)	59405580	59417410
18	ENSG00000101493	ZNF516	Zinc finger protein 516	72201218	72336134
18	ENSG00000220032		cDNA FLJ44313 fis, clone TRACH2025911 (FLJ44313 protein)	72336465	72339033
18	ENSG00000130856	ZNF236	Zinc finger protein 236	72665104	72811668
18	ENSG00000197971	MBP	Myelin basic protein (MBP) (Myelin A1 protein) (Myelin membrane encephalitogenic protein)	72819771	72973788
18	ENSG00000166573	GALR1	Galanin receptor type 1 (GAL1-R) (GALR1)	73090721	73111081

18	ENSG00000151514	SALL3	Sal-like protein 3 (Zinc finger protein SALL3) (hSALL3)	74841263	74858385
18	ENSG00000166377	ATP9B	Probable phospholipid-transporting ATPase IIB	74930385	75239266
18	ENSG00000131196	NFATC1	Nuclear factor of activated T-cells, cytoplasmic 1 (NFAT transcription complex cytosolic component) (NF-ATc1) (NF-ATc) (NFATc)	75256760	75390310
18	ENSG00000178412		CDNA FLJ25715 fis, clone TST05160	75499926	75540733
18	ENSG00000060069	CTDP1	RNA polymerase II subunit A C-terminal domain phosphatase (EC 3.1.3.16) (TFIIF-associating CTD phosphatase)	75540789	75615495
18	ENSG00000178342	KCNG2	Potassium voltage-gated channel subfamily G member 2 (Voltage-gated potassium channel subunit Kv6.2) (Cardiac potassium channel subunit)	75724656	75760804
18	ENSG00000215413		cDNA FLJ44200 fis, clone THYMU3000826	75763454	75805312
18	ENSG00000122490	PQLC1	PQ-loop repeat-containing protein 1	75763476	75812605
18	ENSG00000141759	TXNL4A	Thioredoxin-like protein 4A (Thioredoxin-like U5 snRNP protein U5- 15kD) (Spliceosomal U5 snRNP-specific 15 kDa protein) (DIM1 protein homolog)	75833857	75849520
18	ENSG00000101546	C18orf22	Putative ribosome-binding factor A, mitochondrial precursor	75895346	75907373
18	ENSG00000101544	ADNP2	ADNP homeobox protein 2 (Zinc finger protein 508)	75967903	75999217
18	ENSG00000178184	PARD6G	Partitioning defective 6 homolog gamma (PAR-6 gamma) (PAR6D)	76016114	76106388

8.2 Appendix 2 - List of papers and reviews published during the production of this thesis

PRIMARY RESEARCH ARTICLES:

Replication stress links cancer structural and numerical chromosomal instability. Burrell RA*, McClelland SE*, Endesfelder D et al., **Nature** *accepted - in press*

Genome-wide RNA interference analysis of renal carcinoma survival regulators identifies MCT4 as a Warburg effect metabolic target. Gerlinger M, Santos CR, Spencer-Dene B, Martinez P, Endesfelder D, Burrell RA et al., **J Pathol. 2012 Feb 24. doi: 10.1002/path.4006.**

Relationship of extreme chromosomal instability with long-term survival in a retrospective analysis of primary breast cancer. Roylance R, Endesfelder D, Gorman P, Burrell RA et al., **Cancer Epidemiol Biomarkers Prev. 2011 Oct;20(10):2183-94**

Assessment of an RNA interference screen-derived mitotic and ceramide pathway metagene as a predictor of response to neoadjuvant paclitaxel for primary triple-negative breast cancer: a retrospective analysis of five clinical trials. Juul N, Szallasi Z, Eklund AC, Li Q, Burrell RA et al., **Lancet Oncol. 2010 Apr;11(4):358-65.**

REVIEW ARTICLES:

Cancer chromosomal instability: diagnostic and therapeutic challenges. McGranahan N*, Burrell RA*, Endesfelder D, Novelli M, Swanton C. **EMBO Rep. 2012 May 18**

Targeting chromosomal instability and tumour heterogeneity in HER2-positive breast cancer. Burrell RA*, Juul N, Johnston SR, Reis-Filho JS, Szallasi Z, Swanton C. **J Cell Biochem. 2010 Nov 1;11(4):782-90**

Breast cancer genome heterogeneity: a challenge to personalised medicine? Swanton C, Burrell RA, Futreal PA. **Breast Cancer Res. 2011 Feb 1;13(1):104**.

Advances in personalized therapeutics in non-small cell lung cancer: 4q12 amplification, PDGFRA oncogene addiction and sunitinib sensitivity. Swanton C, Burrell RA. **Cancer Biol Ther. 2009 Nov;8(21):2051**

Chromosomal instability: a composite phenotype that influences sensitivity to chemotherapy. McClelland SE*, Burrell RA*, Swanton C. **Cell Cycle. 2009 Oct 15;8(20):3262-6**

Reference List

AARTS, M., SHARPE, R., GARCIA-MURILLAS, I., GEVENSLEBEN, H., HURD, M. S., SHUMWAY, S. D., TONIATTI, C., ASHWORTH, A. & TURNER, N. C. 2012. Forced mitotic entry of S-phase cells as a therapeutic strategy induced by inhibition of WEE1. *Cancer Discov,* 2**,** 524-39.

ABDEL-RAHMAN, W. M., KATSURA, K., RENS, W., GORMAN, P. A., SHEER, D., BICKNELL, D., BODMER, W. F., ARENDS, M. J., WYLLIE, A. H. & EDWARDS, P. A. 2001. Spectral karyotyping suggests additional subsets of colorectal cancers characterized by pattern of chromosome rearrangement. *Proc Natl Acad Sci U S A,* 98**,** 2538-43.

ABDEL-RAHMAN, W. M., LOHI, H., KNUUTILA, S. & PELTOMAKI, P. 2005. Restoring mismatch repair does not stop the formation of reciprocal translocations in the colon cancer cell line HCA7 but further destabilizes chromosome number. *Oncogene,* 24**,** 706-13.

ACILAN, C., POTTER, D. M. & SAUNDERS, W. S. 2007. DNA repair pathways involved in anaphase bridge formation. *Genes Chromosomes Cancer,* 46**,** 522-31.

ADAMSON, B., SMOGORZEWSKA, A., SIGOILLOT, F. D., KING, R. W. & ELLEDGE, S. J. 2012. A genome-wide homologous recombination screen identifies the RNA-binding protein RBMX as a component of the DNA-damage response. *Nat Cell Biol,* 14**,** 318-28.

ANDERSON, K., LUTZ, C., VAN DELFT, F. W., BATEMAN, C. M., GUO, Y., COLMAN, S. M., KEMPSKI, H., MOORMAN, A. V., TITLEY, I., SWANSBURY, J., KEARNEY, L., ENVER, T. & GREAVES, M. 2011. Genetic variegation of clonal architecture and propagating cells in leukaemia. *Nature,* 469**,** 356-61.

ANDREASSEN, P. R., LOHEZ, O. D., LACROIX, F. B. & MARGOLIS, R. L. 2001. Tetraploid state induces p53-dependent arrest of nontransformed mammalian cells in G1. *Mol Biol Cell,* 12**,** 1315-28.

ANGLANA, M., APIOU, F., BENSIMON, A. & DEBATISSE, M. 2003. Dynamics of DNA replication in mammalian somatic cells: nucleotide pool modulates origin choice and interorigin spacing. *Cell,* 114**,** 385-94.

ARIZ, M., MAINPAL, R. & SUBRAMANIAM, K. 2009. C. elegans RNA-binding proteins PUF-8 and MEX-3 function redundantly to promote germline stem cell mitosis. *Dev Biol,* 326**,** 295-304.

ARLT, M. F., MULLE, J. G., SCHAIBLEY, V. M., RAGLAND, R. L., DURKIN, S. G., WARREN, S. T. & GLOVER, T. W. 2009. Replication stress induces genome-wide copy number changes in human cells that resemble polymorphic and pathogenic variants. *Am J Hum Genet,* 84**,** 339-50.

ARTANDI, S. E., CHANG, S., LEE, S. L., ALSON, S., GOTTLIEB, G. J., CHIN, L. & DEPINHO, R. A. 2000. Telomere dysfunction promotes non-reciprocal translocations and epithelial cancers in mice. *Nature,* 406**,** 641-5.

BACHRATI, C. Z. & HICKSON, I. D. 2008. RecQ helicases: guardian angels of the DNA replication fork. *Chromosoma,* 117**,** 219-33.

BACOLOD, M. D. & BARANY, F. 2011. Molecular profiling of colon tumors: the search for clinically relevant biomarkers of progression, prognosis, therapeutics, and predisposition. *Ann Surg Oncol,* 18**,** 3694-700.

BAKER, D. J., JEGANATHAN, K. B., CAMERON, J. D., THOMPSON, M., JUNEJA, S., KOPECKA, A., KUMAR, R., JENKINS, R. B., DE GROEN, P. C., ROCHE, P. & VAN DEURSEN, J. M. 2004. BubR1 insufficiency causes early onset of aging-associated phenotypes and infertility in mice. *Nat Genet,* 36**,** 744-9.

BAKER, D. J., JIN, F., JEGANATHAN, K. B. & VAN DEURSEN, J. M. 2009. Whole chromosome instability caused by Bub1 insufficiency drives tumorigenesis through tumor suppressor gene loss of heterozygosity. *Cancer Cell,* 16**,** 475-86.

BAKHOUM, S. F., DANILOVA, O. V., KAUR, P., LEVY, N. B. & COMPTON, D. A. 2011. Chromosomal Instability Substantiates Poor Prognosis in Patients with Diffuse Large B-cell Lymphoma. *Clin Cancer Res,* 17**,** 7704-11.

BAKHOUM, S. F., GENOVESE, G. & COMPTON, D. A. 2009a. Deviant kinetochore microtubule dynamics underlie chromosomal instability. *Curr Biol,* 19**,** 1937-42.

BAKHOUM, S. F., THOMPSON, S. L., MANNING, A. L. & COMPTON, D. A. 2009b. Genome stability is ensured by temporal control of kinetochore-microtubule dynamics. *Nat Cell Biol,* 11**,** 27-35.

BARBER, T. D., MCMANUS, K., YUEN, K. W., REIS, M., PARMIGIANI, G., SHEN, D., BARRETT, I., NOUHI, Y., SPENCER, F., MARKOWITZ, S., VELCULESCU, V. E., KINZLER, K. W., VOGELSTEIN, B., LENGAUER, C. & HIETER, P. 2008. Chromatid cohesion defects may underlie chromosome instability in human colorectal cancers. *Proc Natl Acad Sci U S A,* 105**,** 3443-8.

BARDI, G., JOHANSSON, B., PANDIS, N., BAK-JENSEN, E., ORNDAL, C., HEIM, S., MANDAHL, N., ANDREN-SANDBERG, A. & MITELMAN, F. 1993. Cytogenetic aberrations in colorectal adenocarcinomas and their correlation with clinicopathologic features. *Cancer,* 71**,** 306-14.

BAREFIELD, C. & KARLSEDER, J. 2012. The BLM helicase contributes to telomere maintenance through processing of late-replicating intermediate structures. *Nucleic Acids Res*.

BARKLEY, L. R., SONG, I. Y., ZOU, Y. & VAZIRI, C. 2009. Reduced expression of GINS complex members induces hallmarks of pre-malignancy in primary untransformed human cells. *Cell Cycle,* 8**,** 1577-88.

BARTEK, J., LUKAS, C. & LUKAS, J. 2004. Checking on DNA damage in S phase. *Nat Rev Mol Cell Biol,* 5**,** 792-804.

BARTKOVA, J., HAMERLIK, P., STOCKHAUSEN, M. T., EHRMANN, J., HLOBILKOVA, A., LAURSEN, H., KALITA, O., KOLAR, Z., POULSEN, H. S., BROHOLM, H., LUKAS, J. & BARTEK, J. 2010. Replication stress and oxidative damage contribute to aberrant constitutive activation of DNA damage signalling in human gliomas. *Oncogene,* 29**,** 5095-102.

BARTKOVA, J., HOREJSI, Z., KOED, K., KRAMER, A., TORT, F., ZIEGER, K., GULDBERG, P., SEHESTED, M., NESLAND, J. M., LUKAS, C., ORNTOFT, T., LUKAS, J. & BARTEK, J. 2005. DNA damage response as a candidate anti-cancer barrier in early human tumorigenesis. *Nature,* 434**,** 864-70.

BARTKOVA, J., REZAEI, N., LIONTOS, M., KARAKAIDOS, P., KLETSAS, D., ISSAEVA, N., VASSILIOU, L. V., KOLETTAS, E., NIFOROU, K., ZOUMPOURLIS, V. C., TAKAOKA, M., NAKAGAWA, H., TORT, F., FUGGER, K., JOHANSSON, F., SEHESTED, M., ANDERSEN, C. L., DYRSKJOT, L., ORNTOFT, T., LUKAS, J., KITTAS, C., HELLEDAY, T., HALAZONETIS, T. D., BARTEK, J. & GORGOULIS, V. G. 2006. Oncogene-induced senescence is part of the tumorigenesis barrier imposed by DNA damage checkpoints. *Nature,* 444**,** 633-7.

BASS, A. J., LAWRENCE, M. S., BRACE, L. E., RAMOS, A. H., DRIER, Y., CIBULSKIS, K., SOUGNEZ, C., VOET, D., SAKSENA, G., SIVACHENKO, A., JING, R., PARKIN, M., PUGH, T., VERHAAK, R. G., STRANSKY, N., BOUTIN, A. T., BARRETINA, J., SOLIT, D. B., VAKIANI, E., SHAO, W., MISHINA, Y., WARMUTH, M., JIMENEZ, J., CHIANG, D. Y., SIGNORETTI, S., KAELIN, W. G., SPARDY, N., HAHN, W. C., HOSHIDA, Y., OGINO, S., DEPINHO, R. A., CHIN, L., GARRAWAY, L. A., FUCHS, C. S., BASELGA, J., TABERNERO, J., GABRIEL, S., LANDER, E. S., GETZ, G. & MEYERSON, M. 2011. Genomic sequencing of colorectal adenocarcinomas identifies a recurrent VTI1A-TCF7L2 fusion. *Nat Genet,* 43**,** 964-8.

BAUER, V. L., BRASELMANN, H., HENKE, M., MATTERN, D., WALCH, A., UNGER, K., BAUDIS, M., LASSMANN, S., HUBER, R., WIENBERG, J., WERNER, M. & ZITZELSBERGER, H. F. 2008. Chromosomal changes characterize head and neck cancer with poor prognosis. *J Mol Med (Berl),* 86**,** 1353-65.

BAUMANN, C., KORNER, R., HOFMANN, K. & NIGG, E. A. 2007. PICH, a centromere-associated SNF2 family ATPase, is regulated by Plk1 and required for the spindle checkpoint. *Cell,* 128**,** 101-14.

BAXTER, J. & DIFFLEY, J. F. 2008. Topoisomerase II inactivation prevents the completion of DNA replication in budding yeast. *Mol Cell,* 30**,** 790-802.

BECK, H., NAHSE, V., LARSEN, M. S., GROTH, P., CLANCY, T., LEES, M., JORGENSEN, M., HELLEDAY, T., SYLJUASEN, R. G. & SORENSEN, C. S. 2010. Regulators of cyclin-dependent kinases are crucial for maintaining genome integrity in S phase. *J Cell Biol,* 188**,** 629-38.

BENSIMON, A., SIMON, A., CHIFFAUDEL, A., CROQUETTE, V., HESLOT, F. & BENSIMON, D. 1994. Alignment and sensitive detection of DNA by a moving interface. *Science,* 265**,** 2096-8.

BERLINGIERI, M. T., PALLANTE, P., SBONER, A., BARBARESCHI, M., BIANCO, M., FERRARO, A., MANSUETO, G., BORBONE, E., GUERRIERO, E., TRONCONE, G. & FUSCO, A. 2007. UbcH10 is overexpressed in malignant breast carcinomas. *Eur J Cancer,* 43**,** 2729-35.

BEROUKHIM, R., GETZ, G., NGHIEMPHU, L., BARRETINA, J., HSUEH, T., LINHART, D., VIVANCO, I., LEE, J. C., HUANG, J. H., ALEXANDER, S., DU, J., KAU, T., THOMAS, R. K., SHAH, K., SOTO, H., PERNER, S., PRENSNER, J., DEBIASI, R. M., DEMICHELIS, F., HATTON, C., RUBIN, M. A., GARRAWAY, L. A., NELSON, S. F., LIAU, L., MISCHEL, P. S., CLOUGHESY, T. F., MEYERSON, M., GOLUB, T. A., LANDER, E. S., MELLINGHOFF, I. K. & SELLERS, W. R. 2007. Assessing the significance of chromosomal aberrations in cancer: methodology and application to glioma. *Proc Natl Acad Sci U S A,* 104**,** 20007-12.

BEROUKHIM, R., MERMEL, C. H., PORTER, D., WEI, G., RAYCHAUDHURI, S., DONOVAN, J., BARRETINA, J., BOEHM, J. S., DOBSON, J., URASHIMA, M., MC HENRY, K. T., PINCHBACK, R. M., LIGON, A. H., CHO, Y. J., HAERY, L., GREULICH, H., REICH, M., WINCKLER, W., LAWRENCE, M. S., WEIR, B. A., TANAKA, K. E., CHIANG, D. Y., BASS, A. J., LOO, A., HOFFMAN, C., PRENSNER, J., LIEFELD, T., GAO, Q., YECIES, D., SIGNORETTI, S., MAHER, E., KAYE, F. J., SASAKI, H., TEPPER, J. E., FLETCHER, J. A., TABERNERO, J., BASELGA, J., TSAO, M. S., DEMICHELIS, F., RUBIN, M. A., JANNE, P. A., DALY, M. J., NUCERA, C., LEVINE, R. L., EBERT, B. L., GABRIEL, S., RUSTGI, A. K., ANTONESCU, C. R., LADANYI, M., LETAI, A., GARRAWAY, L. A., LODA, M., BEER, D. G., TRUE, L. D., OKAMOTO, A., POMEROY, S. L., SINGER, S., GOLUB, T. R., LANDER, E. S., GETZ, G., SELLERS, W. R. & MEYERSON, M. 2010. The landscape of somatic copy-number alteration across human cancers. *Nature,* 463**,** 899-905.

BERTAGNOLLI, M. M., REDSTON, M., COMPTON, C. C., NIEDZWIECKI, D., MAYER, R. J., GOLDBERG, R. M., COLACCHIO, T. A., SALTZ, L. B. & WARREN, R. S. 2011. Microsatellite instability and loss of heterozygosity at chromosomal location 18q: prospective evaluation of biomarkers for stages II and III colon cancer--a study of CALGB 9581 and 89803. *J Clin Oncol,* 29**,** 3153-62.

BESTER, A. C., RONIGER, M., OREN, Y. S., IM, M. M., SARNI, D., CHAOAT, M., BENSIMON, A., ZAMIR, G., SHEWACH, D. S. & KEREM, B. 2011. Nucleotide deficiency promotes genomic instability in early stages of cancer development. *Cell,* 145**,** 435-46.

BIGNELL, G. R., GREENMAN, C. D., DAVIES, H., BUTLER, A. P., EDKINS, S., ANDREWS, J. M., BUCK, G., CHEN, L., BEARE, D., LATIMER, C., WIDAA, S., HINTON, J., FAHEY, C., FU, B., SWAMY, S., DALGLIESH, G. L., TEH, B. T., DELOUKAS, P., YANG, F., CAMPBELL, P. J., FUTREAL, P. A. & STRATTON, M. R. 2010. Signatures of mutation and selection in the cancer genome. *Nature,* 463**,** 893-8.

BIRKBAK, N. J., EKLUND, A. C., LI, Q., MCCLELLAND, S. E., ENDESFELDER, D., TAN, P., TAN, I. B., RICHARDSON, A. L., SZALLASI, Z. & SWANTON, C. 2011. Paradoxical relationship between chromosomal instability and survival outcome in cancer. *Cancer Res,* 71**,** 3447-52.

BLASCO, M. A., LEE, H. W., HANDE, M. P., SAMPER, E., LANSDORP, P. M., DEPINHO, R. A. & GREIDER, C. W. 1997. Telomere shortening and tumor formation by mouse cells lacking telomerase RNA. *Cell,* 91**,** 25-34.

BLOW, J. J. & GILLESPIE, P. J. 2008. Replication licensing and cancer--a fatal entanglement? *Nat Rev Cancer,* 8**,** 799-806.

BRANZEI, D. 2011. Ubiquitin family modifications and template switching. *FEBS Lett,* 585**,** 2810-7.

BRANZEI, D. & FOIANI, M. 2008. Regulation of DNA repair throughout the cell cycle. *Nat Rev Mol Cell Biol,* 9**,** 297-308.

BRANZEI, D. & FOIANI, M. 2010. Maintaining genome stability at the replication fork. *Nat Rev Mol Cell Biol,* 11**,** 208-19.

BROWN, E. J. & BALTIMORE, D. 2000. ATR disruption leads to chromosomal fragmentation and early embryonic lethality. *Genes Dev,* 14**,** 397-402.

BRYANT, H. E., PETERMANN, E., SCHULTZ, N., JEMTH, A. S., LOSEVA, O., ISSAEVA, N., JOHANSSON, F., FERNANDEZ, S., MCGLYNN, P. & HELLEDAY, T. 2009. PARP is activated at stalled forks to mediate Mre11-dependent replication restart and recombination. *EMBO J,* 28**,** 2601-15.

BUCHET-POYAU, K., COURCHET, J., LE HIR, H., SERAPHIN, B., SCOAZEC, J. Y., DURET, L., DOMON-DELL, C., FREUND, J. N. & BILLAUD, M. 2007. Identification and characterization of human Mex-3 proteins, a novel family of evolutionarily conserved RNA-binding proteins differentially localized to processing bodies. *Nucleic Acids Res,* 35**,** 1289-300.

BUIS, J., WU, Y., DENG, Y., LEDDON, J., WESTFIELD, G., ECKERSDORFF, M., SEKIGUCHI, J. M., CHANG, S. & FERGUSON, D. O. 2008. Mre11 nuclease activity has essential roles in DNA repair and genomic stability distinct from ATM activation. *Cell,* 135**,** 85-96.

BUNZ, F., DUTRIAUX, A., LENGAUER, C., WALDMAN, T., ZHOU, S., BROWN, J. P., SEDIVY, J. M., KINZLER, K. W. & VOGELSTEIN, B. 1998. Requirement for p53 and p21 to sustain G2 arrest after DNA damage. *Science,* 282**,** 1497-501.

BUNZ, F., FAUTH, C., SPEICHER, M. R., DUTRIAUX, A., SEDIVY, J. M., KINZLER, K. W., VOGELSTEIN, B. & LENGAUER, C. 2002. Targeted inactivation of p53 in human cells does not result in aneuploidy. *Cancer Res,* 62**,** 1129-33.

BURRELL, R. A., JUUL, N., JOHNSTON, S. R., REIS-FILHO, J. S., SZALLASI, Z. & SWANTON, C. 2010. Targeting chromosomal instability and tumour heterogeneity in HER2-positive breast cancer. *J Cell Biochem,* 111**,** 782-90.

BURTON, J. L. & SOLOMON, M. J. 2007. Mad3p, a pseudosubstrate inhibitor of APCCdc20 in the spindle assembly checkpoint. *Genes Dev,* 21**,** 655-67.

BYUN, T. S., PACEK, M., YEE, M. C., WALTER, J. C. & CIMPRICH, K. A. 2005. Functional uncoupling of MCM helicase and DNA polymerase activities activates the ATR-dependent checkpoint. *Genes Dev,* 19**,** 1040-52.

CAHILL, D. P., KINZLER, K. W., VOGELSTEIN, B. & LENGAUER, C. 1999. Genetic instability and darwinian selection in tumours. *Trends Cell Biol,* 9**,** M57-60.

CAHILL, D. P., LENGAUER, C., YU, J., RIGGINS, G. J., WILLSON, J. K., MARKOWITZ, S. D., KINZLER, K. W. & VOGELSTEIN, B. 1998. Mutations of mitotic checkpoint genes in human cancers. *Nature,* 392**,** 300-3.

CALDECOTT, K. W. 2008. Single-strand break repair and genetic disease. *Nat Rev Genet,* 9**,** 619-31.

CALDWELL, C. M., GREEN, R. A. & KAPLAN, K. B. 2007. APC mutations lead to cytokinetic failures in vitro and tetraploid genotypes in Min mice. *J Cell Biol,* 178**,** 1109-20.

CARTER, S. L., EKLUND, A. C., KOHANE, I. S., HARRIS, L. N. & SZALLASI, Z. 2006. A signature of chromosomal instability inferred from gene expression profiles predicts clinical outcome in multiple human cancers. *Nat Genet,* 38**,** 1043-8.

CASTETS, M., BROUTIER, L., MOLIN, Y., BREVET, M., CHAZOT, G., GADOT, N., PAQUET, A., MAZELIN, L., JARROSSON-WUILLEME, L., SCOAZEC, J. Y., BERNET, A. & MEHLEN, P. 2012. DCC constrains tumour progression via its dependence receptor activity. *Nature,* 482**,** 534-7.

CELESTE, A., PETERSEN, S., ROMANIENKO, P. J., FERNANDEZ-CAPETILLO, O., CHEN, H. T., SEDELNIKOVA, O. A., REINA-SAN-MARTIN, B., COPPOLA, V., MEFFRE, E., DIFILIPPANTONIO, M. J., REDON, C., PILCH, D. R., OLARU, A., ECKHAUS, M., CAMERINI-OTERO, R. D., TESSAROLLO, L., LIVAK, F., MANOVA, K., BONNER, W. M., NUSSENZWEIG, M. C. & NUSSENZWEIG, A. 2002. Genomic instability in mice lacking histone H2AX. *Science,* 296**,** 922-7.

CHABES, A. & STILLMAN, B. 2007. Constitutively high dNTP concentration inhibits cell cycle progression and the DNA damage checkpoint in yeast Saccharomyces cerevisiae. *Proc Natl Acad Sci U S A,* 104**,** 1183-8.

CHABOSSEAU, P., BUHAGIAR-LABARCHEDE, G., ONCLERCQ-DELIC, R., LAMBERT, S., DEBATISSE, M., BRISON, O. & AMOR-GUERET, M. 2011. Pyrimidine pool imbalance induced by BLM helicase deficiency contributes to genetic instability in Bloom syndrome. *Nat Commun,* 2**,** 368.

CHAN, K. L. & HICKSON, I. D. 2009. On the origins of ultra-fine anaphase bridges. *Cell Cycle,* 8**,** 3065-6.

CHAN, K. L. & HICKSON, I. D. 2011. New insights into the formation and resolution of ultra-fine anaphase bridges. *Semin Cell Dev Biol,* 22**,** 906-12.

CHAN, K. L., NORTH, P. S. & HICKSON, I. D. 2007. BLM is required for faithful chromosome segregation and its localization defines a class of ultrafine anaphase bridges. *EMBO J,* 26**,** 3397-409.

CHAN, K. L., PALMAI-PALLAG, T., YING, S. & HICKSON, I. D. 2009. Replication stress induces sister-chromatid bridging at fragile site loci in mitosis. *Nat Cell Biol,* 11**,** 753-60.

CHAO, W. C., KULKARNI, K., ZHANG, Z., KONG, E. H. & BARFORD, D. 2012. Structure of the mitotic checkpoint complex. *Nature,* 484**,** 208-13.

CHEN, L., GILKES, D. M., PAN, Y., LANE, W. S. & CHEN, J. 2005. ATM and Chk2-dependent phosphorylation of MDMX contribute to p53 activation after DNA damage. *EMBO J,* 24**,** 3411-22.

CHENG, K. C., CAHILL, D. S., KASAI, H., NISHIMURA, S. & LOEB, L. A. 1992. 8-Hydroxyguanine, an abundant form of oxidative DNA damage, causes G----T and A----C substitutions. *J Biol Chem,* 267**,** 166-72.

CHEOK, C. F., WU, L., GARCIA, P. L., JANSCAK, P. & HICKSON, I. D. 2005. The Bloom's syndrome helicase promotes the annealing of complementary single-stranded DNA. *Nucleic Acids Res,* 33**,** 3932-41.

CHIN, S. F., TESCHENDORFF, A. E., MARIONI, J. C., WANG, Y., BARBOSA-MORAIS, N. L., THORNE, N. P., COSTA, J. L., PINDER, S. E., VAN DE WIEL, M. A., GREEN, A. R., ELLIS, I. O., PORTER, P. L., TAVARE, S., BRENTON, J. D., YLSTRA, B. & CALDAS, C. 2007. High-resolution aCGH and expression profiling identifies a novel genomic subtype of ER negative breast cancer. *Genome Biol,* 8**,** R215.

CHOI, C. M., SEO, K. W., JANG, S. J., OH, Y. M., SHIM, T. S., KIM, W. S., LEE, D. S. & LEE, S. D. 2009. Chromosomal instability is a risk factor for poor prognosis of adenocarcinoma of the lung: Fluorescence in situ hybridization analysis of paraffin-embedded tissue from Korean patients. *Lung Cancer,* 64**,** 66-70.

CIMINI, D. 2007. Detection and correction of merotelic kinetochore orientation by Aurora B and its partners. *Cell Cycle,* 6**,** 1558-64.

CIMINI, D., ANTOCCIA, A., TANZARELLA, C. & DEGRASSI, F. 1997. Topoisomerase II inhibition in mitosis produces numerical and structural chromosomal aberrations in human fibroblasts. *Cytogenet Cell Genet,* 76**,** 61-7.

CIMINI, D., CAMERON, L. A. & SALMON, E. D. 2004. Anaphase spindle mechanics prevent mis-segregation of merotelically oriented chromosomes. *Curr Biol,* 14**,** 2149-55.

CIMINI, D., HOWELL, B., MADDOX, P., KHODJAKOV, A., DEGRASSI, F. & SALMON, E. D. 2001. Merotelic kinetochore orientation is a major mechanism of aneuploidy in mitotic mammalian tissue cells. *J Cell Biol,* 153**,** 517-27.

CIMINI, D., MOREE, B., CANMAN, J. C. & SALMON, E. D. 2003. Merotelic kinetochore orientation occurs frequently during early mitosis in mammalian tissue cells and error correction is achieved by two different mechanisms. *J Cell Sci,* 116**,** 4213-25.

COLNAGHI, R., CARPENTER, G., VOLKER, M. & O'DRISCOLL, M. 2011. The consequences of structural genomic alterations in humans: genomic disorders, genomic instability and cancer. *Semin Cell Dev Biol,* 22**,** 875-85.

CONSTANTINOU, A., CHEN, X. B., MCGOWAN, C. H. & WEST, S. C. 2002. Holliday junction resolution in human cells: two junction endonucleases with distinct substrate specificities. *EMBO J,* 21**,** 5577-85.

CONSTANTINOU, A., DAVIES, A. A. & WEST, S. C. 2001. Branch migration and Holliday junction resolution catalyzed by activities from mammalian cells. *Cell,* 104**,** 259-68.

CONSTANTINOU, A., TARSOUNAS, M., KAROW, J. K., BROSH, R. M., BOHR, V. A., HICKSON, I. D. & WEST, S. C. 2000. Werner's syndrome protein (WRN) migrates Holliday junctions and co-localizes with RPA upon replication arrest. *EMBO Rep,* 1**,** 80-4.

COOK, P. J., JU, B. G., TELESE, F., WANG, X., GLASS, C. K. & ROSENFELD, M. G. 2009. Tyrosine dephosphorylation of H2AX modulates apoptosis and survival decisions. *Nature,* 458**,** 591-6.

COUNTER, C. M., AVILION, A. A., LEFEUVRE, C. E., STEWART, N. G., GREIDER, C. W., HARLEY, C. B. & BACCHETTI, S. 1992. Telomere shortening associated with chromosome instability is arrested in immortal cells which express telomerase activity. *EMBO J,* 11**,** 1921-9.

COURBET, S., GAY, S., ARNOULT, N., WRONKA, G., ANGLANA, M., BRISON, O. & DEBATISSE, M. 2008. Replication fork movement sets chromatin loop size and origin choice in mammalian cells. *Nature,* 455**,** 557-60.

COURCHET, J., BUCHET-POYAU, K., POTEMSKI, A., BRES, A., JARIEL-ENCONTRE, I. & BILLAUD, M. 2008. Interaction with 14-3-3 adaptors regulates the sorting of hMex-3B RNA-binding protein to distinct classes of RNA granules. *J Biol Chem,* 283**,** 32131-42.

CRASTA, K., GANEM, N. J., DAGHER, R., LANTERMANN, A. B., IVANOVA, E. V., PAN, Y., NEZI, L., PROTOPOPOV, A., CHOWDHURY, D. & PELLMAN, D. 2012. DNA breaks and chromosome pulverization from errors in mitosis. *Nature*.

DARZYNKIEWICZ, Z., HALICKA, H. D. & ZHAO, H. 2010. Analysis of cellular DNA content by flow and laser scanning cytometry. *Adv Exp Med Biol,* 676**,** 137-47.

DAVIDSON, M. B., KATOU, Y., KESZTHELYI, A., SING, T. L., XIA, T., OU, J., VAISICA, J. A., THEVAKUMARAN, N., MARJAVAARA, L., MYERS, C. L., CHABES, A., SHIRAHIGE, K.

& BROWN, G. W. 2012. Endogenous DNA replication stress results in expansion of dNTP pools and a mutator phenotype. *EMBO J,* 31**,** 895-907.

DAVIES, S. L., NORTH, P. S., DART, A., LAKIN, N. D. & HICKSON, I. D. 2004. Phosphorylation of the Bloom's syndrome helicase and its role in recovery from S-phase arrest. *Mol Cell Biol,* 24**,** 1279-91.

DAVIES, S. L., NORTH, P. S. & HICKSON, I. D. 2007. Role for BLM in replication-fork restart and suppression of origin firing after replicative stress. *Nat Struct Mol Biol,* 14**,** 677-9.

DE ANTONI, A., PEARSON, C. G., CIMINI, D., CANMAN, J. C., SALA, V., NEZI, L., MAPELLI, M., SIRONI, L., FARETTA, M., SALMON, E. D. & MUSACCHIO, A. 2005. The Mad1/Mad2 complex as a template for Mad2 activation in the spindle assembly checkpoint. *Curr Biol,* 15**,** 214-25.

DE BRUIJN, M. T., RAATS, D. A., HOOGWATER, F. J., VAN HOUDT, W. J., CAMERON, K., MEDEMA, J. P., BOREL RINKES, I. H. & KRANENBURG, O. 2010. Oncogenic KRAS sensitises colorectal tumour cells to chemotherapy by p53-dependent induction of Noxa. *Br J Cancer,* 102**,** 1254-64.

DECKBAR, D., BIRRAUX, J., KREMPLER, A., TCHOUANDONG, L., BEUCHER, A., WALKER, S., STIFF, T., JEGGO, P. & LOBRICH, M. 2007. Chromosome breakage after G2 checkpoint release. *J Cell Biol,* 176**,** 749-55.

DEMING, P. B., CISTULLI, C. A., ZHAO, H., GRAVES, P. R., PIWNICA-WORMS, H., PAULES, R. S., DOWNES, C. S. & KAUFMANN, W. K. 2001. The human decatenation checkpoint. *Proc Natl Acad Sci U S A,* 98**,** 12044-9.

DEMIRHAN, O., TASTEMIR, D., HASTURK, S., KULECI, S. & HANTA, I. 2010. Alterations in p16 and p53 genes and chromosomal findings in patients with lung cancer: fluorescence in situ hybridization and cytogenetic studies. *Cancer Epidemiol,* 34**,** 472-7.

DERELI-OZ, A., VERSINI, G. & HALAZONETIS, T. D. 2011. Studies of genomic copy number changes in human cancers reveal signatures of DNA replication stress. *Mol Oncol,* 5**,** 308-14.

DIEP, C. B., KLEIVI, K., RIBEIRO, F. R., TEIXEIRA, M. R., LINDGJAERDE, O. C. & LOTHE, R. A. 2006. The order of genetic events associated with colorectal cancer progression inferred from meta-analysis of copy number changes. *Genes Chromosomes Cancer,* 45**,** 31-41.

DING, L., LEY, T. J., LARSON, D. E., MILLER, C. A., KOBOLDT, D. C., WELCH, J. S., RITCHEY, J. K., YOUNG, M. A., LAMPRECHT, T., MCLELLAN, M. D., MCMICHAEL, J. F., WALLIS, J. W., LU, C., SHEN, D., HARRIS, C. C., DOOLING, D. J., FULTON, R. S., FULTON, L. L., CHEN, K., SCHMIDT, H., KALICKI-VEIZER, J., MAGRINI, V. J., COOK, L., MCGRATH, S. D., VICKERY, T. L., WENDL, M. C., HEATH, S., WATSON, M. A., LINK, D. C., TOMASSON, M. H., SHANNON, W. D., PAYTON, J. E., KULKARNI, S., WESTERVELT, P., WALTER, M. J., GRAUBERT, T. A., MARDIS, E. R., WILSON, R. K. & DIPERSIO, J. F. 2012. Clonal evolution in relapsed acute myeloid leukaemia revealed by whole-genome sequencing. *Nature,* 481**,** 506-10.

DOIL, C., MAILAND, N., BEKKER-JENSEN, S., MENARD, P., LARSEN, D. H., PEPPERKOK, R., ELLENBERG, J., PANIER, S., DUROCHER, D., BARTEK, J., LUKAS, J. & LUKAS, C. 2009. RNF168 binds and amplifies ubiquitin conjugates on damaged chromosomes to allow accumulation of repair proteins. *Cell,* 136**,** 435-46.

DOKSANI, Y., BERMEJO, R., FIORANI, S., HABER, J. E. & FOIANI, M. 2009. Replicon dynamics, dormant origin firing, and terminal fork integrity after double-strand break formation. *Cell,* 137**,** 247-58.

DUESBERG, P., STINDL, R. & HEHLMANN, R. 2000. Explaining the high mutation rates of cancer cells to drug and multidrug resistance by chromosome reassortments that are catalyzed by aneuploidy. *Proc Natl Acad Sci U S A,* 97**,** 14295-300.

DUNN, J. M., HVEEM, T., PRETORIUS, M., OUKRIF, D., NIELSEN, B., ALBREGTSEN, F., LOVAT, L. B., NOVELLI, M. R. & DANIELSEN, H. E. 2011. Comparison of nuclear texture analysis and image cytometric DNA analysis for the assessment of dysplasia in Barrett's oesophagus. *Br J Cancer,* 105**,** 1218-23.

DUNN, J. M., MACKENZIE, G. D., OUKRIF, D., MOSSE, C. A., BANKS, M. R., THORPE, S., SASIENI, P., BOWN, S. G., NOVELLI, M. R., RABINOVITCH, P. S. & LOVAT, L. B. 2010. Image cytometry accurately detects DNA ploidy abnormalities and predicts late relapse to high-grade dysplasia and adenocarcinoma in Barrett's oesophagus following photodynamic therapy. *Br J Cancer,* 102**,** 1608-17.

DURINCK, S., MOREAU, Y., KASPRZYK, A., DAVIS, S., DE MOOR, B., BRAZMA, A. & HUBER, W. 2005. BioMart and Bioconductor: a powerful link between biological databases and microarray data analysis. *Bioinformatics,* 21**,** 3439-40.

ENDESFELDER, D., MCGRANAHAN, N., BIRKBAK, N. J., SZALLASI, Z., KSCHISCHO, M., GRAHAM, T. A. & SWANTON, C. 2011. A breast cancer meta-analysis of two expression measures of chromosomal instability reveals a relationship with younger age at diagnosis and high risk histopathological variables. *Oncotarget,* 2**,** 529-37.

ESHLEMAN, J. R., LANG, E. Z., BOWERFIND, G. K., PARSONS, R., VOGELSTEIN, B., WILLSON, J. K., VEIGL, M. L., SEDWICK, W. D. & MARKOWITZ, S. D. 1995. Increased mutation rate at the hprt locus accompanies microsatellite instability in colon cancer. *Oncogene,* 10**,** 33-7.

FALCK, J., COATES, J. & JACKSON, S. P. 2005. Conserved modes of recruitment of ATM, ATR and DNA-PKcs to sites of DNA damage. *Nature,* 434**,** 605-11.

FALCK, J., FORMENT, J. V., COATES, J., MISTRIK, M., LUKAS, J., BARTEK, J. & JACKSON, S. P. 2012. CDK targeting of NBS1 promotes DNA-end resection, replication restart and homologous recombination. *EMBO Rep*.

FARABEGOLI, F., SANTINI, D., CECCARELLI, C., TAFFURELLI, M., MARRANO, D. & BALDINI, N. 2001. Clone heterogeneity in diploid and aneuploid breast carcinomas as detected by FISH. *Cytometry,* 46**,** 50-6.

FASULLO, M., TSAPONINA, O., SUN, M. & CHABES, A. 2010. Elevated dNTP levels suppress hyper-recombination in Saccharomyces cerevisiae S-phase checkpoint mutants. *Nucleic Acids Res,* 38**,** 1195-203.

FEARON, E. R., CHO, K. R., NIGRO, J. M., KERN, S. E., SIMONS, J. W., RUPPERT, J. M., HAMILTON, S. R., PREISINGER, A. C., THOMAS, G., KINZLER, K. W. & ET AL. 1990. Identification of a chromosome 18q gene that is altered in colorectal cancers. *Science,* 247**,** 49-56.

FODDE, R., KUIPERS, J., ROSENBERG, C., SMITS, R., KIELMAN, M., GASPAR, C., VAN ES, J. H., BREUKEL, C., WIEGANT, J., GILES, R. H. & CLEVERS, H. 2001. Mutations in the APC tumour suppressor gene cause chromosomal instability. *Nat Cell Biol,* 3**,** 433-8.

FURUTA, T., TAKEMURA, H., LIAO, Z. Y., AUNE, G. J., REDON, C., SEDELNIKOVA, O. A., PILCH, D. R., ROGAKOU, E. P., CELESTE, A., CHEN, H. T., NUSSENZWEIG, A., ALADJEM, M. I., BONNER, W. M. & POMMIER, Y. 2003. Phosphorylation of histone H2AX and activation of Mre11, Rad50, and Nbs1 in response to replication-dependent DNA double-strand breaks induced by mammalian DNA topoisomerase I cleavage complexes. *J Biol Chem,* 278**,** 20303-12.

FURUYA, T., UCHIYAMA, T., MURAKAMI, T., ADACHI, A., KAWAUCHI, S., OGA, A., HIRANO, T. & SASAKI, K. 2000. Relationship between chromosomal instability and intratumoral regional DNA ploidy heterogeneity in primary gastric cancers. *Clin Cancer Res,* 6**,** 2815-20.

GAASENBEEK, M., HOWARTH, K., ROWAN, A. J., GORMAN, P. A., JONES, A., CHAPLIN, T., LIU, Y., BICKNELL, D., DAVISON, E. J., FIEGLER, H., CARTER, N. P., ROYLANCE, R. R. & TOMLINSON, I. P. 2006. Combined array-comparative genomic hybridization and single-nucleotide polymorphism-loss of heterozygosity analysis reveals complex changes and multiple forms of chromosomal instability in colorectal cancers. *Cancer Res,* 66**,** 3471-9.

GANEM, N. J., GODINHO, S. A. & PELLMAN, D. 2009. A mechanism linking extra centrosomes to chromosomal instability. *Nature,* 460**,** 278-82.

GARCIA, V., PHELPS, S. E., GRAY, S. & NEALE, M. J. 2011. Bidirectional resection of DNA double-strand breaks by Mre11 and Exo1. *Nature,* 479**,** 241-4.

GASCOIGNE, K. E. & TAYLOR, S. S. 2008. Cancer cells display profound intra- and interline variation following prolonged exposure to antimitotic drugs. *Cancer Cell,* 14**,** 111-22.

GERLINGER, M., ROWAN, A. J., HORSWELL, S., LARKIN, J., ENDESFELDER, D., GRONROOS, E., MARTINEZ, P., MATTHEWS, N., STEWART, A., TARPEY, P., VARELA, I., PHILLIMORE, B., BEGUM, S., MCDONALD, N. Q., BUTLER, A., JONES, D., RAINE, K., LATIMER, C., SANTOS, C. R., NOHADANI, M., EKLUND, A. C., SPENCER-DENE, B., CLARK, G., PICKERING, L., STAMP, G., GORE, M., SZALLASI, Z., DOWNWARD, J., FUTREAL, P. A. & SWANTON, C. 2012. Intratumor heterogeneity and branched evolution revealed by multiregion sequencing. *N Engl J Med,* 366**,** 883-92.

GERLINGER, M. & SWANTON, C. 2010. How Darwinian models inform therapeutic failure initiated by clonal heterogeneity in cancer medicine. *Br J Cancer,* 103**,** 1139-43.

GERMAN, J. 1980. Chromosome-breakage syndromes: different genes, different treatments, different cancers. *Basic Life Sci,* 15**,** 429-39.

GHADIMI, B. M., SACKETT, D. L., DIFILIPPANTONIO, M. J., SCHROCK, E., NEUMANN, T., JAUHO, A., AUER, G. & RIED, T. 2000. Centrosome amplification and instability occurs exclusively in aneuploid, but not in diploid colorectal cancer cell lines, and correlates with numerical chromosomal aberrations. *Genes Chromosomes Cancer,* 27**,** 183-90.

GIANNINI, G., RINALDI, C., RISTORI, E., AMBROSINI, M. I., CERIGNOLI, F., VIEL, A., BIDOLI, E., BERNI, S., D'AMATI, G., SCAMBIA, G., FRATI, L., SCREPANTI, I. & GULINO, A. 2004. Mutations of an intronic repeat induce impaired MRE11 expression in primary human cancer with microsatellite instability. *Oncogene,* 23**,** 2640-7.

GIANNINI, G., RISTORI, E., CERIGNOLI, F., RINALDI, C., ZANI, M., VIEL, A., OTTINI, L., CRESCENZI, M., MARTINOTTI, S., BIGNAMI, M., FRATI, L., SCREPANTI, I. & GULINO, A. 2002. Human MRE11 is inactivated in mismatch repair-deficient cancers. *EMBO Rep,* 3**,** 248-54.

GISSELSSON, D. 2008. Classification of chromosome segregation errors in cancer. *Chromosoma,* 117**,** 511-9.

GISSELSSON, D., HAKANSON, U., STOLLER, P., MARTI, D., JIN, Y., ROSENGREN, A. H., STEWENIUS, Y., KAHL, F. & PANAGOPOULOS, I. 2008. When the genome plays dice: circumvention of the spindle assembly checkpoint and near-random chromosome segregation in multipolar cancer cell mitoses. *PLoS One,* 3**,** e1871.

GISSELSSON, D., JONSON, T., PETERSEN, A., STROMBECK, B., DAL CIN, P., HOGLUND, M., MITELMAN, F., MERTENS, F. & MANDAHL, N. 2001. Telomere dysfunction triggers extensive DNA fragmentation and evolution of complex chromosome abnormalities in human malignant tumors. *Proc Natl Acad Sci U S A,* 98**,** 12683-8.

GISSELSSON, D., PETTERSSON, L., HOGLUND, M., HEIDENBLAD, M., GORUNOVA, L., WIEGANT, J., MERTENS, F., DAL CIN, P., MITELMAN, F. & MANDAHL, N. 2000. Chromosomal breakage-fusion-bridge events cause genetic intratumor heterogeneity. *Proc Natl Acad Sci U S A,* 97**,** 5357-62.

GIUNTA, S., BELOTSERKOVSKAYA, R. & JACKSON, S. P. 2010. DNA damage signaling in response to double-strand breaks during mitosis. *J Cell Biol,* 190**,** 197-207.

GLOVER, T. W. 2006. Common fragile sites. *Cancer Lett,* 232**,** 4-12.

GLOVER, T. W., BERGER, C., COYLE, J. & ECHO, B. 1984. DNA polymerase alpha inhibition by aphidicolin induces gaps and breaks at common fragile sites in human chromosomes. *Hum Genet,* 67**,** 136-42.

GOLDBERG, M., STUCKI, M., FALCK, J., D'AMOURS, D., RAHMAN, D., PAPPIN, D., BARTEK, J. & JACKSON, S. P. 2003. MDC1 is required for the intra-S-phase DNA damage checkpoint. *Nature,* 421**,** 952-6.

GOLDSCHNEIDER, D. & MEHLEN, P. 2010. Dependence receptors: a new paradigm in cell signaling and cancer therapy. *Oncogene,* 29**,** 1865-82.

GORDON, D. J., RESIO, B. & PELLMAN, D. 2012. Causes and consequences of aneuploidy in cancer. *Nat Rev Genet,* 13**,** 189-203.

GORGOULIS, V. G., VASSILIOU, L. V., KARAKAIDOS, P., ZACHARATOS, P., KOTSINAS, A., LILOGLOU, T., VENERE, M., DITULLIO, R. A., JR., KASTRINAKIS, N. G., LEVY, B., KLETSAS, D., YONETA, A., HERLYN, M., KITTAS, C. & HALAZONETIS, T. D. 2005. Activation of the DNA damage checkpoint and genomic instability in human precancerous lesions. *Nature,* 434**,** 907-13.

GRADY, W. M. & CARETHERS, J. M. 2008. Genomic and epigenetic instability in colorectal cancer pathogenesis. *Gastroenterology,* 135**,** 1079-99.

GREEN, R. A. & KAPLAN, K. B. 2003. Chromosome instability in colorectal tumor cells is associated with defects in microtubule plus-end attachments caused by a dominant mutation in APC. *J Cell Biol,* 163**,** 949-61.

GREENMAN, C. D., BIGNELL, G., BUTLER, A., EDKINS, S., HINTON, J., BEARE, D., SWAMY, S., SANTARIUS, T., CHEN, L., WIDAA, S., FUTREAL, P. A. & STRATTON, M. R. 2010. PICNIC: an algorithm to predict absolute allelic copy number variation with microarray cancer data. *Biostatistics,* 11**,** 164-75.

GREGAN, J., POLAKOVA, S., ZHANG, L., TOLIC-NORRELYKKE, I. M. & CIMINI, D. 2011. Merotelic kinetochore attachment: causes and effects. *Trends Cell Biol,* 21**,** 374-81.

GRIM, J. E., KNOBLAUGH, S. E., GUTHRIE, K. A., HAGAR, A., SWANGER, J., HESPELT, J., DELROW, J. J., SMALL, T., GRADY, W. M., NAKAYAMA, K. I. & CLURMAN, B. E. 2012. Fbw7 and p53 cooperatively suppress advanced and chromosomally unstable intestinal cancer. *Mol Cell Biol,* 32**,** 2160-7.

GRIMM, S. 2004. The art and design of genetic screens: mammalian culture cells. *Nat Rev Genet,* 5**,** 179-89.

GROTH, P., AUSLANDER, S., MAJUMDER, M. M., SCHULTZ, N., JOHANSSON, F., PETERMANN, E. & HELLEDAY, T. 2010. Methylated DNA causes a physical block to replication forks independently of damage signalling, O(6)-methylguanine or DNA single-strand breaks and results in DNA damage. *J Mol Biol,* 402**,** 70-82.

HABERMANN, J. K., DOERING, J., HAUTANIEMI, S., ROBLICK, U. J., BUNDGEN, N. K., NICORICI, D., KRONENWETT, U., RATHNAGIRISWARAN, S., METTU, R. K., MA, Y., KRUGER, S., BRUCH, H. P., AUER, G., GUO, N. L. & RIED, T. 2009. The gene expression signature of genomic instability in breast cancer is an independent predictor of clinical outcome. *Int J Cancer,* 124**,** 1552-64.

HAKIMI, M. A., DONG, Y., LANE, W. S., SPEICHER, D. W. & SHIEKHATTAR, R. 2003. A candidate X-linked mental retardation gene is a component of a new family of histone deacetylase-containing complexes. *J Biol Chem,* 278**,** 7234-9.

HALAZONETIS, T. D., GORGOULIS, V. G. & BARTEK, J. 2008. An oncogene-induced DNA damage model for cancer development. *Science,* 319**,** 1352-5.

HANADA, K., BUDZOWSKA, M., DAVIES, S. L., VAN DRUNEN, E., ONIZAWA, H., BEVERLOO, H. B., MAAS, A., ESSERS, J., HICKSON, I. D. & KANAAR, R. 2007. The structure-specific endonuclease Mus81 contributes to replication restart by generating double-strand DNA breaks. *Nat Struct Mol Biol,* 14**,** 1096-104.

HANKS, S., COLEMAN, K., REID, S., PLAJA, A., FIRTH, H., FITZPATRICK, D., KIDD, A., MEHES, K., NASH, R., ROBIN, N., SHANNON, N., TOLMIE, J., SWANSBURY, J., IRRTHUM, A., DOUGLAS, J. & RAHMAN, N. 2004. Constitutional aneuploidy and cancer predisposition caused by biallelic mutations in BUB1B. *Nat Genet,* 36**,** 1159-61.

HARRIGAN, J. A., BELOTSERKOVSKAYA, R., COATES, J., DIMITROVA, D. S., POLO, S. E., BRADSHAW, C. R., FRASER, P. & JACKSON, S. P. 2011. Replication stress induces 53BP1-containing OPT domains in G1 cells. *J Cell Biol,* 193**,** 97-108.

HARTLERODE, A. J. & SCULLY, R. 2009. Mechanisms of double-strand break repair in somatic mammalian cells. *Biochem J,* 423**,** 157-68.

HASTINGS, P. J., IRA, G. & LUPSKI, J. R. 2009. A microhomology-mediated break-induced replication model for the origin of human copy number variation. *PLoS Genet,* 5**,** e1000327.

HAUF, S., COLE, R. W., LATERRA, S., ZIMMER, C., SCHNAPP, G., WALTER, R., HECKEL, A., VAN MEEL, J., RIEDER, C. L. & PETERS, J. M. 2003. The small molecule Hesperadin reveals a role for Aurora B in correcting kinetochore-microtubule attachment and in maintaining the spindle assembly checkpoint. *J Cell Biol,* 161**,** 281-94.

HEIDINGER-PAULI, J. M., MERT, O., DAVENPORT, C., GUACCI, V. & KOSHLAND, D. 2010. Systematic reduction of cohesin differentially affects chromosome segregation, condensation, and DNA repair. *Curr Biol,* 20**,** 957-63.

HELLER, R. C. & MARIANS, K. J. 2006. Replication fork reactivation downstream of a blocked nascent leading strand. *Nature,* 439**,** 557-62.

HERMAN, J. G., UMAR, A., POLYAK, K., GRAFF, J. R., AHUJA, N., ISSA, J. P., MARKOWITZ, S., WILLSON, J. K., HAMILTON, S. R., KINZLER, K. W., KANE, M. F., KOLODNER, R. D., VOGELSTEIN, B., KUNKEL, T. A. & BAYLIN, S. B. 1998. Incidence and functional consequences of hMLH1 promoter hypermethylation in colorectal carcinoma. *Proc Natl Acad Sci U S A,* 95**,** 6870-5.

HERZOG, F., PRIMORAC, I., DUBE, P., LENART, P., SANDER, B., MECHTLER, K., STARK, H. & PETERS, J. M. 2009. Structure of the anaphase-promoting complex/cyclosome interacting with a mitotic checkpoint complex. *Science,* 323**,** 1477-81.

HOLLAND, A. J. & CLEVELAND, D. W. 2012. Losing balance: the origin and impact of aneuploidy in cancer. *EMBO Rep,* 13**,** 501-14.

HOMFRAY, T. F., COTTRELL, S. E., ILYAS, M., ROWAN, A., TALBOT, I. C., BODMER, W. F. & TOMLINSON, I. P. 1998. Defects in mismatch repair occur after APC mutations in the pathogenesis of sporadic colorectal tumours. *Hum Mutat,* 11**,** 114-20.

HONG, Y., MAEDA, Y., WATANABE, R., OHISHI, K., MISHKIND, M., RIEZMAN, H. & KINOSHITA, T. 1999. Pig-n, a mammalian homologue of yeast Mcd4p, is involved in transferring phosphoethanolamine to the first mannose of the glycosylphosphatidylinositol. *J Biol Chem,* 274**,** 35099-106.

HOWELL, B. J., MCEWEN, B. F., CANMAN, J. C., HOFFMAN, D. B., FARRAR, E. M., RIEDER, C. L. & SALMON, E. D. 2001. Cytoplasmic dynein/dynactin drives kinetochore protein transport to the spindle poles and has a role in mitotic spindle checkpoint inactivation. *J Cell Biol,* 155**,** 1159-72.

HSIAO, S. J. & SMITH, S. 2009. Sister telomeres rendered dysfunctional by persistent cohesion are fused by NHEJ. *J Cell Biol,* 184**,** 515-26.

HUANG, L. C., CLARKIN, K. C. & WAHL, G. M. 1996. Sensitivity and selectivity of the DNA damage sensor responsible for activating p53-dependent G1 arrest. *Proc Natl Acad Sci U S A,* 93**,** 4827-32.

HUBNER, N. C., WANG, L. H., KAULICH, M., DESCOMBES, P., POSER, I. & NIGG, E. A. 2010. Re-examination of siRNA specificity questions role of PICH and Tao1 in the spindle checkpoint and identifies Mad2 as a sensitive target for small RNAs. *Chromosoma,* 119**,** 149-65.

HUIPING, C., EIRIKSDOTTIR, G., SIGURDSSON, A., SIGURGEIRSDOTTIR, J. R., BARKARDOTTIR, R. B., EGILSSON, V. & INGVARSSON, S. 1998. High frequency of LOH at chromosome 18q in human breast cancer: association with high S-phase fraction and low progesterone receptor content. *Anticancer Res,* 18**,** 1031-6.

ICHIJIMA, Y., YOSHIOKA, K., YOSHIOKA, Y., SHINOHE, K., FUJIMORI, H., UNNO, J., TAKAGI, M., GOTO, H., INAGAKI, M., MIZUTANI, S. & TERAOKA, H. 2010. DNA lesions induced by replication stress trigger mitotic aberration and tetraploidy development. *PLoS One,* 5**,** e8821.

INANC, B., DODSON, H. & MORRISON, C. G. 2010. A centrosome-autonomous signal that involves centriole disengagement permits centrosome duplication in G2 phase after DNA damage. *Mol Biol Cell,* 21**,** 3866-77.

JACKSON, S. P. & BARTEK, J. 2009. The DNA-damage response in human biology and disease. *Nature,* 461**,** 1071-8.

JACQUEMONT, S., BOCENO, M., RIVAL, J. M., MECHINAUD, F. & DAVID, A. 2002. High risk of malignancy in mosaic variegated aneuploidy syndrome. *Am J Med Genet,* 109**,** 17-21; discussion 16.

JALLEPALLI, P. V. & LENGAUER, C. 2001. Chromosome segregation and cancer: cutting through the mystery. *Nat Rev Cancer,* 1**,** 109-17.

JANSSEN, A., KOPS, G. J. & MEDEMA, R. H. 2009. Elevating the frequency of chromosome mis-segregation as a strategy to kill tumor cells. *Proc Natl Acad Sci U S A,* 106**,** 19108-13.

JANSSEN, A., VAN DER BURG, M., SZUHAI, K., KOPS, G. J. & MEDEMA, R. H. 2011. Chromosome segregation errors as a cause of DNA damage and structural chromosome aberrations. *Science,* 333**,** 1895-8.

JAQAMAN, K., KING, E. M., AMARO, A. C., WINTER, J. R., DORN, J. F., ELLIOTT, H. L., MCHEDLISHVILI, N., MCCLELLAND, S. E., PORTER, I. M., POSCH, M., TOSO, A., DANUSER, G., MCAINSH, A. D., MERALDI, P. & SWEDLOW, J. R. 2010. Kinetochore alignment within the metaphase plate is regulated by centromere stiffness and microtubule depolymerases. *J Cell Biol,* 188**,** 665-79.

JAZAYERI, A., FALCK, J., LUKAS, C., BARTEK, J., SMITH, G. C., LUKAS, J. & JACKSON, S. P. 2006. ATM- and cell cycle-dependent regulation of ATR in response to DNA double-strand breaks. *Nat Cell Biol,* 8**,** 37-45.

JELLUMA, N., BRENKMAN, A. B., MCLEOD, I., YATES, J. R., 3RD, CLEVELAND, D. W., MEDEMA, R. H. & KOPS, G. J. 2008. Chromosomal instability by inefficient Mps1 auto-activation due to a weakened mitotic checkpoint and lagging chromosomes. *PLoS ONE,* 3**,** e2415.

JEN, J., KIM, H., PIANTADOSI, S., LIU, Z. F., LEVITT, R. C., SISTONEN, P., KINZLER, K. W., VOGELSTEIN, B. & HAMILTON, S. R. 1994. Allelic loss of chromosome 18q and prognosis in colorectal cancer. *N Engl J Med,* 331**,** 213-21.

JIN, Y., DAI, M. S., LU, S. Z., XU, Y., LUO, Z., ZHAO, Y. & LU, H. 2006. 14-3-3gamma binds to MDMX that is phosphorylated by UV-activated Chk1, resulting in p53 activation. *EMBO J,* 25**,** 1207-18.

JIN, Y., STEWENIUS, Y., LINDGREN, D., FRIGYESI, A., CALCAGNILE, O., JONSON, T., EDQVIST, A., LARSSON, N., LUNDBERG, L. M., CHEBIL, G., LIEDBERG, F.,

GUDJONSSON, S., MANSSON, W., HOGLUND, M. & GISSELSSON, D. 2007. Distinct mitotic segregation errors mediate chromosomal instability in aggressive urothelial cancers. *Clin Cancer Res,* 13**,** 1703-12.

JONKERS, Y. M., CLAESSEN, S. M., PERREN, A., SCHMID, S., KOMMINOTH, P., VERHOFSTAD, A. A., HOFLAND, L. J., DE KRIJGER, R. R., SLOOTWEG, P. J., RAMAEKERS, F. C. & SPEEL, E. J. 2005. Chromosomal instability predicts metastatic disease in patients with insulinomas. *Endocr Relat Cancer,* 12**,** 435-47.

KANDA, T., OTTER, M. & WAHL, G. M. 2001. Mitotic segregation of viral and cellular acentric extrachromosomal molecules by chromosome tethering. *J Cell Sci,* 114**,** 49-58.

KANDA, T. & WAHL, G. M. 2000. The dynamics of acentric chromosomes in cancer cells revealed by GFP-based chromosome labeling strategies. *J Cell Biochem Suppl,* Suppl 35**,** 107-14.

KANE, M. F., LODA, M., GAIDA, G. M., LIPMAN, J., MISHRA, R., GOLDMAN, H., JESSUP, J. M. & KOLODNER, R. 1997. Methylation of the hMLH1 promoter correlates with lack of expression of hMLH1 in sporadic colon tumors and mismatch repair-defective human tumor cell lines. *Cancer Res,* 57**,** 808-11.

KANEKO, Y. & KNUDSON, A. G. 2000. Mechanism and relevance of ploidy in neuroblastoma. *Genes Chromosomes Cancer,* 29**,** 89-95.

KAPLAN, K. B., BURDS, A. A., SWEDLOW, J. R., BEKIR, S. S., SORGER, P. K. & NATHKE, I. S. 2001. A role for the Adenomatous Polyposis Coli protein in chromosome segregation. *Nat Cell Biol,* 3**,** 429-32.

KAROW, J. K., CONSTANTINOU, A., LI, J. L., WEST, S. C. & HICKSON, I. D. 2000. The Bloom's syndrome gene product promotes branch migration of holliday junctions. *Proc Natl Acad Sci U S A,* 97**,** 6504-8.

KASAI, H., CRAIN, P. F., KUCHINO, Y., NISHIMURA, S., OOTSUYAMA, A. & TANOOKA, H. 1986. Formation of 8-hydroxyguanine moiety in cellular DNA by agents producing oxygen radicals and evidence for its repair. *Carcinogenesis,* 7**,** 1849-51.

KASTAN, M. B. & BARTEK, J. 2004. Cell-cycle checkpoints and cancer. *Nature,* 432**,** 316-23.

KASTAN, M. B., ZHAN, Q., EL-DEIRY, W. S., CARRIER, F., JACKS, T., WALSH, W. V., PLUNKETT, B. S., VOGELSTEIN, B. & FORNACE, A. J., JR. 1992. A mammalian cell cycle checkpoint pathway utilizing p53 and GADD45 is defective in ataxia-telangiectasia. *Cell,* 71**,** 587-97.

KATKOORI, V. R., SHANMUGAM, C., JIA, X., VITTA, S. P., STHANAM, M., CALLENS, T., MESSIAEN, L., CHEN, D., ZHANG, B., BUMPERS, H. L., SAMUEL, T. & MANNE, U. 2012. Prognostic significance and gene expression profiles of p53 mutations in microsatellite-stable stage III colorectal adenocarcinomas. *PLoS One,* 7**,** e30020.

KAWABATA, T., LUEBBEN, S. W., YAMAGUCHI, S., ILVES, I., MATISE, I., BUSKE, T., BOTCHAN, M. R. & SHIMA, N. 2011. Stalled fork rescue via dormant replication origins in unchallenged S phase promotes proper chromosome segregation and tumor suppression. *Mol Cell,* 41**,** 543-53.

KEMP, Z., ROWAN, A., CHAMBERS, W., WORTHAM, N., HALFORD, S., SIEBER, O., MORTENSEN, N., VON HERBAY, A., GUNTHER, T., ILYAS, M. & TOMLINSON, I. 2005. CDC4 mutations occur in a subset of colorectal cancers but are not predicted to cause loss of function and are not associated with chromosomal instability. *Cancer Res,* 65**,** 11361-6.

KHODJAKOV, A. & RIEDER, C. L. 2009. The nature of cell-cycle checkpoints: facts and fallacies. *J Biol,* 8**,** 88.

KLEIN, A., ZANG, K. D., STEUDEL, W. I. & URBSCHAT, S. 2006. Different mechanisms of mitotic instability in cancer cell lines. *Int J Oncol,* 29**,** 1389-96.

KNOWLTON, A. L., LAN, W. & STUKENBERG, P. T. 2006. Aurora B is enriched at merotelic attachment sites, where it regulates MCAK. *Curr Biol,* 16**,** 1705-10.

KOMAROVA, N. 2004. Does cancer solve an optimization problem? *Cell Cycle,* 3**,** 840-4.

KOPS, G. J., FOLTZ, D. R. & CLEVELAND, D. W. 2004. Lethality to human cancer cells through massive chromosome loss by inhibition of the mitotic checkpoint. *Proc Natl Acad Sci U S A,* 101**,** 8699-704.

KOPS, G. J., KIM, Y., WEAVER, B. A., MAO, Y., MCLEOD, I., YATES, J. R., 3RD, TAGAYA, M. & CLEVELAND, D. W. 2005. ZW10 links mitotic checkpoint signaling to the structural kinetochore. *J Cell Biol,* 169**,** 49-60.

KOUZMINOVA, E. A. & KUZMINOV, A. 2006. Fragmentation of replicating chromosomes triggered by uracil in DNA. *J Mol Biol,* 355**,** 20-33.

KREMPLER, A., DECKBAR, D., JEGGO, P. A. & LOBRICH, M. 2007. An imperfect G2M checkpoint contributes to chromosome instability following irradiation of S and G2 phase cells. *Cell Cycle,* 6**,** 1682-6.

KRONENWETT, U., HUWENDIEK, S., OSTRING, C., PORTWOOD, N., ROBLICK, U. J., PAWITAN, Y., ALAIYA, A., SENNERSTAM, R., ZETTERBERG, A. & AUER, G. 2004. Improved grading of breast adenocarcinomas based on genomic instability. *Cancer Res,* 64**,** 904-9.

KUERBITZ, S. J., PLUNKETT, B. S., WALSH, W. V. & KASTAN, M. B. 1992. Wild-type p53 is a cell cycle checkpoint determinant following irradiation. *Proc Natl Acad Sci U S A,* 89**,** 7491-5.

KULUKIAN, A., HAN, J. S. & CLEVELAND, D. W. 2009. Unattached kinetochores catalyze production of an anaphase inhibitor that requires a Mad2 template to prime Cdc20 for BubR1 binding. *Dev Cell,* 16**,** 105-17.

KUMAGAI, A., KIM, S. M. & DUNPHY, W. G. 2004. Claspin and the activated form of ATR-ATRIP collaborate in the activation of Chk1. *J Biol Chem,* 279**,** 49599-608.

KUMAR, D., ABDULOVIC, A. L., VIBERG, J., NILSSON, A. K., KUNKEL, T. A. & CHABES, A. 2011. Mechanisms of mutagenesis in vivo due to imbalanced dNTP pools. *Nucleic Acids Res,* 39**,** 1360-71.

KWON, M., GODINHO, S. A., CHANDHOK, N. S., GANEM, N. J., AZIOUNE, A., THERY, M. & PELLMAN, D. 2008. Mechanisms to suppress multipolar divisions in cancer cells with extra centrosomes. *Genes Dev,* 22**,** 2189-203.

LATIL, A., BARON, J. C., CUSSENOT, O., FOURNIER, G., SOUSSI, T., BOCCON-GIBOD, L., LE DUC, A., ROUESSE, J. & LIDEREAU, R. 1994. Genetic alterations in localized prostate cancer: identification of a common region of deletion on chromosome arm 18q. *Genes Chromosomes Cancer,* 11**,** 119-25.

LAUD, P. R., MULTANI, A. S., BAILEY, S. M., WU, L., MA, J., KINGSLEY, C., LEBEL, M., PATHAK, S., DEPINHO, R. A. & CHANG, S. 2005. Elevated telomere-telomere recombination in WRN-deficient, telomere dysfunctional cells promotes escape from senescence and engagement of the ALT pathway. *Genes Dev,* 19**,** 2560-70.

LEE, A. J., ENDESFELDER, D., ROWAN, A. J., WALTHER, A., BIRKBAK, N. J., FUTREAL, P. A., DOWNWARD, J., SZALLASI, Z., TOMLINSON, I. P., HOWELL, M., KSCHISCHO, M. & SWANTON, C. 2011. Chromosomal instability confers intrinsic multidrug resistance. *Cancer Res,* 71**,** 1858-70.

LEE, J. A., CARVALHO, C. M. & LUPSKI, J. R. 2007. A DNA replication mechanism for generating nonrecurrent rearrangements associated with genomic disorders. *Cell,* 131**,** 1235-47.

LEE, M. G., WYNDER, C., COOCH, N. & SHIEKHATTAR, R. 2005. An essential role for CoREST in nucleosomal histone 3 lysine 4 demethylation. *Nature,* 437**,** 432-5.

LEEDHAM, S. J., GRAHAM, T. A., OUKRIF, D., MCDONALD, S. A., RODRIGUEZ-JUSTO, M., HARRISON, R. F., SHEPHERD, N. A., NOVELLI, M. R., JANKOWSKI, J. A. & WRIGHT, N. A. 2009. Clonality, founder mutations, and field cancerization in human ulcerative colitis-associated neoplasia. *Gastroenterology,* 136**,** 542-50 e6.

LENGAUER, C., KINZLER, K. W. & VOGELSTEIN, B. 1997. Genetic instability in colorectal cancers. *Nature,* 386**,** 623-7.

LENGAUER, C., KINZLER, K. W. & VOGELSTEIN, B. 1998. Genetic instabilities in human cancers. *Nature,* 396**,** 643-9.

LENS, S. M., WOLTHUIS, R. M., KLOMPMAKER, R., KAUW, J., AGAMI, R., BRUMMELKAMP, T., KOPS, G. & MEDEMA, R. H. 2003. Survivin is required for a sustained spindle checkpoint arrest in response to lack of tension. *EMBO J,* 22**,** 2934-47.

LETESSIER, A., MILLOT, G. A., KOUNDRIOUKOFF, S., LACHAGES, A. M., VOGT, N., HANSEN, R. S., MALFOY, B., BRISON, O. & DEBATISSE, M. 2011. Cell-type-specific replication initiation programs set fragility of the FRA3B fragile site. *Nature,* 470**,** 120-3.

LEWIS, A., DAVIS, H., DEHERAGODA, M., POLLARD, P., NYE, E., JEFFERY, R., SEGDITSAS, S., EAST, P., POULSOM, R., STAMP, G., WRIGHT, N. & TOMLINSON, I. 2012. The C-terminus of Apc does not influence intestinal adenoma development or progression. *J Pathol,* 226**,** 73-83.

LI, R., HEHLMAN, R., SACHS, R. & DUESBERG, P. 2005. Chromosomal alterations cause the high rates and wide ranges of drug resistance in cancer cells. *Cancer Genet Cytogenet,* 163**,** 44-56.

LINGLE, W. L., BARRETT, S. L., NEGRON, V. C., D'ASSORO, A. B., BOENEMAN, K., LIU, W., WHITEHEAD, C. M., REYNOLDS, C. & SALISBURY, J. L. 2002. Centrosome amplification

drives chromosomal instability in breast tumor development. *Proc Natl Acad Sci U S A,* 99**,** 1978-83.

LIU, D., VADER, G., VROMANS, M. J., LAMPSON, M. A. & LENS, S. M. 2009. Sensing chromosome bi-orientation by spatial separation of aurora B kinase from kinetochore substrates. *Science,* 323**,** 1350-3.

LIU, D., VLEUGEL, M., BACKER, C. B., HORI, T., FUKAGAWA, T., CHEESEMAN, I. M. & LAMPSON, M. A. 2010. Regulated targeting of protein phosphatase 1 to the outer kinetochore by KNL1 opposes Aurora B kinase. *J Cell Biol,* 188**,** 809-20.

LIU, P., EREZ, A., NAGAMANI, S. C., DHAR, S. U., KOLODZIEJSKA, K. E., DHARMADHIKARI, A. V., COOPER, M. L., WISZNIEWSKA, J., ZHANG, F., WITHERS, M. A., BACINO, C. A., CAMPOS-ACEVEDO, L. D., DELGADO, M. R., FREEDENBERG, D., GARNICA, A., GREBE, T. A., HERNANDEZ-ALMAGUER, D., IMMKEN, L., LALANI, S. R., MCLEAN, S. D., NORTHRUP, H., SCAGLIA, F., STRATHEARN, L., TRAPANE, P., KANG, S. H., PATEL, A., CHEUNG, S. W., HASTINGS, P. J., STANKIEWICZ, P., LUPSKI, J. R. & BI, W. 2011. Chromosome catastrophes involve replication mechanisms generating complex genomic rearrangements. *Cell,* 146**,** 889-903.

LIU, Q., GUNTUKU, S., CUI, X. S., MATSUOKA, S., CORTEZ, D., TAMAI, K., LUO, G., CARATTINI-RIVERA, S., DEMAYO, F., BRADLEY, A., DONEHOWER, L. A. & ELLEDGE, S. J. 2000. Chk1 is an essential kinase that is regulated by Atr and required for the G(2)/M DNA damage checkpoint. *Genes Dev,* 14**,** 1448-59.

LLORENTE, B., SMITH, C. E. & SYMINGTON, L. S. 2008. Break-induced replication: what is it and what is it for? *Cell Cycle,* 7**,** 859-64.

LOBRICH, M. & JEGGO, P. A. 2007. The impact of a negligent G2/M checkpoint on genomic instability and cancer induction. *Nat Rev Cancer,* 7**,** 861-9.

LOPEZ, I., L, P. O., TUCCI, P., ALVAREZ-VALIN, F., R, A. C. & MARIN, M. 2012. Different mutation profiles associated to P53 accumulation in colorectal cancer. *Gene,* 499**,** 81-7.

LUKAS, C., SAVIC, V., BEKKER-JENSEN, S., DOIL, C., NEUMANN, B., PEDERSEN, R. S., GROFTE, M., CHAN, K. L., HICKSON, I. D., BARTEK, J. & LUKAS, J. 2011a. 53BP1 nuclear bodies form around DNA lesions generated by mitotic transmission of chromosomes under replication stress. *Nat Cell Biol,* 13**,** 243-53.

LUKAS, J., LUKAS, C. & BARTEK, J. 2011b. More than just a focus: The chromatin response to DNA damage and its role in genome integrity maintenance. *Nat Cell Biol,* 13**,** 1161-9.

MACDOUGALL, C. A., BYUN, T. S., VAN, C., YEE, M. C. & CIMPRICH, K. A. 2007. The structural determinants of checkpoint activation. *Genes Dev,* 21**,** 898-903.

MAILAND, N., BEKKER-JENSEN, S., FAUSTRUP, H., MELANDER, F., BARTEK, J., LUKAS, C. & LUKAS, J. 2007. RNF8 ubiquitylates histones at DNA double-strand breaks and promotes assembly of repair proteins. *Cell,* 131**,** 887-900.

MAILAND, N., FALCK, J., LUKAS, C., SYLJUASEN, R. G., WELCKER, M., BARTEK, J. & LUKAS, J. 2000. Rapid destruction of human Cdc25A in response to DNA damage. *Science,* 288**,** 1425-9.

MAILHES, J. B., MASTROMATTEO, C. & FUSELER, J. W. 2004. Transient exposure to the Eg5 kinesin inhibitor monastrol leads to syntelic orientation of chromosomes and aneuploidy in mouse oocytes. *Mutat Res,* 559**,** 153-67.

MALOVANNAYA, A., LI, Y., BULYNKO, Y., JUNG, S. Y., WANG, Y., LANZ, R. B., O'MALLEY, B. W. & QIN, J. 2010. Streamlined analysis schema for high-throughput identification of endogenous protein complexes. *Proc Natl Acad Sci U S A,* 107**,** 2431-6.

MANNINI, L., MENGA, S. & MUSIO, A. 2010. The expanding universe of cohesin functions: a new genome stability caretaker involved in human disease and cancer. *Hum Mutat,* 31**,** 623-30.

MARTINEZ, A. C. & VAN WELY, K. H. 2011. Centromere fission, not telomere erosion, triggers chromosomal instability in human carcinomas. *Carcinogenesis,* 32**,** 796-803.

MATHEWS, C. K. 2006. DNA precursor metabolism and genomic stability. *FASEB J,* 20**,** 1300-14.

MATSUOKA, S., BALLIF, B. A., SMOGORZEWSKA, A., MCDONALD, E. R., 3RD, HUROV, K. E., LUO, J., BAKALARSKI, C. E., ZHAO, Z., SOLIMINI, N., LERENTHAL, Y., SHILOH, Y., GYGI, S. P. & ELLEDGE, S. J. 2007. ATM and ATR substrate analysis reveals extensive protein networks responsive to DNA damage. *Science,* 316**,** 1160-6.

MAYDAN, G., NOYMAN, I., HAR-ZAHAV, A., NERIAH, Z. B., PASMANIK-CHOR, M., YEHESKEL, A., ALBIN-KAPLANSKI, A., MAYA, I., MAGAL, N., BIRK, E., SIMON, A. J., HALEVY, A., RECHAVI, G., SHOHAT, M., STRAUSSBERG, R. & BASEL-VANAGAITE,

L. 2011. Multiple congenital anomalies-hypotonia-seizures syndrome is caused by a mutation in PIGN. *J Med Genet,* 48**,** 383-9.

MCCLELLAND, S. E., BURRELL, R. A. & SWANTON, C. 2009. Chromosomal instability: a composite phenotype that influences sensitivity to chemotherapy. *Cell Cycle,* 8**,** 3262-6.

MCDERMOTT, K. M., ZHANG, J., HOLST, C. R., KOZAKIEWICZ, B. K., SINGLA, V. & TLSTY, T. D. 2006. p16(INK4a) prevents centrosome dysfunction and genomic instability in primary cells. *PLoS Biol,* 4**,** e51.

MCGRANAHAN, N., BURRELL, R. A., ENDESFELDER, D., NOVELLI, M. R. & SWANTON, C. 2012. Cancer chromosomal instability: therapeutic and diagnostic challenges. 'Exploring aneuploidy: the significance of chromosomal imbalance' review series. *EMBO Rep*.

MELCHER, R., KOEHLER, S., STEINLEIN, C., SCHMID, M., MUELLER, C. R., LUEHRS, H., MENZEL, T., SCHEPPACH, W., MOERK, H., SCHEURLEN, M., KOEHRLE, J. & AL-TAIE, O. 2002. Spectral karyotype analysis of colon cancer cell lines of the tumor suppressor and mutator pathway. *Cytogenet Genome Res,* 98**,** 22-8.

MERALDI, P., LUKAS, J., FRY, A. M., BARTEK, J. & NIGG, E. A. 1999. Centrosome duplication in mammalian somatic cells requires E2F and Cdk2-cyclin A. *Nat Cell Biol,* 1**,** 88-93.

METTU, R. K., WAN, Y. W., HABERMANN, J. K., RIED, T. & GUO, N. L. 2010. A 12-gene genomic instability signature predicts clinical outcomes in multiple cancer types. *Int J Biol Markers,* 25.

MISHRA, P. K., BHARGAVA, A., RAGHURAM, G. V., JATAWA, S. K., AKHTAR, N., KHAN, S., TIWARI, A. & MAUDAR, K. K. 2009a. Induction of genomic instability in cultured human colon epithelial cells following exposure to isocyanates. *Cell Biol Int,* 33**,** 675-83.

MISHRA, P. K., RAGHURAM, G. V., PANWAR, H., JAIN, D., PANDEY, H. & MAUDAR, K. K. 2009b. Mitochondrial oxidative stress elicits chromosomal instability after exposure to isocyanates in human kidney epithelial cells. *Free Radic Res,* 43**,** 718-28.

MONTGOMERY, E., WILENTZ, R. E., ARGANI, P., FISHER, C., HRUBAN, R. H., KERN, S. E. & LENGAUER, C. 2003. Analysis of anaphase figures in routine histologic sections distinguishes chromosomally unstable from chromosomally stable malignancies. *Cancer Biol Ther,* 2**,** 248-52.

MOYNAHAN, M. E., PIERCE, A. J. & JASIN, M. 2001. BRCA2 is required for homology-directed repair of chromosomal breaks. *Mol Cell,* 7**,** 263-72.

MURAYAMA-HOSOKAWA, S., ODA, K., NAKAGAWA, S., ISHIKAWA, S., YAMAMOTO, S., SHOJI, K., IKEDA, Y., UEHARA, Y., FUKAYAMA, M., MCCORMICK, F., YANO, T., TAKETANI, Y. & ABURATANI, H. 2010. Genome-wide single-nucleotide polymorphism arrays in endometrial carcinomas associate extensive chromosomal instability with poor prognosis and unveil frequent chromosomal imbalances involved in the PI3-kinase pathway. *Oncogene,* 29**,** 1897-908.

MUSACCHIO, A. & SALMON, E. D. 2007. The spindle-assembly checkpoint in space and time. *Nat Rev Mol Cell Biol,* 8**,** 379-93.

NAKAMURA, H., SAJI, H., IDIRIS, A., KAWASAKI, N., HOSAKA, M., OGATA, A., SAIJO, T. & KATO, H. 2003. Chromosomal instability detected by fluorescence in situ hybridization in surgical specimens of non-small cell lung cancer is associated with poor survival. *Clin Cancer Res,* 9**,** 2294-9.

NAKAO, K., MEHTA, K. R., FRIDLYAND, J., MOORE, D. H., JAIN, A. N., LAFUENTE, A., WIENCKE, J. W., TERDIMAN, J. P. & WALDMAN, F. M. 2004. High-resolution analysis of DNA copy number alterations in colorectal cancer by array-based comparative genomic hybridization. *Carcinogenesis,* 25**,** 1345-57.

NEGRINI, S., GORGOULIS, V. G. & HALAZONETIS, T. D. 2010. Genomic instability--an evolving hallmark of cancer. *Nat Rev Mol Cell Biol,* 11**,** 220-8.

NG, T. M., WAPLES, W. G., LAVOIE, B. D. & BIGGINS, S. 2009. Pericentromeric sister chromatid cohesion promotes kinetochore biorientation. *Mol Biol Cell,* 20**,** 3818-27.

NIGG, E. A. & STEARNS, T. 2011. The centrosome cycle: Centriole biogenesis, duplication and inherent asymmetries. *Nat Cell Biol,* 13**,** 1154-60.

NIIDA, H., KATSUNO, Y., SENGOKU, M., SHIMADA, M., YUKAWA, M., IKURA, M., IKURA, T., KOHNO, K., SHIMA, H., SUZUKI, H., TASHIRO, S. & NAKANISHI, M. 2010a. Essential role of Tip60-dependent recruitment of ribonucleotide reductase at DNA damage sites in DNA repair during G1 phase. *Genes Dev,* 24**,** 333-8.

NIIDA, H., SHIMADA, M., MURAKAMI, H. & NAKANISHI, M. 2010b. Mechanisms of dNTP supply that play an essential role in maintaining genome integrity in eukaryotic cells. *Cancer Sci,* 101**,** 2505-9.

O'SULLIVAN, R. J. & KARLSEDER, J. 2010. Telomeres: protecting chromosomes against genome instability. *Nat Rev Mol Cell Biol,* 11**,** 171-81.

OZERI-GALAI, E., LEBOFSKY, R., RAHAT, A., BESTER, A. C., BENSIMON, A. & KEREM, B. 2011. Failure of origin activation in response to fork stalling leads to chromosomal instability at fragile sites. *Mol Cell,* 43**,** 122-31.

PALAKODETI, A., LUCAS, I., JIANG, Y., YOUNG, D. J., FERNALD, A. A., KARRISON, T. & LE BEAU, M. M. 2010. Impaired replication dynamics at the FRA3B common fragile site. *Hum Mol Genet,* 19**,** 99-110.

PALUMBO, E., MATRICARDI, L., TOSONI, E., BENSIMON, A. & RUSSO, A. 2010. Replication dynamics at common fragile site FRA6E. *Chromosoma,* 119**,** 575-87.

PAMPALONA, J., FRIAS, C., GENESCA, A. & TUSELL, L. 2012. Progressive telomere dysfunction causes cytokinesis failure and leads to the accumulation of polyploid cells. *PLoS Genet,* 8**,** e1002679.

PAMPALONA, J., SOLER, D., GENESCA, A. & TUSELL, L. 2010a. Telomere dysfunction and chromosome structure modulate the contribution of individual chromosomes in abnormal nuclear morphologies. *Mutat Res,* 683**,** 16-22.

PAMPALONA, J., SOLER, D., GENESCA, A. & TUSELL, L. 2010b. Whole chromosome loss is promoted by telomere dysfunction in primary cells. *Genes Chromosomes Cancer,* 49**,** 368-78.

PAQUES, F. & HABER, J. E. 1999. Multiple pathways of recombination induced by double-strand breaks in Saccharomyces cerevisiae. *Microbiol Mol Biol Rev,* 63**,** 349-404.

PAREDES-ZAGLUL, A., KANG, J. J., ESSIG, Y. P., MAO, W., IRBY, R., WLOCH, M. & YEATMAN, T. J. 1998. Analysis of colorectal cancer by comparative genomic hybridization: evidence for induction of the metastatic phenotype by loss of tumor suppressor genes. *Clin Cancer Res,* 4**,** 879-86.

PASELLO, G., AGATA, S., BONALDI, L., CORRADIN, A., MONTAGNA, M., ZAMARCHI, R., PARENTI, A., CAGOL, M., ZANINOTTO, G., RUOL, A., ANCONA, E., AMADORI, A. & SAGGIORO, D. 2008. DNA copy number alterations correlate with survival of esophageal adenocarcinoma patients. *Mod Pathol*.

PAULETTI, G., LAI, E. & ATTARDI, G. 1990. Early appearance and long-term persistence of the submicroscopic extrachromosomal elements (amplisomes) containing the amplified DHFR genes in human cell lines. *Proc Natl Acad Sci U S A,* 87**,** 2955-9.

PAULICK, M. G. & BERTOZZI, C. R. 2008. The glycosylphosphatidylinositol anchor: a complex membrane-anchoring structure for proteins. *Biochemistry,* 47**,** 6991-7000.

PAULSSON, K. & JOHANSSON, B. 2009. High hyperdiploid childhood acute lymphoblastic leukemia. *Genes Chromosomes Cancer,* 48**,** 637-60.

PAVELKA, N., RANCATI, G., ZHU, J., BRADFORD, W. D., SARAF, A., FLORENS, L., SANDERSON, B. W., HATTEM, G. L. & LI, R. 2010. Aneuploidy confers quantitative proteome changes and phenotypic variation in budding yeast. *Nature,* 468**,** 321-5.

PETERMANN, E. & HELLEDAY, T. 2010. Pathways of mammalian replication fork restart. *Nat Rev Mol Cell Biol,* 11**,** 683-7.

PETERMANN, E., WOODCOCK, M. & HELLEDAY, T. 2010. Chk1 promotes replication fork progression by controlling replication initiation. *Proc Natl Acad Sci U S A,* 107**,** 16090-5.

PFAU, S. J. & AMON, A. 2012. Chromosomal instability and aneuploidy in cancer: from yeast to man. *EMBO Rep,* 13**,** 515-27.

POLI, J., TSAPONINA, O., CRABBE, L., KESZTHELYI, A., PANTESCO, V., CHABES, A., LENGRONNE, A. & PASERO, P. 2012. dNTP pools determine fork progression and origin usage under replication stress. *EMBO J,* 31**,** 883-94.

POPAT, S. & HOULSTON, R. S. 2005. A systematic review and meta-analysis of the relationship between chromosome 18q genotype, DCC status and colorectal cancer prognosis. *Eur J Cancer,* 41**,** 2060-70.

POPOVA, T., MANIE, E., STOPPA-LYONNET, D., RIGAILL, G., BARILLOT, E. & STERN, M. H. 2009. Genome Alteration Print (GAP): a tool to visualize and mine complex cancer genomic profiles obtained by SNP arrays. *Genome Biol,* 10**,** R128.

PROSSER, S. L., STRAATMAN, K. R. & FRY, A. M. 2009. Molecular dissection of the centrosome overduplication pathway in S-phase-arrested cells. *Mol Cell Biol,* 29**,** 1760-73.

QUINLAN, K. G., NARDINI, M., VERGER, A., FRANCESCATO, P., YASWEN, P., CORDA, D., BOLOGNESI, M. & CROSSLEY, M. 2006. Specific recognition of ZNF217 and other zinc finger proteins at a surface groove of C-terminal binding proteins. *Mol Cell Biol,* 26**,** 8159-72.

RAJAGOPALAN, H., JALLEPALLI, P. V., RAGO, C., VELCULESCU, V. E., KINZLER, K. W., VOGELSTEIN, B. & LENGAUER, C. 2004. Inactivation of hCDC4 can cause chromosomal instability. *Nature,* 428**,** 77-81.

RAJESH, C., BAKER, D. K., PIERCE, A. J. & PITTMAN, D. L. 2011. The splicing-factor related protein SFPQ/PSF interacts with RAD51D and is necessary for homology-directed repair and sister chromatid cohesion. *Nucleic Acids Res,* 39**,** 132-45.

REDDY, S. K., RAPE, M., MARGANSKY, W. A. & KIRSCHNER, M. W. 2007. Ubiquitination by the anaphase-promoting complex drives spindle checkpoint inactivation. *Nature,* 446**,** 921-5.

REINHARDT, H. C., CANNELL, I. G., MORANDELL, S. & YAFFE, M. B. 2011. Is post-transcriptional stabilization, splicing and translation of selective mRNAs a key to the DNA damage response? *Cell Cycle,* 10**,** 23-7.

REINHARDT, H. C., HASSKAMP, P., SCHMEDDING, I., MORANDELL, S., VAN VUGT, M. A., WANG, X., LINDING, R., ONG, S. E., WEAVER, D., CARR, S. A. & YAFFE, M. B. 2010. DNA damage activates a spatially distinct late cytoplasmic cell-cycle checkpoint network controlled by MK2-mediated RNA stabilization. *Mol Cell,* 40**,** 34-49.

RICHARDSON, C. & JASIN, M. 2000. Frequent chromosomal translocations induced by DNA double-strand breaks. *Nature,* 405**,** 697-700.

RICHARDSON, C., MOYNAHAN, M. E. & JASIN, M. 1998. Double-strand break repair by interchromosomal recombination: suppression of chromosomal translocations. *Genes Dev,* 12**,** 3831-42.

RIEDER, C. L., COLE, R. W., KHODJAKOV, A. & SLUDER, G. 1995. The checkpoint delaying anaphase in response to chromosome monoorientation is mediated by an inhibitory signal produced by unattached kinetochores. *J Cell Biol,* 130**,** 941-8.

RODRIGUES, N. R., ROWAN, A., SMITH, M. E., KERR, I. B., BODMER, W. F., GANNON, J. V. & LANE, D. P. 1990. p53 mutations in colorectal cancer. *Proc Natl Acad Sci U S A,* 87**,** 7555-9.

ROGAKOU, E. P., PILCH, D. R., ORR, A. H., IVANOVA, V. S. & BONNER, W. M. 1998. DNA double-stranded breaks induce histone H2AX phosphorylation on serine 139. *J Biol Chem,* 273**,** 5858-68.

ROSCHKE, A. V., STOVER, K., TONON, G., SCHAFFER, A. A. & KIRSCH, I. R. 2002. Stable karyotypes in epithelial cancer cell lines despite high rates of ongoing structural and numerical chromosomal instability. *Neoplasia,* 4**,** 19-31.

ROSCHKE, A. V., TONON, G., GEHLHAUS, K. S., MCTYRE, N., BUSSEY, K. J., LABABIDI, S., SCUDIERO, D. A., WEINSTEIN, J. N. & KIRSCH, I. R. 2003. Karyotypic complexity of the NCI-60 drug-screening panel. *Cancer Res,* 63**,** 8634-47.

ROWAN, A., HALFORD, S., GAASENBEEK, M., KEMP, Z., SIEBER, O., VOLIKOS, E., DOUGLAS, E., FIEGLER, H., CARTER, N., TALBOT, I., SILVER, A. & TOMLINSON, I. 2005. Refining molecular analysis in the pathways of colorectal carcinogenesis. *Clin Gastroenterol Hepatol,* 3**,** 1115-23.

ROYLANCE, R., ENDESFELDER, D., GORMAN, P., BURRELL, R. A., SANDER, J., TOMLINSON, I., HANBY, A. M., SPEIRS, V., RICHARDSON, A. L., BIRKBAK, N. J., EKLUND, A. C., DOWNWARD, J., KSCHISCHO, M., SZALLASI, Z. & SWANTON, C. 2011. Relationship of extreme chromosomal instability with long-term survival in a retrospective analysis of primary breast cancer. *Cancer Epidemiol Biomarkers Prev,* 20**,** 2183-94.

ROYOU, A., GAGOU, M. E., KARESS, R. & SULLIVAN, W. 2010. BubR1- and Polo-coated DNA tethers facilitate poleward segregation of acentric chromatids. *Cell,* 140**,** 235-45.

RUSAN, N. M. & PEIFER, M. 2008. Original CIN: reviewing roles for APC in chromosome instability. *J Cell Biol,* 181**,** 719-26.

SALE, J. E., LEHMANN, A. R. & WOODGATE, R. 2012. Y-family DNA polymerases and their role in tolerance of cellular DNA damage. *Nat Rev Mol Cell Biol,* 13**,** 141-52.

SAMOSHKIN, A., ARNAOUTOV, A., JANSEN, L. E., OUSPENSKI, I., DYE, L., KARPOVA, T., MCNALLY, J., DASSO, M., CLEVELAND, D. W. & STRUNNIKOV, A. 2009. Human condensin function is essential for centromeric chromatin assembly and proper sister kinetochore orientation. *PLoS One,* 4**,** e6831.

SANCAR, A., LINDSEY-BOLTZ, L. A., UNSAL-KACMAZ, K. & LINN, S. 2004. Molecular mechanisms of mammalian DNA repair and the DNA damage checkpoints. *Annu Rev Biochem,* 73**,** 39-85.

SANTAGUIDA, S., TIGHE, A., D'ALISE, A. M., TAYLOR, S. S. & MUSACCHIO, A. 2010. Dissecting the role of MPS1 in chromosome biorientation and the spindle checkpoint through the small molecule inhibitor reversine. *J Cell Biol,* 190**,** 73-87.

SARTORI, A. A., LUKAS, C., COATES, J., MISTRIK, M., FU, S., BARTEK, J., BAER, R., LUKAS, J. & JACKSON, S. P. 2007. Human CtIP promotes DNA end resection. *Nature,* 450**,** 509-14.

SATO, H., MASUDA, F., TAKAYAMA, Y., TAKAHASHI, K. & SAITOH, S. 2012. Epigenetic Inactivation and Subsequent Heterochromatinization of a Centromere Stabilize Dicentric Chromosomes. *Curr Biol*.

SAVITSKY, K., BAR-SHIRA, A., GILAD, S., ROTMAN, G., ZIV, Y., VANAGAITE, L., TAGLE, D. A., SMITH, S., UZIEL, T., SFEZ, S., ASHKENAZI, M., PECKER, I., FRYDMAN, M., HARNIK, R., PATANJALI, S. R., SIMMONS, A., CLINES, G. A., SARTIEL, A., GATTI, R. A., CHESSA, L., SANAL, O., LAVIN, M. F., JASPERS, N. G., TAYLOR, A. M., ARLETT, C. F., MIKI, T., WEISSMAN, S. M., LOVETT, M., COLLINS, F. S. & SHILOH, Y. 1995. A single ataxia telangiectasia gene with a product similar to PI-3 kinase. *Science,* 268**,** 1749-53.

SCHLACHER, K., CHRIST, N., SIAUD, N., EGASHIRA, A., WU, H. & JASIN, M. 2011. Double-strand break repair-independent role for BRCA2 in blocking stalled replication fork degradation by MRE11. *Cell,* 145**,** 529-42.

SCHLACHER, K., WU, H. & JASIN, M. 2012. A Distinct Replication Fork Protection Pathway Connects Fanconi Anemia Tumor Suppressors to RAD51-BRCA1/2. *Cancer Cell,* 22**,** 106-16.

SCHULTZ, L. B., CHEHAB, N. H., MALIKZAY, A. & HALAZONETIS, T. D. 2000. p53 binding protein 1 (53BP1) is an early participant in the cellular response to DNA double-strand breaks. *J Cell Biol,* 151**,** 1381-90.

SCHWARTZ, M., ZLOTORYNSKI, E. & KEREM, B. 2006. The molecular basis of common and rare fragile sites. *Cancer Lett,* 232**,** 13-26.

SFEIR, A., KOSIYATRAKUL, S. T., HOCKEMEYER, D., MACRAE, S. L., KARLSEDER, J., SCHILDKRAUT, C. L. & DE LANGE, T. 2009. Mammalian telomeres resemble fragile sites and require TRF1 for efficient replication. *Cell,* 138**,** 90-103.

SHANG, Y. L., BODERO, A. J. & CHEN, P. L. 2003. NFBD1, a novel nuclear protein with signature motifs of FHA and BRCT, and an internal 41-amino acid repeat sequence, is an early participant in DNA damage response. *J Biol Chem,* 278**,** 6323-9.

SHAY, J. W. & WRIGHT, W. E. 1996. Telomerase activity in human cancer. *Curr Opin Oncol,* 8**,** 66-71.

SHEFFER, M., BACOLOD, M. D., ZUK, O., GIARDINA, S. F., PINCAS, H., BARANY, F., PATY, P. B., GERALD, W. L., NOTTERMAN, D. A. & DOMANY, E. 2009. Association of survival and disease progression with chromosomal instability: a genomic exploration of colorectal cancer. *Proc Natl Acad Sci U S A,* 106**,** 7131-6.

SHELTZER, J. M., BLANK, H. M., PFAU, S. J., TANGE, Y., GEORGE, B. M., HUMPTON, T. J., BRITO, I. L., HIRAOKA, Y., NIWA, O. & AMON, A. 2011. Aneuploidy drives genomic instability in yeast. *Science,* 333**,** 1026-30.

SHERWOOD, R., TAKAHASHI, T. S. & JALLEPALLI, P. V. 2010. Sister acts: coordinating DNA replication and cohesion establishment. *Genes Dev,* 24**,** 2723-31.

SHI, Y., SAWADA, J., SUI, G., AFFAR EL, B., WHETSTINE, J. R., LAN, F., OGAWA, H., LUKE, M. P. & NAKATANI, Y. 2003. Coordinated histone modifications mediated by a CtBP co-repressor complex. *Nature,* 422**,** 735-8.

SHIMADA, M., KOBAYASHI, J., HIRAYAMA, R. & KOMATSU, K. 2010. Differential role of repair proteins, BRCA1/NBS1 and Ku70/DNA-PKcs, in radiation-induced centrosome overduplication. *Cancer Sci,* 101**,** 2531-7.

SHIMADA, M., SAGAE, R., KOBAYASHI, J., HABU, T. & KOMATSU, K. 2009. Inactivation of the Nijmegen breakage syndrome gene leads to excess centrosome duplication via the ATR/BRCA1 pathway. *Cancer Res,* 69**,** 1768-75.

SIEBER, O. M., HEINIMANN, K., GORMAN, P., LAMLUM, H., CRABTREE, M., SIMPSON, C. A., DAVIES, D., NEALE, K., HODGSON, S. V., ROYLANCE, R. R., PHILLIPS, R. K., BODMER, W. F. & TOMLINSON, I. P. 2002. Analysis of chromosomal instability in human colorectal adenomas with two mutational hits at APC. *Proc Natl Acad Sci U S A,* 99**,** 16910-5.

SIGOILLOT, F. D., LYMAN, S., HUCKINS, J. F., ADAMSON, B., CHUNG, E., QUATTROCHI, B. & KING, R. W. 2012. A bioinformatics method identifies prominent off-targeted transcripts in RNAi screens. *Nat Methods*.

SILKWORTH, W. T., NARDI, I. K., PAUL, R., MOGILNER, A. & CIMINI, D. 2012. Timing of centrosome separation is important for accurate chromosome segregation. *Mol Biol Cell,* 23**,** 401-11.

SILKWORTH, W. T., NARDI, I. K., SCHOLL, L. M. & CIMINI, D. 2009. Multipolar spindle pole coalescence is a major source of kinetochore mis-attachment and chromosome mis-segregation in cancer cells. *PLoS One,* 4**,** e6564.

SMID, M., HOES, M., SIEUWERTS, A. M., SLEIJFER, S., ZHANG, Y., WANG, Y., FOEKENS, J. A. & MARTENS, J. W. 2011. Patterns and incidence of chromosomal instability and their prognostic relevance in breast cancer subtypes. *Breast Cancer Res Treat,* 128**,** 23-30.

SMITH, J., THO, L. M., XU, N. & GILLESPIE, D. A. 2010. The ATM-Chk2 and ATR-Chk1 pathways in DNA damage signaling and cancer. *Adv Cancer Res,* 108**,** 73-112.

SMITH, K. J., LEVY, D. B., MAUPIN, P., POLLARD, T. D., VOGELSTEIN, B. & KINZLER, K. W. 1994. Wild-type but not mutant APC associates with the microtubule cytoskeleton. *Cancer Res,* 54**,** 3672-5.

SMOGORZEWSKA, A., KARLSEDER, J., HOLTGREVE-GREZ, H., JAUCH, A. & DE LANGE, T. 2002. DNA ligase IV-dependent NHEJ of deprotected mammalian telomeres in G1 and G2. *Curr Biol,* 12**,** 1635-44.

SNUDERL, M., FAZLOLLAHI, L., LE, L. P., NITTA, M., ZHELYAZKOVA, B. H., DAVIDSON, C. J., AKHAVANFARD, S., CAHILL, D. P., ALDAPE, K. D., BETENSKY, R. A., LOUIS, D. N. & IAFRATE, A. J. 2011. Mosaic amplification of multiple receptor tyrosine kinase genes in glioblastoma. *Cancer Cell,* 20**,** 810-7.

SOLOMON, D. A., KIM, T., DIAZ-MARTINEZ, L. A., FAIR, J., ELKAHLOUN, A. G., HARRIS, B. T., TORETSKY, J. A., ROSENBERG, S. A., SHUKLA, N., LADANYI, M., SAMUELS, Y., JAMES, C. D., YU, H., KIM, J. S. & WALDMAN, T. 2011. Mutational inactivation of STAG2 causes aneuploidy in human cancer. *Science,* 333**,** 1039-43.

SORENSEN, C. S., SYLJUASEN, R. G., LUKAS, J. & BARTEK, J. 2004. ATR, Claspin and the Rad9-Rad1-Hus1 complex regulate Chk1 and Cdc25A in the absence of DNA damage. *Cell Cycle,* 3**,** 941-5.

SOTILLO, R., SCHVARTZMAN, J. M., SOCCI, N. D. & BENEZRA, R. 2010. Mad2-induced chromosome instability leads to lung tumour relapse after oncogene withdrawal. *Nature,* 464**,** 436-40.

STEWART, G. S., WANG, B., BIGNELL, C. R., TAYLOR, A. M. & ELLEDGE, S. J. 2003. MDC1 is a mediator of the mammalian DNA damage checkpoint. *Nature,* 421**,** 961-6.

STEWENIUS, Y., GORUNOVA, L., JONSON, T., LARSSON, N., HOGLUND, M., MANDAHL, N., MERTENS, F., MITELMAN, F. & GISSELSSON, D. 2005. Structural and numerical chromosome changes in colon cancer develop through telomere-mediated anaphase bridges, not through mitotic multipolarity. *Proc Natl Acad Sci U S A,* 102**,** 5541-6.

STOLZ, A., ERTYCH, N., KIENITZ, A., VOGEL, C., SCHNEIDER, V., FRITZ, B., JACOB, R., DITTMAR, G., WEICHERT, W., PETERSEN, I. & BASTIANS, H. 2010. The CHK2-BRCA1 tumour suppressor pathway ensures chromosomal stability in human somatic cells. *Nat Cell Biol,* 12**,** 492-9.

STORCHOVA, Z., BRENEMAN, A., CANDE, J., DUNN, J., BURBANK, K., O'TOOLE, E. & PELLMAN, D. 2006. Genome-wide genetic analysis of polyploidy in yeast. *Nature,* 443**,** 541-7.

STORCHOVA, Z. & PELLMAN, D. 2004. From polyploidy to aneuploidy, genome instability and cancer. *Nat Rev Mol Cell Biol,* 5**,** 45-54.

STOREY, J. D. & SIEGMUND, D. 2001. Approximate p-values for local sequence alignments: numerical studies. *J Comput Biol,* 8**,** 549-56.

STRACKER, T. H., USUI, T. & PETRINI, J. H. 2009. Taking the time to make important decisions: the checkpoint effector kinases Chk1 and Chk2 and the DNA damage response. *DNA Repair (Amst),* 8**,** 1047-54.

SU, K. Y., CHEN, H. Y., LI, K. C., KUO, M. L., YANG, J. C., CHAN, W. K., HO, B. C., CHANG, G. C., SHIH, J. Y., YU, S. L. & YANG, P. C. 2012. Pretreatment epidermal growth factor receptor (EGFR) T790M mutation predicts shorter EGFR tyrosine kinase inhibitor response duration in patients with non-small-cell lung cancer. *J Clin Oncol,* 30**,** 433-40.

SU, L. K., BURRELL, M., HILL, D. E., GYURIS, J., BRENT, R., WILTSHIRE, R., TRENT, J., VOGELSTEIN, B. & KINZLER, K. W. 1995. APC binds to the novel protein EB1. *Cancer Res,* 55**,** 2972-7.

SUDAKIN, V., CHAN, G. K. & YEN, T. J. 2001. Checkpoint inhibition of the APC/C in HeLa cells is mediated by a complex of BUBR1, BUB3, CDC20, and MAD2. *J Cell Biol,* 154**,** 925-36.

SWANTON, C., NICKE, B., SCHUETT, M., EKLUND, A. C., NG, C., LI, Q., HARDCASTLE, T., LEE, A., ROY, R., EAST, P., KSCHISCHO, M., ENDESFELDER, D., WYLIE, P., KIM, S. N., CHEN, J. G., HOWELL, M., RIED, T., HABERMANN, J. K., AUER, G., BRENTON, J. D., SZALLASI, Z. & DOWNWARD, J. 2009. Chromosomal instability determines taxane response. *Proc Natl Acad Sci U S A,* 106**,** 8671-6.

TAALMAN, R. D., JASPERS, N. G., SCHERES, J. M., DE WIT, J. & HUSTINX, T. W. 1983. Hypersensitivity to ionizing radiation, in vitro, in a new chromosomal breakage disorder, the Nijmegen Breakage Syndrome. *Mutat Res,* 112**,** 23-32.

TAKAGI, Y., KOHMURA, H., FUTAMURA, M., KIDA, H., TANEMURA, H., SHIMOKAWA, K. & SAJI, S. 1996. Somatic alterations of the DPC4 gene in human colorectal cancers in vivo. *Gastroenterology,* 111**,** 1369-72.

TAKAMI, S., KAWASOME, C., KINOSHITA, M., KOYAMA, H. & NOGUCHI, S. 2001. Chromosomal instability detected by fluorescence in situ hybridization in Japanese breast cancer patients. *Clin Chim Acta,* 308**,** 127-31.

TAKEMURA, H., RAO, V. A., SORDET, O., FURUTA, T., MIAO, Z. H., MENG, L., ZHANG, H. & POMMIER, Y. 2006. Defective Mre11-dependent activation of Chk2 by ataxia telangiectasia mutated in colorectal carcinoma cells in response to replication-dependent DNA double strand breaks. *J Biol Chem,* 281**,** 30814-23.

TANG, Y. C., WILLIAMS, B. R., SIEGEL, J. J. & AMON, A. 2011. Identification of aneuploidy-selective antiproliferation compounds. *Cell,* 144**,** 499-512.

TCGA 2012. Comprehensive molecular characterization of human colon and rectal cancer. *Nature,* 487**,** 330-7.

THIRLWELL, C., WILL, O. C., DOMINGO, E., GRAHAM, T. A., MCDONALD, S. A., OUKRIF, D., JEFFREY, R., GORMAN, M., RODRIGUEZ-JUSTO, M., CHIN-ALEONG, J., CLARK, S. K., NOVELLI, M. R., JANKOWSKI, J. A., WRIGHT, N. A., TOMLINSON, I. P. & LEEDHAM, S. J. 2010. Clonality assessment and clonal ordering of individual neoplastic crypts shows polyclonality of colorectal adenomas. *Gastroenterology,* 138**,** 1441-54, 1454 e1-7.

THOMPSON, S. L., BAKHOUM, S. F. & COMPTON, D. A. 2010. Mechanisms of chromosomal instability. *Curr Biol,* 20**,** R285-95.

THOMPSON, S. L. & COMPTON, D. A. 2008. Examining the link between chromosomal instability and aneuploidy in human cells. *J Cell Biol,* 180**,** 665-72.

THOMPSON, S. L. & COMPTON, D. A. 2010. Proliferation of aneuploid human cells is limited by a p53-dependent mechanism. *J Cell Biol,* 188**,** 369-81.

THOMPSON, S. L. & COMPTON, D. A. 2011a. Chromosome missegregation in human cells arises through specific types of kinetochore-microtubule attachment errors. *Proc Natl Acad Sci U S A,* 108**,** 17974-8.

THOMPSON, S. L. & COMPTON, D. A. 2011b. Chromosomes and cancer cells. *Chromosome Res,* 19**,** 433-44.

TIGHE, A., JOHNSON, V. L., ALBERTELLA, M. & TAYLOR, S. S. 2001. Aneuploid colon cancer cells have a robust spindle checkpoint. *EMBO Rep,* 2**,** 609-14.

TORRES, E. M., SOKOLSKY, T., TUCKER, C. M., CHAN, L. Y., BOSELLI, M., DUNHAM, M. J. & AMON, A. 2007. Effects of aneuploidy on cellular physiology and cell division in haploid yeast. *Science,* 317**,** 916-24.

TORT, F., BARTKOVA, J., SEHESTED, M., ORNTOFT, T., LUKAS, J. & BARTEK, J. 2006. Retinoblastoma pathway defects show differential ability to activate the constitutive DNA damage response in human tumorigenesis. *Cancer Res,* 66**,** 10258-63.

TOSO, A., WINTER, J. R., GARROD, A. J., AMARO, A. C., MERALDI, P. & MCAINSH, A. D. 2009. Kinetochore-generated pushing forces separate centrosomes during bipolar spindle assembly. *J Cell Biol,* 184**,** 365-72.

TRAUT, T. W. 1994. Physiological concentrations of purines and pyrimidines. *Mol Cell Biochem,* 140**,** 1-22.

TRENZ, K., SMITH, E., SMITH, S. & COSTANZO, V. 2006. ATM and ATR promote Mre11 dependent restart of collapsed replication forks and prevent accumulation of DNA breaks. *EMBO J,* 25**,** 1764-74.

TSAFRIR, D., BACOLOD, M., SELVANAYAGAM, Z., TSAFRIR, I., SHIA, J., ZENG, Z., LIU, H., KRIER, C., STENGEL, R. F., BARANY, F., GERALD, W. L., PATY, P. B., DOMANY, E. &

NOTTERMAN, D. A. 2006. Relationship of gene expression and chromosomal abnormalities in colorectal cancer. *Cancer Res,* 66**,** 2129-37.

TSUDA, H., SAKAMAKI, C., TSUGANE, S., FUKUTOMI, T. & HIROHASHI, S. 1998. Prognostic significance of accumulation of gene and chromosome alterations and histological grade in node-negative breast carcinoma. *Jpn J Clin Oncol,* 28**,** 5-11.

TSUI, M., XIE, T., ORTH, J. D., CARPENTER, A. E., RUDNICKI, S., KIM, S., SHAMU, C. E. & MITCHISON, T. J. 2009. An intermittent live cell imaging screen for siRNA enhancers and suppressors of a kinesin-5 inhibitor. *PLoS One,* 4**,** e7339.

UMAR, A., BOLAND, C. R., TERDIMAN, J. P., SYNGAL, S., DE LA CHAPELLE, A., RUSCHOFF, J., FISHEL, R., LINDOR, N. M., BURGART, L. J., HAMELIN, R., HAMILTON, S. R., HIATT, R. A., JASS, J., LINDBLOM, A., LYNCH, H. T., PELTOMAKI, P., RAMSEY, S. D., RODRIGUEZ-BIGAS, M. A., VASEN, H. F., HAWK, E. T., BARRETT, J. C., FREEDMAN, A. N. & SRIVASTAVA, S. 2004. Revised Bethesda Guidelines for hereditary nonpolyposis colorectal cancer (Lynch syndrome) and microsatellite instability. *J Natl Cancer Inst,* 96**,** 261-8.

VAN DER HEIJDEN, M. S., BRODY, J. R., ELGHALBZOURI-MAGHRANI, E., ZDZIENICKA, M. Z. & KERN, S. E. 2006. Does tumorigenesis select for or against mutations of the DNA repair-associated genes BRCA2 and MRE11?: considerations from somatic mutations in microsatellite unstable (MSI) gastrointestinal cancers. *BMC Genet,* 7**,** 3.

VAN REE, J. H., JEGANATHAN, K. B., MALUREANU, L. & VAN DEURSEN, J. M. 2010. Overexpression of the E2 ubiquitin-conjugating enzyme UbcH10 causes chromosome missegregation and tumor formation. *J Cell Biol,* 188**,** 83-100.

VEIGL, M. L., KASTURI, L., OLECHNOWICZ, J., MA, A. H., LUTTERBAUGH, J. D., PERIYASAMY, S., LI, G. M., DRUMMOND, J., MODRICH, P. L., SEDWICK, W. D. & MARKOWITZ, S. D. 1998. Biallelic inactivation of hMLH1 by epigenetic gene silencing, a novel mechanism causing human MSI cancers. *Proc Natl Acad Sci U S A,* 95**,** 8698-702.

VENKITARAMAN, A. R. 2007. Chromosomal instability in cancer: causality and interdependence. *Cell Cycle,* 6**,** 2341-3.

VOGELSTEIN, B., FEARON, E. R., HAMILTON, S. R., KERN, S. E., PREISINGER, A. C., LEPPERT, M., NAKAMURA, Y., WHITE, R., SMITS, A. M. & BOS, J. L. 1988. Genetic alterations during colorectal-tumor development. *N Engl J Med,* 319**,** 525-32.

WAGNER, K. W., SAPINOSO, L. M., EL-RIFAI, W., FRIERSON, H. F., BUTZ, N., MESTAN, J., HOFMANN, F., DEVERAUX, Q. L. & HAMPTON, G. M. 2004. Overexpression, genomic amplification and therapeutic potential of inhibiting the UbcH10 ubiquitin conjugase in human carcinomas of diverse anatomic origin. *Oncogene,* 23**,** 6621-9.

WALTHER, A., HOULSTON, R. & TOMLINSON, I. 2008. Association between chromosomal instability and prognosis in colorectal cancer: a meta-analysis. *Gut,* 57**,** 941-50.

WANG, H., ZENG, Z. C., BUI, T. A., DIBIASE, S. J., QIN, W., XIA, F., POWELL, S. N. & ILIAKIS, G. 2001. Nonhomologous end-joining of ionizing radiation-induced DNA double-stranded breaks in human tumor cells deficient in BRCA1 or BRCA2. *Cancer Res,* 61**,** 270-7.

WANG, L. H., SCHWARZBRAUN, T., SPEICHER, M. R. & NIGG, E. A. 2008. Persistence of DNA threads in human anaphase cells suggests late completion of sister chromatid decatenation. *Chromosoma,* 117**,** 123-35.

WANG, Q., LIU, T., FANG, Y., XIE, S., HUANG, X., MAHMOOD, R., RAMASWAMY, G., SAKAMOTO, K. M., DARZYNKIEWICZ, Z., XU, M. & DAI, W. 2004a. BUBR1 deficiency results in abnormal megakaryopoiesis. *Blood,* 103**,** 1278-85.

WANG, Z., CUMMINS, J. M., SHEN, D., CAHILL, D. P., JALLEPALLI, P. V., WANG, T. L., PARSONS, D. W., TRAVERSO, G., AWAD, M., SILLIMAN, N., PTAK, J., SZABO, S., WILLSON, J. K., MARKOWITZ, S. D., GOLDBERG, M. L., KARESS, R., KINZLER, K. W., VOGELSTEIN, B., VELCULESCU, V. E. & LENGAUER, C. 2004b. Three classes of genes mutated in colorectal cancers with chromosomal instability. *Cancer Res,* 64**,** 2998-3001.

WANZEL, M., KLEINE-KOHLBRECHER, D., HEROLD, S., HOCK, A., BERNS, K., PARK, J., HEMMINGS, B. & EILERS, M. 2005. Akt and 14-3-3eta regulate Miz1 to control cell-cycle arrest after DNA damage. *Nat Cell Biol,* 7**,** 30-41.

WASAN, H. S., PARK, H. S., LIU, K. C., MANDIR, N. K., WINNETT, A., SASIENI, P., BODMER, W. F., GOODLAD, R. A. & WRIGHT, N. A. 1998. APC in the regulation of intestinal crypt fission. *J Pathol,* 185**,** 246-55.

WATANABE, T., WU, T. T., CATALANO, P. J., UEKI, T., SATRIANO, R., HALLER, D. G., BENSON, A. B., 3RD & HAMILTON, S. R. 2001. Molecular predictors of survival after adjuvant chemotherapy for colon cancer. *N Engl J Med,* 344**,** 1196-206.

WATSON, J. V., CHAMBERS, S. H. & SMITH, P. J. 1987. A pragmatic approach to the analysis of DNA histograms with a definable G1 peak. *Cytometry,* 8**,** 1-8.

WEAVER, B. A., SILK, A. D., MONTAGNA, C., VERDIER-PINARD, P. & CLEVELAND, D. W. 2007. Aneuploidy acts both oncogenically and as a tumor suppressor. *Cancer Cell,* 11**,** 25-36.

WECHSLER, T., NEWMAN, S. & WEST, S. C. 2011. Aberrant chromosome morphology in human cells defective for Holliday junction resolution. *Nature,* 471**,** 642-6.

WELCKER, M. & CLURMAN, B. E. 2008. FBW7 ubiquitin ligase: a tumour suppressor at the crossroads of cell division, growth and differentiation. *Nat Rev Cancer,* 8**,** 83-93.

WESTHORPE, F. G., DIEZ, M. A., GURDEN, M. D., TIGHE, A. & TAYLOR, S. S. 2010. Re-evaluating the role of Tao1 in the spindle checkpoint. *Chromosoma*.

WILLIAMS, B. R., PRABHU, V. R., HUNTER, K. E., GLAZIER, C. M., WHITTAKER, C. A., HOUSMAN, D. E. & AMON, A. 2008. Aneuploidy affects proliferation and spontaneous immortalization in mammalian cells. *Science,* 322**,** 703-9.

WILLIAMS, R. S. & TAINER, J. A. 2005. A nanomachine for making ends meet: MRN is a flexing scaffold for the repair of DNA double-strand breaks. *Mol Cell,* 19**,** 724-6.

WOODFORD-RICHENS, K. L., ROWAN, A. J., GORMAN, P., HALFORD, S., BICKNELL, D. C., WASAN, H. S., ROYLANCE, R. R., BODMER, W. F. & TOMLINSON, I. P. 2001. SMAD4 mutations in colorectal cancer probably occur before chromosomal instability, but after divergence of the microsatellite instability pathway. *Proc Natl Acad Sci U S A,* 98**,** 9719-23.

WU, L. & HICKSON, I. D. 2003. The Bloom's syndrome helicase suppresses crossing over during homologous recombination. *Nature,* 426**,** 870-4.

WU, X., NORTHCOTT, P. A., DUBUC, A., DUPUY, A. J., SHIH, D. J., WITT, H., CROUL, S., BOUFFET, E., FULTS, D. W., EBERHART, C. G., GARZIA, L., VAN METER, T., ZAGZAG, D., JABADO, N., SCHWARTZENTRUBER, J., MAJEWSKI, J., SCHEETZ, T. E., PFISTER, S. M., KORSHUNOV, A., LI, X. N., SCHERER, S. W., CHO, Y. J., AKAGI, K., MACDONALD, T. J., KOSTER, J., MCCABE, M. G., SARVER, A. L., COLLINS, V. P., WEISS, W. A., LARGAESPADA, D. A., COLLIER, L. S. & TAYLOR, M. D. 2012. Clonal selection drives genetic divergence of metastatic medulloblastoma. *Nature,* 482**,** 529-33.

WU, ZH., SHI, Y., TIBBETTS, R., MIYAMOTO, S. 2006. Molecular linkage between the kinase ATM and NF-kappaB signaling in response to genotoxic stimuli. *Science* 311(5764):1141-6

XIA, F., TAGHIAN, D. G., DEFRANK, J. S., ZENG, Z. C., WILLERS, H., ILIAKIS, G. & POWELL, S. N. 2001. Deficiency of human BRCA2 leads to impaired homologous recombination but maintains normal nonhomologous end joining. *Proc Natl Acad Sci U S A,* 98**,** 8644-9.

XIAO, A., LI, H., SHECHTER, D., AHN, S. H., FABRIZIO, L. A., ERDJUMENT-BROMAGE, H., ISHIBE-MURAKAMI, S., WANG, B., TEMPST, P., HOFMANN, K., PATEL, D. J., ELLEDGE, S. J. & ALLIS, C. D. 2009. WSTF regulates the H2A.X DNA damage response via a novel tyrosine kinase activity. *Nature,* 457**,** 57-62.

XUE, W., KITZING, T., ROESSLER, S., ZUBER, J., KRASNITZ, A., SCHULTZ, N., REVILL, K., WEISSMUELLER, S., RAPPAPORT, A. R., SIMON, J., ZHANG, J., LUO, W., HICKS, J., ZENDER, L., WANG, X. W., POWERS, S., WIGLER, M. & LOWE, S. W. 2012. A cluster of cooperating tumor-suppressor gene candidates in chromosomal deletions. *Proc Natl Acad Sci U S A,* 109**,** 8212-7.

YADA, T., SUGIURA, R., KITA, A., ITOH, Y., LU, Y., HONG, Y., KINOSHITA, T., SHUNTOH, H. & KUNO, T. 2001. Its8, a fission yeast homolog of Mcd4 and Pig-n, is involved in GPI anchor synthesis and shares an essential function with calcineurin in cytokinesis. *J Biol Chem,* 276**,** 13579-86.

YAP, T. A., GERLINGER, M., FUTREAL, P. A., PUSZTAI, L. & SWANTON, C. 2012. Intratumor heterogeneity: seeing the wood for the trees. *Sci Transl Med,* 4**,** 127ps10.

YATSUOKA, T., SUNAMURA, M., FURUKAWA, T., FUKUSHIGE, S., YOKOYAMA, T., INOUE, H., SHIBUYA, K., TAKEDA, K., MATSUNO, S. & HORII, A. 2000. Association of poor prognosis with loss of 12q, 17p, and 18q, and concordant loss of 6q/17p and 12q/18q in human pancreatic ductal adenocarcinoma. *Am J Gastroenterol,* 95**,** 2080-5.

ZEGERMAN, P. & DIFFLEY, J. F. 2010. Checkpoint-dependent inhibition of DNA replication initiation by Sld3 and Dbf4 phosphorylation. *Nature,* 467**,** 474-8.

ZHONG, X., MALHOTRA, R. & GUIDOTTI, G. 2003. ATP uptake in the Golgi and extracellular release require Mcd4 protein and the vacuolar H+-ATPase. *J Biol Chem,* 278**,** 33436-44.

ZHOU, H., KUANG, J., ZHONG, L., KUO, W. L., GRAY, J. W., SAHIN, A., BRINKLEY, B. R. & SEN, S. 1998. Tumour amplified kinase STK15/BTAK induces centrosome amplification, aneuploidy and transformation. *Nat Genet,* 20**,** 189-93.

ZOU, L. & ELLEDGE, S. J. 2003. Sensing DNA damage through ATRIP recognition of RPA-ssDNA complexes. *Science,* 300**,** 1542-8.